REPORT DOCUMENTATION PAGE

1a. REPORT SECURITY CLASSIFICATION: Unclassified	1b. RESTRICTIVE MARKINGS
2a. SECURITY CLASSIFICATION AUTHORITY	3. DISTRIBUTION/AVAILABILITY OF REPORT: Approved for public release; distribution unlimited.
2b. DECLASSIFICATION/DOWNGRADING SCHEDULE	
4. PERFORMING ORGANIZATION REPORT NUMBER(S)	5. MONITORING ORGANIZATION REPORT NUMBER(S): ARO 26372.1-MS-CF
6a. NAME OF PERFORMING ORGANIZATION: Virginia Polytechnic Inst. and State Univ. / 6b. OFFICE SYMBOL (If applicable)	7a. NAME OF MONITORING ORGANIZATION: U. S. Army Research Office
6c. ADDRESS (City, State, and ZIP Code): Blacksburg, VA 24061	7b. ADDRESS (City, State, and ZIP Code): P. O. Box 12211, Research Triangle Park, NC 27709-2211
8a. NAME OF FUNDING/SPONSORING ORGANIZATION: U. S. Army Research Office / 8b. OFFICE SYMBOL (If applicable)	9. PROCUREMENT INSTRUMENT IDENTIFICATION NUMBER: DAAL03-88-G-0043
8c. ADDRESS (City, State, and ZIP Code): P. O. Box 12211, Research Triangle Park, NC 27709-2211	10. SOURCE OF FUNDING NUMBERS: PROGRAM ELEMENT NO. / PROJECT NO. / TASK NO. / WORK UNIT ACCESSION NO.

11. TITLE (Include Security Classification): Smart Materials, Structures and Mathematical Issues

12. PERSONAL AUTHOR(S): Craig A. Rogers (Principal Investigator on Project)

13a. TYPE OF REPORT	13b. TIME COVERED	14. DATE OF REPORT (Year, Month, Day)	15. PAGE COUNT
Final	FROM 8/8/88 TO 8/7/89	1989	

16. SUPPLEMENTARY NOTATION: The view, opinions and/or findings contained in this report are those of the author(s) and should not be construed as an official Department of the Army position, policy, or decision, unless so designated by other documentation.

17. COSATI CODES		
FIELD	GROUP	SUB-GROUP

18. SUBJECT TERMS (Continue on reverse if necessary and identify by block number): Smart Materials, Smart Structures, Actuators, Sensors, Intelligence, Control, Constitutive Modeling

19. ABSTRACT (Continue on reverse if necessary and identify by block number)

This workshop on "Smart Materials, Structures, and Mathematical Issues" is one of a series of workshops organized by the U. S. Army Research Office to identify recent significant developments and breakthroughs in science and technology. Its main objective is to evolve a consensus on the definition and characteristics of a 'smart'/'intelligent' material or structure, and discuss mechanisms and possible methods to produce them. Another objective is to identify directions of future research in this field.

This report includes the abstracts/papers presented at the three sessions. The three sessions related to (1) Smart Structures, (2) Smart Materials, and (3) Related Mathematical Issues, contain a wide range of presentations concerning numberous technologies for actuators, sensors, intelligence,

(CONT'D ON BACK)

20. DISTRIBUTION/AVAILABILITY OF ABSTRACT	21. ABSTRACT SECURITY CLASSIFICATION
☐ UNCLASSIFIED/UNLIMITED ☐ SAME AS RPT. ☐ DTIC USERS	Unclassified
22a. NAME OF RESPONSIBLE INDIVIDUAL	22b. TELEPHONE (Include Area Code) / 22c. OFFICE SYMBOL

control, constitutive modeling, and other scientific fields that have become essential to the emerging science and technologies of smart materials and structures. At the end of each session a discussion period was held to address some of issues of general concern related to the mission of the workshop.

U. S. Army Research Office Workshop

SMART MATERIALS, STRUCTURES and MATHEMATICAL ISSUES

September 15-16, 1988

Donaldson Brown Continuing Education Center
Virginia Polytechnic Institute and State University
Blacksburg, Virginia 24061

Workshop Co-chairman:
Iqbal Ahmad, ARO
Craig Rogers, VPI&SU

Editor:
C. A. Rogers
Smart Materials & Structures Laboratory
Mechanical Engineering Department
Virginia Polytechnic Institute and State University

"The views, opinions, and/or findings contained in this report are those of the author(s) and should not be construed as an official Department of the Army position, policy, or decision, unless so designated by other documentation."

Accession For	
NTIS GRA&I	☑
DTIC TAB	☐
Unannounced	☐
Justification	
By	
Distribution/	
Availability Codes	
Dist	Avail and/or Special
A-1	

U. S. Army Research Office Workshop
"Smart Materials, Structures, and Mathematical Issues"

FORWARD

This workshop on "Smart Materials, Structures, and Mathematical Issues" is one of a series of workshops organized by the U. S. Army Research Office to identify recent significant developments and breakthroughs in science and technology. Its main objective is to evolve a consensus on the definition and characteristics of a 'smart'/'intelligent' material or structure, and discuss mechanisms and possible methods to produce them. Another objective is to identify directions of future research in this field.

In the following pages the abstracts/papers as received by the invited speakers are presented. The three sessions related to i) Smart Structures, ii) Smart Materials, and iii) Related Mathematical Issues, contain a wide range of presentations concerning numerous technologies for actuators, sensors, intelligence, control, constitutive modeling, and other scientific fields that have become essential to the emerging science and technologies of smart materials and structures. At the end of each session a discussion period has been scheduled to address some of issues of general concern related to the mission of the workshop. It is hoped that all in attendance will contribute to the discussion and share with all of us your impressions, experiences and desires for the future of smart materials and structures research.

Craig Rogers
Iqbal Ahmad
Workshop Co-chairman

U. S. Army Research Office Workshop
"Smart Materials, Structures, and Mathematical Issues"

Donaldson Brown Continuing Education Center
Virginia Polytechnic Insitute and State University
Blacksburg, Virginia 24061
September 15-16, 1988

Workshop Co-chairman:
Dr. Iqbal Ahmad, ARO
Dr. Craig A. Rogers, VPI&SU

- **Wednesday September 14, 1988**
  - 6:00 PM - 7:00 PM Registration and Reception at the Donaldson Brown Continuing Education Center

- **Thursday September 15, 1988** - Conference Room F
  - 8:00 AM - 8:30 Coffee and Danish (Registration)
  - 8:30 AM - 8:50 Opening Remarks - Conference Room F
    - Prof. Craig A. Rogers, VPI&SU : Workshop Co-Chairman
    - Dr. F. W. Stephenson, Assoc. Dean - College of Engineering, VPI&SU
    - Dr. Iqbal Ahmad, ARO : Workshop Co-Chairman
  - **Session 1 - Smart Structures - Chair: Dr. Gary Anderson, ARO**
    - 8:50 - 9:15 "Dynamic Control Concepts Using Shape Memory Alloy Reinforced Plates", Prof. C. A. Rogers, VPI&SU
    - 9:15 - 9:40 "Optical Fiber Sensors and Signal Processing for Smart Materials and Structures Applications", Prof. R. O. Claus, VPI&SU
    - 9:40 - 10:05 "A New Generation of Revolutionary Ultra-Advanced Intelligent Composite Materials Featuring Electro-Rheological Fluids", Prof. M. V. Gandhi, Michigan State Univ.
    - 10:05 - 10:20 Coffee Break
    - 10:20 - 10:45 "Piezoceramic Devices and PVDF Films as Sensors and Actuators for Intelligent Structures", Prof. S. Hanagud, GA Tech
    - 10:45 - 11:10 "Variable Geometry Trusses", Prof. H. H. Robertshaw, VPI&SU
    - 11:10 - 11:35 "Passive Self-Adaptive Structures", Prof. E. Rivin, Wayne State University
    - 11:35 - 12:00 "Applications for Smart Materials in the Field of Vibration Control", Dr. T. G. Duclos, Lord Corporation
    - 12:00 - 12:30 Discussion - Moderator: Dr. G. Anderson, ARO

- 12:30 - 1:30 PM Lunch at CEC
- **Session 2 - Smart Materials - Chair: Dr. Iqbal Ahmad, ARO**
  - 1:30 - 1:50 "Materials Issues for Smart Structures", Prof. G. L. Wilkes, VPI&SU
  - 1:50 - 2:30 "Smart Ceramics", Prof. R. E. Newnham, Penn State Univ.
  - 2:30 - 3:30 "Self Assembly and 'Smart Materials'", Dr. B. B. Rath, Naval Research Laboratory
  - 3:00 - 3:15 Coffee Break
  - 3:15 - 3:45 "Basic Principles for the Improvement of Shape-Memory and Related Materials", Prof. James, Univ. of Minnesota
  - 3:45 - 4:15 "Tribopolymerization: A New Concept of Boundary Lubrication", Prof. M. J. Furey, VPI&SU
  - 4:15 - 5:00 Discussion - Moderator: Dr. I. Ahmad, ARO
- 6:00 - 7:00 Reception
- 7:00 - Dinner at CEC - Speaker: Dr. James Robertson, C. P. Miles Professor of History, VPI&SU - "THE AMERICAN PRESIDENCY: WHAT WE WANT AND WHAT WE GET"

- **Friday September 16, 1988**
  - 8:00 - 8:30 Coffee and Danish - Conference Room B
  - **Session 3 - Mathematical Issues - Chair: Dr. Julian Wu, ARO**
    - 8:30 - 9:00 "Extremal Composites and Structural Optimization", Prof. R. V. Kohn, Courant Institute
    - 9:00 - 9:30 "Wave Propagation in Layered Elastic Media", Prof. R. Rostamian, Univ. of Maryland
    - 9:30 - 10:00 "Optimization and Homogenization for Elastic Materials", W. W. Hager, University of Florida
    - 10:00 - 10:15 Coffee Break
    - 10:15 - 10:45 "Computational Results for Phase Transitions in Shape Memory Materials, Prof. M. Luskin, Univ. of Minnesota
    - 10:45 - 11:15 "Dynamics of Phase Transitions", Prof. M. Slemrod, Univ. of Wisconsin-Madison
    - 11:15 - 11:30 Discussion - Moderator: Dr. J. Wu, ARO
  - **Session 4 - Direction of Future Research - Chair: Dr. Chandra**
    - 11:30 - 12:30 Panel Discussion - Moderator: Dr. Chandra, ARO
  - 12:30 - Lunch & End of Workshop

"SMART" STRUCTURES AND MATERIALS

I. AHMAD

U.S. Army Research Office, Research Triangle Park, NC

ABSTRACT

The definition of 'smart' and the characteristics of 'smart' structures and materials are reviewed.

As Professor Rogers has stated, the objectives of this workshop are as follows:

1. To arrive at a concensus about the definition of 'smart'/'intelligent' structures or materials.
2. Identify their characteristics.
3. Discuss the logic and methodology of producing them.
4. Discuss mathematical issues relating to modeling and predictive relationships.

This paper is addressed to the first two objectives. The terms 'smart', 'adaptive' and 'intelligent' have been used recently quite frequently in the technical meetings and literature, interchangeably and rather loosely. For example Professor Gandhi, who is one of the speakers at this workshop, reports an electrorheological fluid as 'smart structural material' as it can change properties' on demand'. In principle this fluid is placed in a graphite epoxy composite beam as shown in Figure 1. When an electrical potential is applied, the fluid stiffens, thereby stiffening the beam. This phenomenon can be used to dampen vibrations in structures. Response time less than a millisecond is reported. Professor Roger, who is the co-chairman of the workshop, uses the term 'adaptive' to shape memory alloy wires which act as actuators in a composite beam. He has developed a system (Figure 2) in which prestrained Nitinol (an alloy of nickel and titanium) wires are embedded in an off-axis position in the graphite fiber reinforced epoxy composite beam. When these wires are heated by passing an electrical current they try to contract to their original length, which generates a uniformly distributed shear load along their length, causing the beam to bend in a predictive manner. In a recent issue of Laser Focus (May 1988) a concept of 'smart structure' that contains embedded fiber-optic sensors has been presented. The idea is to incorporate the sensors at the time of the manufacture of the structure to monitor the manufacturing process, check the integrity of the structure before installation in the system and monitor its health during service. The output from various sensors is multiplexed for transition to optical/electronic preprocessors whose output goes to control computers. A fiber optical link can be used in connection with the control system to activate actuators when required. So in this example, the 'smart' structure includes sensors, a control system and actuators.

Use of piezoelectric actuators as elements of 'intelligent' structures has been actively pursued by many researchers. In the large space structures, these

actuators are required to control both the rigid body and elastic deformations. The feasibility of using segmented actuators for vibration and shape control has been demonstrated both analytically and experimentally by Crawley et al (AIAA Journal, vol 25, No. 10, p 1373-1385).

No intrinsically 'smart' or 'intelligent' material has been reported as such in the literature. However, a careful search does indicate a few materials, which may qualify as 'intrinsically' smart. In other words, they have intrinsic capability of sensing the stimulus and responding in a controlled manner, as a result of their atomic or molecular structure. The former is exemplified by photochromic glass and the latter is prevelant in the biosystems. These examples will be very briefly described in the following.

Photochromic glass used in the popular ophthalmic lenses for the protection of eyes from the ultraviolet radiation, was discovered by Arimstead and Stooky of Corning Glass in 1964. This glass has the remarkable property of becoming dark in the sunlight and reverting to the clear state indoors. This is accomplished by incorporating in an appropriate glass composition, a small quantity of very fine crystallites of silver chloride containing traces of copper. Figure 4 shows the arrangement of ions in one of the silver chloride crystals, before and after darkening. The process responsible for darkening can be summarized by the following equations:

$$Cl^- + h\nu_+ = Cl^0 + e \quad (1)$$

$$e + Ag^+ = Ag^0 \text{ (Trapped electron)} \quad (2)$$

$$Cu^+ + Cl^0 = Cl^- + Cu^{++} \text{ (Trapped hole)} \quad (3)$$

$$Cu^+ + Ag^+ = Ag^0 + Cu^{++} \quad (4)$$

Thus the silver halide which is sensitive to the ultraviolet radiation acts both as a sensor and as an actuator, as the darkening is the result of the clustering of silver atoms (Ag^0). The fading is the reverse of reaction (4) which is energetically favorable in the absence of ultraviolet radiation.

From the biosystems a large number of examples of molecular entities, which can be termed as 'smart' or 'intelligent' can be mentioned. One simple example (Encyclopedia Britanica, 'Science and the Future' 1981 Year Book, p 122-137) is the cell membrane. All living beings are composed of cells which carry out specialized functions with greatest efficiency. The life and performance of living systems is due to the integration of these functions. Cells themselves are highly complex systems. They are kept separate by a thin wall called cell membrane. Until recently cell wall was considered to be a passive system through which certain constituents can pass. But more recently, the structure and function of this membrane have been elucidated, according to which it is now believed that it is a dynamic system which controls (1) transport of raw materials into the cell and secretory and waste materials out of the cell, and (2) it carries specialized receptor molecules which function as sensors for the cell and provides it with means to react with the outside stimuli such as hormones, regulatory substances such as drugs or even other cells.

The cell membrane is essentially composed of phospholipid molecules which are hydrophobic on one end and hydrophilic on the other (Fig 5a). In aqueous solutions, they form stable bilayers as shown in Figure 5(b), with the hydrophilic groups on the surface. In these layers are incorporated protein molecules, which consist of chains of amino acids some of which are hydrophobic and others are hydrophilic. These molecules in aqueous solutions fold into three dimensional structures (Figure 6a) that satisfy the surface properties of individual amino acids. In the aqueous medium the protein chains fold in such a way that the hydrophobic amino acids are collected together within the structure, while the hydrophilic portions are on the surface. Although cells use about 20 types of amino acids, essentially any one of them can appear at any position on the protein chain which could have anywhere from 50-50,000 amino acids. This provides these molecules a large number of functional capabilities. These chains are flexible and are quite sensitive to the conditions that effect chemical reactions- temperature, pressure, acidity and exposure to other molecules. Also some carbohydrate groups occur as chains attached to the phospholipid and protein molecules of the membrane, which act as sensors. The configuration of the protein molecule is very sensitive to an is determined by the chemical environment in and outside the cell. For transport of molecules such as glucose, the protein chain forms hydrophilic channels as shown in Figure 7. whereby the attached molecule is transported into the cell. As soon as the molecule detaches (caused by the environment in the cell interior) from the protein surface, the chain reconfigures into the original shape as in Figure 7a. Thus the protein molecule acts as a sensor and because of its ability to configure dictated by the environment, as an actuator. Control mechanisms are provided by the chemical environment. The key factor is the intrinsic nature of the molecular structure. Other functions and the mechanisms of transport used by the protein molecules are described in the literature.

From the above examples, the common features of the so called 'smart' or 'intelligent' structures or materials, can be identified as follows:

1. They have embedded (or bonded) or intrinsic sensor/s which recognize and measure the intensity of the stimulus, such as stress, strain, thermal, electric, magnetic, electromagnetic, chemical or nuclear etc.
2. They have embedded or intrinsic actuator/s to respond to the stimulus.
3. For controlling the response in a predetermined manner they have available mechanisms of control and sometime of selecting a particular response if more than one option is available.
4. Time of response is short/appropriate.
5. The system returns to its original state as soon as the stimulus is removed.

Now the question arises whether the above described structures or materials should be termed as 'smart' 'adaptive', 'intelligent' or something else. According to the Webster's International Dictionary, 'smart' is:

> Suggesting vigor, speedy, spirited, lively; showing mental alertness and quickness of perception, shrewd, informed, resourceful; sharp and of questionable integrity, well turned out, neat, trim, spruce, tidy, natty

This dictionary also defines 'intelligence' as follows:

> To perceive ones environment;
> to know/comprehend and learn;
> to understand;
> to foresee problems;
> to use symbols and relationships and create new ones;
> think abstractly;
> to work towards a goal;

McGraw Hill Encyclopedia of Science and Technology (Vol. 9, p. 272) defines 'intelligence' as:

> "general mental ability due to integrative and adaptive functions of the brain that permit complex, unstereotyped, purposive response to novel and changing situations, involving discrimination, generalization, learning, concept formation, inference, mental manipulations of memories, images, words and abstract symbols, education of relations and correlations and problem solving"

Then there is 'machine intelligence' which is defined as:

> "that can accomplish its specified task in the presence of uncertainty and variability in its environments. Machine's ability to monitor its environments allowing it to adjust its action based on what it has sensed is a prerequisite of intelligence"

Examples of 'machine intelligence' quoted in the literature include robots equipped with sensors, computers equipped with voice recognition etc. Atomatic feedbacks, regulatory systems such as thermostats, automobile cruise controls, photoelectric door opener etc are not considered as machine intelligence. In fact the term 'intelligence' represents an hierarchy which ranges from the simple automatic feedback systems, 'machine intelligence', artificial intelligence, and intelligence in vegetable kingdom, to that of viruses, bacteria and higher order species including mammals and homosapiens.

In the light of the above discussion of the characteristics and definitions of 'smart' and 'intelligent', neither of these terms appear to be appropriate for the systems described in the literature as "smart" or "intelligent". However, the term 'smart' has acquired some acceptability in the technical popular literature. To avoid confusion one way out is to sanctify it as a technical term and define it as follows:

'A system or a material which has built-in or intrinsic sensor/s, actuator/s and control mechanism/s whereby it is capable of sensing a stimulus, responding to it in a predetermined manner and extent, in a short/appropriate time and reverting to its original state as soon as the stimulus is removed.'

If this definition is adopted, then electrorheological fluids, shape memory alloys or piezoelectric transducers are not 'smart' materials as such, but they can be an important component (for example as a sensor or an actuator) of a 'smart' structure or a system. On the other hand photochromic glasses and certain protein molecules can be termed as 'smart'.

It is hoped that these ideas about the definition and characteristics of 'smart' structures and materials, will be discussed in this work shop thoroughly, as their clear conceptualisation is important for the furtherance of this emerging technology.

List of Figures:

Figure 1. 'Smart Structural Material.' Prof. Gandhi

Figure 2. 'Novel 'Adaptive/Smart Composite Material'. Prof. Rogers

Figure 3. Embedded sensors make structure 'smart'

Figure 4. Darkening mechanism of photochromic glasses.

Figure 5. (a) A monomolecular layer of phospholipid molecules.

(b) Self assembled two molecule thick layer.

Figure 6. (a) A folding pattern of protein molecule in an aqueous medium in which hydrophobic regions face upwards
(b) Unfolded protein molecule.

Figure 7. (a) Showing the configuration of the protein molecule as the molecule to be transported from the exterior of the cell, attaches to it.

(b) Showing the configuration of the protein chain as the molecule to be transported detaches in the interior of the cell.

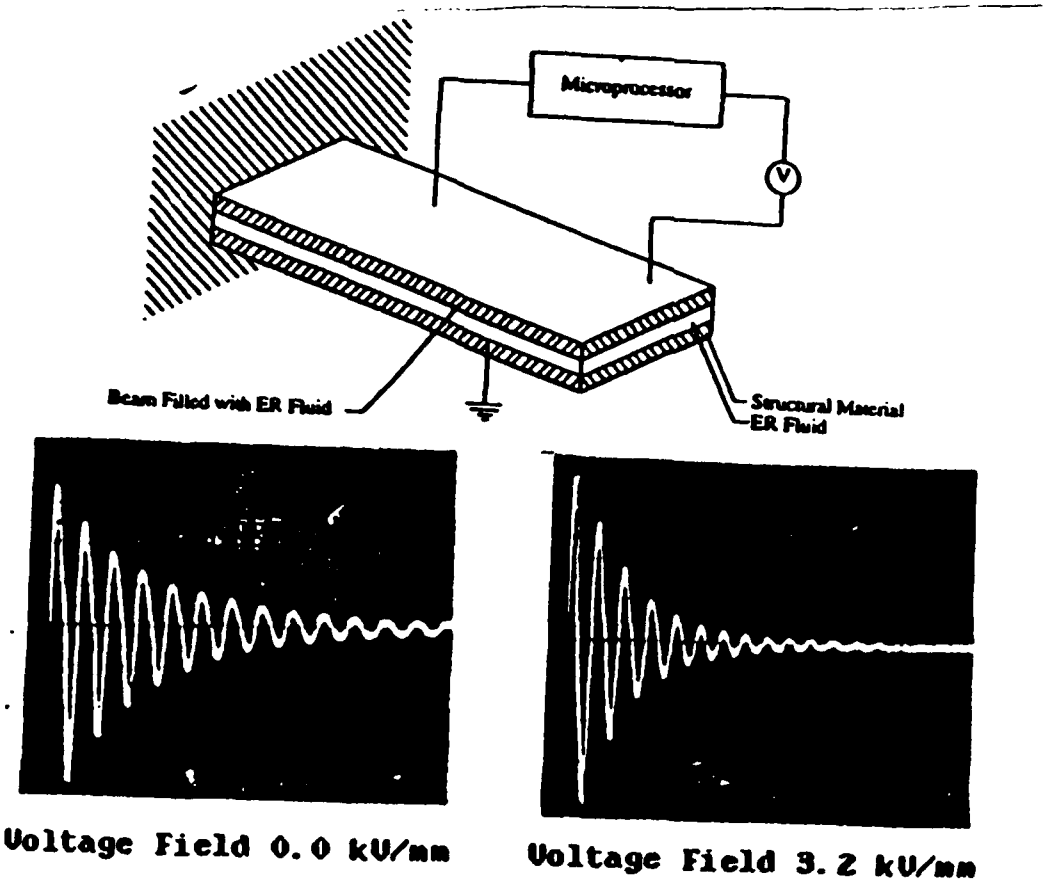

Figure 1: Electrorheological Fluid termed as 'smart' structural material. (Gandhi in J.O.M.)

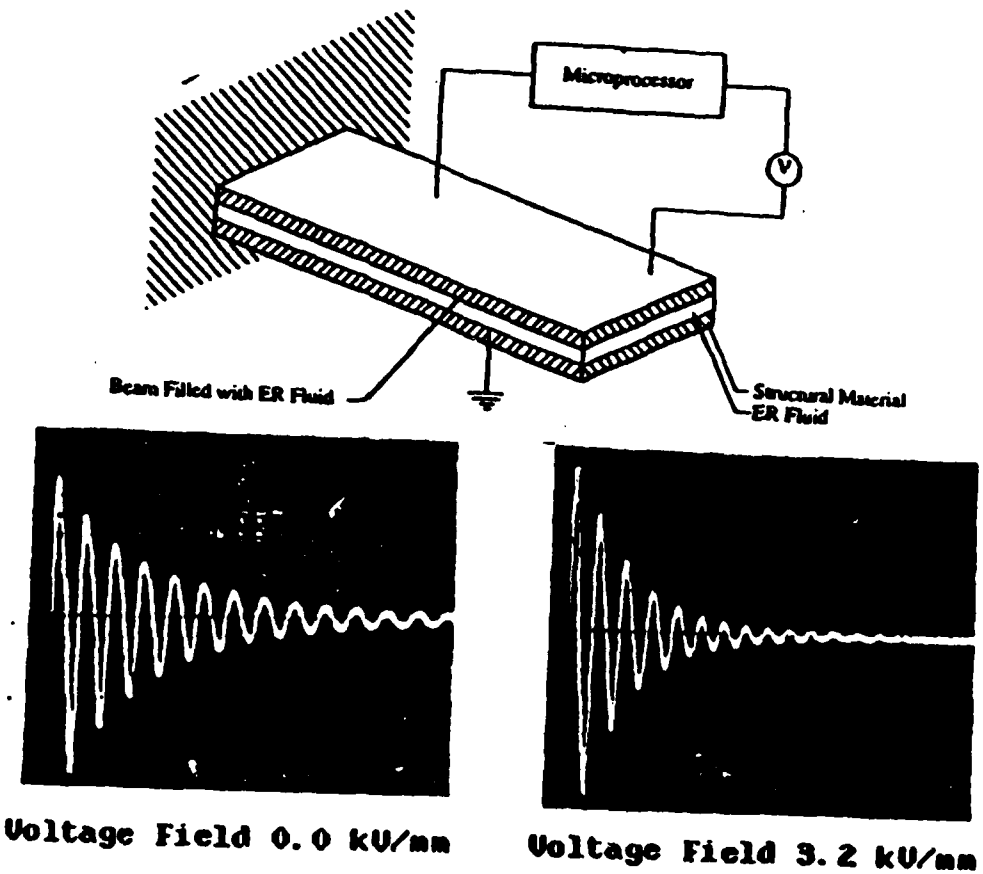

Figure 1: Electrorheological Fluid termed as 'smart' structural material. (Gandhi in J.O.M.)

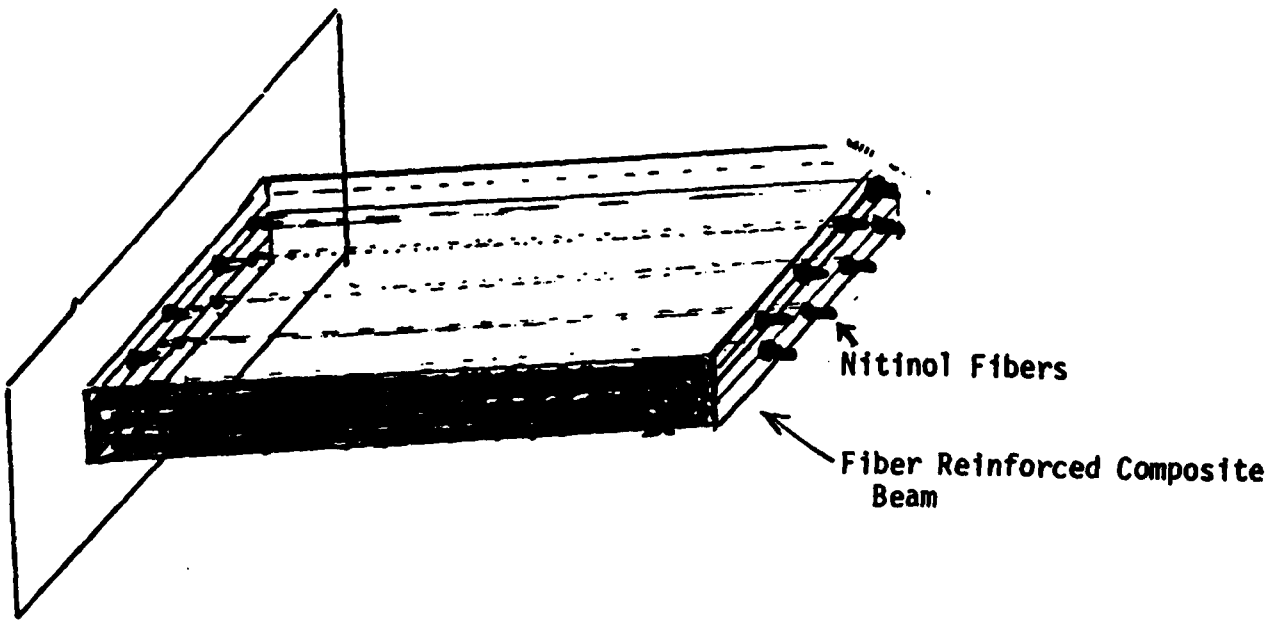

Figure 2: Novel 'Adaptive/Smart Composite Material' utilizing Nitinol Fibers. (Craig Rogers, VPI)

EMBEDDED SENSORS MAKE STRUCTURES "SMART"

Fiberoptic sensors and data links efficiently monitor the manufacture, health, and performance of various structures.

By Eric Udd

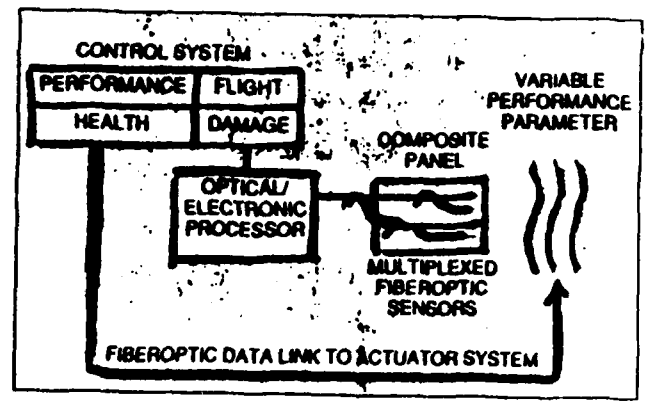

The diagram shows a basic smart-structure system. Sensors embedded in the panel monitor variations in the environment. The output from the sensors, multiplexed for transition to the preprocessors, goes to the control-systems computers.

Figure 3: 'Smart' structure with fiber-optic sensors.

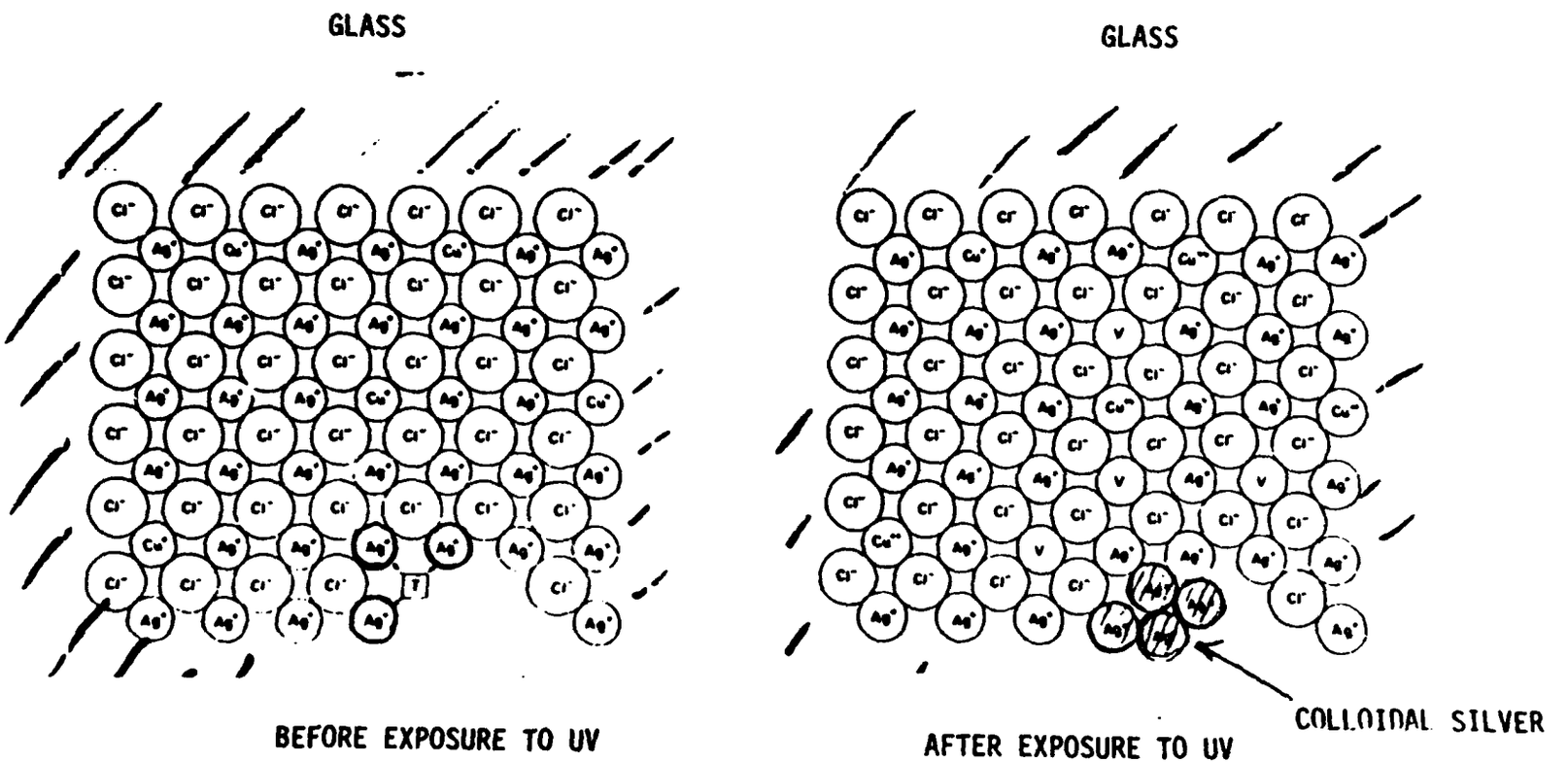

Figure 4 : Darkening Mechanism of photochromic glass

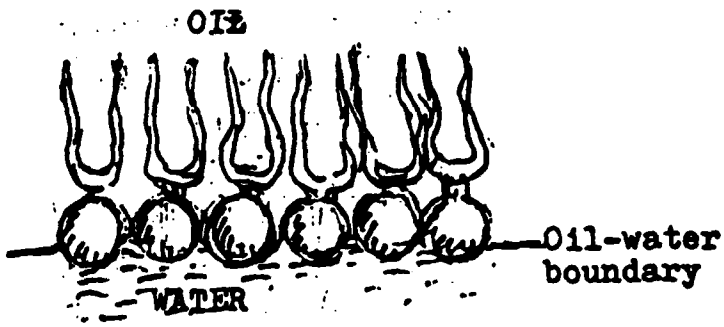

Figure 5(a)

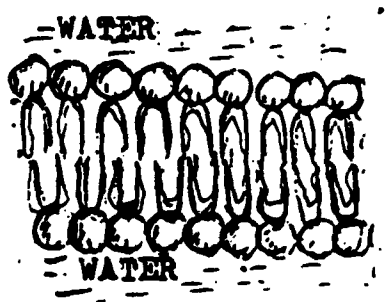

Figure 5(b)

Figure 5 : (a) Phospholipid molecules orient prefentially at oil-water boundary, forming a monomolecular film. (b) When immersed under water, phospholipids form extended layers exactly two molecules thick.

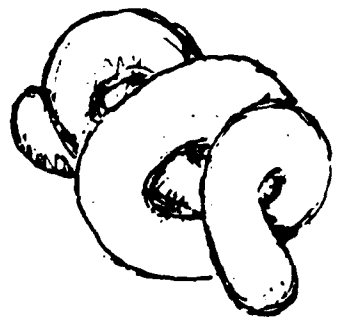

Figure 6 (a)

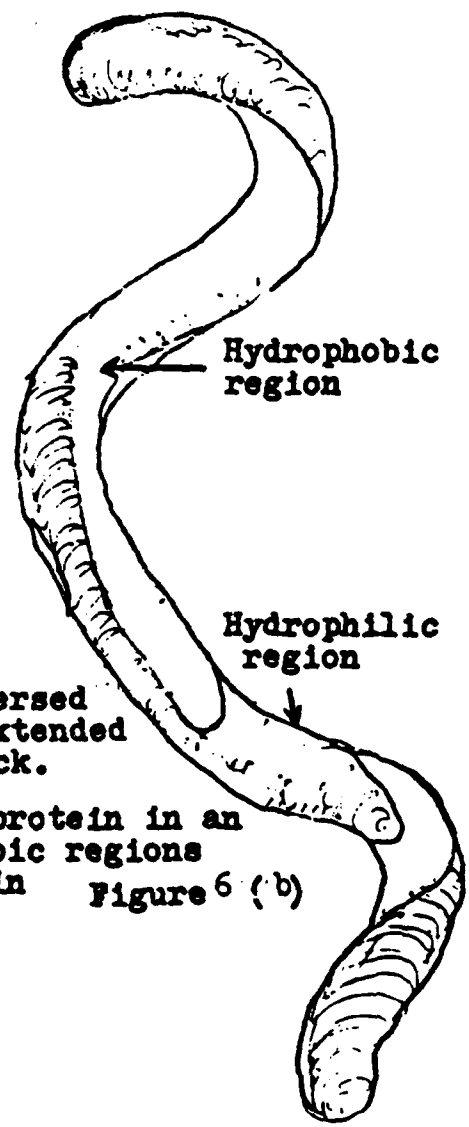

Figure 6 (b)

Figure 6 :A folding pattern of a protein in an aqueous medium in which hydrophobic regions face outward. (b) Unfolded protein chain.

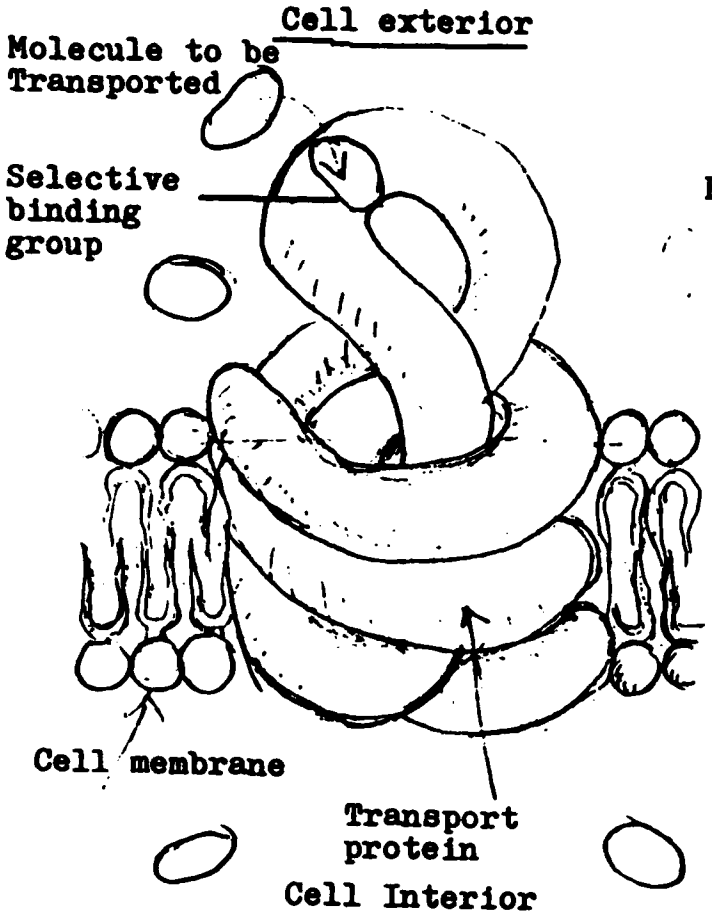

Figure 7(a): Configuration of the protein molecule at the time the molecule to be tranported from the cell exterior to the interior attaches on its surface.

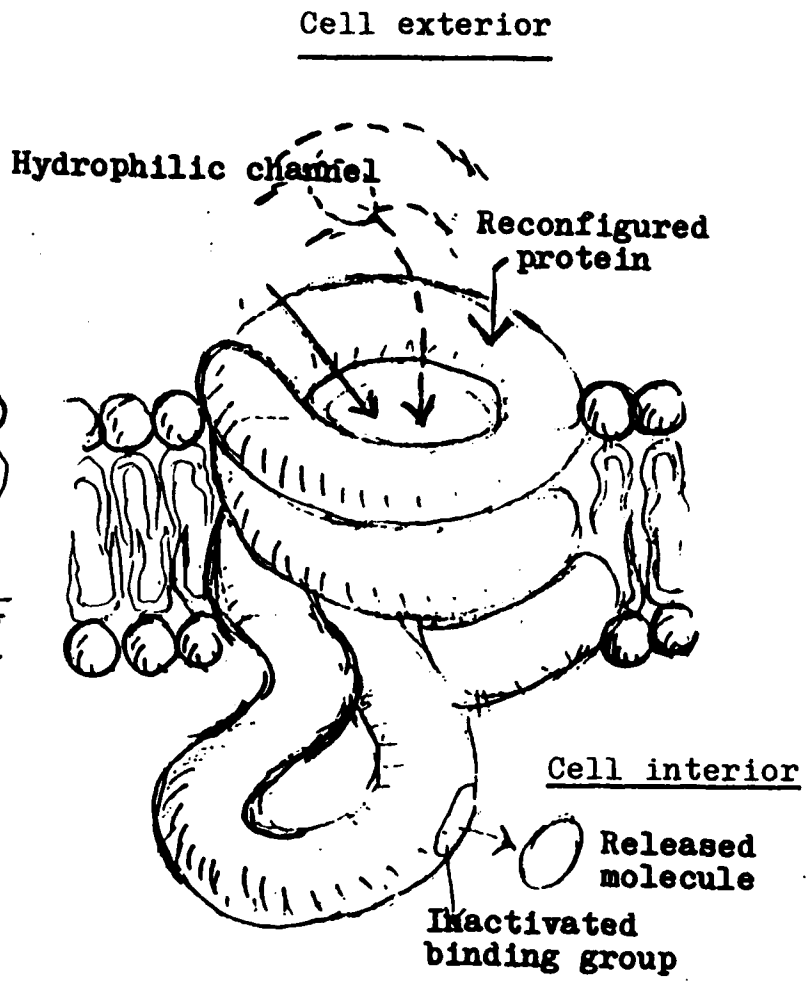

Figure 7(b): Showing the configuration of the protein molecule after the the molecule to be transported has passed through the hydrophilic channel. The protein chain will revert back to configuration as in (a) after the transported molecule detaches.

AN OVERVIEW OF SMART MATERIALS & STRUCTURES

Carol A. Jaeger
Craig A. Rogers

Smart Materials & Structures Laboratory
Department of Mechanical Engineering
Virginia Polytechnic Institute and State University
Blacksburg, Virginia 24061

Abstract

'Smart', 'Intelligent', 'Sense-able', and 'Adaptive' have all been used to described and/or classify materials and structures which contain their own sensors, actuators and computational/control capabilities and/or hardware. One of the definitions of Smart Materials that has been proposed may be materials that possess adaptive capabilities to external stimuli such as load or environment with inherent or integral intelligence. The control or intelligence of the material could perhaps be 'programmed' by material composition, processing, defect and microstructure, or conditioning to adapt in a controlled manner to various levels of stimulus. Smart structures may simply be constructed of Smart materials or may have dedicated or integrated actuators, sensors, and intelligence in a more discrete form. The early 'Smart Materials' contained for the most part embedded and/or distributed sensors for strain and temperature. However, the complexity and utility of smart materials has increased rapidly to the present time where major advancements seem to be occurring on a monthly basis in the areas of materials, actuators, sensors, and controls. Although smart materials and structure concepts may be applied to the design and implementation of buildings, dams, bridges, pipelines, ships, and ground-based vehicles, recent research efforts have been concentrated on potential aerospace applications in advanced aircraft, launch vehicles, and large space-based platforms. This paper will present a brief overview of the history of smart materials and structures and some of the diverse technologies that have contributed to this dynamic field.

Introduction

'Smart' is only one of the many adjectives that have been used to describe and/or classify materials and structures which contain their own sensors, actuators and computational/control capabilities and/or hardware. No true consensus has been reached concerning what categorizes a material or structure as 'smart,' 'intelligent,' 'sense-able' and/or 'adaptive.' The shape memory alloy is aptly named for it remembers a shape and can remake that shape with the addition of heat (an external stimuli). One is 'smart or 'adaptive' in the sense that it can respond or react to stimuli or input. An electro-rheological fluid is adaptive in that it can be either a solid or a liquid, as need be. The 'adaptiveness' of the materials could be in any one of many forms. For shape memory alloys it is added in the annealing process, for piezoelectric actuators and sensors it is achieved in the polarization of a polymer, in fiber optics it is a characteristic of the glass fibers, and in variable viscosity fluids it is found in the ability to react to temperature. Smart structures are more difficult to

categorize. They may be made of smart materials, they may have embedded or distributed actuators or sensors, and they may have dedicated intelligence in the form of microcomputers or microchips to perform dedicated control tasks. Most smart structures research has been done in the aerospace industry – in the control and adaptations of space structures. The stringent controls and demands of the space industry have created a need for controllable structures, where the structures demand built-in control. Now there is added interest in building structures that know how to damp out vibrations, control shapes and attitudes, adapt to severe or extreme environments, perform orbit transfers and stationkeeping maneuvers, reduce and process data, model systems, and reject noises and disturbance. These applications an controls can apply to bridges, dams and skyscrapers. The possibilities continue to grow. The structures vary, and the 'intelligence' is groomed to meet new needs. Smart structures and materials have a great range of possibilities, and definitions.

The definition of 'Smart Materials and Structures' has been a topic of discussion and controversy since the late 1970's when a 'Smart Material' simply consisted of optical fiber sensors embedded in a composite material. Some definitions state that the material or structure simply have integral (perhaps embedded) sensors, actuators, and 'intelligence.' The intelligence is most often dedicated (or integral) computation/control hardware. However, other definitions state that all sensing, actuating and intelligence capabilities be inherent to the material or structure.

The purpose of this paper is not to presume to set a hard and fast definition. The definitions have evolved with the technology and they will continue to evolve. Instead, a look at the technology will yield an understanding and insight into these definitions. The technology began with fiber optics, perhaps, that is where this paper should begin as well.

Review

Fiber optics can be traced back about 20 years when they entered the communications field, and revolutionized it as well. The success of fiber optics in communications can be attributed to the many advantages fiber optic communications have over the other technologies. Main (1985) enumerates the following advantages:

- freedom from influence by external electromagnetic disturbances
- immunity from 'crosstalk'
- signal flow is unidirectional if desired
- no problems with ground loops and offset dissimilar voltages where conductors meet
- very high data transmission rates – up to several GHz and more
- simple signal multiplexing by a variety of means
- reduced costs for equivalent transmission capabilities
- lower losses and less electrical power consumption
- a high degree of security against 'tapping' into signal trains
- greatly reduced electrical hazards and no problems with arcing or sparking
- highly resistant to adverse environmental conditions

•thinner, lighter, and more rugged than electrical cabling

Again, about ten years ago, they entered the sensor technology, and they are about to revolutionize it too. As a transmitter, the optic fiber was a marvel, therefore it seemed appropriate to use these fibers for the transmission of a sensor's signal -- for the same reasons. Fiber optics found a use in extrinsic sensors. Fiber optic sensors can be classified into one of two types. Extrinsic sensor are the sensors where the fiber itself operates as a light transmitter only, it performs none of the sensing. An example of an extrinsic fiber optic sensor would be a light beam where the fiber is used to detect the light from a source and what is being checked for is a break in the beam. Such a sensor is often used in robotics to sense the presence of a workpiece. An intrinsic utilizes some intrinsic property of the fiber to detect a phenomenon or to quantify a measurement. An example of this would be the detection of radiation from radiation-induced luminescence. A list of properties intrinsically measurable from fibers is given in Table 1.

Table 1. Fiber Optic Sensing (Main, 1985, Mann, 1985).

Variable	Methodology
Force	Induced birefringence
Pressure	Piezoelectric Effect
Bending	Piezoabsorption
Density Change	Luminescence
Electric Field	Electro-Optical Effect
Dielectric Polarization	Electrochromatism
Electric Current	Electroluminescence
Magnetic Field	Magneto-optical effect, Farraday Effect
Magnetic Polarization	Magnetoabsorption
Temperature	Thermal change in refractive index,absorptive properties, or fluorescence, thermoluminescence
Photoelectric Emission	Fiber defects leading to alteration in refractive index and absorptive properties
X-rays, Gamma rays	Radiation-induced luminescence
Changes in chemical composition	Changes in absorption and refractive index owing to chemical effects,chemoluminescence

The future of fiber optics is indeed exciting and more sophisticated sensors are sure to be developed. Examples of some sensing capabilities are shown in fig. 1 through fig. 3. The fiber optic sensors will make the present day sensors seem rather cumbersome and painstaking (Main, 1985;Mann, 1985).

What are fiber optics finding uses in now? The list is quite long, but a list of some applications and research should prove instructive of what the technology has to offer and can accomplish. In 1979 and 1980, R. O. Claus participated in the first documented smart structures experiments, conducted at NASA Langley, which demonstrated the use of embedded optical fiber sensors for the measurement of strain in low temperature composite materials. Since then R. O. Claus has worked on the development of optical fiber interferometric, blackbody, evanescent, modal domain and time domain sensors for the evaluation of composite cure, in-service

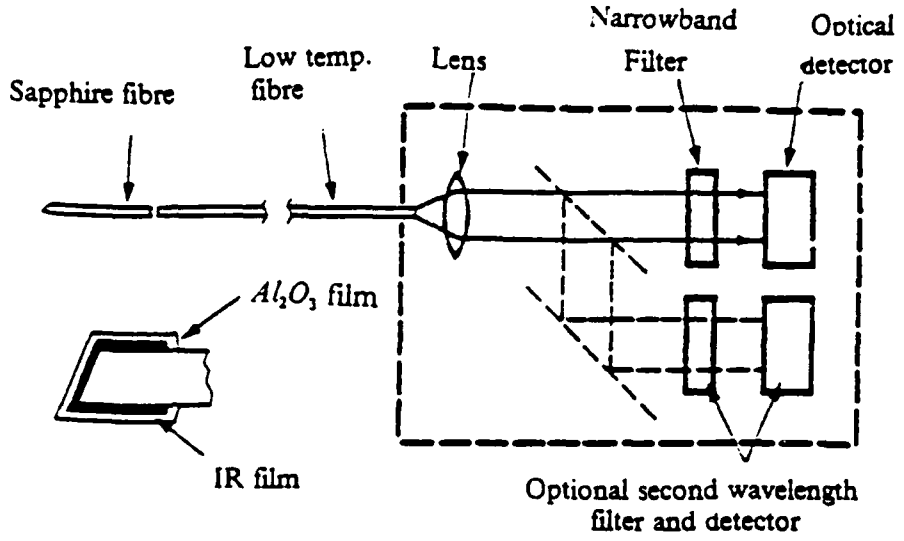

Figure 1. The Accufibre optical thermometer.

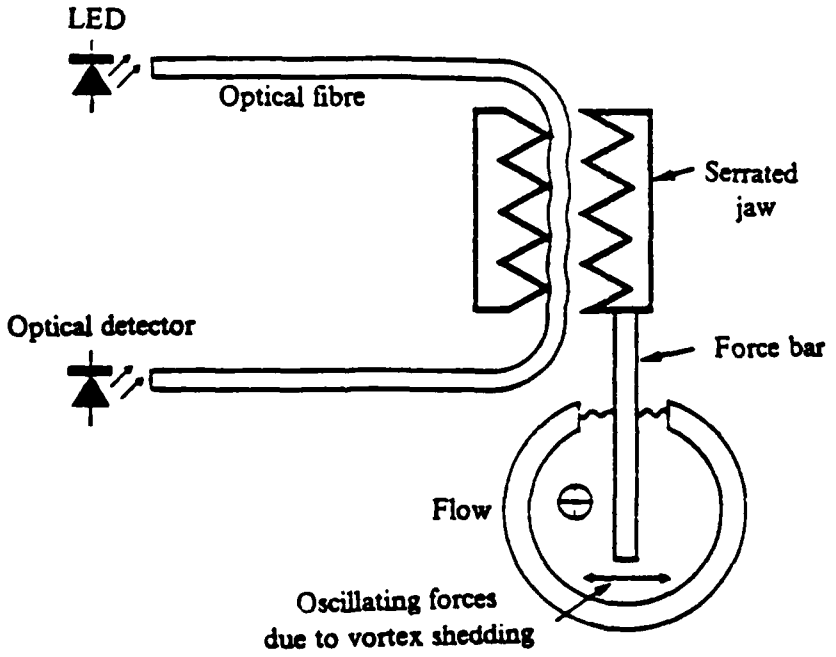

Figure 2. A vortex flowmeter detecting light intensity modulation caused by microbending losses.

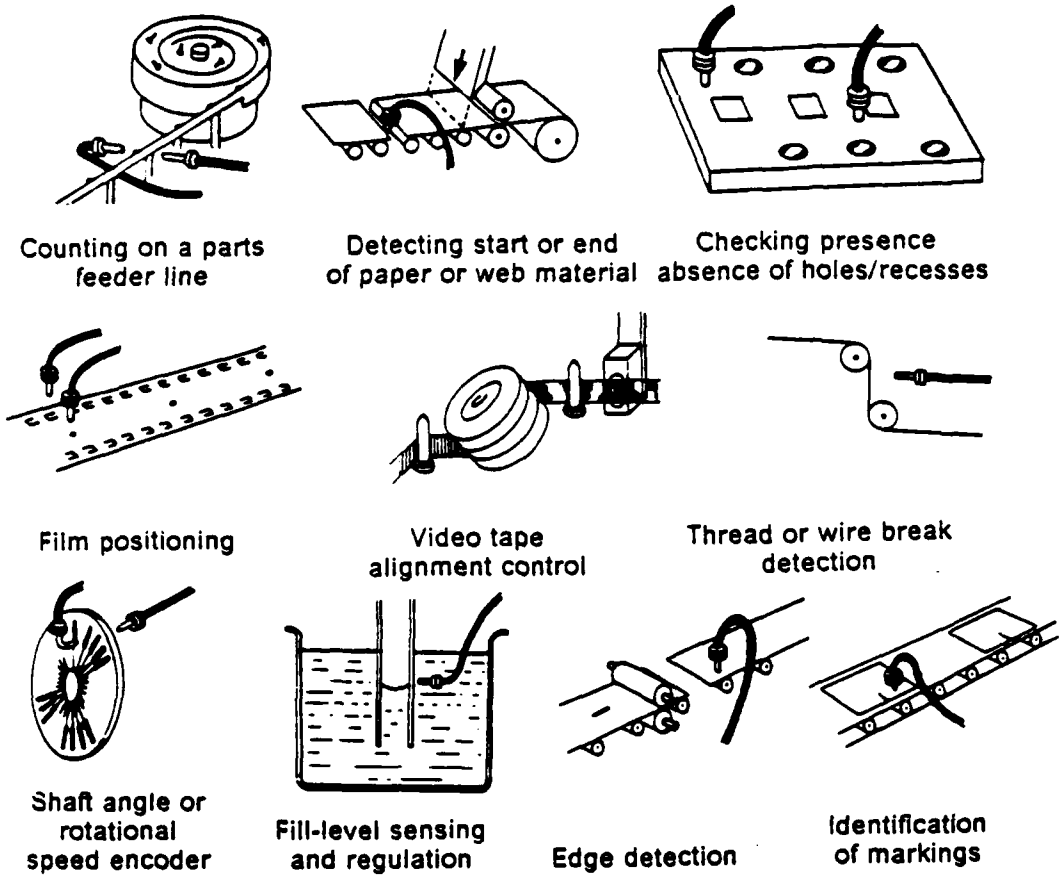

Figure 3. Various sensors using fiber optics.

structural component monitoring, nondestructive materials evaluation, and damage detection and evaluation. Claus, Jackson and May (1985) have developed an optical waveguide embedded in composites that can be used to determine the two dimensional dynamic strain by using the optical refractometry and signal processing of the fibers. Electro-absorption phenomenon has been used by Su (1985) to show magnetic field sensing capabilities. Martinelli (1984) describes a fiber optic interferometer that can measure deformations and vibrations. Baumbick (1985) notes the use of fiber optics and optical sensors in propulsion systems because of the severe environmental conditions present there. Bucholtz, Kersey and Dandridge (1986) describe a fiber optic accelerometer based on the displacement to strain conversion suitable for use at DC and low frequencies.

Two separate sources speak of the possibilities of fiber optic actuators(Collier, McGlade, and Stephens, 1985; Morikawa, 1985). Although a brand new technology, Collier, McGlade and Stephens claim that total electrical isolation can be achieved by complementing optical sensors with optical actuators -- the 'control-by-light' concept. Jones (1984) also proposes the 'control-by-light concept' in an article about fiber optics' role in industry and discusses the use of intensity, wavelength, or rate modulation for multimode technology and point-source sensors. Bogue (1984) addresses the use of fiber optics in accelerometers. Allan (1985) describes the development of one of the first tactile sensors at Tactile Robotics Systems using fiber optic bundles, and a fine resolution development of 1190 fibers at MIT Mechanical

Engineering department (Allan, 1985, Pennywitt, 1986). An improved design was investigated that uses the fibers as both emitter and receiver, allowing for greater resolution -- the resolution of the sensor is limited by the size of the fiber.

The advantage of fiber optics, as is fast becoming evident, is that 'the glass and silica fibers are themselves the basis for a broad range of sensors which utilize fiber properties to provide optoelectronic signals indicative of external parameters to be measured.'(Main, 1985). These intrinsic properties of the glass and the silica are what qualify fiber optics as smart materials. Fiber optics are capable of performing as the sensor as well as performing the transmission of the sensor's signal. They have a wide area of applications and will become more and more prevalent as new applications are developed and refined. These include measurements of temperature, pressures, displacement, magnetic fields, chemical composition, and others.

Other sensors have been incorporated into the 'smart' world, and one of the most prevalent is the piezoelectric. Piezoelectric sensors are built of materials that generate an electrical response to an applied force; that is their adaptive reaction to stimuli. Piezoelectric materials can be crystals and ceramics, but because they have a brittle nature the piezoelectric sensors are generally made of one of the family of polymers, polyvinyldene fluoride also known as PVDF or PVF_2. Because it is a polymer, it can be formed into very thin sheets and adhered to almost any surface. It outperforms many other sensors in its mechanical strength and its high sensitivity to pressure changes. Nevill and Patterson of the University of Florida have developed a piezoelectric tactile sensor that is able to recognize objects with about 100 percent accuracy, it is sensitive enough to distinguish the letters of the braille alphabet and different grades of sandpaper, showing great promise in exploratory sensing or object identification (Pennywitt, 1986). Researchers at the University of Pisa have been working on a skin-like sensor utilizing piezoelectric material. It basically replicates the temperature and pressure sensing capabilities of the human skin. In different modes of operation it can detect edges, corners, and geometric features, or it can distinguish between different grades of fabric (Allan, 1985,Pennywitt, 1986). Its construction can be seen in a schematic in fig. 4 (Allan, 1985). Nakamura et al propose a tactile sensor for robots in their paper using a ultra-thin film (200-300 μm) and back this with mathematical analysis and numerical simulation (Nakamura, Hanafusa, Ueno, 1985). It also exhibits what is called the pyroelectric effect in that it exhibits response to temperature changes as well; this can be an advantage or disadvantage contingent on the application. The polymer is made piezoelectric by polarizing it in either a uniaxial or biaxial film. The uniaxial film indicates stress in one direction by producing a voltage. Biaxial films indicate stress in one or two directions with voltage (Bailey and Hubbard, 1985).

Piezoelectric materials are very versatile in that they can also be used as actuators. Piezoelectric actuators are PVDF used in the reciprocating way of the sensors. By putting a voltage across the piezoelectric, the material creates a distributed force. Piezoelectric usage has increased in positioning applications because piezoelectric polymers generate little heat and can conserve energy as compared to their electromechanical counterparts. The piezoelectric actuator is a true distributed actuator and can be analyzed and controlled in distributed systems using distributed-parameter control theory. The high precision work is also prevalent in piezoelectric actuators. A printer head is position driven by the piezoelectric effect (Tanoshima, Araki, and Tsukada, 1984). Tojo and Sugihara (1985) have developed a turntable driven with the piezoelectric effect and exhibiting very high positioning accuracy – under 4.8×10^{-7} rad. Burke and Taft (1984) report the use of piezoelectric benders in an electrofluidic converter. Takahashi proposes two types of piezoelectric

actuators , one with two piezoelectric plates stuck together and the other where are number of plates are laminated together. These actuators can be driven with low power and can be mass produced (Takahashi, 1985). Bailey and Hubbard (1985) of MIT designed an active vibration damper using a piezoelectric actuator and distributed-parameter control theory.

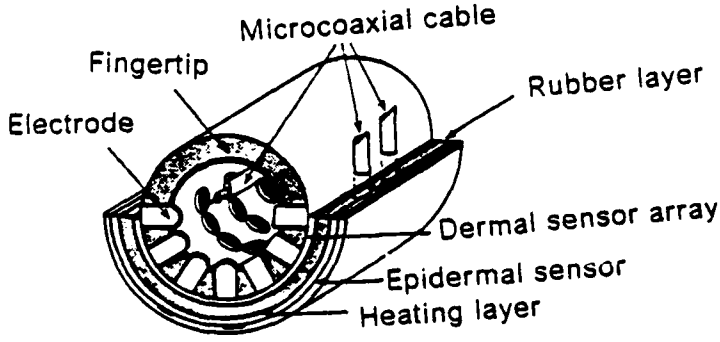

Figure 4. A portion of the University of Pisa robot finger.

The force – or strain – created in these piezoelectric actuators is proportional to the voltage or field put across the crystal. This simple relation makes for simplistic control algorithms and distributed analysis. The relationship is

$$\varepsilon_p(x,t) = V(x,t)\times(d_{31}/h_2)$$

where ε_p is the strain, V is the applied voltage, d is the appropriate piezoelectric constant and h is the thickness of the PVF $_2$ layer (Bailey and Hubbard, 1985). The equation is valid for both actuator and sensor applications. It is clear that piezoelectric crystal/polymers have a vast assortment of applications. They can be used both as actuators and sensors. Perhaps more important is that they are distributed devices, and can be readily used in control schemes for distributed systems.

Another distributed actuator is shape memory alloys. Shape memory alloys (SMA) devices convert the thermal energy of a compound into kinetic energy by the martensitic transformation. A SMA remembers the shape in which it was annealed, be that a straight or curved form. Upon heating it tries to remake that shape if possible, creating large and tapable forces in the process. There are a few alloys that exhibit the shape memory effect, but the most popular is the Nickel and Titanium (Ni-Ti or Nitinol) alloy. Shape memory alloys have been applied to a number of items including connectors and heat engines, but have usually found application in bang-bang type actuators. This has begun to change. Recently in Japan, SMAs have been developed into robot manipulators. The shape memory alloy has only recently begun to attract serious attention as an actuator. Most of the work presently being done seems to be occurring in Japan. Because of Japan's dominance in the SMA research and since little of that work has been documented in English, it is hard to know where the Japanese have taken the technology. The sampling available is sufficient to give an overview of the technology. Hashimoto, et al., (1985) show the use of SMAs in robotic actuators. Two types are discussed, biased and differential. Biasing uses a spring to obtain the bias force against the unidirectional force of the SMA. In the differential type, the spring is replaced with another SMA and the opposing forces control the actuation (Hashimoto, et al., 1985). Figure 5 shows

two configurations for SMA actuators. Yaeger (1984) has developed a one-pound three-quarter-inch-stroke linear actuator using a spring made of nitinol wire; the design includes prevention from ancillary jams. Miwa (1985) discusses the use of SMA actuator to sequential robotic control of multiple degree of freedom robots.

Rogers and Robertshaw have developed Nitinol into a new class of adaptive materials This class of adaptive materials utilize a shape-memory-alloy (Nitinol) in a laminated, fiber-reinforced composite. Adaptive materials using shape memory alloys are a relatively new class of materials that have the capability of changing their physical geometry, or of altering their physical properties. The basic concept behind the adaptive material developed at VPI&SU is that shape memory alloys are integrated in a bulk material (i.e., laminated fiber-reinforced composite) as an actuator for force, motion, and/or variable stiffness. Possible applications for this class of adaptive materials are: in structures that are part of long-duration, unattended space missions (for which the material must be able to compensate for damage by redistributing the load around failed portions of the structure); in active vibration control of large flexible structures, in active acoustic control for aircraft to reduce interior sound levels, and in robotic manipulators. A more detailed account of this technology will be presented by C. A. Rogers in companion paper published at these proceedings.

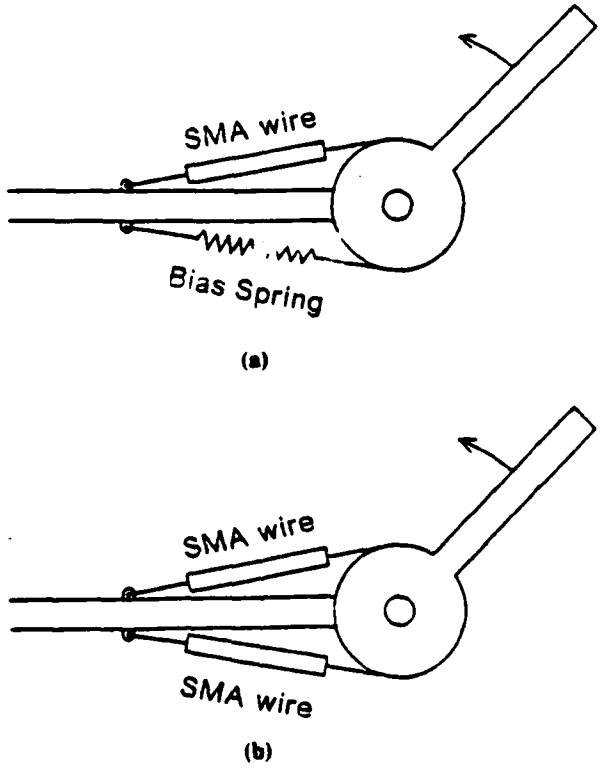

Figure 5. SMA actuators (a) the bias-type actuator (b) the differential-type actuator.

With advances in the control algorithms, biasing with springs or opposing SMA's, active cooling techniques, and the creation of SMA composites, the shape memory alloys have improved their range of applications and are becoming more reliable and promising actuators.

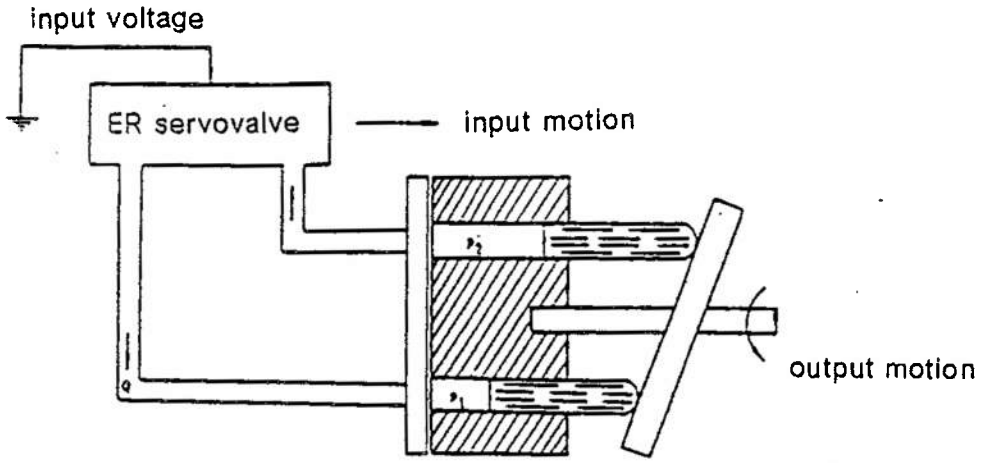

Figure 6. Schematic Diagram of a proposed Hydraulic Servomotor (Choi, Thompson, and Ghandl, 1987)

station keeping. Static shape distortion can be caused in a number of ways including incorrect deployment, and outside forces including gravity and temperature gradients (Weeks, 1984b).

Shape Control

Shape and attitude control are a paramount group of problems. Without this achievement the structure is ineffectual. If an antenna is not pointed to the right location its transmission is useless, and an optical reflector loses its integrity as its shape fails. Dynamic problems can contribute to these conditions with the system's low natural frequency, joint conditions, and normally low damping (Nurre, et al., 1984). Previously shape control was accomplished at the design stage by stiffening the structure and providing a separation between the natural frequencies of the structure and the control system bandwidth. Shape control problem is actually the dual problem of shape determination followed by shape control. The method for determining and controlling the shape of continuous structures by means of discrete of point wise observation and control devices is required. This is referred to as the continuous- discrete nature of the problem. Static shape control is generally accomplished after the damping of dynamic vibration (Weeks, 1984a). Weeks uses the green function to convert boundary value problems into integral equations for shape determination of the continuous-discrete mathematics. Static shape control and determination algorithms are illustrated on a space antenna and simple beam (Weeks, 1984a,Weeks, 1984b).

Damping

Damping vibrations in space structures is critical to maintaining the integrity of any structure, space structures included. McClamroch develops a simple form of hierarchical control for structures consisting of interconnected flexible members where control forces are generated by electromechanical member dampers. The control scheme consisting of feedback of structural signals and compensation for the member dampers (McClamroch, 1985). Juang present a technique for applying expressions of the optimal tuning law for an elastic system including a truss beam (Juang, 1984). Soni et al deal with methods of enhancing passive damping of spacecraft structures. First they examine various methods for synthesis of damping and a improved method was proposed. Viscoelastic passive damping was

incorporated into the design of joints and honeycombs of flexible space structures, verification was noted (Soni, Kluesener, and Drake, 1985). Ryaciotaki-Broussalis and Broussalis consider flexible members in decentralized control using Lyapunov functions. Controlled modes as well as residual modes must be considered in order to obtain sufficient conditions for exponential stability (Ryaciotaki-Broussalis and Broussalis, 1985). Kissel and Hegg apply linear-quadratic-Guassian/loop transfer recovery techniques to the active control of flexible spaceborne optical support structure. Closed-loop stability in the presence of 150 elastic modes is maintained (Kissel and Hegg, 1986). Miller discusses a computational control method discussed in the context of vibration suppression of large flexible space structures. Emphasis is given in the proper specification of weighting matrices is the design and determination of the combined optimization of the structural and control design. Numerical simulations using finite element analysis for two and three bay trusses are given in support. This specifically deals with the numerical and computational questions of analysis (Miller, Venkayya, and Tischler, 1985). Sundararajan and Montgomery of NASA Langley propose an indirect adaptive control scheme for the control of flexible structures using least squares lattice filters for on-line identification of the number of modes, mode shapes, and modal amplitudes. The control law developed is based on modal pole placement. Successful implementation is demonstrated using the simulations for the apparatus at NASA Langley Research Center (Sundarajan and Montgomery, 1984). Plant excitation is another problem because its low-frequency modes and low damping limit vibrational attenuation (Nurre, et al., 1984). Rajaram and Junkins present novel identification schemes to determine model parameters of vibrating structures. Three methods are discussed, one using nonresonant harmonic excitation, another method is a time domain identification using transient response, and finally a unique method using both free and forced response methods (Raharam and Junkins, 1985). Joshi speaks of the robustness of velocity feedback controllers and proves that the closed-loop system using such controllers is asymptotically stable (Joshi, 1985).

Modelling

Large space structures are those structures which are designed exclusively for the near zero g environment of space and are large by some measure. The difficulties of large space structures are many. the design of a control system with natural frequencies above several major structural resonant frequencies must be achieved to ensure that the design is robust enough to accommodate tolerances in the structural model. An accurate model must be established usually implies a high order model that reflects the many degrees of freedom of the structure processed to a workable size through some means of model reduction. Numerical algorithms must be available or developed to manipulate these models. (Nurre, et al., 1984). Hale and Lisowski consider optimization based on a reduced order model. They find optimization based on a reduced order model can yield an accurate numerical solution to the integrated design problem (Hale and Lisowski, 1984). Silverberg and Meirovitch propose a compromise between coupled control and independent modal-space control, a block-independent control method is proposed. The method is designed to combine the computational advantages of independent modal-space control with a reduced number of actuators for coupled control. The reduction is achieved, but the number of actuators is not significantly lower (Silverberg and Meirovitch, 1985). Goh and Caughey apply the concept of stiffness modification to the vibration suppression of large space structures. They guarantee global stability by virtue of the positive definite rate of energy decay (Goh and Caughey, 1985).

Control Schemes

Goh and Caughey consider position feedback in addressing stability problems of finite actuator dynamics in the collocated control of large space structures. These authors contend that if with the addition of the complicated 'tuning filters' restrictive sufficient conditions can be derived like those with velocity feedback that can guarantee stability for all modes, including the uncontrolled and unmodelled modes. This technique is much less sensitive to to the uncertain natural damping and model structure of the system than the velocity feedback counterpart. Numerical simulations of a simply supported shear beam are used as verification (Goh and Caughey, 1983). With collocation of sensors and actuators good stable control of flexible structures is easy to achieve. Without it it is very difficult, particularly if structural damping is very low and spacecraft stiffness and inertial values are changing as they often are. A crucial problem for some flexible spacecraft is that the location of points at extremities must often be controlled, sometimes to very high precision as with space antennas. Too often this must be done by controlling some other section of the structure thus the noncollocated control problem. Cannon and Rosenthal contend that there are noncollocated configurations where there are no practical alternatives to adaptive control. Systems with sensor actuator noncollocation can exhibit pole zero flipping when parameters vary (Greene, 1985). An adaptive control technique deemed suitable for large structural systems is the direct multivariable model reference adaptive control, developed by Sobel et al and extended by Bar-Kana and Kaufman with the conditions that the system used velocity feedback and sensors and actuators are collocated (Sobel, Kaufman, and Mabius, 1982,Bar-Kana and Kaufman, 1983). Bar-Kana applied the control algorithm to systems with non collocated sensors and actuators and with position and velocity control. Simulation results show satisfactory behavior (Bar-Kana and Kaufman, 1983). A flexible structure can be simply categorized as one that cannot be accurately described with rigid body formulations. Accurate , here, is a relative term, and must be governed by the application. Here are some of the problems inherent with flexible bodies. rigid body mode cannot be controlled without affecting flexible modes. disturbances activate flexible modes. damping factors for flexible modes are usually quite low. in flexible systems points exist where no modal motion can be detected and no modal motion can be produced. the presence of both control and observer system spillover can easily cause closed-loop instability where spillover is an excitement of higher states that undesirable for control and the presence of higher states in the observer control. damping factors may not be constant modal shapes and frequency can vary with the system configuration (Weeks, 1984a). Balas has determined bounds on controller interaction with unmodelled part of structures that can be used to guarantee the success of linear control even in the presence of nonlinear interactions. This is good for those cases when the spillover from the interaction of the controller and the unmodelled parts of distributed parameter systems. Limitations of these theorems are given (Balas, 1985). Buchanan et al discuss the on-orbit dynamic testing of a large solar array as well as the design of a proposed experiment to demonstrate control technique applicable to large systems. Results show that the amount of control authority is dependent on many factors including the placement and slope of sensors and effectors. (Buchanan, Schock, and Waites, 1984). Avramovic et al develop a control method for flexible structures using a frequency domain algorithm to compute optimal gains and requiring spectral factorization as a crucial step. This system was applied to control a simply supported Euler beam (Avcamovic, Barkakati, and Blankenship,1983).

Space Applications

Schaechter and Eldred have demonstrated active shape control, active dynamic control, adaptive control of flexible structures. Excellent results were obtained in shape, dynamic and adaptive control (Schaechter and Eldred, 1984). Wie and Plescia present a reaction jet attitude control system for a spacecraft having large flexible solar arrays since these interact strongly with pulse width and pulse-frequency modulators. The stability margin and performance are verified from the three axis nonlinear simulations (Wie and Plescia, 1983). Robertshaw et al., have developed a variable geometry truss for use in control of broadband vibrations, both steady-state and transient, of the truss and its attachments. The truss is controlled via motor driven variable length links. Experimental control data and a schematic of the truss can be found in fig. 7 and fig. 8 (Robertshaw, et al., 1988). Clark, Robertshaw, and Warrington compare the effectiveness of four actuators in controlling the planar vibrations of a truss-beam. These actuators are the proof-mass actuator, the reaction wheel actuator, the planar truss actuator, and the planar truss proof-mass actuator, see fig. 9. For the Tip deflection comparison of these actuators see fig. 10 (Clark, Robertshaw, and Warrington, 1988).

Conclusions

Smart materials and structures have grown in scope the last few decades from including only fiber optic sensors to variable geometry trusses and new material systems such as shape memory alloy reinforced composites. Despite the recent appearance of the terms 'smart,' adaptive,' 'sense-able,'and 'intelligent,' adaptive materials have existed for many years; but have only recently begun being used in a wide variety of applications. The possibilities continue to grow. Smart materials and structures have found applications in varied areas, and as the technology advances and refines itself, it may find continuing uses and applications. The adaptive materials are adapting themeselves to meet the needs of the technology that birthed them.

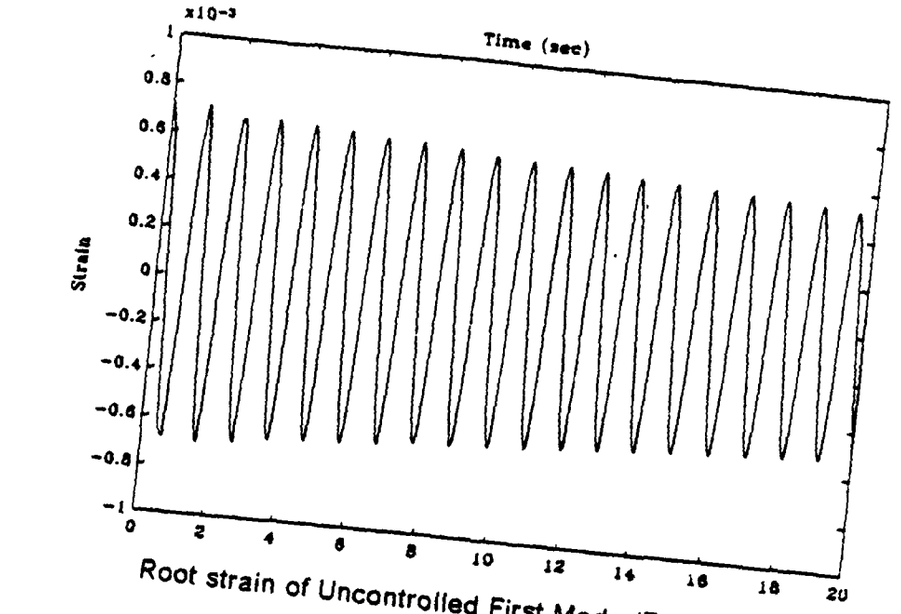

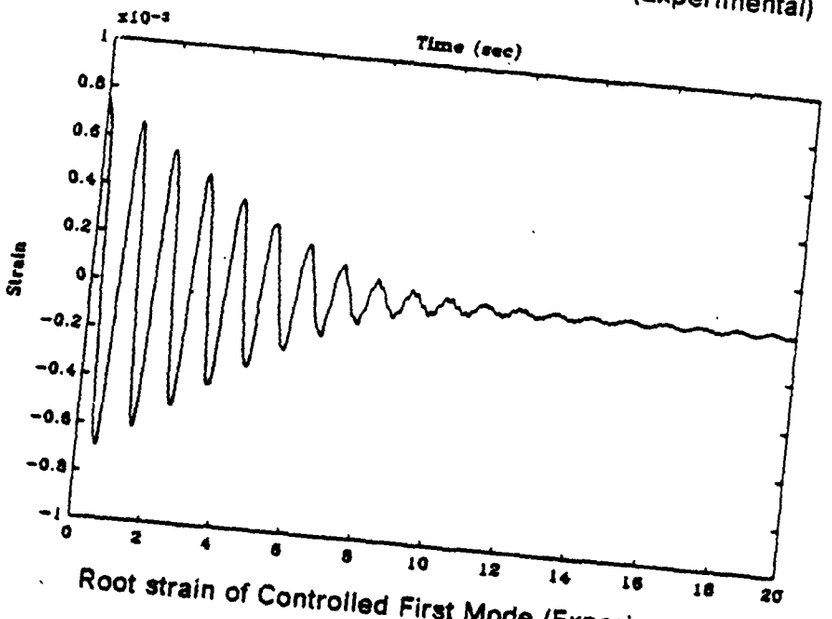

Figure 7. Strain vs. time for (a) uncontrolled and (b) controlled 2 bay truss.

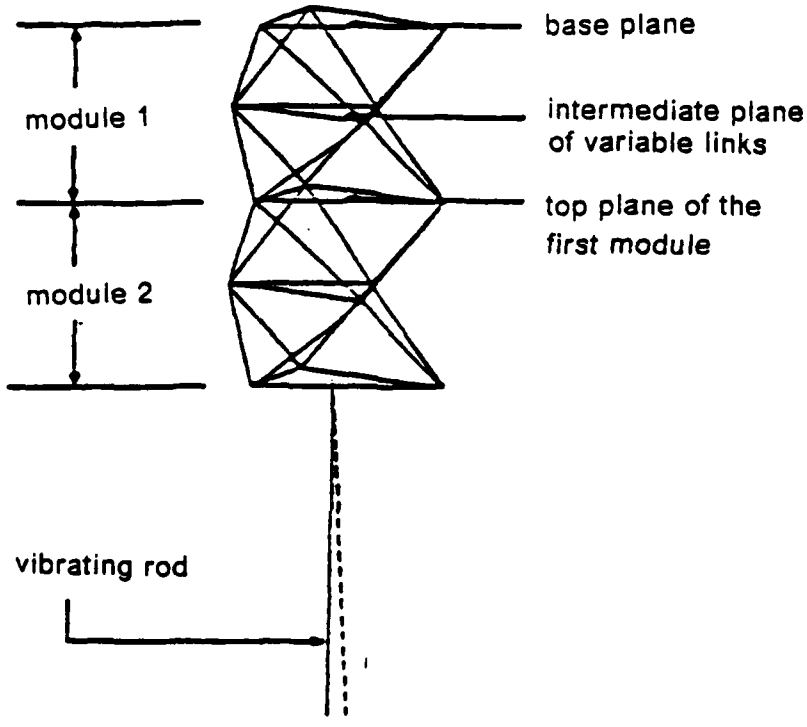

Figure 8. Active Spatial Truss Actuator Schematic.

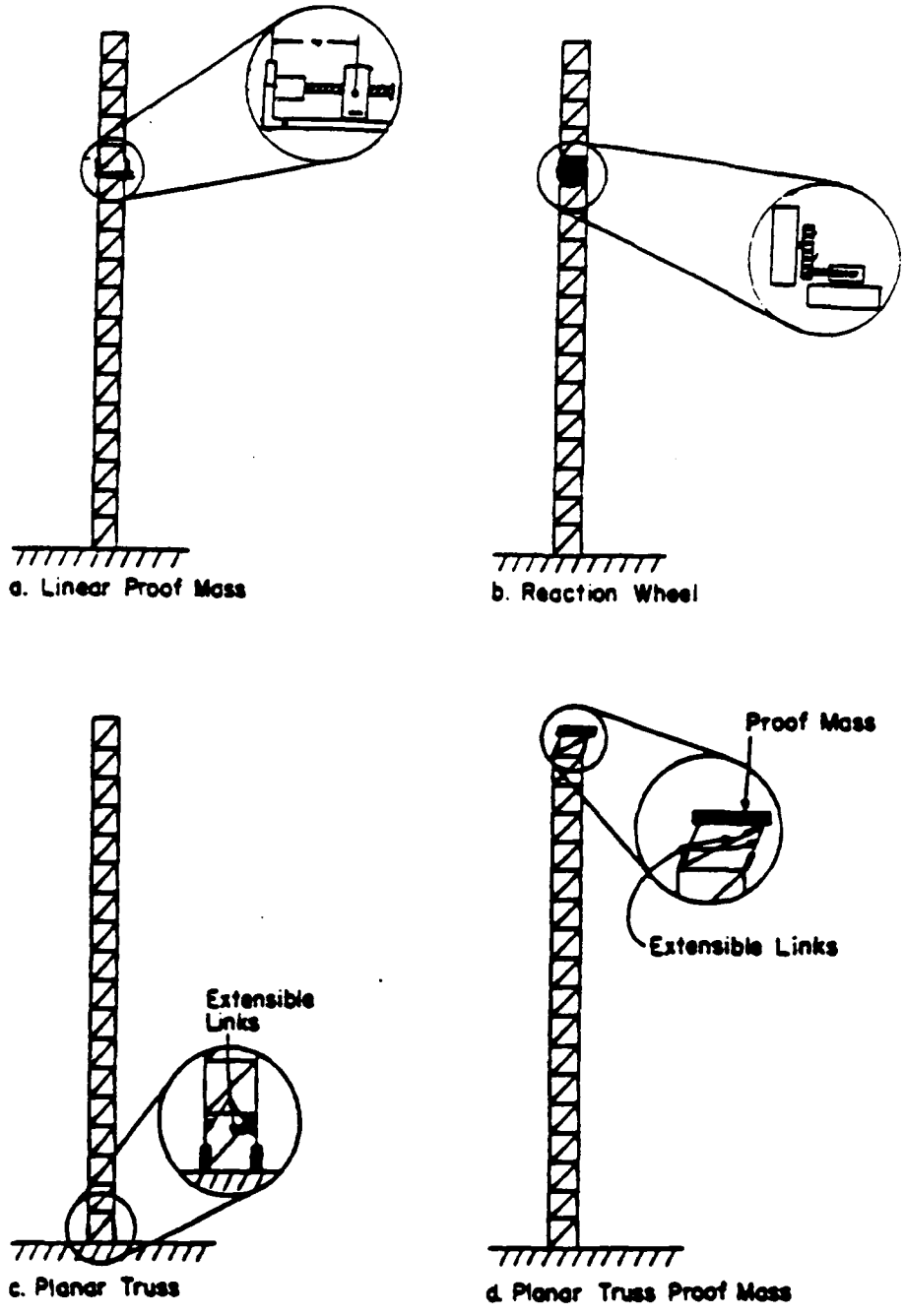

Figure 9. Actuators

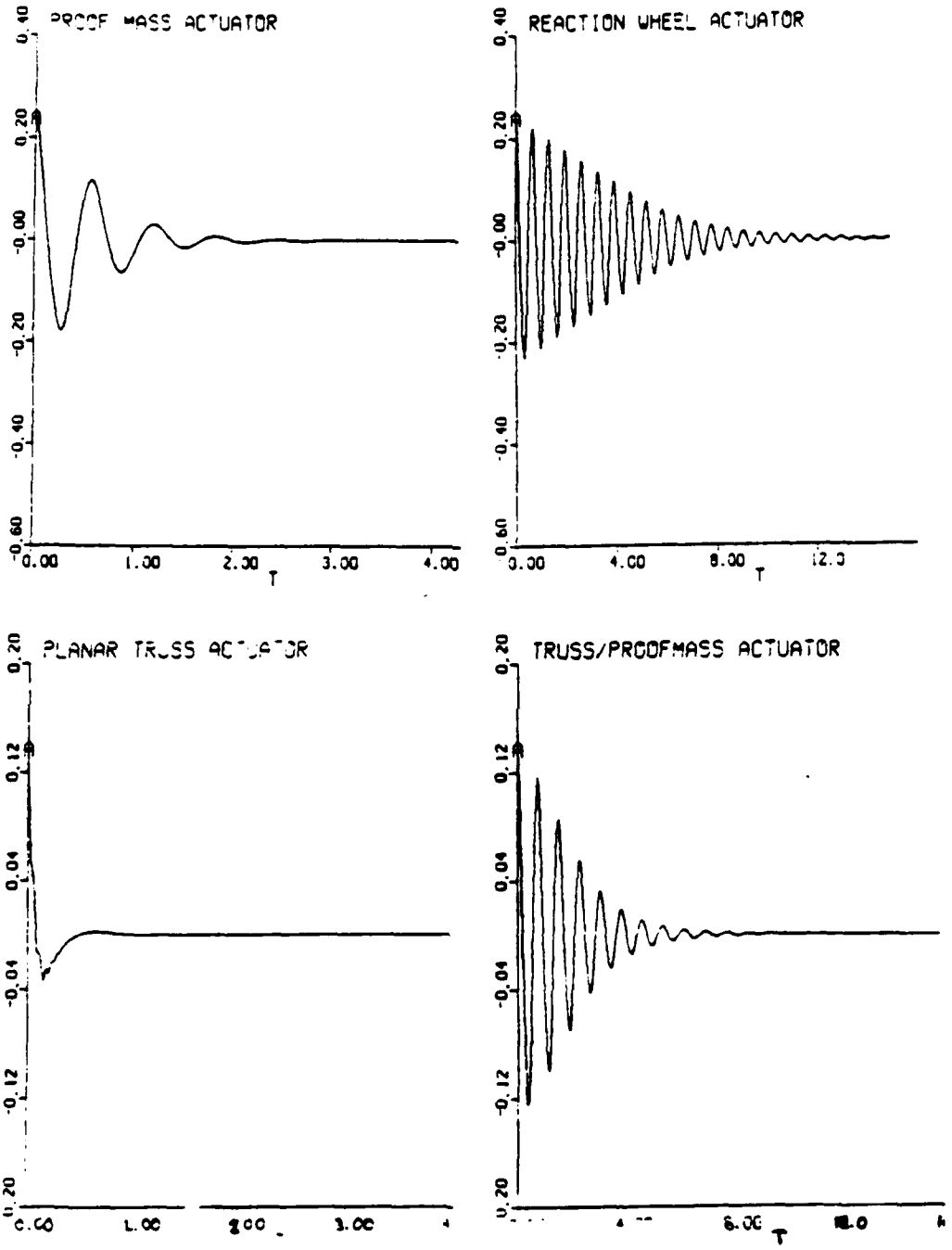

Figure 10. Tip deflection comparison.

References

Allan, R. "Nonvision sensors," **Electronic Design.** (27 June 1985) vol. 33, no. 15, p.103-15.

Avramovic, B., N. Barkakati, and G. L. Blankenship. "Application of a spectral factorization approach to the control of flexible structures," **Proceedings of the 23rd IEEE Conference on Decision and Control.** Las Vegas, NV, vol. 3, (Dec 1984) p.1695-6.

Bailey, T., and J. E. Hubbard. "Distributed piezoelectric-polymer active vibration control of a cantilever beam," **Journal of Guidance, Control, and Dynamics.** vol. 8, no. 5, (Sept.-Oct., 1985) p. 605-11.

Balas, M. J. "Distributed parameter control of nonlinear flexible structures with linear finite-dimensional controllers," **Journal of Mathematical Analysis and Applications.** vol. 108, (1985), p. 528-45.

Bar-Kana, I. and H. Kaufman. "Model reference adaptive control for time-variable input commands," **Proceedings of the 1982 Conference on Information Sciences, and Systems.** Princeton, NJ, 1982, p.208-211.

Bar-Kana I. and H. Kaufman. "Some applications of direct adaptive control to large structural systems," **Journal of Guidance, Control, & Dynamics.** vol. 7, no. 6, (Nov.-Dec., 1984) p.717-24.

Baumbick, R. J. "Fiber optics for propulsion control systems," **Transactions of ASME Journal of Engines,Gas Turbines and Power.** vol. 107, no. 4, p.851-5 (Oct. 1985).

Bogue, R. "Developing Science of Accelerometers," **Control and Instrumentation (GB).** (Oct 1984) ,vol. 16, no. 10, p.69, 71.

Buchanan, H. J., R. W. Schock, and H. B. Waites. "An on-orbit experiment for dynamics and control of large structures," **Journal of Guidance, Control, & Dynamics.** vol. 7, no. 5, Sept-Oct, 1984. p.554-62.

Bucholtz, F., A.D. Kersey, A. Dandridge. "DC fibre optic acceleromter with sub-μg sensitivity," **Electronic Letter (GB).** vol 22, no.9, p. 451-3 (24 April 1986).

Burke, T. S., C. K. Taft. **Proceedings of the 1984 American Control Conference, San Diego, Calif.** 6-8 June 1984, vol. 2. p.1026-31.

Cannon, R. H. Jr., and D. E. Rosenthal. "Experiments in control of flexible structures with noncollocated sensors and actuators," **Journal of Guidance, Control, & Dynamics.** vol. 7, no. 5, (Sept.-Oct., 1984) p. 546-53.

Choi, S. B., B. S. Thompson, and M. V. Gandhi. "Electro-rheological fluids technology stimulates a new generation of robotic and machine systems," **Proceedings of the Oklahoma State University's Applied Mechanisms Conference.** vol. 1, 6-9 Dec, 1987.

Clark, W. W., H. H. Robertshaw, and T. J. Warrington. "A planar comparison of actuators for vibration control of flexible structures," 1988.

Claus, R. O., B. S. Jackson, R. G. May. "Nondestructive evaluation of composites by optical time domain reflectometry in embedded optical fibers," **Conference Proceedings IEEE SOUTHEASTCON '85,** Raleigh, NC, USA, 31 March - 3 April 1985 (New York, USA IEEE 1985), p.241-5.

Collier, M. J., S. M. McGlade P. E. Stephens. "The optical actuation of a process control valve," **Automation and Control (New Zealand).** (June 1985) vol. 15, no.5, p. 52-3, 56-7.

"Damping synthesis and damped design for flexible spacecraft and structures," **Computers and Structures** vol. 20, no. 1-3, (1985), p. 563-74.

Goh, C. J. and T. K. Caughey. "On the stability problem caused by finite actuator dynamics in the collocated control of large space structures," **International Journal of Control** vol. 41, no. 3, (1985), p. 787-802.

Goh, C. J. and T. K. Caughey "A quasi-linear vibration suppression technique for large space structures via stiffness modification," **International Journal of Control** vol. 41, no. 3, (1985), p. 803-12.

Greene. M. "Control of flexible bodies: new challenges in control engineering," **Proceedings of the Seventeenth Southeastern Symposium on System Theory.** Auburn, Al., 24-26 March 1985 p. 89-92.

Hale, A. L. and R. J. Lisowski. "Reduced-order modeling applied to optimal design of maneuvering flexible structures," **Proceedings of the 1985 American Control Conference.** San Diego, CA, 6-8 June 1984, vol. 3, p.1685-90.

Hashimoto, et al. "Application of shape memory alloys to robotic actuators," **Journal of Robotic Systems**. vol. 2, no. 1, (Spring, 1985) p. 3-25.

Jones, B. E. **Electrotechnology (GB).** (Oct. 1984) vol. 12, no.4, p.n148-5.

Joshi, S. M. "Robustness of velocity feedback controllers for flexible spacecraft," **IEEE Transactions of Aerospace and Electronics Systems.** vol. AES-21, no. 1, (Jan 1985), p. 2-7.

Juang, J. "Optimal Design of a passive vibration absorber for a truss beam," **Journal of Guidance, Control, & Dynamics.** vol. 7, no. 6, (Nov-Dec, 1984) p. 733-9.

Kissel, G. J., and D. R. Hegg. "Stability enhancement of flexible space structure control," **Proceeding of the 1985 American Control Conference.** 19-21 June 1985, p. 1194-202.

Main, R. P. "Fibre optic sensors – future light," **Sensor Review, (GB).** vol. 5, no. 3, (July 1985) p.133-9.

Mann, R. "So what future do you see in fibre optics ? " **Process Engineering (GB)** vol. 66, no. 6, (June, 1985) p.79-81.

Martinelli, M. "Fibre optic sensors," **Elettron Oggi. (Italy)** no.4, (April 1984) p.115-16, 118, 120, 122, 124.

McClamroch, N. H. "Vibration control of flexible structures using member dampers," **Proceedings of the 24th Conference on Decision and Control.** 11-13 Dec. 1985, Ft. Lauderdale, FL, vol. 2, p. 936 - 9.

Miller. D. F., V. B. Venkayya, and V. A. Tischler. "Integration of structures and controls - some computational issues," **Proceedings of the 24th Conference on Decision and Control.** Fort Lauderdale, Florida, (Dec 1985) p.924-31.

Miwa, Y. "Shape memory alloy application for sequential operation control," **System and Control (Japan).** vol. 29, no. 5, (May 1985). p. 303-10.

Morikawa, T. "Optical actuators," **J. Soc. Instrumentation and Control Engineering (Japan).** (Sept.1985) vol. 24, no.9, p.827-31.

Nakamura, Y., H. Hanafusa, N. Ueno. "A piezoelectric film sensor with uniformly expanded surface to detect tactile information for robotic end-effectors," **Proceedings of the '85 International Conference on Advanced Robotics.** Tokyo, Japan, 9-10 Sept. 1985, p.137-44.

Nurre, G. S. et al. "Dynamics and control of large space structures," **Journal of Guidance, Control, & Dynamics.** vol. 7, no. 5, (Sept.-Oct., 1984) p.514-26.

Pennywitt, K. E. "Robotic Tactile Sensing," **Byte.** (Jan. 1986) vol.11, no.1, p.177-200.

Rajaram, S. and Junkins, J. L. "Identification of vibrating structures," **Journal of Guidance, Control, & Dynamics.** vol. 8, no. 4, (July-August, 1985) p. 463-70.

Robertshaw, H. H. et al., "Dynamics and control of a spatial active truss actuator," 1988.

Rogers, C. A. and H. H. Robertshaw. "Investigation of processing techniques for adaptive materials utilizing shape memory alloys," 1988.

Ryaciotaki-Broussalis, H. A., and Broussalis, D. "Stable decentralized control of flexible space structures," **Conference Record Eighteenth Asimolar Conference on Circuits, Systems and Computers.** Pacific Grove California, 5-7 Nov. 1984, p.293-5.

Schaechter D. B. and Eldred, D. B. "Experimental Demonstration of the control of flexible structures," **Journal of Guidance, Control, & Dynamics.** vol.7, no. 5, (Sept-Oct, 1984) p.527-34.

Silverberg, L. M. and L. Mierovitch. "Block-independent control of distributed structures," **Optimal Control Applications and Methods.** vol. 6, (1985), p.281-9.

Sobel, K., H. Kaufman, and L. Mabius. "Implicit adaptive control for a class of MIMO systems," **IEEE Transactions on Aerospace and Electronic Systems** no. 5, Sept. 1982, p.576-90.

Su, S. F. "Fiber-optic electric field sensors utilizing electro-absorption," **Conference Proceedings IEEE SOUTHEASTCON '85,** Raleigh, NC, USA, 31 March - 3 April 1985 (New York, USA IEEE 1985), p.241-5.

Sundararajan, N. and R. C. Montgomery. "Adaptive control of a flexible bean using least square lattice filters," **IEEE Transactions on Aerospace and Electronic Systems.** vol. AES-20, no.5, ,Sept 1984). p. 541-6.

Takahashi, S. "Piezoelectric ceramic actuator and it applications," **Oyo Buturi (Japan).** vol. 54, no. 6, p.587-8 (June 1985). In Japanese.

Tanoshima, K., T. Araki, and M. Tsukada. "Vibration analysis of piezoelectric actuators," **IEEE 1984 Ultrasonics Symposium Proceedings.** Dallas, Texas, 14-16 Nov. 1984, vol. 2. p.882-7.

Tojo, T., K. and Sugihara. "Piezoelectricdriven turntable with high positioning accuracy," **Bulletin of the Japanese Society of Precision Engineers.** vol.19, no.2, (June 1985). p.135-7.

Weeks, C. J. "Static shape determination and control for large space structures. I. The flexible beam," **Transactions of ASME, Journal of Dynamic Systems Measurement and Control.** vol. 106 (Dec., 1984) p. 261-6.

Weeks, C. J. "Static shape determination and control for large space structures. II. A large space antenna," **Transactions of ASME, Journal of Dynamic Systems Measurement and Control.** vol. 106 (Dec., 1984) p. 266-72.

Wie, B. and C. T. Plescia. "Attitude stabilization of flexible spacecraft during stationkeeping maneuvers," **Journal of Guidance, Control, & Dynamics.** vol.7, no.4, (July-August, 1984) p.430-6.

Yaeger, J. R. "A practical shape-memory electromechanical actuator," **ISATA 84 Proceedings, International Symposium on Automotive Technology and Automation.** , Milan, Italy, 24-28 Sept., 1984, vol. I. p. 633-42.

Session 1 - Smart Structures

C. A. Rogers, C. Liang, D. K. Barker, "Dynamic Control Concepts Using Shape Memory Alloy Reinforced Plates", Virginia Polytechnic Institute and State University.

R. O. Claus, J. C. Mckeeman, R. G. May, and K. D. Bennett, "Optical Fiber Sensors and Signal Processing for Smart Materials and Structures Applications", Virginia Polytechnic Institute and State University.

M. V. Gandhi, and B. S. Thompson, "A New Generation of Revolutionary Ultra-Advanced Intelligent Composite Materials Featuring Electro-Rheological Fluids", Michigan State University.

S. Hanagud, M. W. Obal, and A. G. Calise, "Piezoceramic Devices and PVDF Films as Sensors and Actuators for Intelligent Structures", Georgia Institute of Technology.

H. H. Robertshaw, and C. F. Reinholtz, "Variable Geometry Trusses", Virginia Polytechnic Institute and State University.

E. I. Rivin, "Passive Self-Adaptive Structures", Abstract, Wayne State University

T. G. Duclos, J. P. Coulter, and L. R. Miller, "Applications for Smart Materials in the Field of Vibration Control", Thomas Lord Research Center.

DYNAMIC CONTROL CONCEPTS USING SHAPE MEMORY ALLOY REINFORCED PLATES

C. A. Rogers
C. Liang
D. K. Barker

Smart Materials & Structures Laboratory
Mechanical Engineering Department
Virginia Polytechnic Institute & State University
Blacksburg, Virginia 24061

ABSTRACT

'Active modal modification' and 'active strain energy tuning' are concepts that have only recently become a possibility with the recent development of shape memory alloy (SMA) reinforced composites. Shape memory alloy reinforced composites is a class of materials that have the ability to; change thier material properties, induce large internal forces in the materials, modify the stress and strain state of the structure, and alter its configuration, all in a controlled fashion. Active modal modification uses the shape memory alloy's capability of changing its stiffness during a temperature activated, reversible, phase transformation thereby modifying the modal response of the structure. Active strain energy tuning adds to the active modal modification concept the ability to use the shape memory alloys ability to impart large distributed loads throughout the material to alter the stored strain energy within the composite structure and therby modify the modal response of the structure.

This paper will present simulations of the modal response of square, quasi-isotropic, SMA reinforced composite plates demonstrating several new concepts and applications for active control of composite structures. Naturally, when the Young's modulus of SMA 'fibers' is increased or large forces are distributed throughout the structure during the reversible phase transformation, not only is the modal response varied, such as the natural frequency and mode shapes, but the maximum deflection and its location on the plate is also changed. Both static deflection (stiffness) and modal response simulations will be presented.

INTRODUCTION

Shape memory alloy reinforced composites are an extremely versatile class of materials recently developed at VPI&SU. Using shape memory alloys as fiber reinforcement gives structures numerous adaptive capabilities. Adaptive and 'Smart' materials, which contain distributed actuators, sensors, and microprocessor capabilities, can be used in many applications requiring a high degree of adaptability to changing external and internal conditions. External conditions may consist of environment, loads, or the desire to change the scope, purpose, or geometry of the structure after it has been built and is in service. Internal conditions may be damage or failure to isolated portions of the material or structure.

The number of applications requiring or desiring such adaptability is increasing rapidly and more are sure to follow as the technology is more readily transfered to the production level. One of the current needs is for long-duration unattended materials and structures that can be used in isolated environments (i.e., submarines, Naval

vessels, defense vehicles, and the space station) or in biomedical applications. Using adaptive/intelligent materials may result in structures with self-inspection and self-identification capabilities which can direct the adaptive response based on the environment and/or damage to the structure.

The ability to adaptively alter the mission, scope, objectives, and geometry of a structure will have tremendous impact on the design philosophy of structures in the future. For example, a structural member made of Shape Memory Alloy (SMA) reinforced composites can compensate for deterioration in absorptivity and thermal expansion properties that result in excessive change in length of that or other members as well as control the motion and vibration of the structure. The same material can be used to change load paths in a structure or within the material so that the component can be replaced or repaired before it causes catastrophic failure of the system or unacceptable degradation of performance.

Applications for adaptive/intelligent materials include:

- Failure detection/prevention of structures (i.e., bridges, walkways, phone and electrical cables, and mechanical components).
- Active vibration control and structural acoustic suppression for acoustic enclosures, propeller aircraft, large flexible structures, etc.
- Active vibration control of helicopter rotor blades.
- Thermal expansion balancing.
- Robot manipulators (fingers).
- Thermally activated valves and ducts.
- Thermal switches.
- Structural dimension adjustment and environment adaptation for large reflector antennas.

The development and subsequent production of this class of materials could have tremendous impact on several diverse technological fields, i.e., material science, vibrations and controls, ocean and aerospace structures, biotechnology, and may act as a catalyst for the development of many new devices and technologies. Brief descriptions of some the applications and the corresponding basic operational modes of the shape memory alloy reinforced composites appear in Ref. [1].

Introduction to Shape Memory Alloys

In 1965, Buehler and Wiley of the U.S. Naval Ordnance Laboratory received a United States Patent on a series of engineering alloys that possess a unique mechanical (shape) "memory" [2]. The generic name of the series of alloys is 55-Nitinol. These alloys have chemical compositions in the range of 53 to 57 weight percent nickel. A great deal of effort was expended over the next ten years in characterizing the material and developing new applications to exploit its remarkable shape memory effect (SME) and its unusual mechanical properties. The Naval Ordnance Laboratory (now known as the Naval Surface Weapons Center) was and still is the leader in characterizing Nitinol. Several other laboratories have made significant contributions to the understanding of the Nitinol, in particular is Battelle Memorial Institute and NASA.

The shape-memory effect (SME) can be described very basically as follows: an object in the low-temperature martensitic condition, when plastically deformed and the external stresses removed will regain its original (memory) shape when heated. The process, or phenomenon, is the result of a martensitic transformation taking place during heating. Although the exact mechanism by which the shape recovery takes place is a subject of controversy, a great deal has been learned about the unique properties of this class of materials in the past twenty years [10-12]. It appears clear

however that the process of regaining the original shape is associated with a reverse transformation of the deformed martensitic phase to the higher temperature austenite phase.

Many materials are known to exhibit the shape memory effect. They include the copper alloy systems of Cu-Zn, Cu-Zn-Al, Cu-Zn-Ga, Cu-Zn-Sn, Cu-Zn-Si, Cu-Al-Ni, Cu-Au-Zn, Cu-Sn, and the alloys of Au-Cd, Ni-Al, Fe-Pt, and others. The most common of the shape memory alloys or transformation metals is a nickel-titanium alloy known as Nitinol.

Nickel-titanium alloys (Nitinol, NiTi) of proper composition exhibit unique mechanical "memory" or restoration force characteristics. The name is derived from Ni (Nickel) - Ti (Titanium) - NOL (Naval Ordinance Laboratory). The shape recovery performance of Nitinol is phenomenal. The material can be plastically deformed in its low-temperature martensite phase and then restored to the original configuration or shape by heating it above the characteristic transition temperature. This unusual behavior is limited to NiTi alloys having near-equiatomic composition. Plastic strains of typically six-to-eight percent may be completely recovered by heating the material so as to transform it to its austenite phase. Restraining the material from regaining its memory shape can yield stresses of 100,000 psi (the yield strength of martensitic Nitinol is approximately 12,000 psi).

For some applications, creating large internal forces within the material or structure are not needed or desireable. Shape memory alloys have the unique ability of changing its material properties, reversiblly, and this characteristic can be exploited without embedding plastically deformed SMA 'fibers' nor creating large forces and deformations of the structure. This capability is exploited in the concept that will be further explained below, termed "Active Modal Modification".

Substantial progress has been made in understanding the nature of the "shape memory effect" (SME). A great deal of literature has been published over the past twenty years presenting detailed thermal, electrical, magnetic, and mechanical characterizations of this unusual alloy [3-10]. However, there is still much to be learned about the influence of residual stress and high temperatures, that may be used in composite fabrication and processing, on the extent, duration and repeatability on SME as well as the dynamic actuator and sensing characteristics of Nitinol.

Shape Memory Alloy Reinforced Composites

The class of the material referred to as SMA reinforced composites in this paper is simply a composite material that contains shape memory alloy fibers (or films) in such a way that the material can be stiffened or controlled by the addition of heat (i.e., apply a current through the fibers) [1,2]. Shape memory alloys and the mechanism by which they exhibit the characteristic shape memory effect (SME) is explained very briefly below and in greater detail in references [3-9]. One of the many possible configurations of the SMA reinforced composite material is one in which the shape memory alloy fibers are embedded in a material off of the neutral axis on both sides of the beam in agonist-antagonist pairs. Before embedding the fibers, the shape memory alloy fibers are plastically elongated and constrained from contracting to their 'normal' or 'memorized' length upon curing the composite material with high-temperature. The plastically deformed fibers are therefore an integral part of the composite material and the structure. When the fibers are heated, generally by passing a current through the shape memory alloy, the fibers 'try' to contract to their 'normal' or 'memorized' length and therefore generate a uniformly distributed shear load along the entire length of the fibers. The shear load offset from the neutral axis

of the structure will then cause the structure to bend in a known and predictable manner.

There are numerous other configurations, such as creating 'sleeves' within the composite laminate which the plastically elongated shape-memory alloy can be inserted and then clamped to both ends. When the shape memory alloy is heated, the fibers try to contract in the same fashion as explained above. When one end of the beam is free, the fibers in a sleeve will exert a concentrated force on the ends of the structure in a direction that is always tangent to the structure at the point where the fibers are clamped to the structure. When both ends of the beam are fixed, heating the SMA results in 'fibers' with a siginificantly increased stiffness and applied tension that will resist any transverse motion. The difference between the embedded fibers and the fibers in a sleeve is that in the first case the force of the shape memory alloy is distributed over the length of the fiber and in the later case the force is concentrated at the end of the structure.

Shape Memory Alloy (SMA) reinforced composites have tremendous potential for creating new paradigms for material-structures interaction [11]. The list of scientific areas that can be influenced by novel approaches possible with SMA reinforced composites is quite large. For example, vibration control can be accomplished by using the distributed force actuator capabilities similar to the common piezoelectric systems. However, two unique approaches to active control are possible with a material that can change its stiffness, physical properties and in the second case, apply large distributed loads throughout the structure; i) Active Strain Energy Tuning, and ii) Active Modal Modification. Simulation results showing the potential for SMA reinforced composites to vary the modal response of a composite plate will be presented below.

Transient and steady-state vibration control can be accomplished with SMA reinforced composites using several techniques. Transient vibration control is defined here as the ability to suppress or damp structural vibration by applying forces (distributed and/or point) to the structure in such a way as to dissipate the energy within the structure. This is accomplished generally by applying point transverse loads to the structure or applying an 'actuator film' to the surface of the structure. The approach with SMA reinforced composites is to simply embed the actuators (shape memory alloys) in the structure such that, when actuated correctly, they exert agonist-antagonist forces off the neutral axis thereby reducing vibrations [1]. Steady state vibration control is the ability to change the modal characteristics of the structure. The mechanism in SMA reinforced composites is to increase the stiffness of the composite in different directions by predetermined amounts through the SMA actuators.

Applications for SMA reinforced composites extend far beyond vibration control tasks. Active buckling control, or more generically active structural modification schemes, can be imagined in which SMA fibers are stiffened within a composite to alter the critical buckling load of the structure. SMA composites that are used for various vibration control tasks would also be used for motion or shape control, allowing a structure to maintain a given shape or orientation for an extended period of time. The physical, thermal, and controller design will be much more critical than in the transient vibration control scenario. Motion and shape control will in all likelihood involve the simultaneous use of force actuators (SMA) and stiffness actuators (the technique in which the SMA is heated to change its modulus of elasticity) to create a structure that behaves much like a mechanical muscle. Another possible design approach is to actuate single fibers with pulse-type signals, much like the all-or-nothing actuation of the individual muscle fibers in the human muscle.

Active Control Concepts

Steady-state vibration control which may also be used for structural acoustic control can be accomplished with SMA reinforced composites using a novel technique termed "Active Modal Modification" [12]. The modal response of a structure or mechanical component (i.e., plate or beam) can be tuned or modified by simply heating the SMA fibers or lamina to change the stiffness of all or portions of the structure. When Nitinol is heated to cause the material transformation from the martensitic phase to the austenite phase, the Young's modulus changes by a factor of approximately four as shown in Fig 1. Not only is the stiffness increased by a factor of four but the yield strength also increases by a factor of ten. This change in the material properties occur because of a phase transformation and does not result in any appreciable force and does not need to be initiated by any plastic deformation.

In 'Active Strain Energy Tuning' the shape memory alloy fibers are placed in or on the structure in such a way that when activated there is no resulting deflections but instead the structure is placed in a 'residual' state of strain. The resulting stored strain energy (tension or compression) changes the energy balance of the structure and modifies the modal response much like tuning a guitar string.

Active strain energy tuning utilizes both the embedded fiber and sleeve method described earlier. The difference between the epoxied fibers and the fibers in a sleeve is that in the first case the force of the shape memory alloy is distributed over the length of the fiber and in the latter case the force is concentrated at the end of the structure or is used to resist transverse motion. Both of the design concepts described above have been incorporated into prototypes and their potential demonstrated on a limited scale. The simulations presented below assume embedded fibers unless otherwise specified.

FORMULATION

Simulations of active strain energy tuning by tuning the material properties of deformed SMA fibers and imparting distributed loads along the length of the fibers of a 'SMA-Epoxy' quasi-isotropic square plate will be presented by evaluating the free vibration response and also the variation of the square plate's variation of bending stiffness. Investigating the effect of active strain energy tuning on a quasi-isotropic plate constrains the following formulation and discussion to midplane symmetric laminates ($B_{ij} = 0$) with the distributed 'fiber' loads assumed to be 'inplane loads'. Therefor, the simulation for active strain energy tuning and active modal modification use similar developments with the only difference being the inclusion of inplane loads for ASET.

Bending of Simply-Supported Plates

The geometry used for all of the simulations and discussion presented in this paper is shown in Fig. 2. Neglecting inertia terms, for static bending analysis, the governing differential equation of motion is

$$D_{11}\frac{\partial^4 w}{\partial x^4} + 4D_{16}\frac{\partial^4 w}{\partial x^3 \partial y} + 2(D_{12} + 2D_{66})\frac{\partial^4 w}{\partial x^2 \partial y^2} + 4D_{26}\frac{\partial^4 w}{\partial x^3 \partial y} + D_{22}\frac{\partial^4 w}{\partial x^4} \qquad [1]$$

$$+ \bar{N}_x\frac{\partial^2 w}{\partial x^2} + \bar{N}_y\frac{\partial^2 w}{\partial y^2} + 2\bar{N}_{xy}\frac{\partial^2 w}{\partial x \partial y} = q$$

The boundary conditions for simply-supported edges are

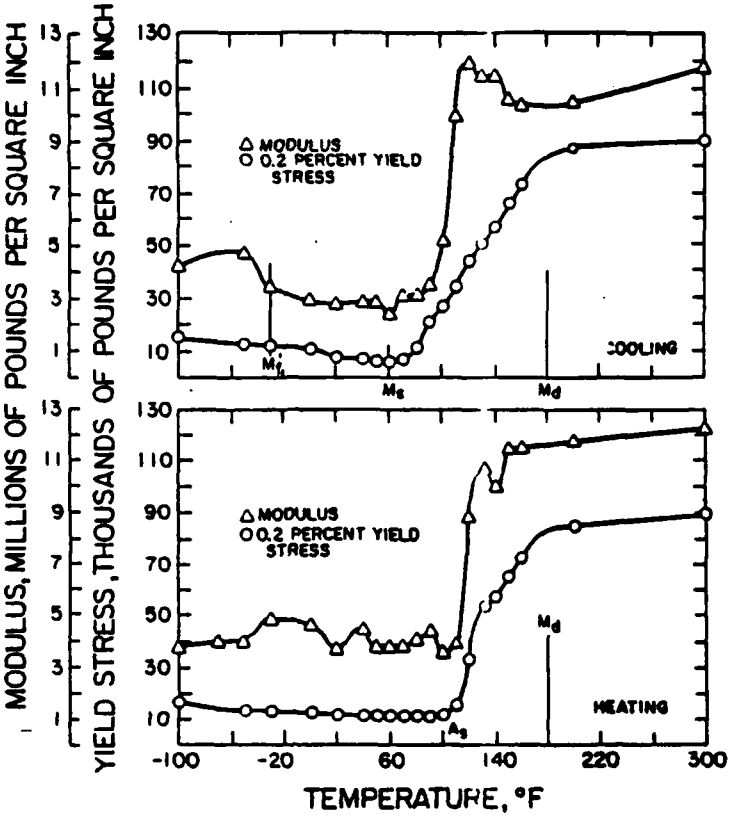

Figure 1. Yield Stress and Elastic Modulus vs. Temperature

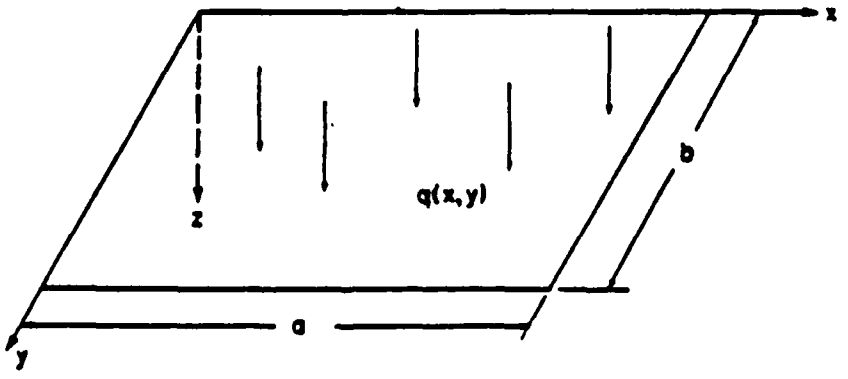

Figure 2. Restoring Stress vs. Temperature for Nitinol

at x = 0 and a :
$$w = M_x = -D_{11}\frac{\partial^2 w}{\partial x^2} - 2D_{16}\frac{\partial^2 w}{\partial x \partial y} - D_{12}\frac{\partial^2 w}{\partial y^2} = 0 \qquad [2]$$

at y = 0 and b :
$$w = M_y = -D_{12}\frac{\partial^2 w}{\partial x^2} - 2D_{26}\frac{\partial^2 w}{\partial x \partial y} - D_{22}\frac{\partial^2 w}{\partial y^2} = 0 \qquad [3]$$

Using the Ritz method to obtain an approximate solution to the governing equation yields the energy expression

$$\frac{1}{2}\int_0^b\int_0^a\left[D_{11}\left(\frac{\partial^2 w}{\partial x^2}\right)^2 + 2D_{12}\frac{\partial^2 w}{\partial x^2}\frac{\partial^2 w}{\partial y^2} + D_{22}\left(\frac{\partial^2 w}{\partial y^2}\right)^2\right] \qquad [4]$$
$$+\left[4\left(D_{16}\frac{\partial^2 w}{\partial x^2} + D_{26}\frac{\partial^2 w}{\partial y^2}\right)\frac{\partial^2 w}{\partial x \partial y} + 4D_{66}\left(\frac{\partial^2 w}{\partial x \partial y}\right)^2\right]$$
$$+\left[\bar{N}_x\left(\frac{\partial w}{\partial x^2}\right)^2 + \bar{N}_y\left(\frac{\partial w}{\partial y}\right)^2 + 2\bar{N}_{xy}\frac{\partial w}{\partial x}\frac{\partial w}{\partial y} - 2qw\right]dx\,dy$$
$$= \textit{stationary value}$$

The assumed solution for the energy expression, Eq. 4, using the separation of variables is

$$w = \sum_{m=1}^{M}\sum_{n=1}^{N} A_{mn}X_m(x)Y_n(y) \qquad [5]$$

Substituting this series into the energy expression, Eq. 4, the following set of equations result.

$$\sum_{i=1}^{M}\sum_{j=1}^{N}\left\{D_{11}\int_0^a \frac{d^2X_i}{dx^2}\frac{d^2X_m}{dx^2}dx\int_0^b Y_jY_n dy \right. \qquad [6]$$
$$+D_{12}\left[\int_0^a X_m\frac{d^2X_i}{dx^2}dx\int_0^b Y_j\frac{d^2Y_n}{dy^2}dy + \int_0^a X_i\frac{d^2X_m}{dx^2}dx\int_0^b Y_n\frac{d^2Y_j}{dy^2}\right]$$
$$+\left[D_{22}\int_0^a X_iX_m dx\int_0^b \frac{d^2Y_j}{dy^2}\frac{d^2Y_m}{dy^2}dy + 4D_{66}\int_0^a \frac{dX_i}{dx}\frac{dX_m}{dx}dx\int_0^b \frac{dY_j}{dy}\frac{dY_n}{dy}dy\right]$$
$$+2D_{16}\left[\int_0^a \frac{d^2X_i}{dx^2}\frac{dX_m}{dx}dx\int_0^b Y_j\frac{dY_n}{dy}dy + \int_0^b Y_n\frac{dY_j}{dy}dy\right]$$
$$+2D_{26}\left[\int_0^a X_m\frac{dX_i}{dx}dx\int_0^b \frac{dY_j}{dy}\frac{d^2Y_n}{dy^2}dy + \int_0^a X_i\frac{dX_m}{dx}dx\int_0^b \frac{d^2Y_j}{dy^2}\frac{dY_n}{dy}dy\right]$$
$$\left.+\int_0^a\int_0^b\left[\bar{N}_xY_nY_j\frac{dX_m}{dx}\frac{dX_i}{dx} + \bar{N}_yX_mX_i\frac{dY_j}{dy}\frac{dY_n}{dy} + \bar{N}_{xy}\left[X_mY_j\frac{dX_i}{dx}\frac{dY_n}{dy} + X_iY_n\frac{dX_m}{dx}\frac{dY_j}{dy}\right]\right]dx\,dy\right\}$$
$$= q_0\int_0^a X_m dx\int_0^b Y_n dy \qquad \begin{matrix} m = 1, 2, \ldots, M \\ n = 1, 2, \ldots, N \end{matrix}$$

The *MxN* linear simultaneous equations are then rewritten in matrix form as

$$[K]\{A_{mn}\} = \{q_{mn}\} \qquad [7]$$

Using the Ritz method to solve the energy equation allows for the assumed solution to only satisfy the displacement boundary conditions (a solution in a variables separable form which satisfies the moment equations does not exist). For a simply-supported plate, the double sine series in conjunction with the assumed solution given by Eq. 5 is sufficient.

$$X_m(x) = \sin\frac{m\pi x}{a} \qquad [8]$$

$$Y_n(y) = \sin\frac{n\pi y}{b}$$

At this point, the unknown coefficients, A_{mn}, are determined and the deflections calculated using the assumed solution of Eq. 5. Because of the approximate nature of the Ritz method, care must be taken to insure convergence of the solution and that the coupling terms, D_{16} and D_{26}, are accounted for appropriately (see ref. [13]).

Free Vibration of Simply-Supported Plates

The formulation of free vibration response of rectangular anisotropic plates is very similar to that described above for the bending problem. The primary difference in the two solutions is that inertia terms must be added to the governing equation for free vibration analysis and the external load, $q(x,y)$, used in the bending formulation may now be neglected. However, the same basic approach must be followed, namely, the Ritz solution method is followed which involves as before, writing the energy equation governing free vibration (assuming no lateral loads).

$$\frac{1}{2}\int_0^b\int_0^a\left[D_{11}\left(\frac{\partial^2 w}{\partial x^2}\right)^2 + 2D_{12}\frac{\partial^2 w}{\partial x^2}\frac{\partial^2 w}{\partial y^2} + D_{22}\left(\frac{\partial^2 w}{\partial y^2}\right)^2\right] \qquad [9]$$

$$+\left[4\left(D_{16}\frac{\partial^2 w}{\partial x^2} + D_{26}\frac{\partial^2 w}{\partial y^2}\right)\frac{\partial^2 w}{\partial x\partial y} + 4D_{66}\left(\frac{\partial^2 w}{\partial x\partial y}\right)^2\right]$$

$$+\left[\bar{N}_x\left(\frac{\partial w}{\partial x^2}\right)^2 + \bar{N}_y\left(\frac{\partial w}{\partial y}\right)^2 + 2\bar{N}_{xy}\frac{\partial w}{\partial x}\frac{\partial w}{\partial y} - \rho\omega^2 w^2\right]dx\,dy$$

$$= \textit{stationary value}$$

The natural modal response of the plate is found by using the same assumed solution as given above, Eq. 4, and by substituting the same double sine series into the resulting *MxN* homogeneous simultaneous equations

$$\sum_{i=1}^{M}\sum_{j=1}^{N}\left\{D_{11}\int_0^a\frac{d^2X_i}{dx^2}\frac{d^2X_m}{dx^2}dx\int_0^b Y_jY_n dy\right. \qquad [10]$$

$$+D_{12}\left[\int_0^a X_m\frac{d^2X_i}{dx^2}dx\int_0^b Y_j\frac{d^2Y_n}{dy^2}dy + \int_0^a X_i\frac{d^2X_m}{dx^2}dx\int_0^b Y_n\frac{d^2Y_j}{dy^2}\right]$$

$$+D_{22}\int_0^a X_iX_m dx\int_0^b\frac{d^2Y_j}{dy^2}\frac{d^2Y_m}{dy^2}dy + 4D_{66}\int_0^a\frac{dX_i}{dx}\frac{dX_m}{dx}dx\int_0^b\frac{dY_j}{dy}\frac{dY_n}{dy}dy$$

$$+2D_{16}\left[\int_0^a\frac{d^2X_i}{dx^2}\frac{dX_m}{dx}dx\int_0^b Y_j\frac{dY_n}{dy}dy + \int_0^b Y_n\frac{dY_j}{dy}dy\right]$$

$$+ 2D_{26}\left[\int_0^a X_m \frac{dX_i}{dx}dx \int_0^b \frac{dY_j}{dy}\frac{d^2Y_n}{dy^2}dy + \int_0^a X_i \frac{dX_m}{dx}dx \int_0^b \frac{d^2Y_j}{dy^2}\frac{dY_n}{dy}dy\right]$$

$$+ \int_0^a \int_0^b \left[\bar{N}_x Y_n Y_j \frac{dX_m}{dx}\frac{dX_i}{dx} + \bar{N}_y X_m X_i \frac{dY_j}{dy}\frac{dY_n}{dy} + \bar{N}_{xy}\left[X_m Y_j \frac{dX_i}{dx}\frac{dY_n}{dy} + X_i Y_n \frac{dX_m}{dx}\frac{dY_j}{dy}\right]\right] dx\, dy$$

$$- \left[\rho\omega^2 \int_0^a X_i X_m dx \int_0^b Y_j Y_n dy\right]\} A_{ij} = 0 \qquad \begin{matrix} m = 1, 2, \ldots, M \\ n = 1, 2, \ldots, N \end{matrix}$$

Since the *MxN* simultaneous equations are homogeneous, a nontrivial solution can be obtained only if the determinant of the coefficient matrix, [K], is zero. Therefor, the eigenvalues of [K] are determined which then reflect the natural frequencies of free vibration.

The formulation must be further expanded for SMA reinforced composites as the bending stiffnesses (D_{ij}) are functions of temperature and can be tuned by activating individual plys of a laminate resulting in a change of the fiber modulus (see Fig. 1) by as much as a factor of four. The change in the fiber modulus occurs over a relatively small temperature range (selectable from 10 to 20°C) and is a result of a solid phase material transformation between the martensite and austenite phases. Therefore, the superscripts 'M' and 'A' are used to denote the physical and mechanical properties in each phase. Unsuperscripted values are intended to represent instantaneous values which are 'tunable' between the martensitic and austenitic (extreme) values.

Determination of Inplane 'Fiber' Loads

One of the basic assumptions or conditions used in the analysis described herein is that the laminate remain midplane symmetric at all times. This means that corresponding lamina with the same fiber orientation (on both sides of the midplane) are activated simultaneously. This assumption then allows for the induced distributed loads to be modeled as general inplane loads as they cause no transverse displacements or moments.

The first numerical procedure that must be performed is to determine the resulting inplane load that can be applied to the plate's boundary to model the distributed 'fiber' loads. The method involves first considering a small element containing the appropriate fraction of fiber and matrix. Recall that prior to embedding the SMA fiber in the matrix, the SMA fiber is strained plastically an amount ε_r. The initial strain in the fiber can then be used to generate large restoring stresses, σ_r, in the composite when the fiber is 'activated'. Fig. 3 shows a typical maximum restoring stress vs. initial strain for Nitinol. Therefore, upon activating the SMA fibers in a particular lamina the fibers exert a large stress distributed throughout the laminate resulting in a reduced strain of the fiber and an increased strain in the laminate, ε (assuming the boundary is free). The stress needed to recover the compressive strain, ε, of the laminate is the equivalent inplane load that is to applied to the laminate boundaries. For example, if $\varepsilon_r = 2.0\%$ then from Fig. 3 the restoring stress is 24 kpsi. However, the 24 kpsi will compress the matrix material in some sense (assuming free boundary conditions) and internal equilibrium will be satisfied by letting the fiber and matrix stresses being equal, $\sigma_f = \sigma_m$. Now assuming that the fiber and matrix have the same deformation in the fiber direction the laminate strain is determined:

$$\sigma_r = E_m \varepsilon \qquad [11]$$

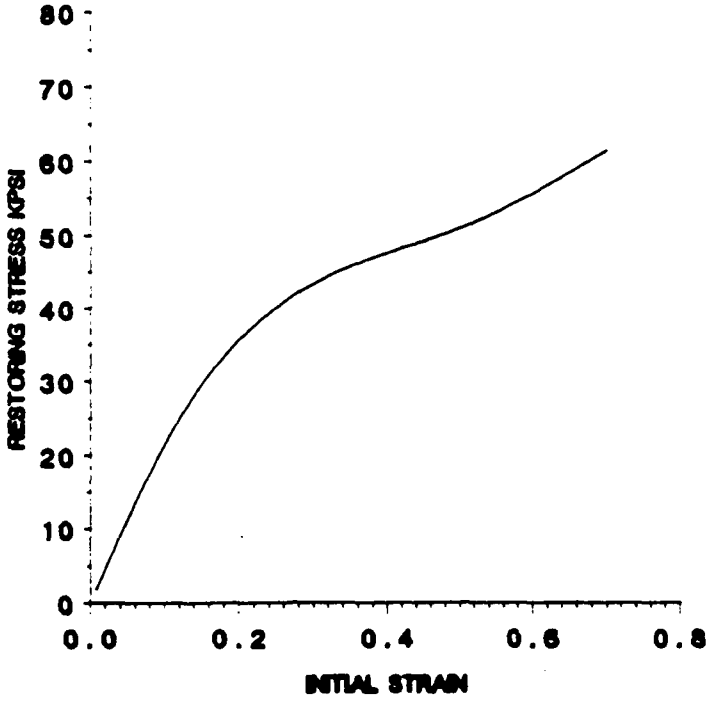

Figure 3. Maximum Restoring Stress vs. Initial Strain

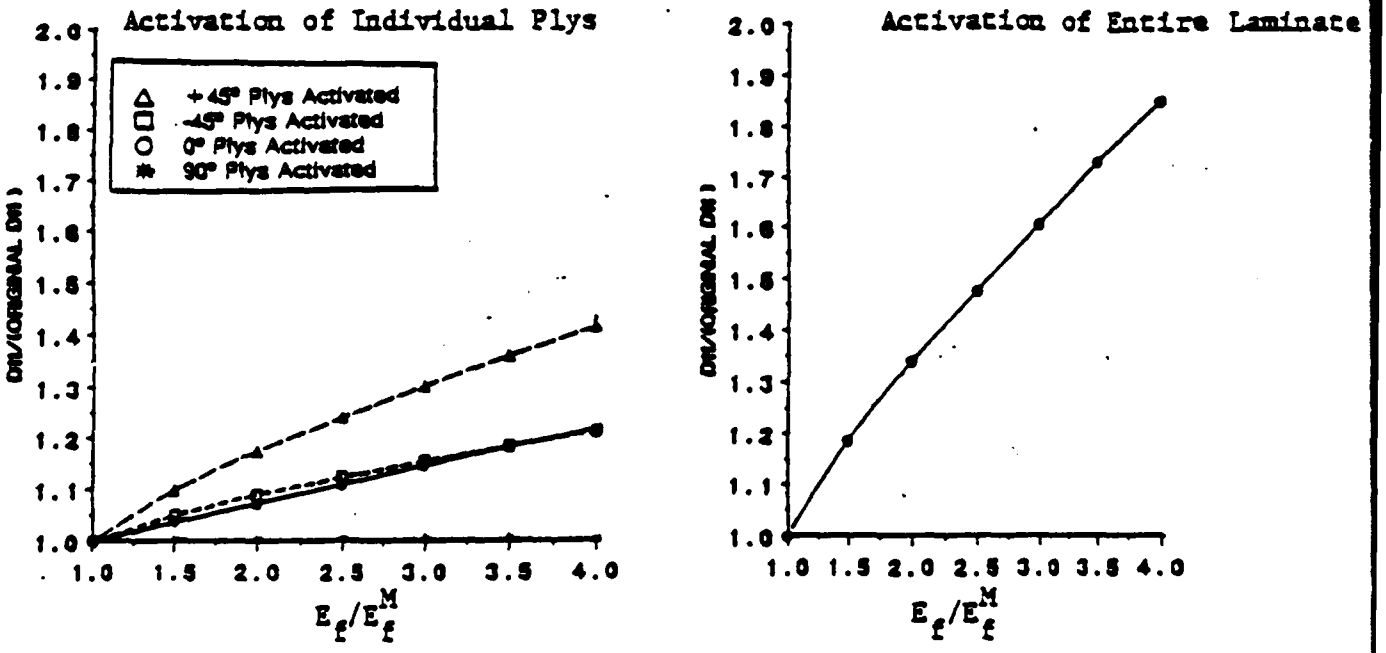

Figure 4. Flexural Stiffness Tuning of Quasi-Isotropic Plate

assuming $E_m = 4mpsi$ and $\sigma_r = 24kpsi$ results in the laminate strain, ε, being 0.6 %. The 0.6 percent strain then reduces the SMA fiber strain to 1.4% from the free contraction of the laminate and therefore the corresponding restoring stress is decreased nonlinearly as shown in Fig. 3. Continuing the numerical example above; for 1.4% SMA fiber strain the σ_r is 20 kpsi resulting in the total laminate strain being 0.5%. This iterative procedure is then continued to convergence and may be described bt the expressions below.

$$\sigma_r^{(n)} = \sigma_f^{(n)} = E_m \varepsilon^{(n)} \qquad [12]$$

$$\sigma_r^{(n)} = f(\varepsilon_f - \varepsilon^{(n)})$$

Upon convergence, the resulting ε is then used to determine the necessary inplane loads, $\bar{N}_x, \bar{N}_y$, and $\bar{N}_{xy}$.

RESULTS

Problem Definition

The simulation results have been generated based upon several assumptions. First, the laminates are all quasi-isotropic, $[+45°, -45°, 0°, 90°]_s$, in the unactivated state and always remain midplane symmetric which means that the lamina pairs above and below the midplane with the same fiber orientation are activated simultaneously. Secondly, all of the plates are square (even though the formulation allows for general rectangular plates) with simply-supported boundaries.

The material used in all simulations is Nitinol/Epoxy with a fiber volume fraction of 50% unless otherwise noted. The macroscopic lamina properties are determined from the rule-of-mixtures. Several simplifying assumptions were adopted relating to the restoring stress of Nitinol and the variation of the fiber's elastic modulus upon activation. The initial restoring stress, σ_r, of the SMA fibers as a function of fiber strain was determined from Fig. 3, however in simulations in which the fibers are partially activated the restoring stress is varied linearly from zero to its maximum stress and the Young's modulus is also varied linearly from 4 mpsi to 16 mpsi. Future work will generalize the nonlinear functions of restoring stress and elastic modulus with temperature as well as consider thermal effects.

ACTIVE MODAL MODIFICATION (AMM)

Variation of Plate Stiffness and Maximum Deflections

The stiffness of a composite plate, extension or bending, can be taylored within reasonable bounds. However, SMA reinforced composites can be taylored to not only have a specified stiffness but can be taylored to have a range of material properties that can be controlled or tuned. For example, Fig. 4 shows the change in the flexural stiffness (D_{11}) of the square plate when one or all of the individual lamina are activated such that the fiber modulus increases. Simply activating the top and bottom +45° ply can modify the plate flexural stiffness by over 40 percent. Activating all of the plys to increase the fiber modulus by a factor of four increases the flexural stiffness by approximately 90 percent. By utilizing the numerous permutations of activated laminae to unactivated laminae and using modulation schemes in which some lamina can be only partially activated can result in subtle and versatile control possibilities. Changing the stiffness of a composite structure has some important practical implications. One prime example is in active structural acoustic control where the radi-

ated sound pressure levels can be reduced dramatically by reducing the amplitude of the structural acoustic vibrations. Obviously changing the stiffness of the plate also changes its dynamic response and has other significant implications on vibration and acoustic control which will be described below.

Variation of Natural Frequencies and Mode Shapes

Naturally, changing the stiffness of a structure impacts on more than the maximum deflection but also modifies the modal response of the structure, hence the term 'Active Modal Modification'. One of the objectives of Active Modal Modification is to tune the structure based upon various performance criteria or external conditions such as periodic force or pressure inputs to the structure that may be near resonant frequencies or result in low transmission loss. Active or adaptive control of the stiffness of the structure will influence the nature of the modal response of the structure by changing the natural frequencies and the characteristic mode shapes. Utilizing classical composite technology in which structures are fabricated with taylored properties and various orientations of individual plys allow for tremendous flexibility in the structural design of these tunable structures for various applications.

Figure 5 illustrates the potential for changing the natural frequency of a square quasi-isotropic plate by activating one or all of the individual plys. Again, the greatest authority is achieved, for single lamina activation, by activating the +45° plys that are positioned on the top and bottom surfaces of the plate. However, by activating various permutations of lamina the control of the natural frequencies and stiffnesses can be accomplished in a more sophisticated manner perhaps allowing for dual-requirements associated with the orthotropy of the structure and the modal response in a coupled fashion.

The authority of SMA reinforced composites is quite dramatic for active modal modification. Activating the +45° plys result in approximately a 25 percent increase in the natural frequencies and activating all of the plys increase the natural frequencies by about 50 percent. The impact of tuning the stiffness of the fibers is also seen in the modification of the mode shapes which naturally occur because of the increased orthotropy introduced by changing the stiffness of a ply or plys of an initially quasi-isotropic structure. Again, the concept of tuning the mode shapes of a structure is another novel approach to composite design.

Modification of the mode shapes associated with the fourth natural frequency are shown in Figs. 6 and 7. Figure 6 shows the mode shape for the quasi-isotropic square plate without any activated fibers or plys. Note that quasi-isotropic plate does not have an anti-node line in the center of the plate as it is only quasi-isotropic in extension and is but only a close approximation to isotropic in bending. When the +45° plys are activated in the plate, the flexural stiffness increases, the natural frequency increases and the characteristic mode shapes also change as illustrated in Fig. 6. Comparing Figs. 6 and 7 show the dramatic change in the location of the nodes and anti-node lines which also indicate the possiblity of tuning the impedance and mobility of any point on the plate. Lastly, Fig. 8 shows some of the variations in mode shapes and natural frequencies that can be accomplished by activating individual plys of the entire structure.

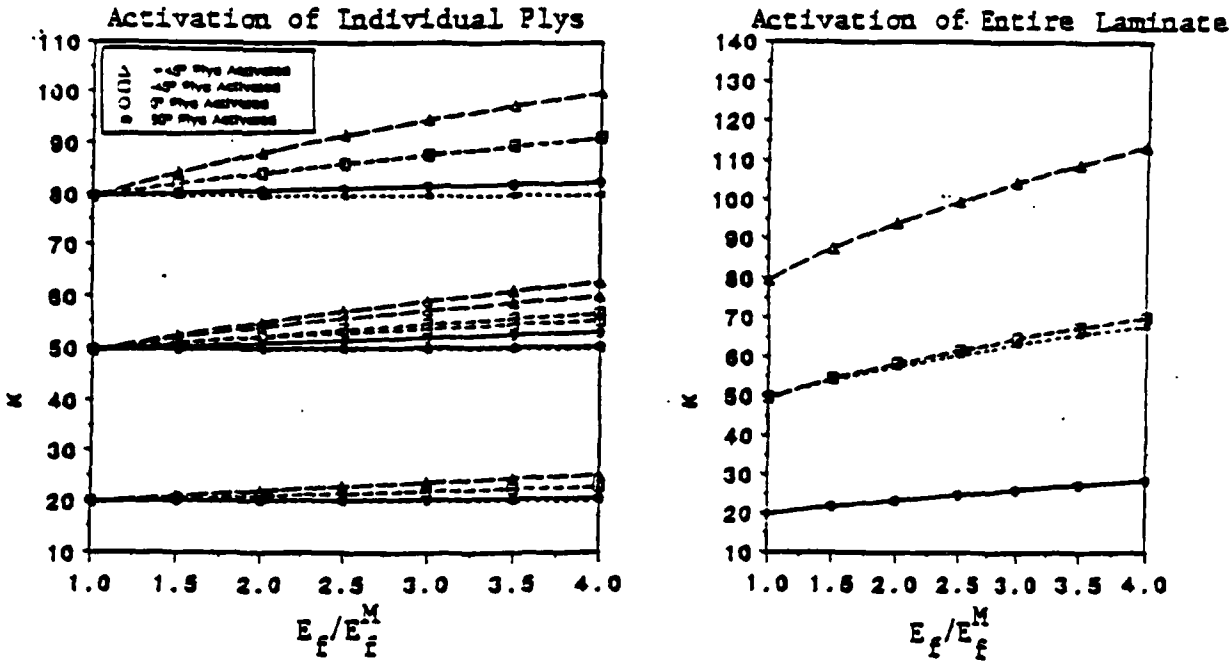

Figure 5. Natural Frequency Tuning of Quasi-Isotropic Plate

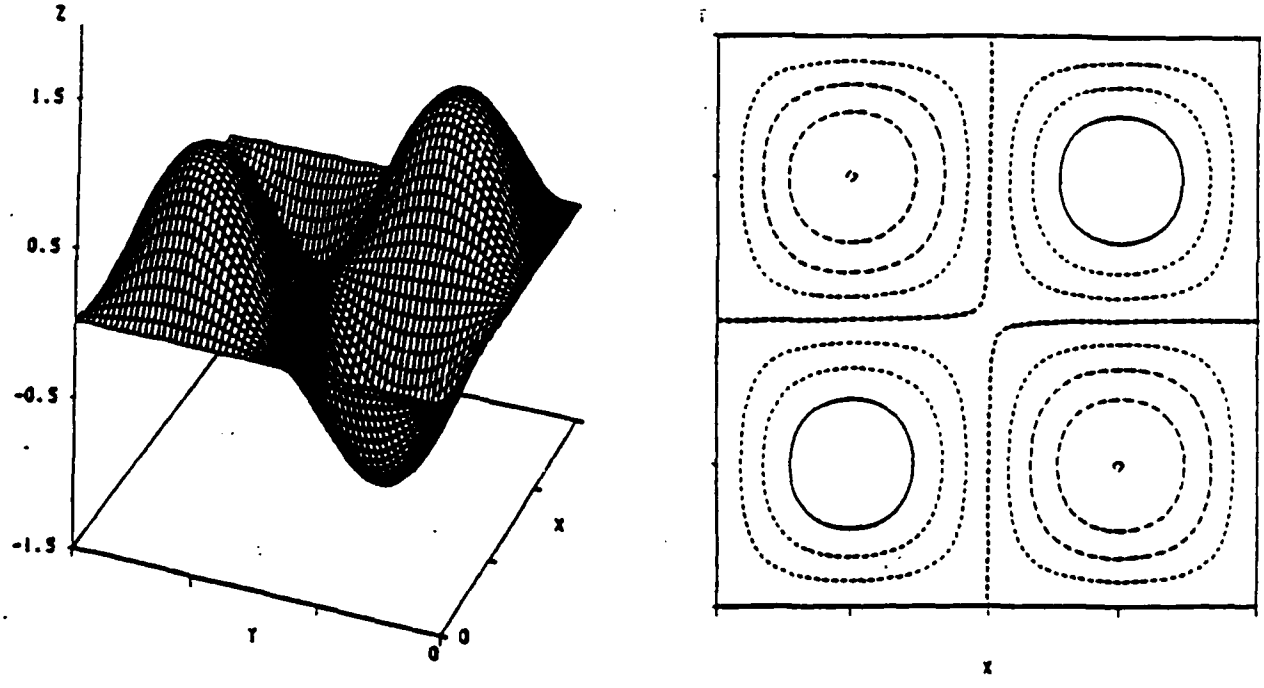

Figure 6. Mode Shape of Unactivated [+45, – 45,0,90], Plate

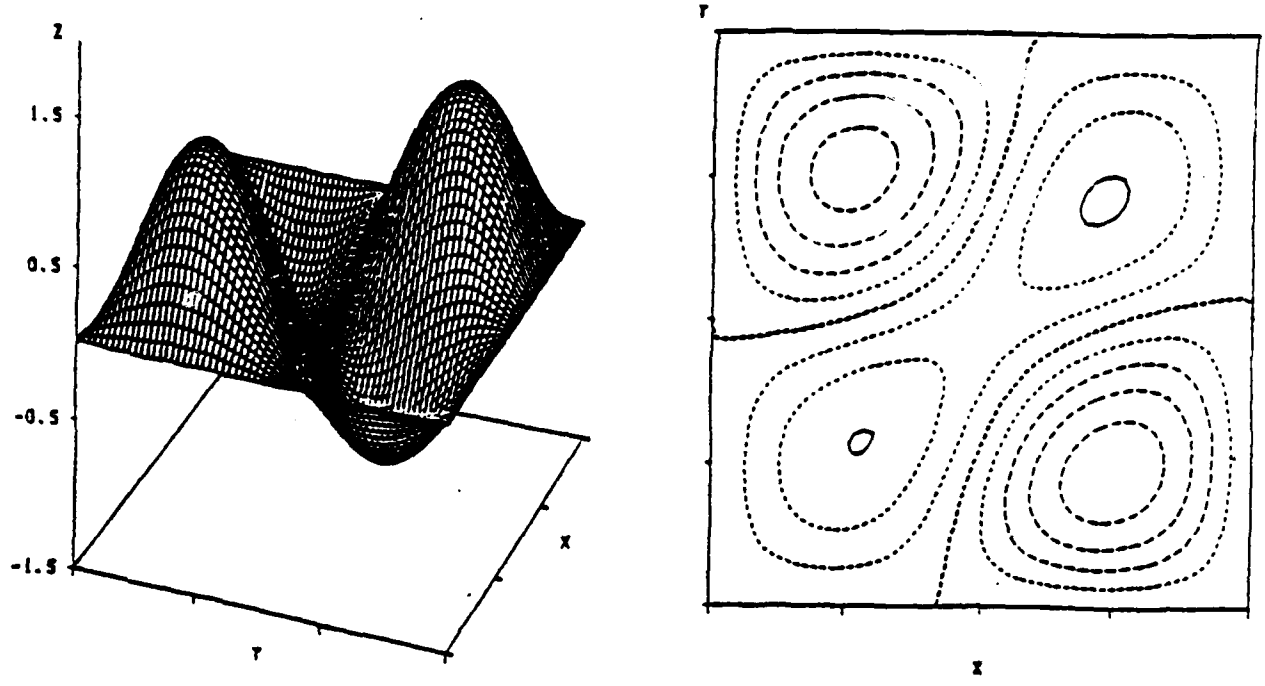

Figure 7. Mode Shape of [+45, − 45,0,90]$_s$ Plate with Activated +45° Plys

E_f/E_f^M = 1.0		E_f/E_f^M = 4.0				
Activated Laminae		+45°	−45°	+0°	+90°	all
1st Mode						
k =	19.9	25.2	22.8	20.0	20.6	28.5
2nd Mode						
k =	49.9	60.1	55.4	49.7	50.3	68.2
3rd Mode						
k =	49.6	62.9	56.8	50.0	53.2	70.4
4th Mode						
k =	79.5	100	91.2	79.9	81.5	114.0

Figure 8. Comparison of Mode Shapes for [+45, − 45,0,90]$_s$ SMA Reinforced Plate

ACTIVE STRAIN ENERGY TUNING (ASET)

Variation of Plate Stiffness and Maximum Deflections

One of the unique capabilities of SMA reinforced composite materials is that structures (or components) can be designed with a specific range of material properties that can be controlled or tuned over a relatively large range. For example, Fig. 4 shows the change in the flexural stiffness (D_{11}) of the square plate when one or all of the individual lamina are activated by active modal modification [12], i.e., the fiber modulus is increased by a factor of four. However, active strain energy tuning allows for even greater authority. Figure 9 illustrates the increased authority over maximum displacements for a uniformly loaded plate by comparing active modal modification and active strain energy tuning. Recall that active strain energy tuning incorporates the response of active modal modification as the Young's modulus of Nitinol is assumed to increase linearly with restoring stress and the percent activation. The results shown in Fig. 9 also assumes an initial strain of the SMA 'fibers' of only 2% even though Nitinol can regain 8% plastic strain and the maximum restoring stress is also realized at 8% strain.

The authority of active strain energy tuning is obvious for SMA/Epoxy composites and even greater authority may be possible if larger initial strains could be used in the embedded fibers. The limiting initial strain of the fibers is dependent on several physical considerations, including; the choice of resin system, the reliability and durability of bond between the fibers and matrix, the maximum, average, and distribution of stresses throughout the matrix material. However, it is somewhat clear that 50% fiber volume fraction is not necessary and in many situations is not desireable. Because of the effect of the inplane distributed loads, the fiber volume fraction can be reduced without significantly increasing the maximum deflection relative to active modal modification. Figure 10 shows the effect of the flexural stiffness, D_{11}, as a function of fiber volume fraction. Similarly, Fig. 9 shows the maximum plate displacement normalized with respect to the maximum plate displacement for active modal modification with a 50% fiber volume fraction.

Variation of Natural Frequencies and Mode Shapes

Active strain energy tuning can be applied to a structure to influence numerous structural interactions such as deflections, buckling, and of course, natural frequencies and mode shapes. As was explained in Ref. [12], the primary objective of active modal modification and active strain energy tuning is to 'tune' the structure based upon various performance criteria or external conditions such as periodic force or pressure inputs to the structure that may be near resonant frequencies or result in low transmission loss. Active strain energy tuning again allows for greater authority and versatility of control to be excersized over active modal modification to vary the natural frequencies and to alter the modal shapes of the structure.

Simulations of the first ten mode shapes of the quasi-isotropic plate for a totally unactivated plate, activation of only the 45° and 90° plys, and when all the layers are activated, are shown in Fig. 11. Naturally the mode shapes for the unactivated and totally activated plate are identical, however, the natural frequencies for the totally activated plate are from five to ten times higher for the totally activated case. Table 1 shows the range of control of the natural frequencies that is possible with a Nitinol/Epoxy composite with a 50% fiber volume fraction. Even though the range of frequencies is quite broad, it is also somewhat clear that for most adaptive control schemes that less dramatic variations will suffice and perhaps simplify fabrication, processing, reliability, and durability of such a structure. Figure 12 shows the effect

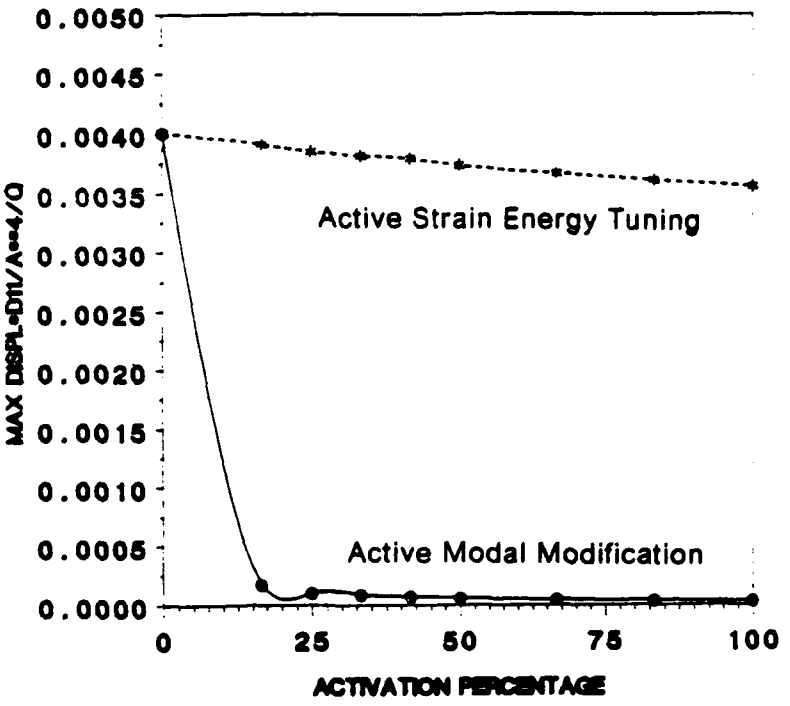

Figure 9. Maximum Plate Deflection Under a Uniform Pressure Load Using Active SMA Control

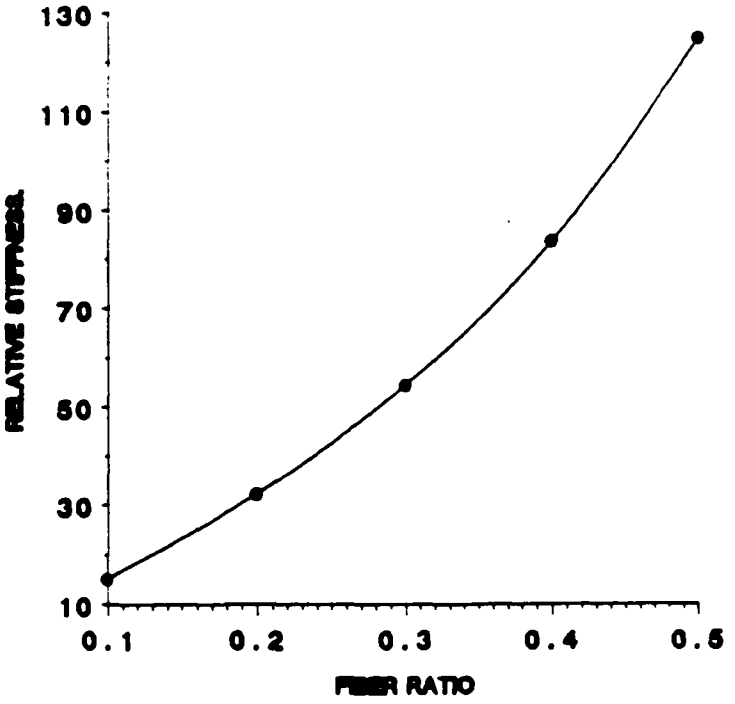

Figure 10. Flexural Stiffness Tuning of Quasi-Isotropic Plates Using Active Strain Energy Tuning

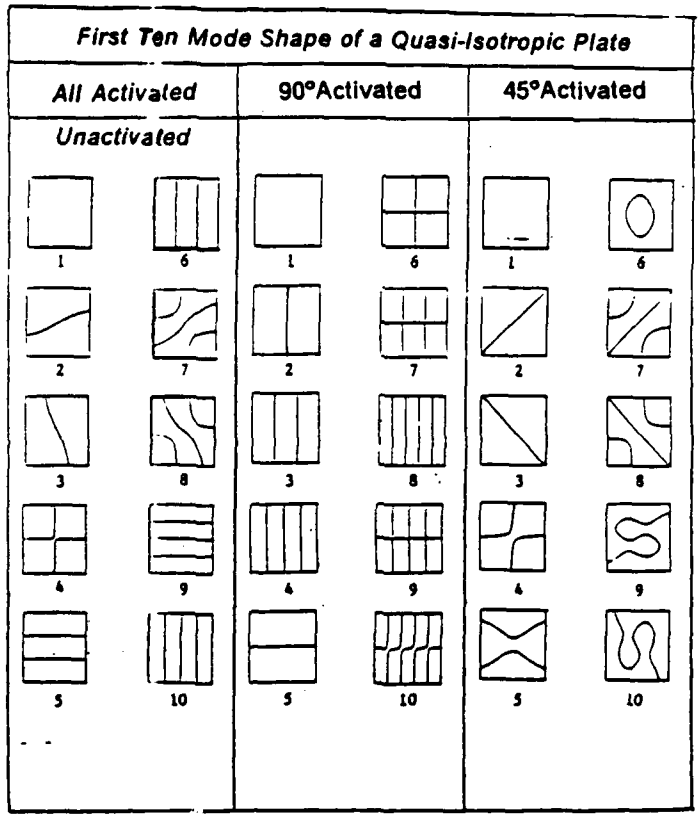

Figure 11. Comparison of Mode Shapes of Quasi-Isotropic Plates Using Active Strain Energy Tuning

Table 1. Natural Frequency of [+45°, −45°, 0°, 90°]$_s$ Plate Using Active Strain Energy Tuning

Mode	Unactivated Plate	Activated Plys				
		+45°	−45°	0°	90°	All
1	20	111	119	113	124	225
2	49	179	192	120	132	358
3	50	180	193	143	157	358
4	80	233	249	190	208	456
5	99	263	281	227	250	511
6	99	264	281	234	258	512
7	129	305	326	252	277	587
8	129	312	330	260	285	588
9	167	360	382	287	315	674
10	168	360	382	345	378	676

of fiber volume fraction on the variation of the first four natural frequencies when all layers of the plate are activated (recall that the second and third mode of a quasi-isotropic plate are essentially degenerative, hence only three lines for the four modes in Fig. 12). The first mode for 0.1% fiber volume fraction is approximately four times greater than the unactivated plate. The fourth natural frequency is more than a factor of two greater than unactivated plate. Figure 12 indicates that embedding relatively small amounts of SMA fibers in conventional composites, (i.e., graphite/epoxy or glass/epoxy), could prove to produce significant variations of the natural frequencies.

EXPERIMENT

Experimental Procedure and Apparatus

A nitinol reinforced fiber-glass beam was fabricated at the Composite Materials and Structures Fabrication Center at VPI&SU. The beam was made of mainly 90 degree plys to minimize the natural frequency of the beam. Thin strips of zero degree plys were appropriately placed in the lay-up to create open channels along the neutral axis of the beam. Teflon fibers, the same size as the nitinol wire, were placed in the channels during the lay-up proceedure so that the epoxy in the fiber-glass would flow around the teflon fibers during the cure cycle to create circular sleeves along the entire length of the beam. After the cure cycle, the teflon fibers were removed from the beam and plastically elongated nitinol wires were inserted in the sleeves. A 2.25 x .125 x 36 inch nitinol reinforced fiber-glass beam was created in this fashion with six nitinol wires accounting for 1.6% of the volume of the beam. The nitinol used had an austenite finish temperature of 63°C and a diameter of 0.031 inches.

The SMA composite beam was clamped at both ends so that it would vibrate out of the gravitional field. The nitinol wires were also clamped at both ends of the beam to prevent them from returning to their original length (memory shape). A mass was added at the center of the composite beam to lower the natural frequency. A schematic of this set-up and other apparatus is shown in Fig. 13.

A fiber optic sensor was used in this set-up to sense the dynamic response in the composite beam. A length of Andrew type 48280-1-P fiber was threaded through a sleeve in the beam and epoxied at both ends. When this elliptical core fiber is excited at 633 nm by a linearly polarized HeNe laser, one polarization of the LP_{01} and the even LP_{11} mode are supported, resulting in the desired two lobe output pattern. Optical detection was accomplished using a Hamamatsu silicon pin diode, along with appropriate amplification and a.c. coupling circuitry.

A standard piezo-electric accelerometer was also used to take data to compare with the optical fiber data. Data was sampled in real time and an FFT was performed on the discrete data points so that the frequency components of the data could be examined and compared.

The actuators were heated by applying a constant current through the nitinol wires. Testing was done so that the beam had the same steady state temperature for each test. Six actuators were used in the first test. The beam was allowed to reach a steady state temperature and then data was taken using both the optical fiber and the accelerometer. Two actuators were then released from the clamping device. Current was applied through all six actuators giving the same steady state beam temperature as the previous test, but only four actuators were used. Again, the composite beam was allowed to reach steady state temperature before data was taken. Data for two and zero actuators was obtained in a similar manner.

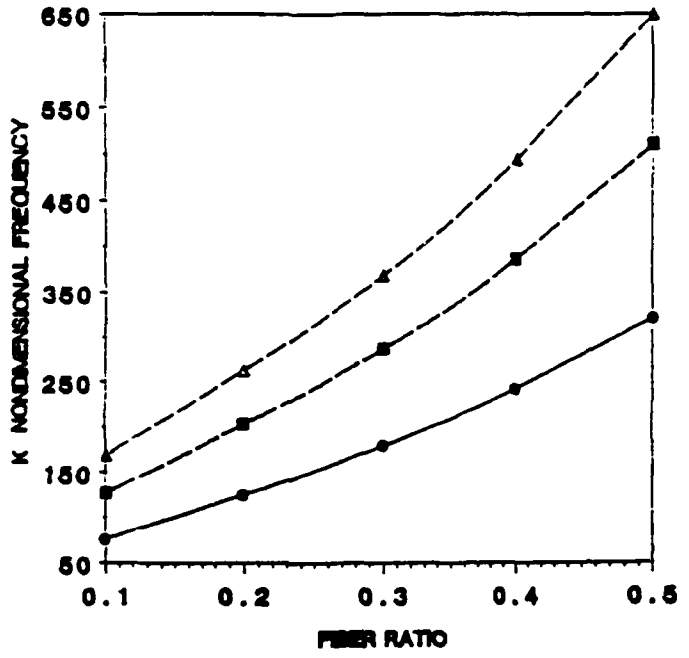

Figure 12. Variation of Natural Frequencies as a Function of Fiber Volume Fraction

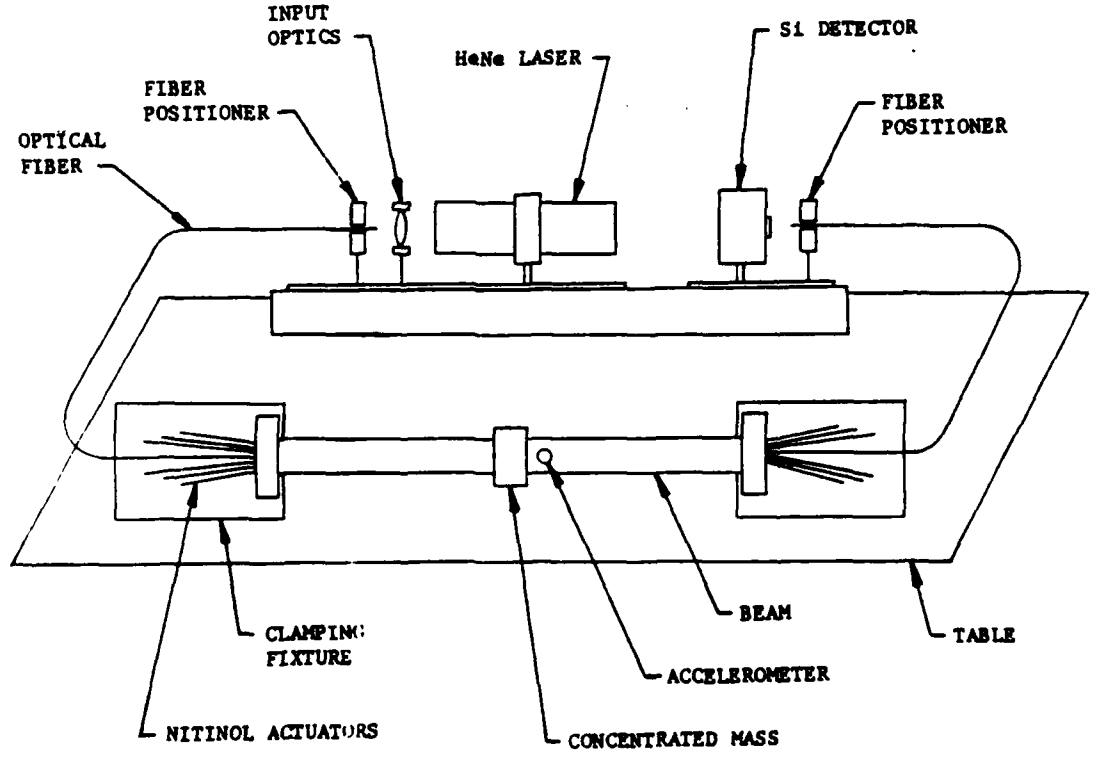

Figure 13. Experimental Apparatus

Results - Active Strain Energy Tuning (ASET)

Data was taken in real real time using both the optical fiber and the accelerometer. An FFT was then performed on the real time data. A comparison of the FFT's for both sensors, Fig. 14, shows good correlation at the natural frequency of the beam. The optical fiber data does, however, contain a much lower signal to noise ratio than the data obtained using the accelerometer. This is expected since the fiber optic sensor is a distributed sensor, and is capable of sensing vibrations in the longitudinal and lateral directions. The actual signal sensed is an integrated value over the entire sensor length and in all directions. The accelerometer, on the other hand, is a discrete sensor capable of sensing vibration in only one position and direction. The accelerometer is strategically placed to measure only the first mode lateral vibration of the beam and should therefor be expected to have a higher signal to noise ratio than the optical fiber. The optical fiber output also contains a d.c. offset. This explains the peak seen at low frequency below 0.5 Hz. A 2.2 and 5.0 Hz signal is contained in the data collected by the optical fiber but is not seen by the accelerometer. A plot of the FFT of the optical fiber data taken from a stationary beam, Fig. 15, also contains the 2.2 and 5.0 Hz signal. This confirms that these signals are not sensed within the beam, but are sensed along the length of the optical fiber outside the beam (refer to schematic of experimental apparatus, Fig. 13), and are regarded as ambient noise.

Active strain energy tuning was accomplished. The natural frequency of the composite beam was changed from 3.8 Hz, when six actuators were used, to 2.2 Hz, when no actuators were used. This can be seen in Figs. 16 and 17. Fig 18 shows the FFT of the data taken by the accelerometer when zero, two, four, and six actuators are used. All four cases are shown on the same plot for comparison. The mechanism for active strain energy tuning is the increased strain in the nitinol wires upon heating. When the wires are heated above 63°C (the austenite finish temperature), the wires try to contract to their original length. Because the nitinol wires are constrained from returning to their original length, strain is effectively added to the wires even though no change in length has occured. When the temperature of the nitinol is below 63°C, there is no strain in the wire. The nitinol wires can therefor be used as actuators to modulate the amount of strain energy in the composite beam. Increased strain energy has the effect of increasing the natural frequency of the beam. The natural frequency of the composite beam when no actuators are used was extracted from the frequency domain of the FFT and, using classical lumped parameter methods, can be used to calculate the spring rate of an un-actuated beam. Elastic spring theory is used to calculate the spring rate of an individual nitinol wire, assuming 75 lb tension in an actuated wire. Predicted values of frequency were calculated assuming actuators act as springs in parallel with the spring rate of the composite beam with no actuators used. These values are tabulated and compared with actual experimental results and pesented in Table 2.

CONCLUSIONS

Active Strain Energy Tuning shows much promise for active structural control and can be designed to have much greater authority than Active Modal Modification. However, several problems have been identified with developing the material with active strain energy tuning capabilities. It is clear that active strain energy tuning and active modal modification represent two new concepts towards active control of structural responses and may act as a catalyst for future developments in both material and structures technology. Demonstrating, even computationally, the ability to change the effective stiffness, natural frequencies and mode shapes of plates will hopefully inspire new material/structural interaction paradigms.

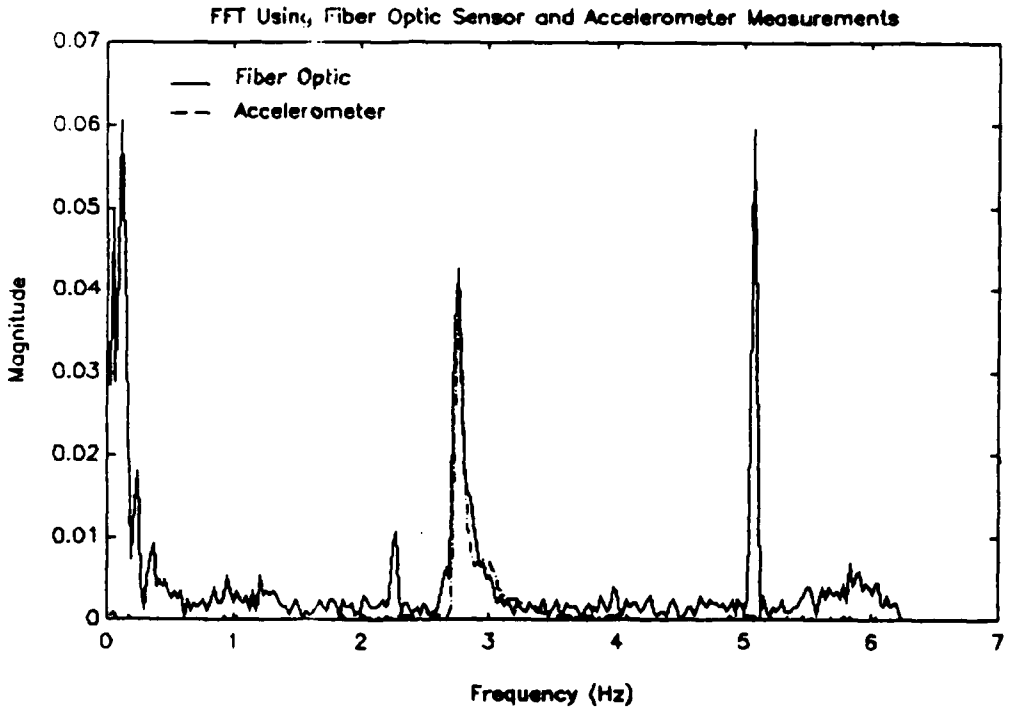

Figure 14. Comparison of Optical Fiber Measurement to Accelerometer Measurements

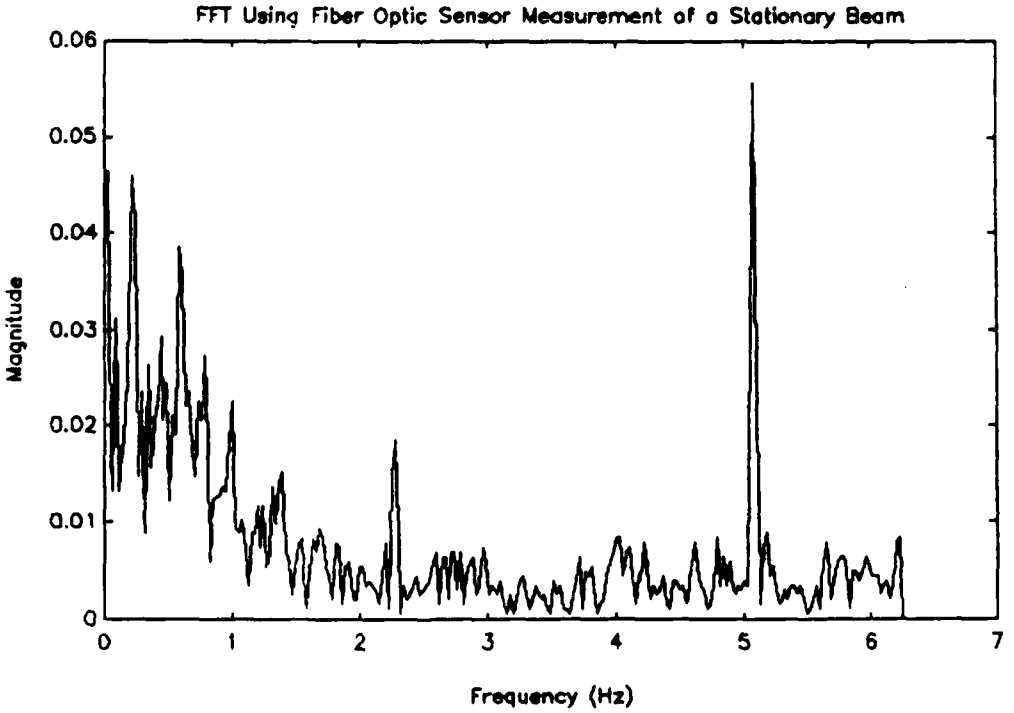

Figure 15. Noise Signals in Optical Fiber Measurement of a Stationary Beam

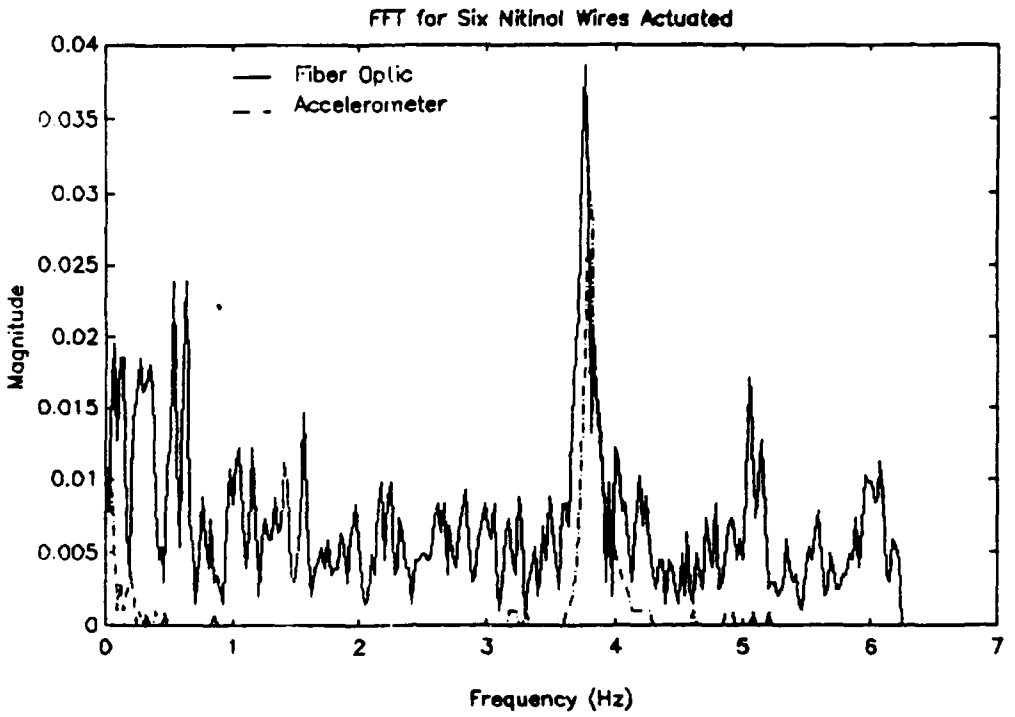

Figure 16. Natural Frequency of SMA Composite Beam Using Six Actuators

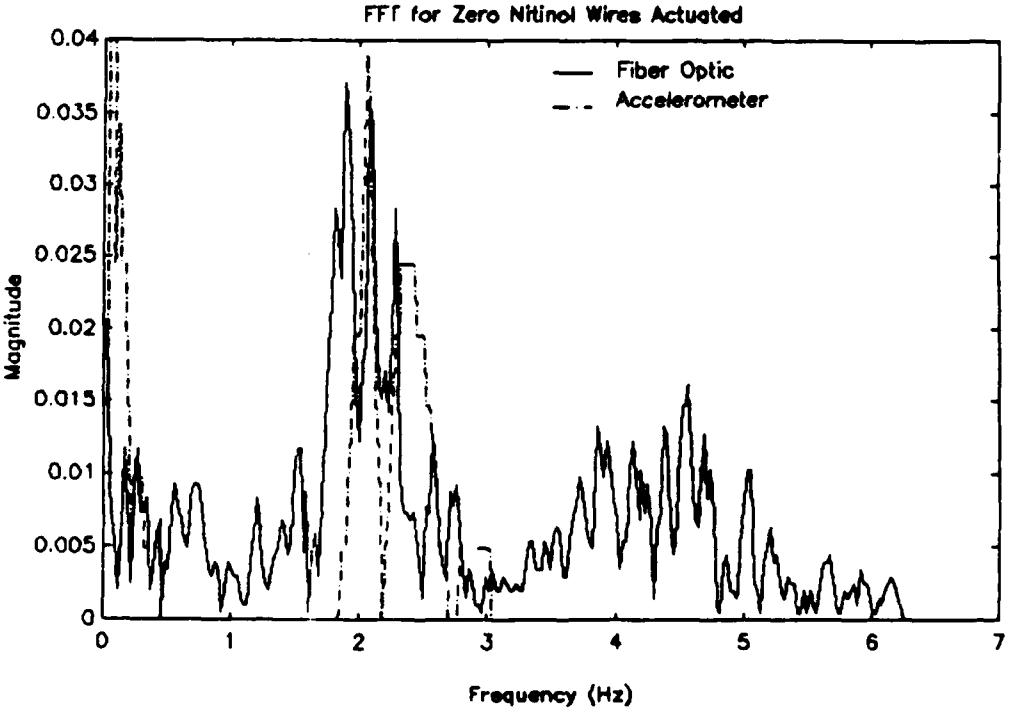

Figure 17. Natural Frequency of SMA Composite Beam With No Actuators

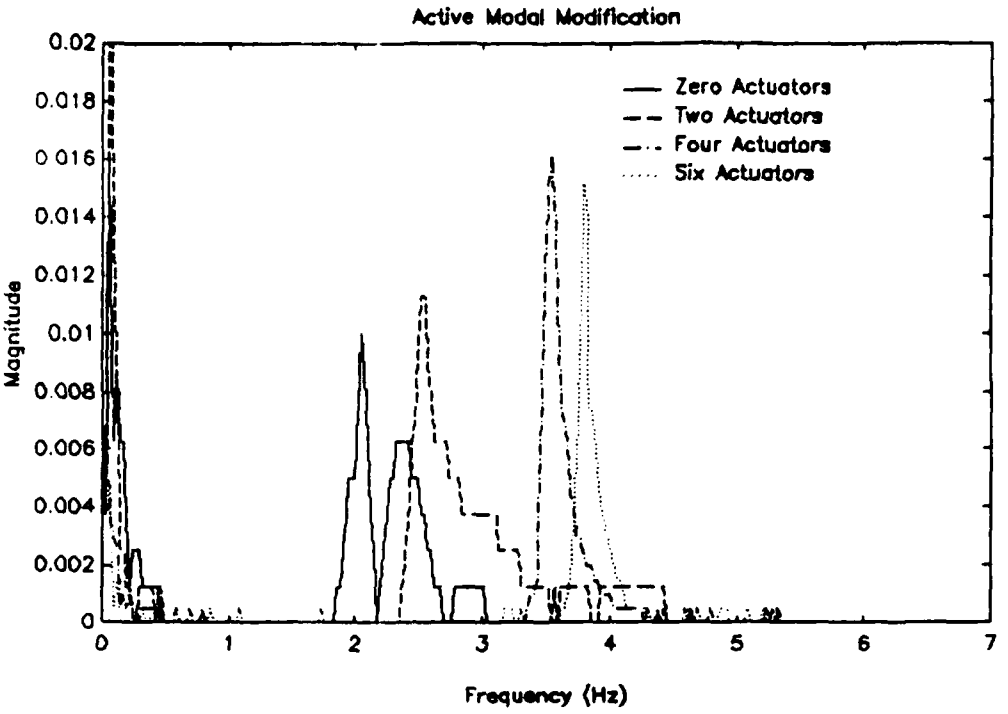

Figure 18. Natural Frequencies of SMA Composite Beam With Zero, Two, Four, and Six Actuators

Table 2. Comparison of Theoretical and Experimental Normalized Natural Frequencies of SMA Composite Beam

NO. OF ACTUATORS	NORMALIZED RESONANT FREQUENCY	
	PREDICTED	ACTUAL
0	1.00	1.00
2	1.13	1.18
4	1.24	1.64
6	1.35	1.73

ACKNOWLEDGEMENTS

The author respectfully acknowledges the support for this research effort by the Virginia Center for Innovative Technology, U. S. Nitinol, and the Office of Naval Research Young Investigator Program.

REFERENCES

1. Rogers, C. A., and H. H. Robertshaw, "Shape Memory Alloy Reinforced Composites," *Engineering Science Preprints 25*, ESP25.88027, Society of Engineering Sciences, Inc., June 20-22, 1988.

2. Buehler, W. J., and R. C. Wiley, "Nickel-Base Alloys," U. S. Patent 3,174,851, March 23, 1965.

3. Wayman, C. M., and K. Shimizu, "The Shape Memory ('Marmem') Effect in Alloys," *Metal Science J.*, Vol. 6, 1972, p. 175.

4. Perkins, J., ed., *Shape Memory Effects in Alloys*, Plenum Press, New York, 1975.

5. Goldstein, D., "A Source Manual for Information on Nitinol and NiTi," Naval Surface Weapons Center, Silver Spring, Maryland, Report NSWC/WOL TR 78-26, 1978.

6. Schetky, L., "Shape Memory Alloys," *Scientific American*, Vol. 241, 1979, p.74.

7. Jackson, C. M., H. J. Wagner, and R. J. Wasilewski, "55-Nitinol - The Alloy with a Memory : Its Physical Metallurgy, Properties, and Applications," *NASA-SP-5110*, 1972, 91 p.

8. Delaey, R. V., H. Tas Krishnan, and H. Warlimont, "Thermoelasticity, Pseudoelasticity and the Shape Memory Effects Associated with Martensitic Transformations," *Journal of Material Science*, Vol. 9, 1974, pp. 1521-1545.

9. Saburi, T., and C. M. Wayman, "Crystallographic Similarities in Shape Memory Martensites," *Acta Metallurgica*, Vol. 27, 1979, p. 979.

10. Cross, W. B., A. H. Kariotis, and F. J. Stimler, "Nitinol Characterization Study," *NASA CR-1433*, Sept. 1969.

11. Rogers, C. A., and H. H. Robertshaw, "Development of a Novel Smart Material," *Proceedings of the ASME 1988 Winter Annual Meeting*, November 28 - December 2, 1988 (in publication).

12. Rogers, C. A., and Liang, Chen, "Active Modal Modification of Quasi-Isotropic Shape Memory Alloy Reinforced Plates," *Proceedings of the 30th Structures, Structural Dynamics and Materials Conference*, Mobile, Al, april 3-5, 1989 (submitted for review)

13. Whitney, J. M., *Structural Analysis of Laminated Anisotropic Plates*, Technomic Publishing Co., Lancaster, PA, 1987.

OPTICAL FIBER SENSORS AND SIGNAL PROCESSING FOR SMART MATERIALS AND STRUCTURES APPLICATIONS

R.O. Claus, J.C. Mckeeman, R.G. May, and K.D. Bennett
Fiber and Electro-Optics Research Center
Virginia Tech
Blacksburg, VA 24061

ABSTRACT

Optical fiber sensors are one of the candidate sensor technologies for applications in smart materials and structures. The potential advantages of such sensors are their small size and low weight, EMI and EMP immunity, geometrical flexibility, large bandwidth, low power, multiple multiplexing options, and all-dielectric profile. Although fiber sensors may be attached to the external surfaces of structures, they also may be directly embedded within materials such as some advanced composites to provide in situ measurements of composite cure as well as a method for dynamic material evaluation during the normal use lifetime and degradation period of the material. During the past nine years, we have studied a number of fiber sensor methods based upon the measurement of optical intensity, phase, polarization, mode, time, and wavelength to determine strain, temperature, chemical concentration, resin cure, acoustic vibration, acoustic emission, crack propagation, and impact and battle damage. We have also considered inline optical signal processing techniques which improve the signal multiplexing and pre-processing capabilities of reviews the capabilities of both optical fiber sensors and optical fiber sensor signal processing for smart materials and structure applications.

1. INTRODUCTION

The desired complexity and missions of advanced aerospace, marine and transportation materials and structures demands the development of intrinsic analysis and control systems which are capable of independently optimizing structural properties in response to particular external disturbances. Materials and structures which incorporate environmental and material sensors, mechanical actuators, and electronic signal processing and adaptive control systems to produce either appropriate readouts or actuator responses for particular sensor inputs have been termed "smart," "intelligent," "sense-able" or "organic" during the past several years. The primary advantage of such materials and structures is that they may be designed to adapt to a wide range of conditions during their normal use lifetimes. Some types of sensors and actuators, particularly small and lightweight optical fiber sensors and shape memory metal actuators, may be directly embedded without seriously affecting material integrity. Additionally, the optical fibers embedded in such material systems may be used as life cycle sensors to monitor the way in which composite and metal structures are fabricated, the in service lifetime performance conditions of the material, and the

onset of material degradation due to a variety of causes including fatigue and impact damage.

Since 1979, sponsored research at Virginia Tech has led to the development of novel sensors, actuators and control system concepts for smart structure applications. To address the goals of this Workshop, this paper borrows heavily from this previous body of work [1] and reviews efforts directed at understanding 1) the micormechanics of materials which contain embedded sensor fibers, 2) the performance of optical fiber sensors for materials testing, and 3) multiplexing and signal processing issues.

2. MICROMECHANICS OF EMBEDDED MATERIAL SENSORS

Central to the smart structures scenario is the concept that optical fiber sensors, and fiber, wire or arrayed discrete element actuators, can be embedded within the structural material without compromising structural integrity. The incorporation of these devices into composite materials prior to cure potentially allows the subsequent in situ monitoring of the cure process as well as the internal application of local forces to enhance local mechanical conditions during cure. Such embedding is of course required if post-cure internal characterization of the material is to be realized.

Preferred optical sensor fiber orientation within multi-ply composite laminates is determined by the intended application of the sensor; Udd, Measures and their co-workers have considered fiber orientation specifically for the minimization of the resulting perturbation to the laminate [2] and the detection of impact damage via the observation of optical fiber breakage [3], respectively. Part of our recent related work at Virginia Tech has involved the design and fabrication of fibers and fiber coatings to improve the mechanical coupling between the core and cladding waveguide structure of the fiber and the composite matrix [4], and the modeling and direct measurement of the micromechanical effects resulting from fiber embedding [5]. Representative results of those measurements, obtained graphite/epoxy coupon containing a single 50/125 glass-on-glass optical fiber near its component parallel to the applied load. A series of measurements similar to these but obtained for different load levels on the composite specimen indicate strain concentration. Factors of approximately 4 at the fiber-to-matrix boundary for an applied load equal to half the failure load of the eight-ply specimens tested. These large interface strain concentrations may pose significant limits on the long term structural integrity of materials containing embedded sensor fibers.

3. OPTICAL FIBER SENSOR IMPLEMENTATION

Optical fiber sensors may be used to evaluate the internal properties of materials, and hence the performance of structures fabricated using those materials, during three periods of the birth-to-retirement lifetime of the structure which require very different sensor information. First, such sensors may be directly embedded in composite prepreg lay-ups and subsequently used to monitor composite cure. Second, embedded sensors may be used to monitor normal environmental factors such as strain, temperature and vibration. And third, the same sensors may in principle be capable of

determining the onset of material degradation. This section describes sensor implementations in each of these ways.

A. Fiber Sensors for Advanced Composite Cure Monitoring

Material cure or fabrication monitoring is the first application of internal sensors as part of complete life cycle testing. In situ fiber optic cure monitoring has been investigated for several years by Levy [6] who used distal end fiber components capable of indicating changes in both curing adhesive color and index of refraction. More recently, Afromowitz [7] has demonstrated the in-line adaptation of similar elements which can be addressed via through transmission in an optical fiber instrumentation system. Extensions of this type of sensor instrumentation may allow the distributed measurement of the index of the curing matrix material throughout large workpieces of varying thicknesses [8].

Our work in this area has been concentrated in the area of "sensitive-clad sensors" (SCS) which are capable of direct localized sensing of the cure process via the implementation of modified waveguide cladding/coatings. Glass-on-glass fibers are acid etched to remove the clad, then re-clad and coated with a layer or layers of appropriate polymers capable of effectively coupling to the glass core and interacting with the surrounding curing matrix in such a way that the wavelength transmission function of the "sensitive clad" region of fiber changes as a function of cure [4]. A simple sketch of a single SCS element is shown in Figure 2. The use of this type of sensor is intended to allow the in situ monitoring of reaction path throughout the cure process and throughout the workpiece.

Temperature, strain, and compaction pressure may be measured during materials processing using fiber sensor systems similar to the interferometric configuration shown in Figure 3. Analysis indicates that for shot noise limited detector performance, a 1.0hz bandwidth, and reasonable laboratory equipment parameters, the minimum detectable strain is on the order of micro-strain per centimeter of fiber sensor length [9]; this demonstrates the excellent sensitivity of interferometric fiber sensor devices. Although conventional interferometric fiber sensor designs are impeded by indistinguishable multiparameter influences on output signal response, alternative configurations which we have studied avoid such problems by compensated mechanical designs or post-detection signal processing [10,11].

B. Strain, Vibration and Stress Wave Sensing

The in-service mechanical performance of materials fabricated with internal sensors may be evaluated using those sensors. Many authors have considered the development of optical fiber sensors for this type of evaluation [12]. Our group has specifically placed most emphasis on the research of optical time domain and fiber modal domain sensor systems, system components, and their evaluation.

Optical time domain reflectometry (OTDR) techniques may be used to measure both distributed and localized strain in structures [13]. Our efforts here include both amplitude and time measurement methods. Our early work utilized the principle of transmitted optical power attenuation due to the localized bending of optical fibers embedded within composite materials [14,15]. Because the spatial transient distance of most optical fibers is larger than the desired spatial resolution, this OTDR method is not applicable to high resolution system implementation which may be necessary in some smart skins applications.

Alternatively, partially reflecting splices may be inserted along the length of a sensor fiber and OTDR methods used to determine the time of arrival of the optical pulses reflected from each splice [16]. Since position changes in such splices produce variations in the times of arrival of the pulses from the splices, observation of the time dependent arrival times yields the distributed strain. Extensions of the use of basic in-line splices for the measurement of strain between adjacent splices are 1) the multiplexing of a network of fiber sensor arms with adequate time delay length fibers between the arms to permit time domain separation of back reflected pulses and subsequent resolution of two-dimensional strain distributions (Figure 4), 2) the use of fiber-to-fiber intensity coupling loss in a single strained splice housing to determine strain localized to the vicinity of the housing, and 3) the low-profile packaging of in-line splices to permit the embedding of such sensors within advanced composite materials [17].

Another sensor method developed for the in-service lifetime monitoring of materials monitors the interference between two or more modes in a few mode fiber [18]. We have applied such sensors to the detection of quasi-static strain, low frequency structural vibrations and relative high frequency stress waves [19]. For the evaluations of structural vibrations such as those of the panel shown in Figure 5, it can be shown that the output signal from a modal domain sensor may be interpreted to yield the mode shape amplitudes of the vibrating structure's mechanical response [20]. This type of response is essential for the type of vibration damping control described below.

Modal sensing has also been applied to the detection of stress waves generated by acoustic emission (AE) events in mechanically loaded graphite/epoxy specimens. As shown in the fiber-detected AE event shown in Figure 6, the observed risetime of such systems is on the order 1.0 microsecond [21].

4. OPTICAL FIBER SENSOR MULTIPLEXING AND SIGNAL PROCESSING

Although the internal evaluation of materials and the distributed characterization of structures is an attractive concept in principle, sensor signal multiplexing and processing limits the spatial resolution of the embedded or attached sensor network. Damage detection in advanced composites, for example, would require spatial resolution perhaps as high as one measurement for every square millimeter of surface area [22], and thus would place a significant demand on signal processing hardware and/or software. Several damage detection systems have been proposed. Early work by Crane and coworkers [23] and recent work by Measures and coworkers [3] relies upon the internal breakage of fibers embedded in an array to locate regions of impact damage or excessive local strain. Signal processing suggested by this work includes the visual observation of a number of illuminated and non-illuminated fiber ends, the use of a multi-element optical detector to perform the same observation, or the visual inspection of light leakage from fiber break locations in transparent or translucent materials.

For quantitative sensing of the type of impact shown in Figure 8, we have investigated the use of in-line fiber signal processing elements such as the one shown in Figure 9 [24]. Here, 2x2 biconical fused tapered couplers having different s-parameters are interconnected in such a way as to yield a single valued output intensity to indicate the three-dimensional location of damage. Since such processors operate as fast as the light signals can propagate through the coupler system, their use is especially attractive

for structural analysis systems requiring good spatial resolution and minimal processing time.

5. SENSORS, ACTUATORS AND STRUCTURAL CONTROL

Recent work at Virginia Tech has stressed the incorporation of fiber sensors with actuators in a material structure which can be controlled via external electronics. Current research includes the evaluation of the type of beam shown in Figure 9 containing both optical fiber modal sensors and distributed resistive strain gauges to verify fiber system outputs. The sensor output signals are used as inputs to the control system electronics developed by implementing a polynomical model of beam response. In a companion paper presented at this ARO Workshop [24], the performance of both this system and that of a beam containing both embedded fiber sensors and nitinol wire actuators are described [25].

6. SUMMARY

The area of smart skins includes elements from a number of disciplines. Since 1979 the smart skins research and teaching program at Virginia Tech has involved basic analysis and development of 1) optical fiber sensors for cure monitoring, in-service lifetime structural testing, and nondestructive evaluation of gradual material degradation, 2) fiber sensor multiplexing and signal processing demanded by such systems, and 3) the integration of embedded sensors, actuators and control electronics to affect structural control systems.

7. ACKNOWLEDGEMENTS

This research has been supported in particular by sustained cooperation from the NASA-Langley Research Center, Hercules Aerospace and the Virginia Center for Innovative Technology. Additional related support has been provided by contracts, grants and agreements from General Dynamics, Lockheed, McDonnell Douglas, Grumman, Litton, Martin Marietta and other companies.

8. REFERENCES

[1] R.O. Claus, A. Safaai-Jazi, K.D. Bennett, R.G. May, B.D. Duncan and A.M. Vengsarkar, Proc. Review of Quantitative NDE (La Jolla, CA), August 1988.

[2] E. Udd, NASA Workshop on Nondestructive Evaluation (Cocoa Beach, FL), December 1987.

[3] R.M. Measures, Review of Progress in Quantitative NDE (La Jolla, CA), August 1988.

[4] C. DiFrancia, "Sensitive Clad Fiber Optic Sensors," M.S. Thesis, Virginia Tech, 1987.

[5] R. Czarnek, Y.F. Guo, K.D. Bennett and R.O. Claus, Proc. SPIE O-E Fiber Lase (Boston, MA), September 1988.

[6] R.L. Levy and S.D. Schwab, Polym. Mat. Sci. Engr. 56, 169-174 (1987).

[7] M.A. Afromowitz, Proc. Optical Fiber Sensors Conf. (New Orleans, LA), January 1988.

[8] M.A. Afromowitz, Review of Progress in Quantitative NDE (San Diego, CA), August 1988.

[9] C.D. Butter and G.B. Hocker, Applied Optics 17, 2867-2869 (1978).

[10] A. Vengsarkar, K.A. Murphy, C.J. Chung and R.O. Claus, Review of Progress in Quantitative NDE (San Diego, CA), August 1988.

[11] A. Vengsarkar, K.A. Murphy, C.J. Chung, and R.O. Claus, Proc. SPIE O-E Fiber Lase (Boston, MA), September 1988.

[12] NASA Workshop on Intelligent Materials and Structures, NASA Langley Research Center, February 1987.

[13] B.S. Jackson, K.D. Bennett and R.O. Claus, Proc. SPIE Conf. (San Diego, CA), August 1985.

[14] B.S. Jackson, "Optical Time Domain Reflectometry as a Nondestructive Evaluation Technique for Composite Materials," M.S. Thesis, Virginia Tech, 1984.

[15] R.O. Claus and K.D. Bennett, Opt. Soc. Am. Natl. Mtg. (Washington, DC), October 1985.

[16] B.D. Zimmermann, K.A. Murphy and R.O. Claus, Proc. Review of Progress in Quantitative NDE (Williamsburg, VA), June 1987.

[17] R.O. Claus, S. Sudora, K.A. Murphy and K.D. Bennett, Proc. Review of Progress in Quantitative NDE (San Diego, CA), August 1988.

[18] K.D. Bennett and R.O. Claus, Proc. IEEE Ultrasonics Symp. (Williamsburg, VA), November 1986.

[19] P.A. Ehrenfeuchter and R.O. Claus, Proc. 20th Intl. Symp., Intl. Metallographic Soc. (Monterey, CA), July 1987.

[20] R.O. Claus and R.E. Rogers, Proc. SENSORS EXPO (Detroit, MI), September 1987.

[21] K.D. Bennett, R.O. Claus and M.J. Pindera, Proc.Rev. Quant. NDE Conf., (San Diego, CA), August 1986.

[22] G. Sendeckyj, NASA Workshop on Intelligent Materials and Structures, NASA-Langley Research Center, February 1987.

[23] R.M. Crane, A.B. Macander and J. Gagorik, Proc. Review of Progress in Quantitative NDE, 1983.

[24] C.A. Rogers, Proc. ARO Workshop on Smart Materials, Structure and Mathematical Issues (Blacksburg, VA), September 1988.

[25] C.A. Rogers, D.H. Barker, K.D. Bennett, and R.H. Wynn Jr., Proc. SPIE O-E Fiber Lase (Boston, MA), September 1988.

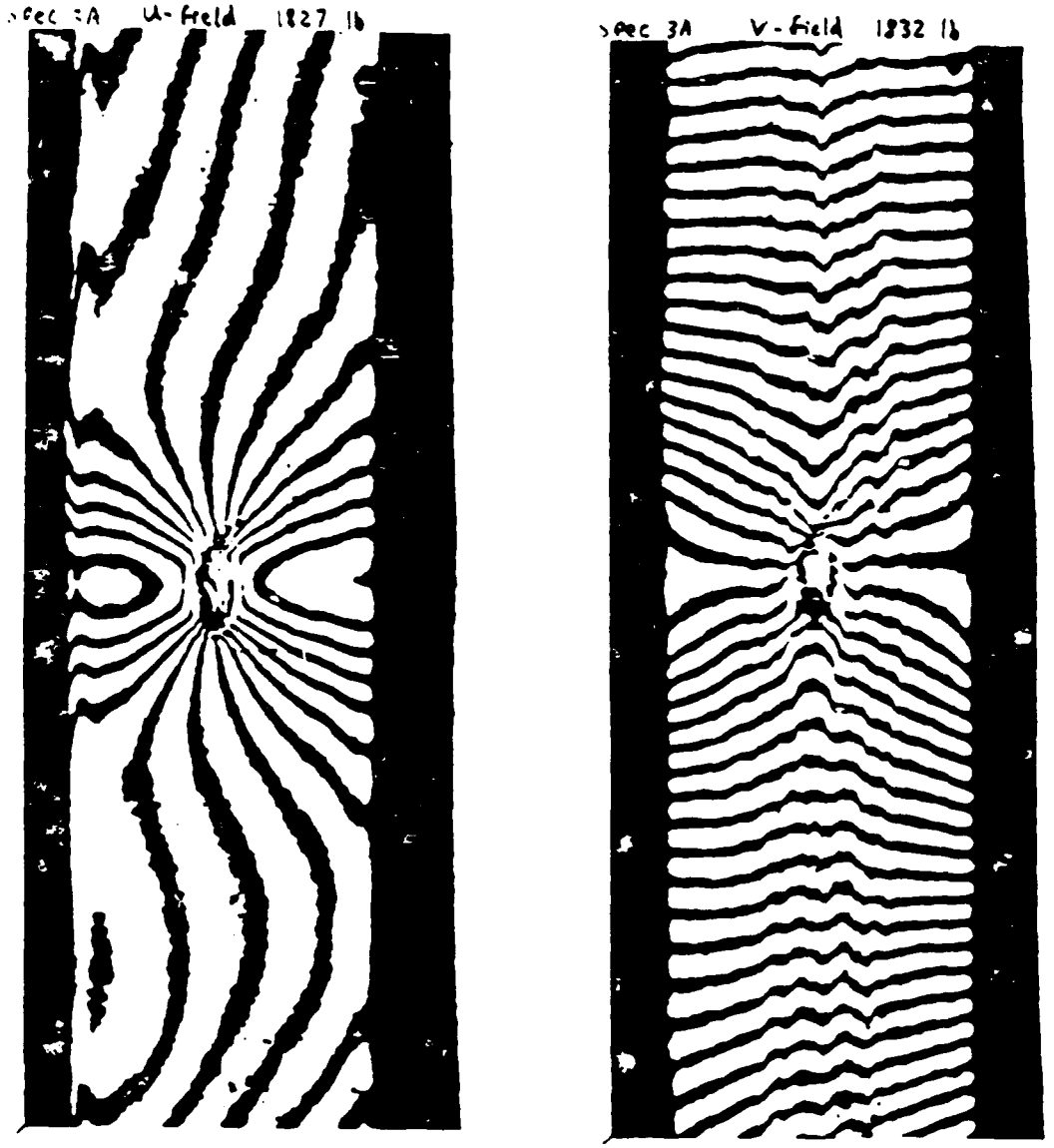

Figure I. U and V dispalcement fields in fiber-embedded composite laminate [5].

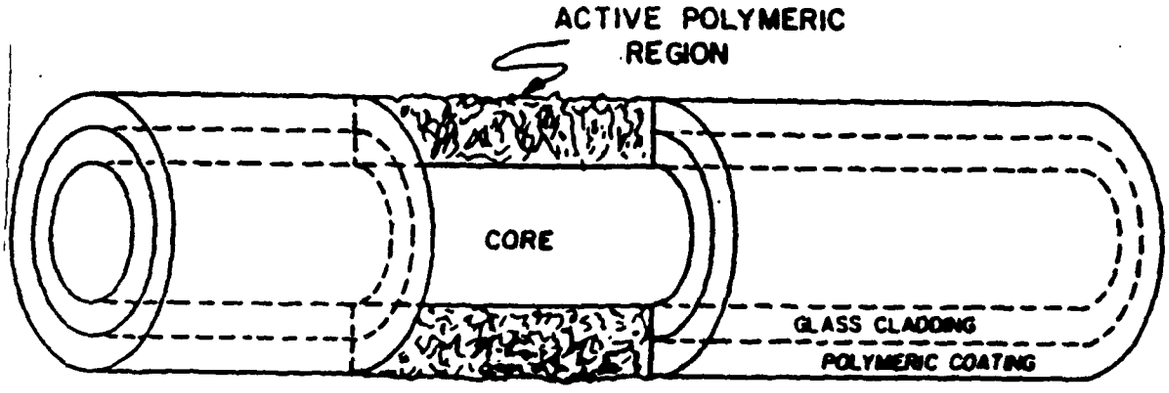

Figure 2. Sensitive clad sensor element [4].

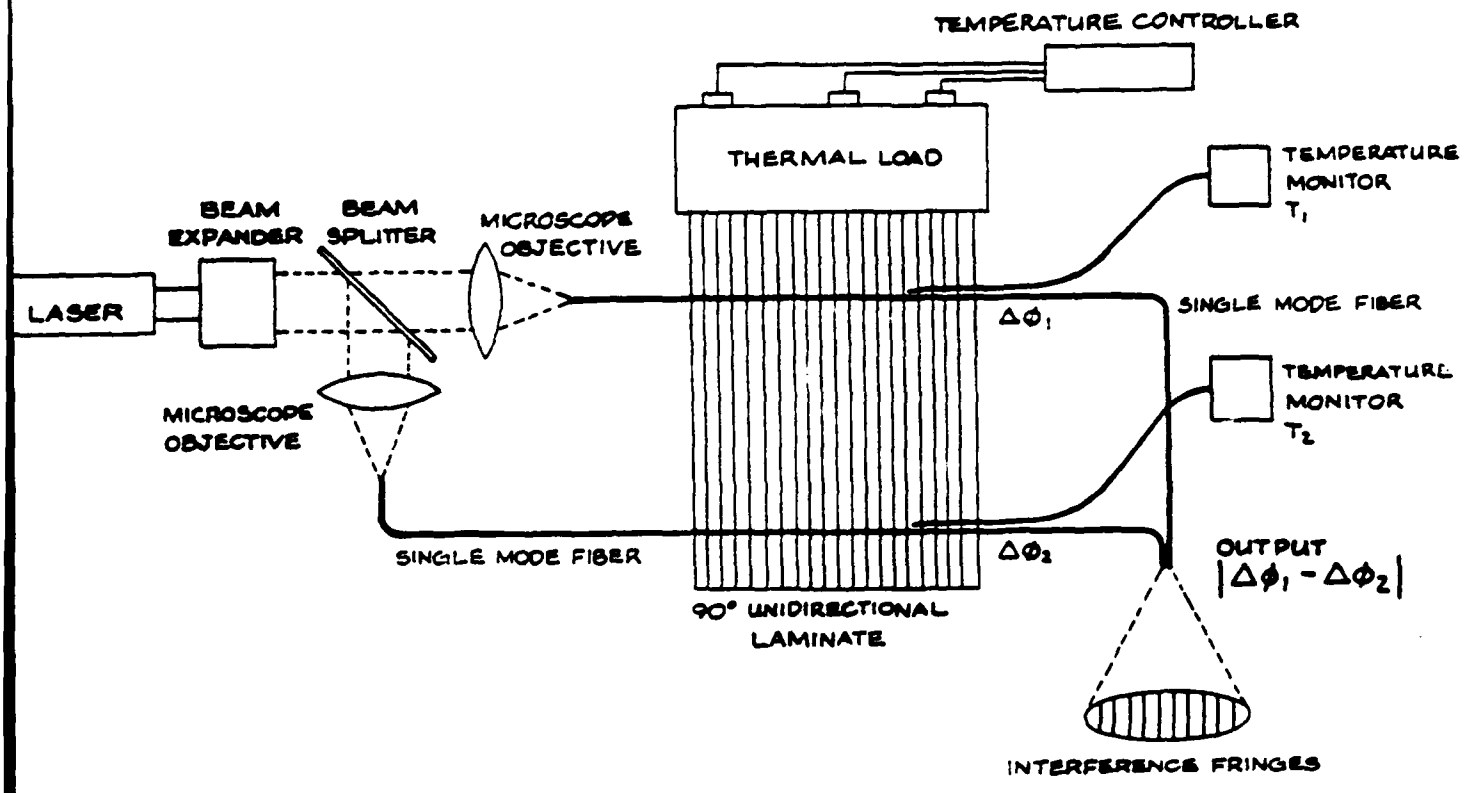

Figure 3. Interferometric fiber system for sensing of heat flow in composites [24].

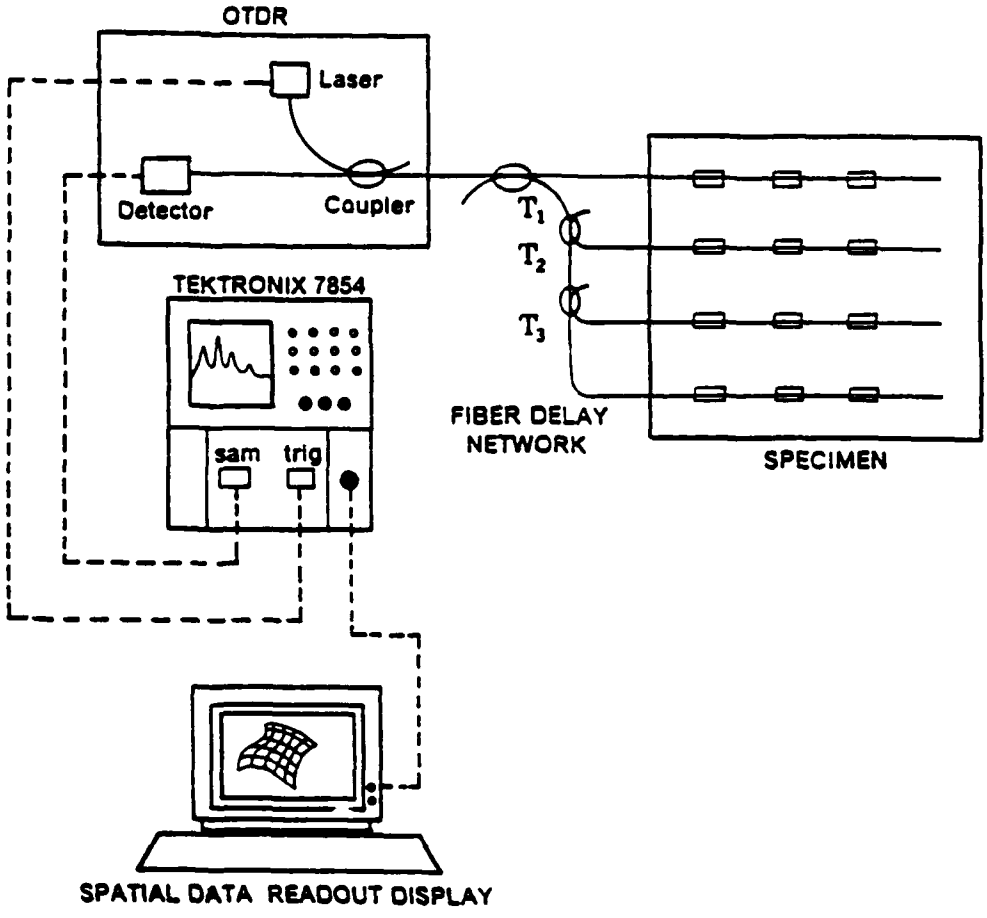

Figure 4. Distributed OTDR sensor system [16]

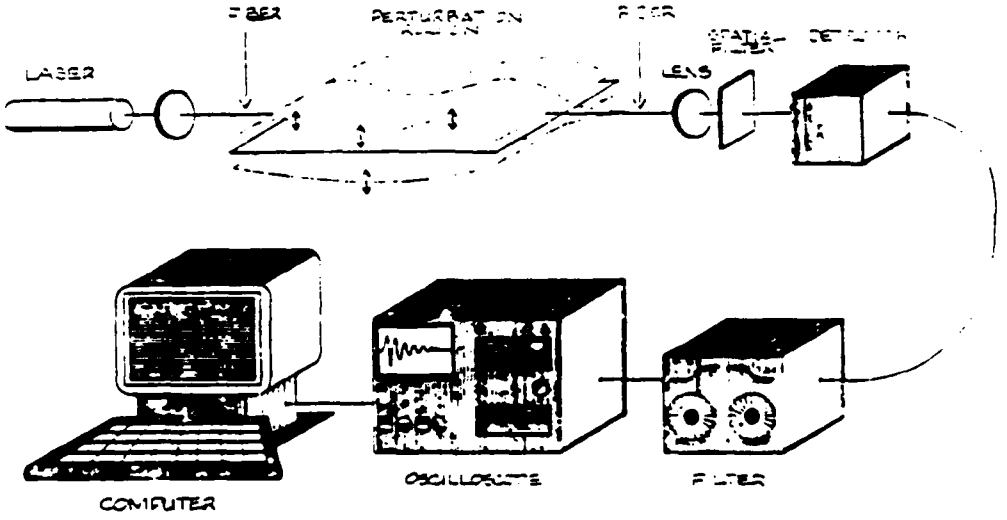

Figure 5. Modal domain sensor system for vibrational mode shape analysis [19].

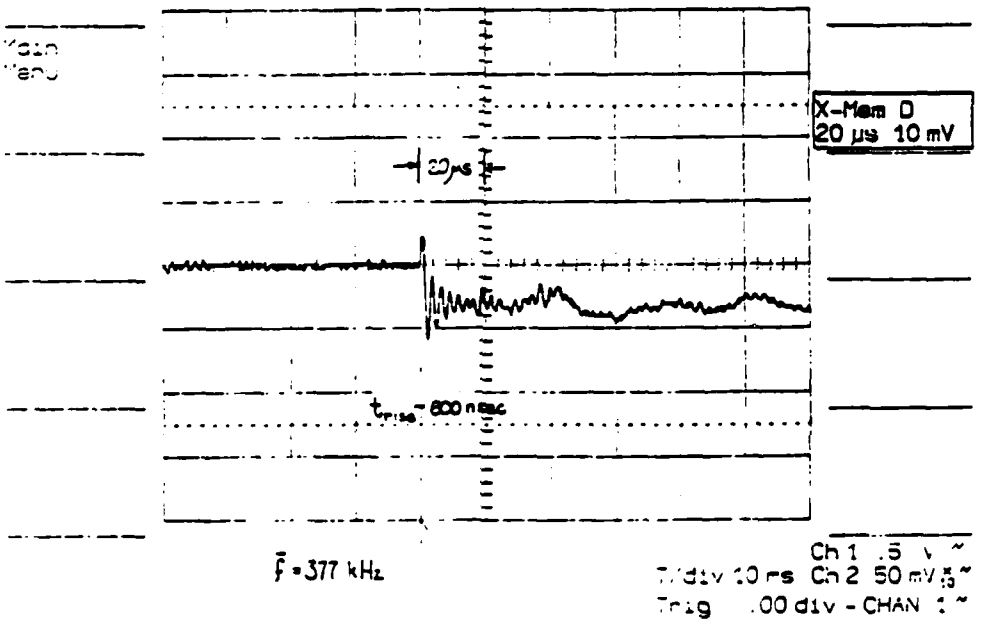

Figure 6. Fiber-detected AE event in loaded graphite-epoxy laminate [21].

EMBEDDED FIBER SENSOR ARRAY FOR IMPACT ANALYSIS

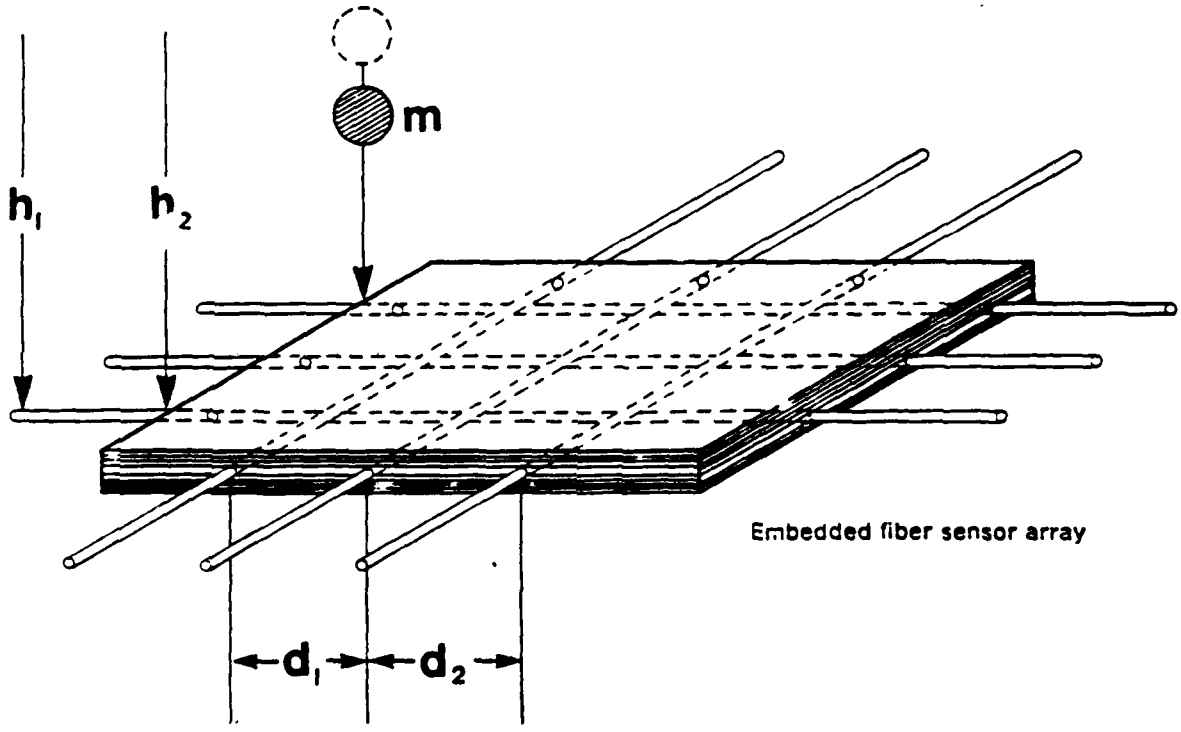

Figure 7 Embedded fiber array for three-dimensional damage detection [24]

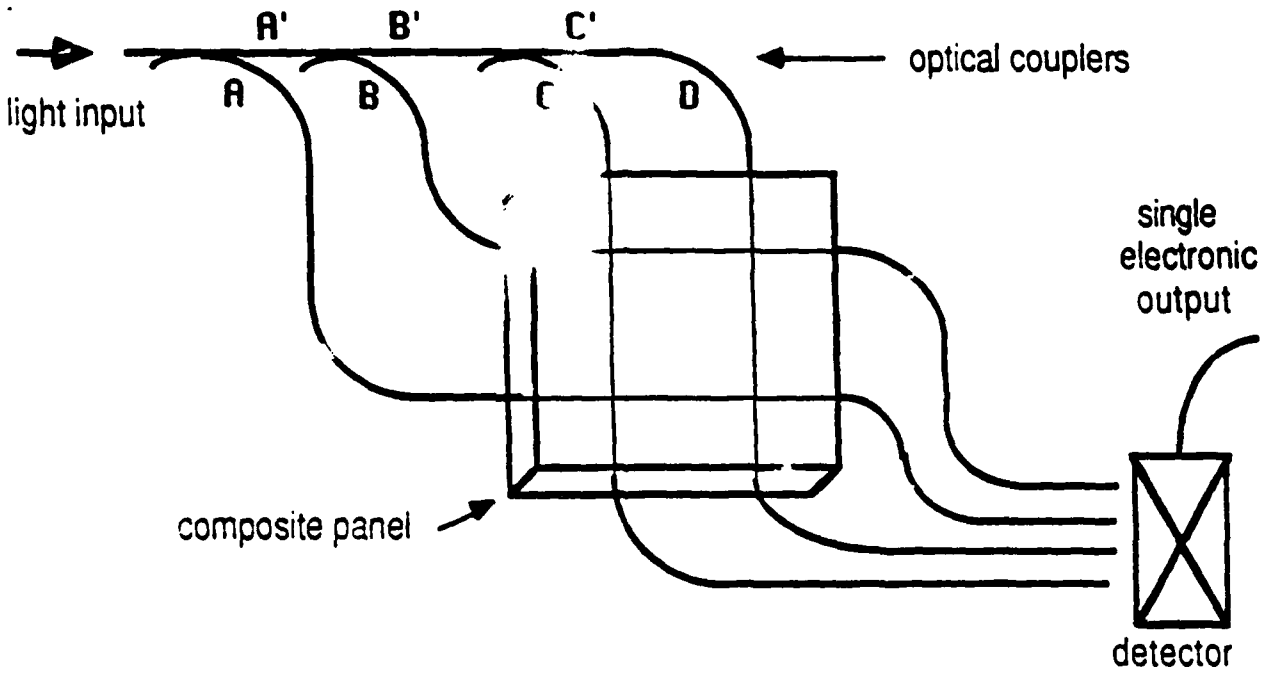

Figure 8. In-line fiber signal processor [24].

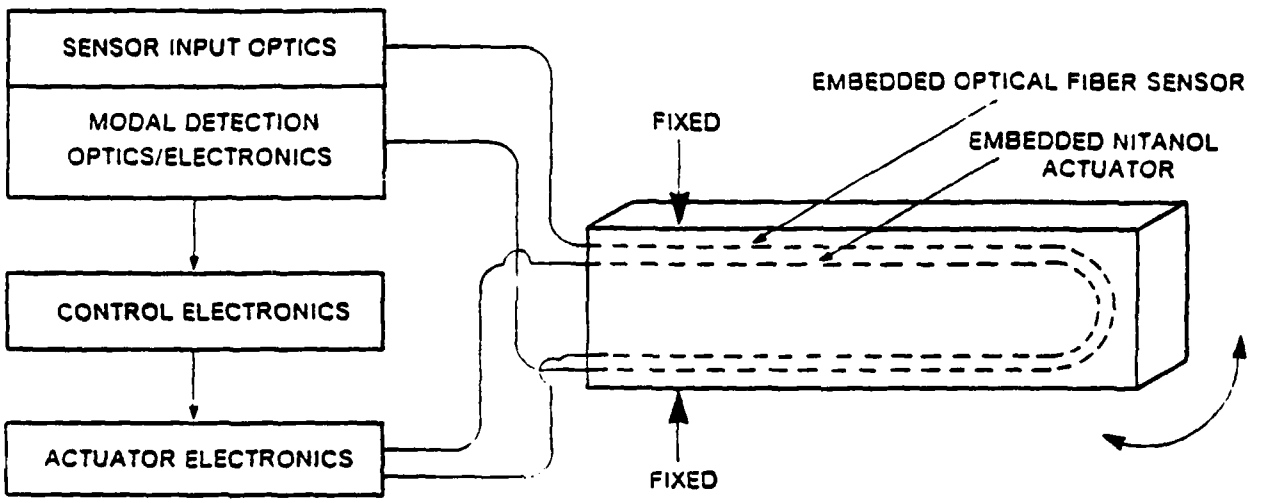

Figure 9.- Smart composite beam consisting of sensor, actuator and control electronics [23].

A NEW GENERATION OF REVOLUTIONARY ULTRA-ADVANCED INTELLIGENT COMPOSITE MATERIALS FEATURING ELECTRO-RHEOLOGICAL FLUIDS

by

M.V. Gandhi and B.S. Thompson
Intelligent Materials and Structures Laboratory
Composite Materials and Structures Center
Michigan State University
East Lansing, MI 48824-1326

ABSTRACT

A new generation of revolutionary, intelligent, ultra-advanced composite materials featuring electro-rheological fluids is presented herein for the active continuum vibration-control of structural and mechanical systems. These ultra-advanced composite materials capitalize on the superior characteristics of advanced composite materials which are interfaced with dynamically-tunable ER fluids contained in voids in the advanced composite structure. Changes in the electrical field imposed upon the electrorheological fluids can dramatically alter the rheological characteristics of the fluids and hence the global mass, stiffness and dissipative characteristics of the ultra-advanced composite structures. The instantaneous response-time of the ER fluids and the inherent ability of these materials to interface with solid-state electronics and modern control systems provides designers, for the first time, with a unique capability to synthesize ultra-advanced intelligent composite structures, whose continuum electro-elastodynamic response can be actively controlled in real-time. The revolutionary capabilities of these materials can be exploited by integrating fundamental phenomenological theories with intelligent sensor technologies and modern control strategies in order to significantly accelerate the evolution of this innovative class of multi-functional, dynamically-tunable, ultra-advanced, intelligent composite materials for military, aerospace, and advanced manufacturing applications.

PREFACE: BACKGROUND ON ELECTRO-RHEOLOGICAL FLUIDS

Electro-rheological (ER) fluids are typically suspensions of micron-sized hydrophilic particles suspended in suitable hydrophobic carrier liquids, which undergo significant instantaneous reversible changes in material characteristics when subjected to electrostatic potentials. The most significant change in the material characteristics of an ER fluid is associated with the bulk viscosity of the suspension, which varies dramatically upon applying an electrical field to the fluid. The tailoring of

this rheological property by the imposition of a suitable electrical potential can be usefully exploited in vibration-control applications. Figure 1 presents photomicrographs of an ER fluid subjected to electrical field intensities of 0 kV/mm and 2 kV/mmm respectively. The current levels associated with the high voltage states are typically in the order of a few micro-amperes, consequently, the power consumption is minimal.

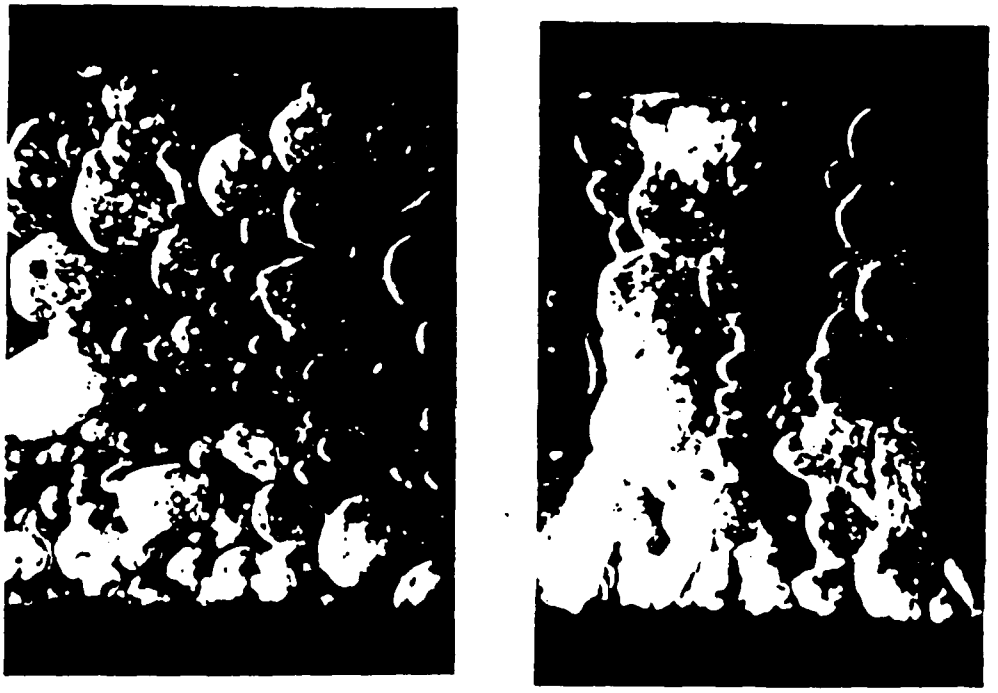

Figure 1. Photomicrograph of ER fluid microstructure at two discrete voltage states.

PREVIOUS WORK: PROOF-OF-CONCEPT STUDIES

Experimental investigations have been undertaken by the authors by employing hollow cantilevered beams fabricated with graphite-epoxy prepreg material filled with various electro-rheological fluids. Typical experimental results are presented in Figure 2 for two discrete voltage states. The dramatic difference in the two elastodynamic response characteristics clearly demonstrates for the first time the viability of the proposed concept of employing ultra-advanced intelligent composite materials for vibration control applications.

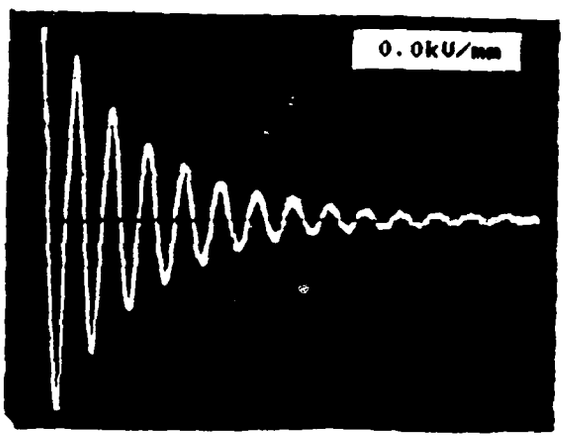

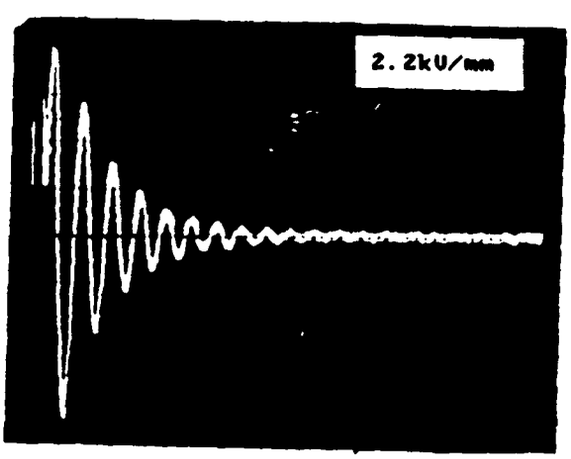

Figure 2. Experimental results demonstrating the controllability of beam vibrations by employing constant voltage fields on smart materials incorporating ER fluids.

The real-time controllability of this revolutionary class of intelligent ultra-advanced composite materials employing variable time- histories of the voltage field is demonstrated in Figure 3.

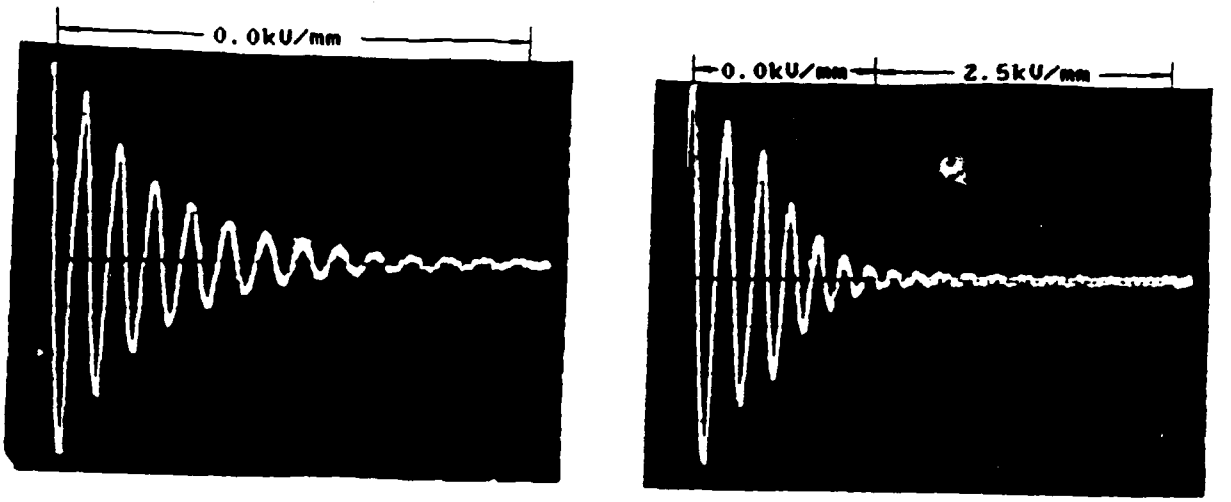

Figure 3. Experimental results demonstrating the controllability of beam vibrations by employing time-dependent variable voltage fields on smart materials incorporating ER fluids.

MOTIVATION

The preliminary research being undertaken in the Intelligent Materials and Structures Laboratory (IMSL) and the Composite Materials and Structures Center (CMSC) at Michigan State University is a coherent experimental and theoretical program of basic research on a revolutionary class of ultra-advanced intelligent composite materials incorporating electro-rheological (ER) fluids for active continuum vibration control applications. These ultra-advanced composite materials capitalize on the superior characteristics of advanced composite materials which are interfaced with dynamically-tunable ER fluids contained in voids in the composite structure. Changes in the electrical field imposed upon ER fluids dramatically alter the rheological characteristics of the fluids, and hence the global stiffness and dissipative characteristics of the ultra-advanced composite structure. The research program is motivated by the promising results from the pioneering proof-of-concept studies on cantilevered beams fabricated from ultra-advanced intelligent composite materials, which clearly demonstrate for the first time how the elastodynamic response of beam-like continua can be dynamically tuned in real-time by actively controlling the electrical field imposed upon the ER fluid , shown in Figure 2.

The capability of these materials to interface with modern solid-state electronics can be exploited by integrating fundamental phenomenological theories with intelligent sensor technologies and modern control strategies in order to significantly accelerate the evolution of this innovative class of

multi-functional, dynamically-tunable, ultra-advanced, intelligent composite materials for military, aerospace, and advanced manufacturing applications.

This class of innovative materials derive their versatility from the merger of sensors, built into the finite element control segments of the ultra-advanced composite material continuum, microprocessors, and dynamically-tunable electro-rheological fluids. The sensors monitor the elastodynamic behavior of the ultra-advanced composite structure, and the signals from the sensors are fed to the appropriate microprocessor which evaluates the signals prior to determining an appropriate control strategy in order to synthesize the desired elastodynamic response characteristics. An application of this philosophy to control the vibrational response of an aircraft wing is schematically represented in Figure 4.

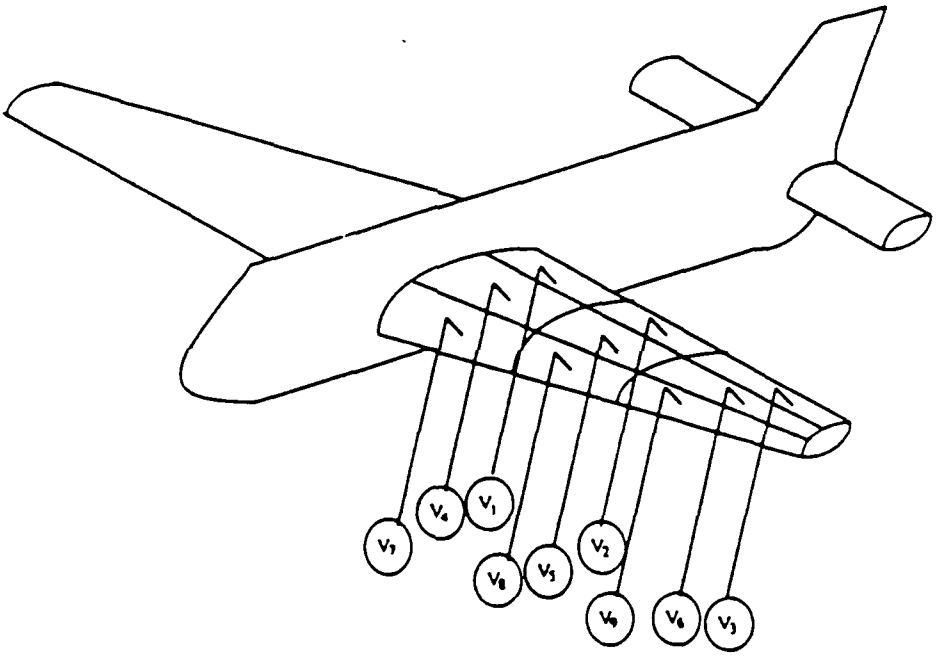

Figure 4. Schematic of an intelligent aircraft wing.

The technology on smart materials presented herein represents a quantum jump in the technology-base relative to the current generation of advanced composite materials in the marketplace at this time. This can be readily illustrated by considering the response of a helicopter rotor. With traditional advanced composite materials, the optimization strategies result in an optimal design, which is passive in nature, and cannot respond to unstructured environments, and changes in the rotational speed, aerodynamic loading, payload, and the ambient hygrothermal environment. Therefore, even an optimally-tailored rotor designed in a traditional advanced composite material is clearly sub-optimal for all service conditions except the one for which the rotor was optimally designed. In sharp contrast to this undesirable scenario, if the rotor were fabricated in one of the intelligent ultra-advanced composite materials presented herein, then the performance of the

rotor could be dynamically tuned to ensure optimal performance under various service conditions and unstructured environments.

Since elastodynamic phenomena manifest themselves in practically all applications such as submarines, machine tools, aerospace environments, and high-speed machinery and robotics, for example, clearly there is a significant need for the evolution of a new class of advanced composite materials whose elastodynamic response can be optimally tailored in real-time in order to significantly enhance the performance of structural and mechanical systems under diverse operating conditions. The successful evolution of this class of revolutionary materials is crucial to U.S. Army's mission, since it would significantly enhance the development of a new generation of advanced mechanical systems, such as, helicopter rotors, adaptive suspension vehicles, and robotized applications in armament, ammunition-supply and matériel-handling systems. An application of intelligent ultra-advanced composite materials to control the elastodynamic response of a typical robotic system is schematically presented in Figure 5. A methodology for synthesizing this class of smart materials is presented in Figure 6.

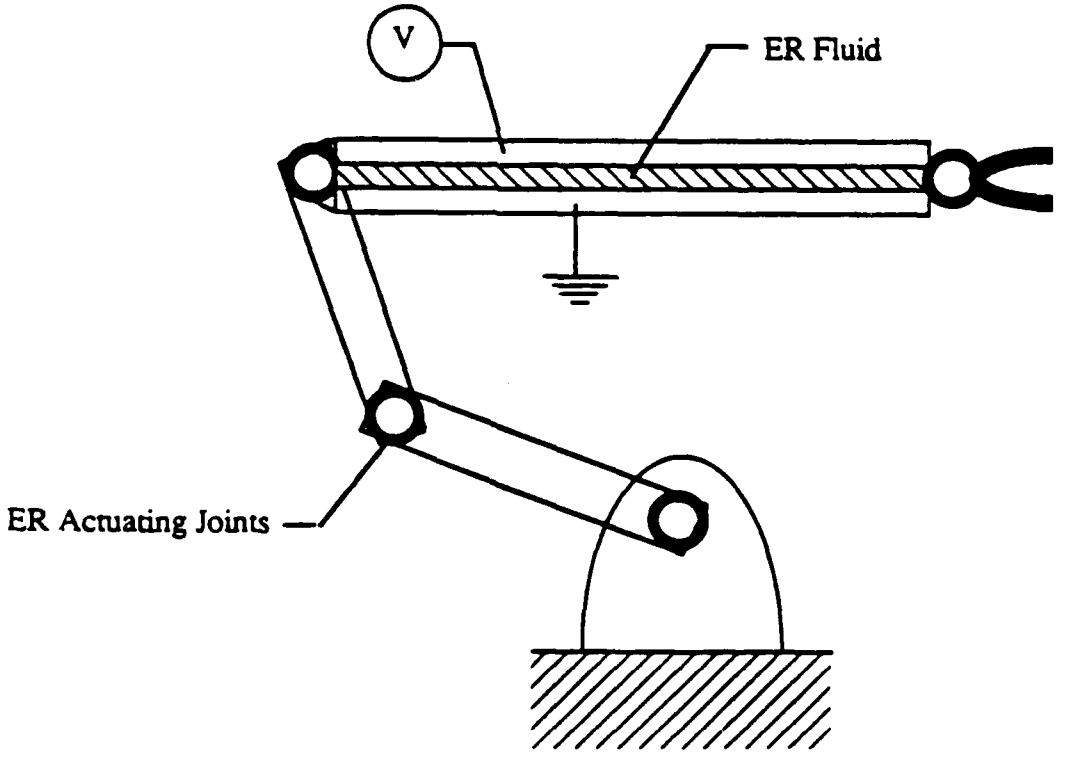

Figure 5. Schematic of Intelligent Robot Arm

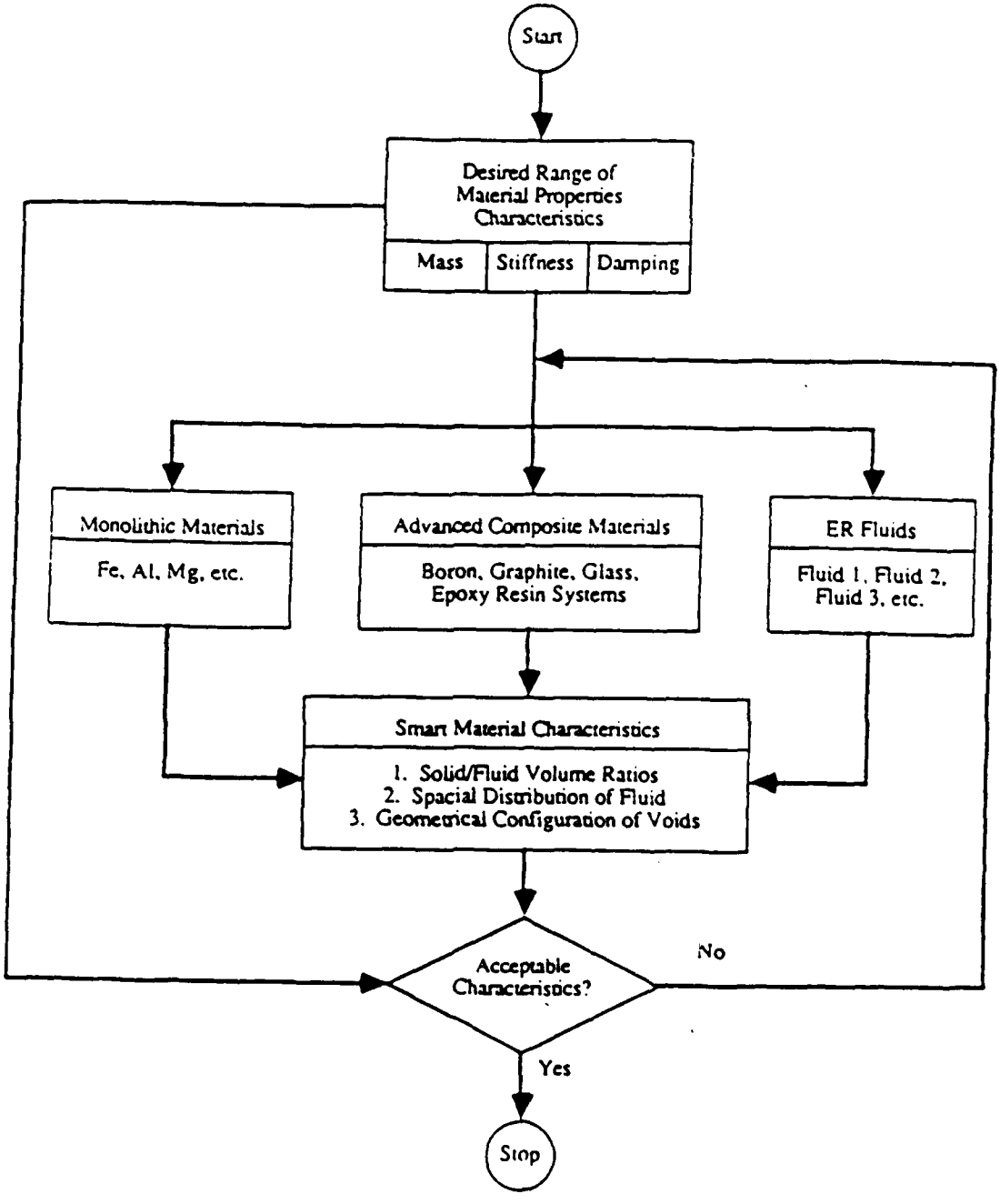

Figure 6. Optimal Synthesis of Smart Materials.

It is anticipated that the successful execution of this research program will transform this embryonic technology on smart materials and structures into an emerging technology, and significantly accelerate the evolution of this innovative class of multi-functional, dynamically-tunable, ultra-advanced, intelligent composite materials for the industrial, defense, and aerospace environments of the future.

PIEZOCERAMIC DEVICES AND PVDF FILMS AS SENSORS AND ACTUATORS FOR INTELLIGENT STRUCTURES

by

S. Hanagud, M.W. Obal,* and A.G. Calise
Georgia Institute of Technology
School of Aerospace Engineering
Atlanta, Georgia 30332-0150

ABSTRACT

During the past few years, developments in the area of intelligent structures and active vibration control of flexible structures have resulted in a significant amount of research work leading to an exploration of the associated benefits of embedded and bonded sensors and actuators. Amongst the available choice for sensors and actuators, piezoceramic transducers fall in the category of devices that can be used as both sensors and actuators. These piezoceramic transducers consist of piezoceramic materials sandwiched between conductive surfaces and polarized in a direction suitable for the particular application. When used as a sensor, deformations of the bonded dynamic structure produce an electric charge resulting in an electric current in the sensing circuit. When used as an actuator, a high voltage signal is applied to the same piezoceramic device. This results in the deformation of the transducer and transmission of energy to the bonded structure. A desired control strategy can be developed by an appropriate conditioning of the sensed signal before feeding the signal to the actuator. A selection of the spatial placement of the actuators also influences the control strategy.

In earlier works, procedures have been developed for optimum control of flexible beam like structures by using a limited state feedback and the minimization of a quadratic performance index of state and control. The problem of optimum spatial location of actuators has also been discussed. During the course of the performance of these research tasks certain research areas have been identified. In this presentation, following a brief review of the previous research work, the identified research areas and their importance in developing the concept of an intelligent structure will be discussed.

INTRODUCTION

During the past few years, there has been a considerable amount of interest in the use of bonded and embedded sensors and actuators for vibration control and failure detection in flexible structures. The discussions in this paper are concerned with the use of bonded piezoceramic sensors and piezoceramic actuators to control vibrations in structural dynamic systems. The rate

*Dr. Obal is currently with the flight testing group at Edwards Air Force Base.

of deformation of the bonded piezoceramic transducer results in an electrical voltage in the sensor detection unit. This signal is conditioned by operations such as filtering, phase shift and amplification. The conditioned signals are used as an input to bonded piezoceramic actuators located at selected locations. The piezoceramic actuators transmit mechanical energy to the flexible structure. The objective of the operations of sensing the deformation, conditioning the sensed signal and the transmission of energy to the flexible structure is to control the vibration of the flexible structure.

Some of the reported applications of piezoceramics to active vibration control are due to Mchennie,[1] Forward,[2] Forward and Liu,[3] Forward and Swigert,[4] Forward, Swigert, and Obal,[5] Hanagud and Obal,[6] and Crawley and deLuis.[7]

Bailey and Hubbard[8] have discussed the use of distributed PVDF film actuators instead of piezoceramic actuators to control flexible structures. In a recent article Hubbard[9] has also discussed the problem of using varying geometrics of PVDF films to obtain different types of actuator forces applied to selected flexible structures. The development of an optimal control procedure for a flexible structure with limited state feedback and the use of piezoceramic sensors and actuators has been discussed by Hanagud, Obal, and Calise.[10] In reference (10) a quadratic performance index of state and control has been used. In such an optimal control problem the choice of control design variable include the gain, weights to be used on the state and control variables, location or placement of the sensors and actuators, number of sensors and actuators, dimensions of the sensors and actuators, centralized or decentralized control, methods of bonding the sensors and actuators to the structure and the types of signal conditioning. In reference (10), issues of gain optimization have been discussed. Differences due to centralization and decentralization have been illustrated in example problems, along with the effects of different selected weights in the quadratic performance index.

The emphasis in this paper is on a brief review of the developments of the optimal control strategy and discussion of research areas to improve the state of the technology.

OPTIMAL CONTROL PROCEDURE

In an earlier paper,[10] finite element models have been developed by the authors for a structural dynamic systems of a Bernouli-Euler beam, bonded piezoceramic sensors, signal conditioning systems and piezoceramic actuators. In the model, a strain rate feedback and a filtered feedback centered around selected frequencies and bandwidths have been considered. Equations for the strain rate feedback are simpler in comparison to the filtered feedback equations. For a beam similar to the one illustrated in figure 1 the finite element model with rate feedback is[10]

$$\ddot{M}q + C\dot{q} + Kq = \hat{F} + F^{C} \tag{1}$$

$$F^{cT} = (C_{ED}\dot{q})^{T} = \{0, -M_1^e, 0, \ldots, M_r^e\} \tag{2}$$

$$\{q\}^{T} = \{w_1, \theta_1, \ldots\ldots w_n, \theta_n\} \tag{3}$$

In this equation M, C, K are the mass, damping, and stiffness matrices. The external force vector is F^e and the control force vector is F^c. In equation (2), C_{ED} for on element is given by

$$C^e_{ED} = G^* K^e_D K^e_s \begin{bmatrix} 0 & 0 & 0 & 0 \\ 0 & 1 & 0 & -1 \\ 0 & 0 & 0 & 0 \\ 0 & -1 & 0 & 1 \end{bmatrix} \tag{4}$$

$$K^e_D = \beta^{-1} H b^a h \, \xi_D \tag{5}$$

$$k^e_s = b^s \beta^{-1} h H R_f \xi_S \tag{6}$$

In these equations $G^* = -G$ is the gain, K^e_D and K^e_s are the sensor and actuator piezoelectric constants resulting in control moments M^a_i. The width and height of the piezoceramic devices are denoted by b and k respectively.

Quantities β and H represent constants in piezoceramic constitutive relationships. The reduced electromechanical coupling efficiency due to bonding has been represented by ξ_s for the sensor and ξ_D for the actuator. In general ξ_s and ξ_D have been assumed to be constants. The deflection and slope of the beam at nodes have been denoted by w_i and θ_i.

The equations have been reduced to the form required for the derivation of optimal output feedback gains:

$$\dot{x} = Ax + Bu, \; x \epsilon R^n \tag{7}$$

$$y = \bar{C}x, \; y \epsilon R^r \tag{8}$$

$$u = -\bar{G}y \tag{9}$$

where

$$A = \begin{bmatrix} 0 & I \\ -M^{r-1}K^r & -M^{r-1}C^r \end{bmatrix} \tag{10}$$

$$B = \begin{bmatrix} 0 \\ -M^{r-1}\bar{K}_D \end{bmatrix} \tag{11}$$

$$\bar{C} = [0 \; K_s] \tag{12}$$

$$x^T = \{x_1, \ldots, x_{2n}\} = \{\theta_1, \ldots, \theta_n; \dot{\theta}_1, \ldots, \dot{\theta}_n\} \tag{13}$$

The reduced size matrices M^r, K^r, and C^r have been obtained by eliminating the translational degrees of freedom from M, K, C by using Guyan condensation procedure.

$$Y = [\ [0]\ [K_s]\ ]\ x \tag{14}$$

and

$$G = K_D \bar{G} \tag{15}$$

Index of performance is defined as[11]

$$J = E_{x_0} \int_0^\infty (x^T \bar{Q}\ x + u^T R\ u)dt \quad + \gamma(G) \tag{16}$$

$$E\{x_o\} = 0;\ E\{x_o x_o^T\} = X_o \tag{17}$$

where the quantity $\gamma G)$ is any scalar function having continuous gradients in G. Minimization yields the following set of equations

$$(A-B\bar{G}\bar{C})L + L(A-B\bar{G}\bar{C})^T + X_o = 0$$

$$S_c(\bar{G},\bar{K}_c)=(A-B\bar{G}\bar{C})^T\bar{K}_c+\bar{K}_c(A-B\bar{G}\bar{C})+\bar{Q}\ \bar{c}^T\bar{G}R\bar{G}\bar{C} = 0$$

$$\bar{G} = R^{-1}\{B^T\bar{K}c\ L\bar{C}^T - \frac{1}{2}\ Y_G(\bar{G})](\bar{C}L\bar{C}^T)^{-1} \tag{18}$$

A convergent numerical solution procedure for these equations have been discussed in reference (11).

For a system, with filtered feedback, equations for the closed system can be summarized as follows. In particular, for a beam with n elements, r piezoceramic actuators and r signal conditioners the equations are as follows:

$$I\ddot{v}_D + A^{\cdot}\dot{v}_D + B^{\cdot}v_D = \bar{K}s\ T_s\ \ddot{q} \tag{19}$$

$$M\ddot{q} + C\dot{q} + Kq = T^D K_D v_D + F \tag{20}$$

In these equations elements of v_d vector are the output from the signal conditioning systems

$$v_D^T = \{v_{D1}, \ldots, v_{Dr}\} \tag{21}$$

The matrices A* and B* are diagonal matrices with diagonal elements.

$$A^*_{jj} = \omega_{fj}/Q_j \qquad j = 1, \ldots r \tag{22}$$

$$B^*_{jj} = \omega^2_{fj}; \qquad j = 1, \ldots r \tag{23}$$

where ω_{fj} is the filter center frequency and Q_j is the band width of the i^{th} signal conditioning system. The matrix $\bar{K}_s$ is also a diagonal matrix with elements.

$$\overline{K_{sjj}} = \frac{G_j \omega_{fj}}{Q_j} K_{sj} \tag{24}$$

where G_j is gain of the i^{th} signal conditioning system and K_{si} is the sensor constant of the i^{th} piezoceramic sensor

$$k_s = b^s \beta^{-1} hHR_f \tag{25}$$

In this equation b is the width, h is the thickness, β is the dielectric constant and H is the piezoelectric constant of the piezoceramic sensor. The quantity R_f is the resistance in the sensor signal analyser portion of the signal conditioning system illustrated in figure 2. The efficiency of the energy transfer from the beam to the sensor through the bonding has been defined by a coupling coefficient ξ_s. In general ξ_s can be a function of space and time. As a first step, in this analysis ξ_s has been assumed to be a constant. Quantities M, C, and K are the system mass, damping and stiffness matrices. The vector q is the displacement vector.

$$\{q\}^T = \{w_1, \theta_1 \ldots . W_n, \theta_n\} \tag{26}$$

$$\{F\}^T = \{V_1, M_1, \ldots . V_n, M_n\} \tag{27}$$

The matrix K_D represents the actuator characteristics and is assembled from element matrices

$$\bar{K}_D^e = \begin{bmatrix} 0 & 0 & 0 & 0 \\ 0 & 1 & 0 & 0 \\ 0 & 0 & 0 & 0 \\ 0 & 0 & 0 & 1 \end{bmatrix} \beta^{-1} Hb^a h \, \xi_d \tag{28}$$

The matrices T_D and T_S are actuator and sensor location matrices used in assembling the sparsely located sensor and actuator contributions into global matrices. The coupling of coefficient ξ_d has been defined similar to ξ_s. Equations (19) and (28) can be used to develop optimal control strategies.

Numerical Results

An example of a cantilever beam has been considered to illustrate the developed procedure for optimal vibration control of structures by the use of piezoceramic sensors, actuators and rate feedbacks with appropriate gains. The cantilever beam is of length 22.86 cm and cross sectional dimensions 1.65 cm x 0.44 cm. The beam is made of an aluminum alloy. Two piezoceramic transducers made of lead zirconate titanate (G1195) of sizes 1.91 cm x 1.91 cm x 0.02154 cm and 3.9;6 cm x 0.02154 cm have been selected for use as collocated sensors and actuators as shown in Figure . In this study, sensor and actuator pairs have been assumed to be at given locations. Optimization of the sensor/actuator placement has not been considered. A finite element model with ten degrees of freedom has been initially formulated for the open loop beam without feedback. In the current state of the art, the desired finite element model does not contain the values of the damping matrices. An assumed linear viscous damping matrix has been determined from tests conducted on the beam and a structural dynamic system identification procedure. The first ten eigenvalues, ten eigenvectors and an a priori model are required in the use of the selected identification procedure which is based on the equation error approach. The derived finite element model has been used as an a priori model. Laboratory tests have been conducted and the required eigendata have been obtained using a GENRAD computer aided data acquisition system and SDRC modal plus software. The identified model resulting from the identification algorithm yields the experimentally obtained eigendata and a symmetric damping matrix. This damping matrix has been noted as the baseline matrix in the paper to distinguish it from the augmented damping matrix due to an active control input vector to the piezoceramic actuators.

The matrices A, B, and $\bar{C}$ for the cantilever beam have been obtained from the identified mass, stiffness and damping matrices. In the process of obtaining matrices A, B, and $\bar{C}$, five translational degrees of freedom have been eliminated by using a Guyan condensation technique. The function $\gamma(G)$ has been selected to be

$$\gamma(G) = \frac{v}{2}\left(g_{12}^2 + g_{21}^2\right) \tag{29}$$

whenever off diagonal gain terms are not desired. Three different types of weight have been selected. The diagonal elements of the weighting matrix are inversely proportional to the square of the eigenvalues, inversely proportional to the eigenvalues and an identity matrix. For all cases R=I. Optimal gains have been obtained for cases in which off diagonal terms have been penalized in accordance with (29), and cases where off diagonal terms have not been penalized. The latter case corresponds to the case where each sensor output fed back to both actuators with appropriate gains.

Figure 2 is the time history of an open loop sensor output at x=16.60 cm. Figure 3 is the corresponding closed loop time history of sensory output When off diagonal terms have been penalized. Figures 4 and 5 are closed loop time histories for sensor output and tip velocity for systems with cross feedback, where it is not necessary to penalize the off diagonal terms.

RESEARCH AREAS AND FUTURE DIRECTIONS

Dynamic coupling and Constitutive Equations: During the course of the performance of reviewed tasks and the the current work in progress at Georgia Tech, it has been observed that a significant amount energy is not transferred from the piezoceramic actuator to the structure. This energy is lost in the bonding material or the adhesive. The efficiency is as low as 10 to 20 percent. Research efforts are needed in improving the efficiency. Furthermore, most of the current analytical work is based on classical linear piezoelectric constitutive relations. These equations were derived and used to study these crystals at resonant conditions. Very likely, they are valid for our purposes of active control. However, it is necessary to reexamine these constitutive relations including their effects with varying temperature and aging. It is necessary to design appropriate experiments and identify the appropriate parameters.

Load and Energy Transfer: Following discussions of the previous paragraph, it is necessary to understand the energy and load transfer mechanisms for PVDF films, piezoceramic sensors or other actuators to the structural dynamic system. This problem should be addressed for both bonded and embedded actuators. It is also necessary to consider the effect of the adhesive material. A thorough understanding is possible by progressively considering one, two, and three dimensional models with their dynamic analysis. It is also important to consider different types of structures. A specific area of concern will be the multiple layers of the film actuators.

Composite Structures: An important area of the application of the smart structure concept will be in the use of embedded sensors and actuators in composite structures. Modeling these composite structures with embedded sensors and actuators and verifying the accuracy of the model results are necessary in evaluating the performance of composite structures.

Optimal Dynamic Compensation: In the results presented thus far, only the case of constant gain output feedback has been considered. The output signal conditioning were prespecified using highly tuned bandpass filtering. This approach is in general not robust in that it relies on accurate knowledge of the modal frequencies. An alternative approach is to use LQG theory to define the compensation. Unfortunately, this also can be shown to lead to highly turned notch filtering. Moreover, the order of the system would preclude the practical implementation of a full order observer (compensator). An alternative approach is to design a fixed order dynamic compensator, of order less than the minimal order observer. This in concept is a straight forward extension of constant gain output feedback. However, there are a number of difficulties associated with this approach which have been recently addressed in the literature. One problem is that the compensator formulation is over parameterized, which invariably leads to convergence problems when attempting to numerically optimize the design. several authors[12,13] have adopted canonical formulations which yield a minimal parameterization. A second

problem is that there are few guidelines for penalizing plant and compensator states in the performance index to achieve desirable performance.[14] Finally, there are no guarantees on stability margins. In a recent paper[14] a Loop Transfer recovery procedure is outlined for approximating the properties of a full state feedback design, including the well known stability robustness margins. In addition, this approach leads to a well defined approach for defining the weighting matrices in the performance index, and the initial condition distribution matrix (X_0) as well. A singular perturbation method for extending this approach to two time scale design appears in Reference (15). In this setting, fast and slow compensators result, that operate in a parallel architecture with different sampling rates. This approach offers the possibility of decentralized control. These approaches warrant further investigation and development for potential application to control of flexible structures.

Estimation and Identification: Accurate models are necessary from the point of view of sensing the information only or sensing and control. Accurate model improvement procedures for adaptive control techniques and optimum control. Because of the coupling between the smart structural elements and benign structural elements and uncertainties such as adhesive material (or bonding) effects and noise in the process models and measurement it is very important that appropriate model and parameter identification techniques as well as State estimation techniques are developed. Estimation is very important in structures where smart elements are primarily used for sending and monitoring the health of the structure.

Distributed Controls: One of the benefits of PVDF films, piezoceramic or other similar actuators is that control of distributed parameter system can be developed by using distributed actuators. Techniques for exploiting the maximum benefits of the distributed sensor and actuators are needed.

References

1. H. F. Olsen, "Electronic Control of Mechanical Noise, Vibration and Reverberation," Journal of the Acoustical Society of America, pp. 966, 972, 1956.

2. R. E. McKechnie, "A Method of Damping the Piezoelectric Accelerometer," Instr. Soc. of Am., Vol. 11, pp. 45-51, c. 1972.

3. R. L. Forward, "Electronic Damping of Vibration in Optimal Structures," Applied Optics, pp. 690, 697, March 1979.

4. R. L. Forward, C. P. Liu, "Electronic Damping of Resonances in Gimbal Structures," AIAA paper No. 81-0556, Proceedings AIAA/ASME/ASCE/AIS, 22nd Structures, Structural Dynamics, and Materials Conference, Atlanta, GA, April 6-8, 1981.

5. R. L. Forward and J. Swigert, "electronic Damping of Orthogonal Bending Modes in a Cylindrical Mast, AIAA 81-4017/4018, J. Spacecraft and Rockets, Jan. -Feb. 1981.

6. R. L. Forward, C. J. Swigert, M. W. Obal, "Electronic Damping of a Large Optical Bench," Shock and Vibration Bulletin, No. 53, pp. 51-61, May 1983.

7. T. Bailey and J. E. Hubbard, "Distributed Piezoelectric Polymer Active Vibration Control of a Cantilever Beam," J. Guidance and Control, p. 605, 1985.

8. V. Komkou, "Optimal Control Theory for Damping of Vibration of Simple Elastic Systems," Lecture notes in Math, Spring Verlag, New York, 1972.

9. E. W. Crawley and J. deLuis, "use of Piezoceramics as Distributed Actuators in Large Space Structures," AIAA Paper No. 85-0626, Proc. AIAA S.D.M. Conference, 1985.

10. S. Hanagud, M. Obal, and A. J. Calise, "Optimal Vibration Control by the Piezoceramic Sensors and Actuators," Proceedings of AIAA/ASME/ASCE/AHS Structures, Structural Dynamics, and Materials Conference, 1987, pp. 987-997.

11. Moerder, D.D., A.J. Calise, "Convergence of a Numerical Algorithm for Calculating Optimal Output Feedback Gains," IEEE Trans. Auto. Control, Vol., AC-30, No. 9, pp. 900-903, September 1985.

12. Martin, G.D., and A.E. Bryson, "Attitude Control of a Flexible Spacecraft," Journal of Guidance and Control, Vol. 3, No. 1, Jan.-Feb., 1980.

13. Kramer, F.S. and A.J. Calise, "Fixed Order Dynamic Compensation for Multivariable Linear Systems," Journal of Guidance, Control and Dynamics, Vol. 11, No. 1, Jan.-Feb., 1988.

14. Calise, A.J., J.V.R. Prasad, "An Approximate Loop Transfer Recovery Method for Designing Fixed-Order Compensators," AIAA Guid., Nav. and Control Conf., Minneapolis, MN, Aug. 1988.

15. Calise, A.J., J.V.R. Prasad, B. Siciliano, "Design of Optimal Output Feedback Regulators in Two-Time Scale Systems," IEEE Conf. on Decision and Control, Los Angeles, CA, Dec. 1987.

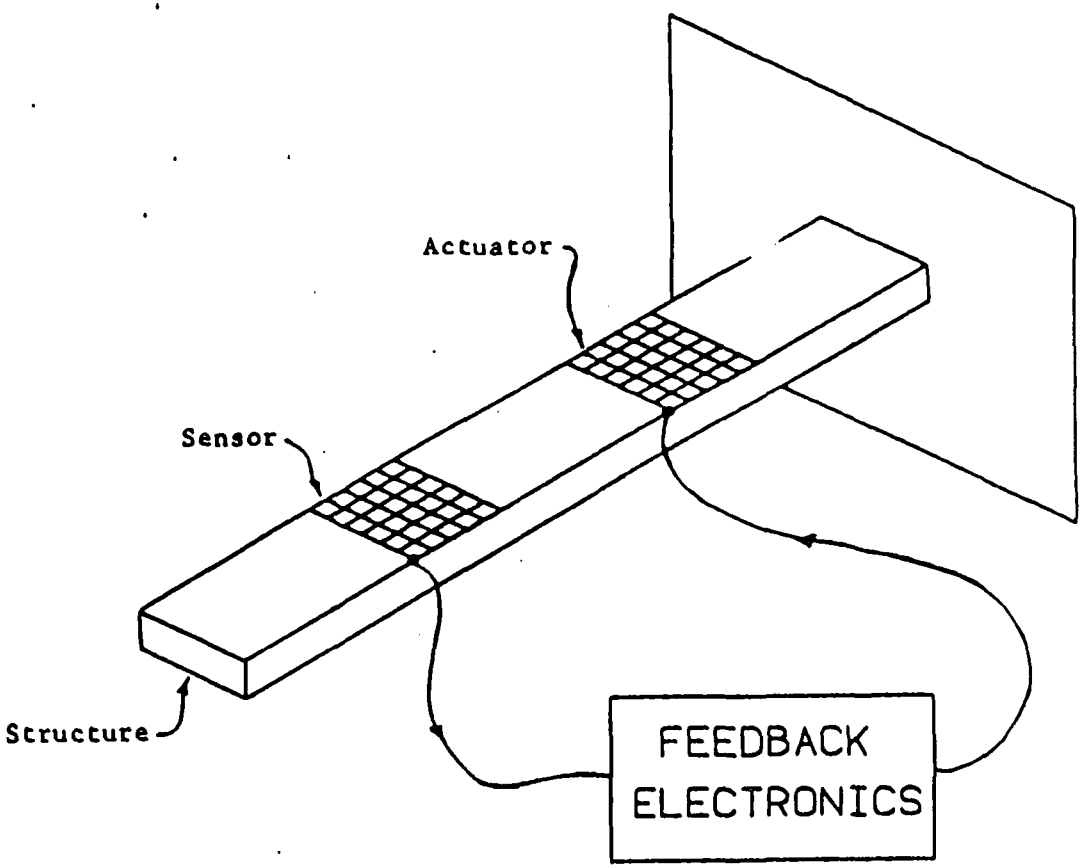

Fig. 1. Active Control of Structures with Piezoelectric Sensors and Actuators.

Experiment Beam

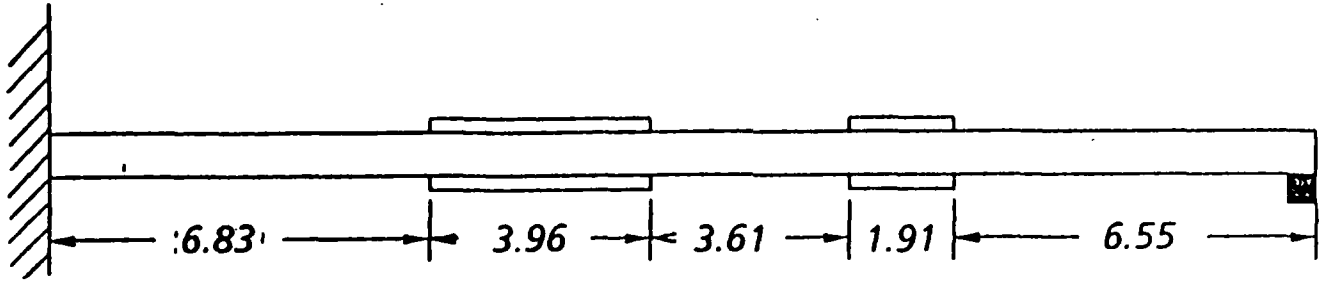

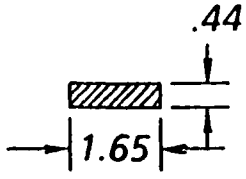

Finite Element Model

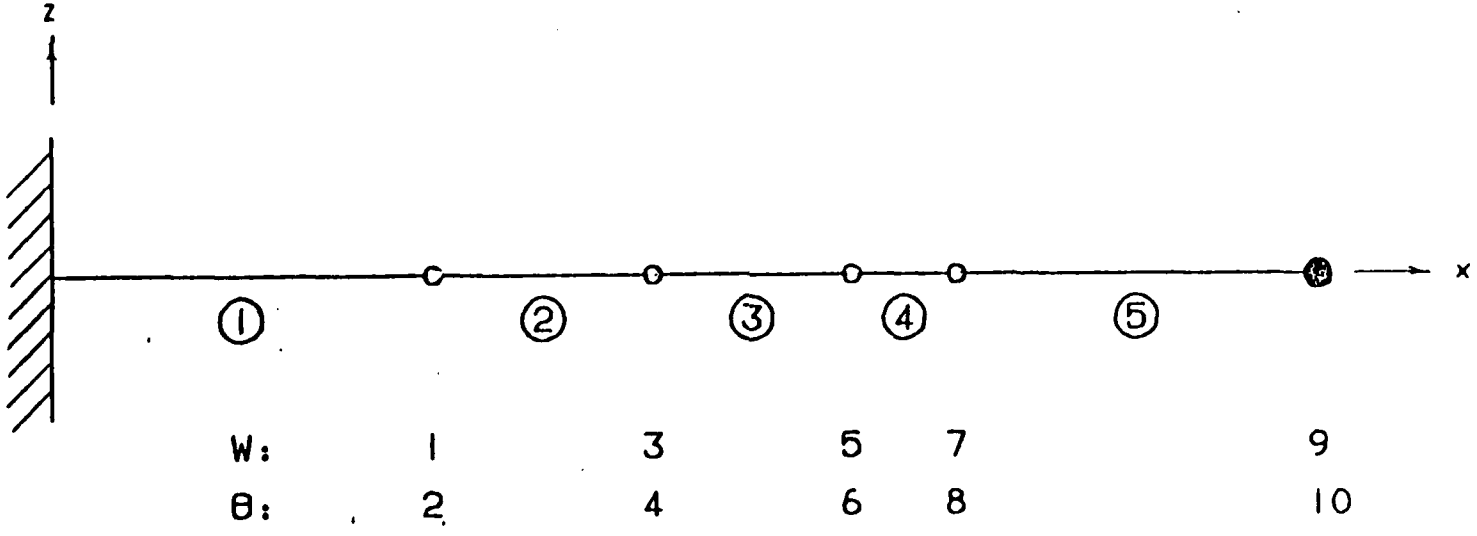

Fig. 2. Test Beam's Collocated Sensor and Actuator Locations

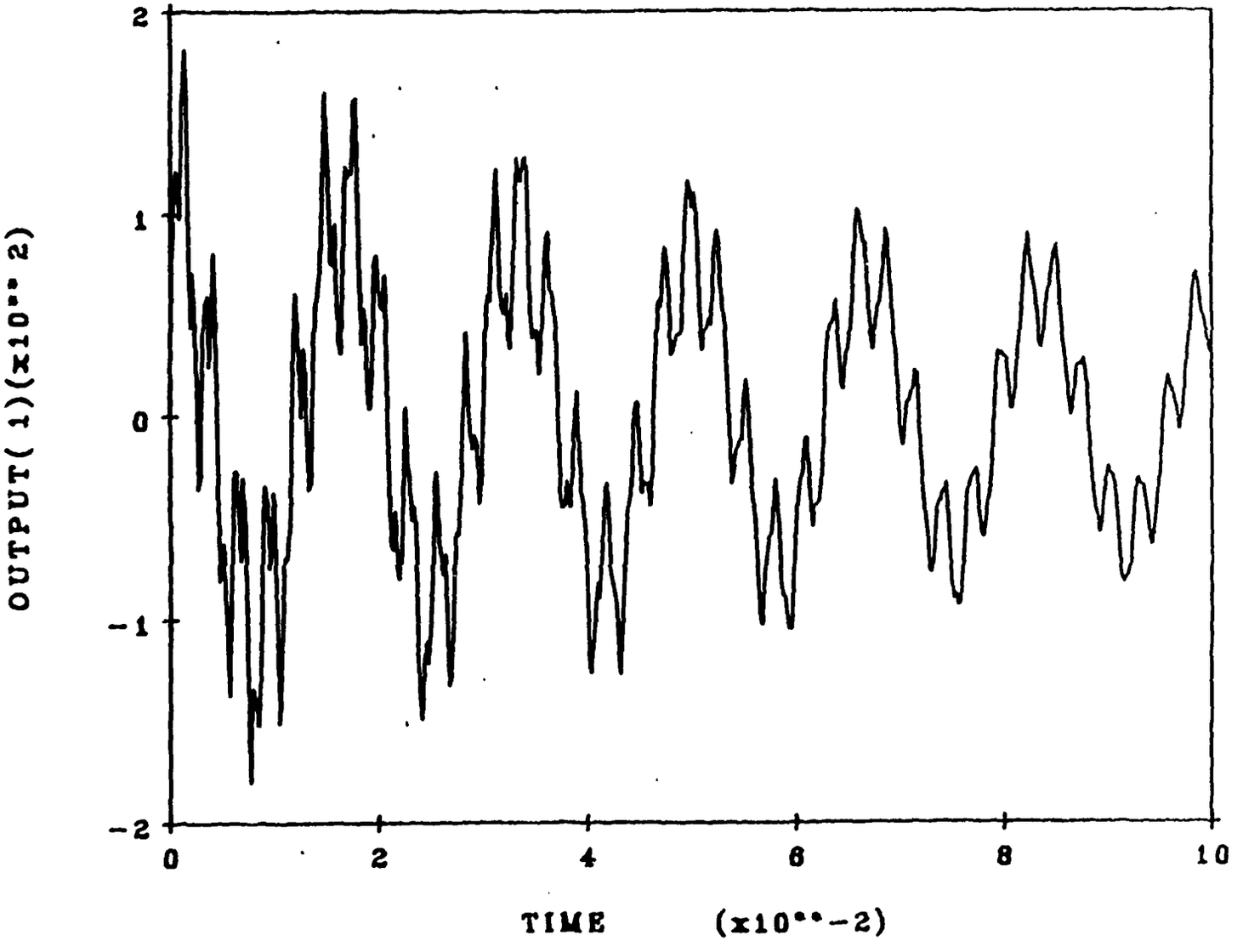

Fig. 2. Time history of Sensor #1 output, no control.

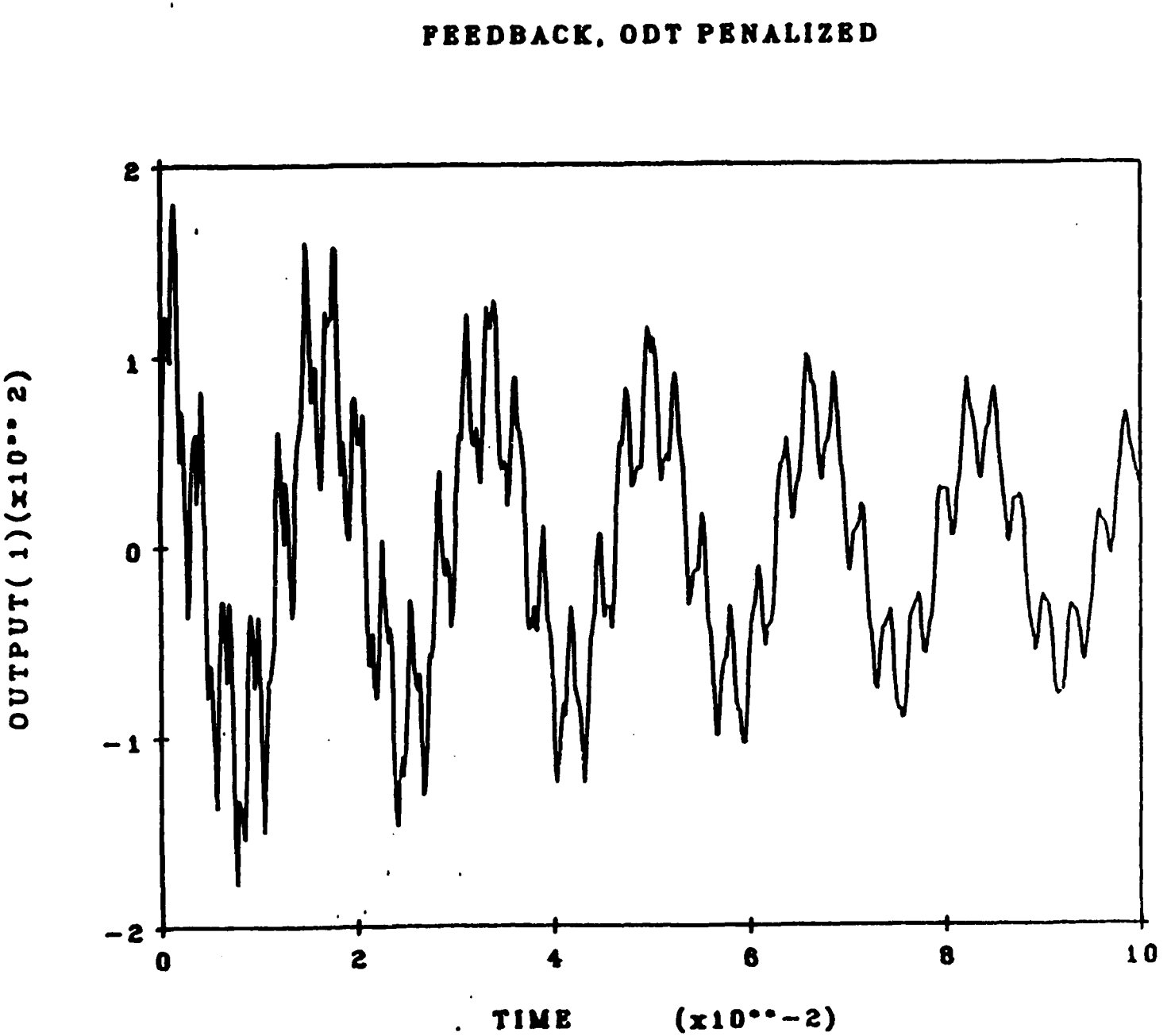

Fig. 3. Time history of Sensor#1 output for penalized ODT gain matrix.

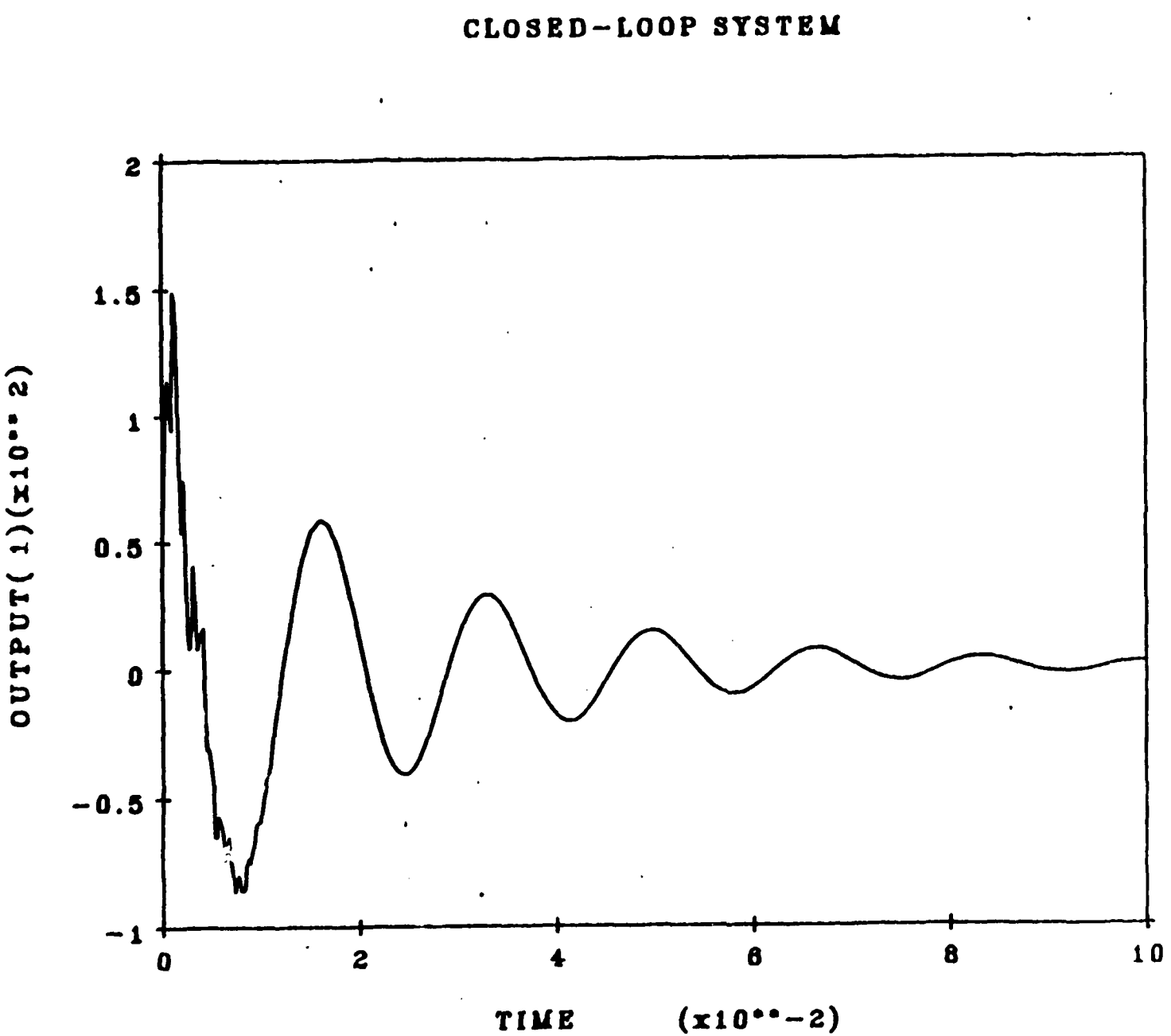

Fig. 4. Closed-loop time hist[illegible] of Sensor#1 output

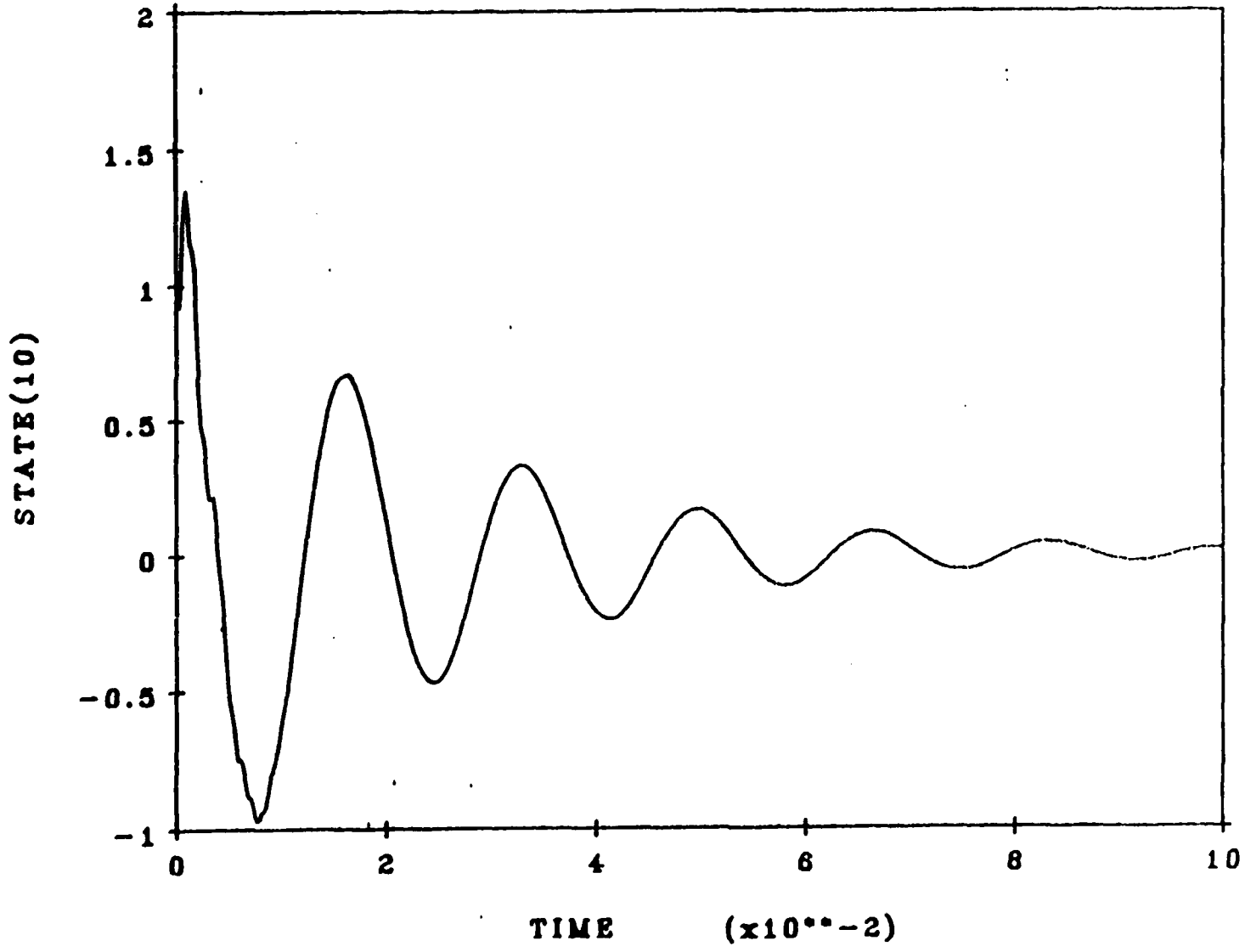

Fig. 9. Closed-loop time history of tip velocity for the general gain matrix with cross feedback.

Variable Geometry Trusses

Harry H. Robertshaw
Charles F. Reinholtz

Smart Materials and Structures Laboratory
Department of Mechanical Engineering
Virginia Polytechnic Institute and State University

Introduction

Work into the analysis and experimentation with Variable Geometry Trusses (VGT's) has been carried out in the Mechanical Engineering Department at VPI&SU since 1985. The purpose of the work at that time was to explore the vibration control capabilities of these VGT's. The first focus for the work was a four-bar linkage with three variable-length links used to give the structure three degrees of freedom (DOF). The structure was grounded at one end and had a continuum attached at the other end with the object being to control the vibration, the dynamics, of the continuum. Since that time a spatial three DOF active truss (with an octohedral-octohedral configuration) has been analyzed and tested for vibration control and for performing rudimentary robotic tasks. A twenty-one DOF truss has been designed and is being assembled for testing.

Varible geometry trusses are an embodiment of the "Smart Structure" concept: possessing the three needed attributes of integral actuators, integral sensors, and some intelligence to direct the actuators. There are many terms currently being used for structures that have some or all of the concepts inferred by "smart": variable, adaptable, adaptive, active, adjustable, and organic. It seems that "smart" has been chosen because of it's alliterative qualities and not because of it's emphasis on the intelligence aspect, the most developed of the three needed attributes. "Organic" may be the best choice.

"Organic" suggests the biological process, at least the musculo-skeletal processes, that we attempt, directly or indirectly, to mimic with our smart structures. Looking at the macroscopic and possibly microscopic behavior of organisms will lead us to developing goals and perhaps mechanisms for actuators, sensors, and intelligence for structures and materials. For example, the human arm when performing any of the advanced tasks it is capable of (e.g. painting, pitching, punching, or piano-playing) can be considered as a variable stiffness actuator with a control law (the intelligence) that has significant open-loop, preprogrammed, behavior. These observations (and others) may have significant impact on the development of new smart structures.

The development of VGT's at VPI&SU, described below, is in the beginning stages. The overall goal of this work is to design, build, and test variable geometry structures that are adaptable and controllable. The work has focused on vibration control and robotic tasks using "integral" actuators composed of dc motors driving machine screws, sensors composed of resistive devices to measure motions and strains, and intelligence composed of desktop digital microcomputers.

Vibration Control With VGT's

Vibration control of continua with VGT's has been studied and carried out using a planar three DOF truss (Lovejoy, 1987, Patten, 1988) (Fig. 1) and a three DOF spatial octahedral-octahedral truss (Robertshaw, 1988) (Fig. 2). Additionally, an analytical, planar, comparison of inertia-type actuators and VGT actuators has been carried out for a planar structure (Clark, 1988).

A particular area of interest is the vibration control of truss structures built up as long flexible beams. Many future space applications, such as the proposed space station, incorporate such truss-beams in their main structures and appendages. There have been various methods introduced in the literature to actively damp these truss-beams. Some of these include the use of piezoelectric

materials (Bailey, 1985, Fanson, 1986, Hanagud, 1987) and applications of thermal gradients to enhance the structure's own internal damping capabilities (Edberg, 1987). One of the primary methods being studied today is the use of inertia-type actuators to apply controlling forces to the beam. These actuators produce forces and moments on the structure by using inertial reaction forces of a small mass or rotational inertia. The oldest and most tested of these actuators are various configurations of the reaction wheel (a rotational actuator), (Anderson, 1975, Aubrun, 1985, Joshi, 1980, Margulies, 1978), which was followed several years later by the development of the proof mass (a linear actuator), (Aubrun, 1980, Doane, 1986, Ham, 1987, Zimmerman, 1984). In 1981 Mills performed a theoretical case study comparing the effectiveness of those two inertia-type actuators (Mills, 1981). He modelled the actuators as having dc motors driving the inertial elements. In the study he placed the actuators at the tip of a cantilevered beam and determined each actuator's effectiveness in damping the first three modes of the beam. His results showed that for first mode the two actuators were very evenly matched, but for second and third modes, the reaction wheel actuator proved to be superior to the proof mass actuator.

Even though inertia-type actuators have been studied a great deal over the past years for their vibration control capabilities, they lack the ability to perform pointing or slewing maneuvers. VGT's can provide both forces and moments to the structure and accomplish slewing maneuvers as well. VGT's had been studied in the past for their vibration characteristics, and for their pointing and shape control capabilities (Natori, 1987), but they had never been applied directly to vibration control. In 1987 Lovejoy showed that a planar truss actuator could be used to damp the vibrations of a beam, and in so doing, showed that the truss has a great deal of authority over the beam. This work has opened the possibility of three-dimensional truss actuators which are built into the structure, thus eliminating the added weight of inertial elements.

Inertia-type actuators and VGT's represent two distinct concepts for controlling vibrations of flexible structures. Each concept brings with it characteristics which may or may not be beneficial in performing the vibration control task. Clark (1988) describes the method and results of a study comparing the effectiveness of four actuators in controlling the planar vibrations of a truss-beam. The four actuators studied are the proof-mass actuator, the reaction wheel actuator, the planar truss actuator (a VGT), and the planar truss proof-mass actuator (a combination VGT/inertia-type actuator), Fig. 1. The work involves simulating the response of a finite element model of a cantilevered truss-beam to initial conditions, with each of the actuators acting in turn to damp the imposed vibrations.

The analytical approach taken was to model each actuator with lumped masses and model the beam with finite elements, including in each model the generalized reaction forces from the beam on the actuator or vice versa. The two systems (beam and actuator) are combined by solving for corresponding reaction forces and then setting the resulting equations equal to one another to form the complete system. All actuators are assumed to have no means of storing appreciable amounts of potential energy. Figure 3 shows that the VGT actuators each have three active parts while the proof mass and reaction wheel actuators have only one active part. To make up for this disadvantage, three proof mass and three reaction wheel actuators are placed on the beam at different locations. For the proof mass and reaction wheel actuator models, parameters such as motor constants, secondary masses, and ballscrew leads are chosen based on the results of a parametric study. The study involved varying the actuator parameters and choosing the set which provided the best closed loop system response (determined by eigenvalue location). The parameters for the truss actuator models (motors and ballscrews) in this study were chosen from an experimental setup of a similar system. A parametric study of the planar truss actuators has not yet been carried out. Using the previous method for choosing actuator parameters means that any disadvantage seen by the reaction wheel or proof mass actuators is brought about by actuator configuration and not by choice of parameters. In order to be consistent a constant, full-state-feedback, linear, optimal control law (Linear Quadratic Regulator) is used for all actuators.

Three performance indices are used to evaluate the actuators in this study. One obvious choice is the linear quadratic regulator performance index used to determine the feedback control gains. Perhaps a better, more meaningful index of performance is the energy consumed by the actuators during control, since, for practical purposes, the energy consumed by each actuator may be the limiting factor in actual control situations. The LQR performance index, J, does not adequately represent energy consumed. Where J is a function of the motor input voltage, it should be a function of both the input voltage and armature current. A different performance index which does

represent energy consumed, J_E, is calculated during each simulation for each actuator system. The third performance index, J_D, was chosen to represent the damping added to the system. Integrating the energy in the system over time provides a relative "damping factor" (dependent upon initial conditions) which can be used to compare one actuator to another for a given set of initial conditions. All three of these performance indices are tabulated with the results of the simulations.

The response of each beam/actuator system was simulated to various initial condition inputs. The results of the simulations are shown in Table 1. Figure 4 shows the response plots of the system controlled by the VGT actuator for the initial condition of all modes. The figure shows two plots; the first shows the energy of the system versus time, and for an illustration of what would actually be seen in the real system, the second plot shows the tip deflection of the beam versus time.

The data in Table 1 show that the planar truss actuator does the best job of damping the vibrations of a beam excited by first mode initial conditions. The third column shows the integral of the total system energy over time, that is, the area under the energy curve shown. From these numbers it is seen that all actuators do a better job of damping higher modes than lower modes, and all actuators are very similar in their ability to damp higher modes. The planar truss proof mass actuator lags behind the other actuators in its controlability, however this is due in large part to the fact that it adds a large lumped mass to the end of the beam. Placing more actuators at different locations on the beam should improve its performance.

Table 1 also shows that the inertia-type actuators are all very close in the amount of energy consumed in controlling any mode. The planar truss actuator, however, consumes significantly more energy than the inertia-type actuators. This can be explained by the fact that the planar truss actuator must affect rigid body motion on the beam, a process which consumes more energy than moving a secondary mass. Placing the planar truss actuator at some other position along the truss should cause the energy required for control to decrease because the part of the beam being moved rigidly is decreased.

There are several final points concerning various actuator characteristics which should be considered when comparing one actuator to another. These points are not drawn directly from the simulation results, but have an impact on actuator design or on the choice of an actuator for a particular application. An important characteristic of the VGT actuator is that it can be an extension, by one bay, of the truss-beam to which it is attached, with the difference that the links making up the actuator are active. This active bay could be located anywhere along the beam, which makes the planar truss actuator convenient for applications such as pointing or shape control. Global beam motions can be applied and controlled by the actuator to accomplish tasks such as positioning solar arrays or antennas. Global motions cannot be applied by the inertia-type actuators. Another advantage of the planar truss is that it does not require the added mass necessary for the operation of inertia-type actuators. That added mass will be costly when these ideas are implemented in space.

The conclusion to be drawn from this discussion is that, from an operational standpoint, the VGT actuator is more favorable than the inertia-type actuators. It allows for global positioning (slewing, shape control) of the beam, it does not come with the penalty of an added secondary mass, and the planar VGT actuator is effective in controlling vibrations of a flexible beam.

Experimental work with a planar VGT actuator has been carried out by Lovejoy (1987) and Patten (1988). The experimental work was carried out on the same experimental appparatus but used different control laws. Unlike the control laws used by Clark (1988) in his comparison study, both Lovejoy and Patten did not have the full state measurements available for feedback during the experiments; rate information is notoriously difficult to measure. Both these investigators used partial state feedback with similarly good results. The response of Lovejoy's control law in controlling a continuum with a clamped-free first mode of approximately 0.5 Hz and almost zero open-loop damping is shown in Fig. 5. Patten's more advanced control law used open-loop responses between widely spaced sampling periods to perform this control and resulted in better yet similar responses.

Experiments and analyses with a spatial VGT have been carried out, Robertshaw (1988). As in the planar case, the spatial VGT is actuated via variable-length links that are driven by dc motors and machine screws. The truss used for the experiments and as the focus of the analysis is a three degree-of-freedom, statically-determinate, two-bay, octahedral-octahedral truss developed at the

NASA Langley Research Center to demonstrate deployment concepts, (Rhodes, 1985). The truss has been adapted to perform closed-loop position control and vibration control at VPI&SU.

A schematic diagram of the spatial truss actuator with an attached generic beam continuum is shown in Fig. 2. The truss is a two bay, statically determinate, octahedral-octahedral structure with three motor/lead screw actuators. Joshi, (1988) has analyzed many different cases for variable geometry trusses and has shown that the three variable-length links give this structure three degrees of freedom. The continuum attached could represent the remainder of an unactuated truss structure. The continuum chosen for use is a 1/4" dia. brass rod 75" long. The combination of the rod and the two truss bays is nearly fourteen feet in length. The equations of motion for the system were developed and then were used to develop the linear, suboptimal control laws for the system and to simulate the system response.

The approach taken in deriving the equations of motion was to consider the actuator and beam continuum separately. The spatial VGT actuator was modeled by identifying coefficients of a second-order differential equation model for each of the variable-length links using experimental frequency response and time response data. The truss base motion was found from these link motions using a linearized version of the non-linear, iterative, kinematic transformation developed by Reinholtz (1987). The truss, therefore, supplied kinematic inputs to the rod continuum equations. The rod continuum was modelled using energy methods (with a Ritz discretization) and the resulting ordinary differential equations were linearized about the operating point.

In the development of the system model five different coordinate systems are utilized at one time or another. The Newtonian coordinates of the base of the truss (the root of the clamped rod) can be described in terms of the primitive coordinates or in terms of the variable-link lengths. Once the base position is known, the rod continuum can be located in the Newtonian frame using either the Ritz time-dependent coordinates or by using coordinates consisting of strain measurements along the beam.

Finding an optimal, linear state-variable feedback, control law for this system is a variation of the classic Digital Linear Quadratic Regulator (LQR) problem. Iterations with different penalty matrices produced sets of gains which had acceptable eigenvalues. With an eye toward the experimentation the eigenvalues were computed assuming that there were no rates available for feedback; therefore, the computed rate Kalman gains were set to zero for the eigenvalue determinations. Additionaly, the digital computer calculation delays, one for each of the active links, were included in the eigenvalue calculations as well as the simulations. In order to verify the anlytical model and the control approach an experiment was performed.

The active link positions were measured with linear potentiometers and the beam strains at six locations (three in each direction) were transduced using full (four-arm) bridges at each location. The digital control algorithm was implemented on an AT style computer using two commercially available data acquisition boards to perform the A/D and D/A operations. The controlled response of the nearly undamped rod to first-mode like initial conditions is shown in Fig. 6. Note that this controlled response shows some energy being moved into the second mode and also being controlled by the algorithm. The control algorithm gain sets chosen produced output voltages that saturated at certain times during the transient response. The linear control algorithm was robust in the face of this saturation non-linearity.

As a further check of the system model an ACSL smulation of the system equations was carried out. The saturation non-linearities, the digital calculation delays, as well as the effects of the zero-order hold in the D/A circuit were included in the simulations. Figure 8 shows the simulation of the controlled root strain in response to a first mode excitation. Care was taken to account for all transducer and amplifier constants so that comparisons can be made between actual and simualted strain values. Comparison of the experimental and simulated control voltages showed that the simulation took longer to come off the saturation non-linearity. However, the agreement between the experimental and simulated responses is encouraging as was the response of the spatial VGT in controlling vibrations of the continuum attached to it.

Kinematic Control With VGT's

Reinholtz (1987) has presented work that shows the complexity of the forward and inverse kinematic solutions for any of the possible configurations of the basic unit of a VGT. The solution of these equations are mostly iterative and have optimized at VPI&SU in order that they may be used in the real-time code designed to move the experimental VGT's. The spatial VGT has been used to test out rudimentary robotic tasks by programming it to draw letters with a pen fixed to the tip of a stiff rod attached to it. As in the vibration control experiments, the whole apparatus is approximately 14 ft. long. The letters NASA among others have been drawn with what may amount to the worlds longest pen. Figure 8 shows a reduction of two of these letters. Note the irregularities. These have been shown to reproduceable when the letters are traced overmore than one time. The irregularities were caused by the discretization of the letters and the fact that the resultant trajectories between points were dominated by motor differnces and not by needed shapes between the letters. The reproduceability of these trajectories is encouraging and indicates that VGT's have a strong future as so-called VGT (parallel) manipulators.

Salerno (1988) has discussed the problem of determining the desired link lengths in a truss that may have more degrees of freedom than are needed to satisfy the terminal constraints of the end of a long chain VGT manipulator, such as the one shown in Fig. 8. Many geometric configurations, both planar and spatial are possible candidates for VGT manipulators. Salerno presented only two geometries: the 3 degree-of-freedom (DOF) spatial octahedral/octahedral truss and the 3 DOF planar tetrahedral truss. These truss geometries were used as the fundamental element in a repeating chain of trusses. This resulted in a highly dexterous manipulator with perhaps 30 or 60 degrees of freedom that retains the favorable stiffness properties of a conventional truss. From a fixed base, this type of manipulator could perform shape or vibration control while extending and "snaking" through complex passageways or moving around obstacles to perform robotic tasks.

In order for this new technology to be useful in terms of robotic applictions the forward and inverse kinematic solutions must be efficiently solved. The approach taken here was to first concentrate on fully understanding the forward and inverse kinematics of the fundamental elements and then utilizing the insight thus gained to solve the more complex problem of the kinematic chains. Obstacle avoidance criteria and assumed shapes for the overspecified VGT chain were used as criteria to choose the needed VGT variable link lengths.

Conclusions

The present state of the art in the analysis and application of variable geometry trusses has been reviewed. The development of the potential of these smart structures is still in it's beginning. Future work will focus on implementation of high degree of freedom VGT's, the implementation of parallel intelligence to operate these high order systems, and the implementation of new actuators and sensors to drive the systems.

This work was supported by NASA Langley Research Center, Spacecraft Dynamics Branch, under grant NAG-1-570.

Table 1. Results of Multiple Actuator Comparison

Actuator	*Initial Conditions	LQR Performance Index J	Energy Consumed By Actuators J_E (Joules)	System Energy Performance Index J_D (Joule-sec)
Proof Mass	1st Mode	13,600	8.93	40.9
	2nd Mode	2,090	58.5	5.77
	3rd Mode	869	9.77	2.01
	All Modes	7,780	40.5	12.4
Reaction Wheel	1st Mode	70,800	57.2	289
	2nd Mode	4,600	14.9	19.4
	3rd Mode	99?	37.4	3.80
	All Modes	13,960	17.8	49.8
Planar Truss/ Proof Mass	1st Mode	32,800	92.6	183.
	2nd Mode	18,000	778.	191.
	3rd Mode	6,350	236.	29.4
	All Modes	19,400	93.5	72.7
Planar Truss	1st Mode	5,640	137.	8.75
	2nd Mode	6,010	501.	30.2
	3rd Mode	5,150	427.	11.5
	All Modes	25,400	396.	8.4

*Single mode initial conditions imparted 100J of strain energy to the beam; multiple mode initial conditions imparted 160J of strain energy to the beam (20J for each modelled mode).

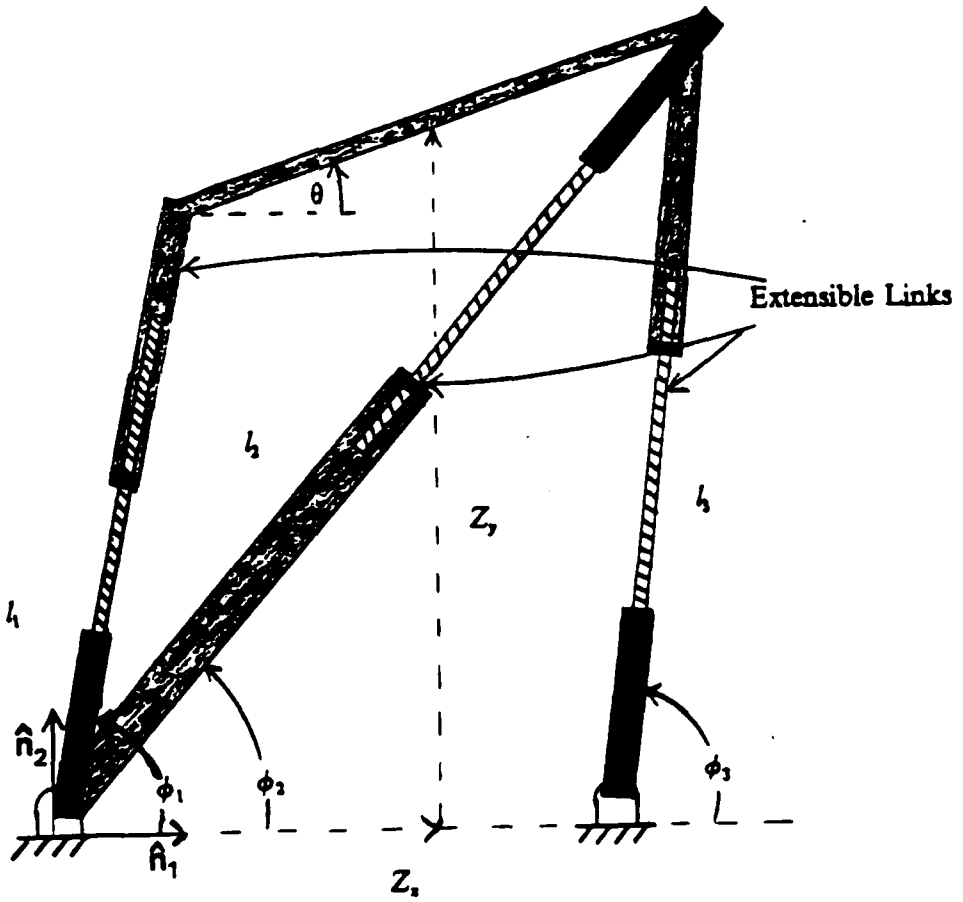

Figure 1. Planar Variable Geometry Truss Actuator

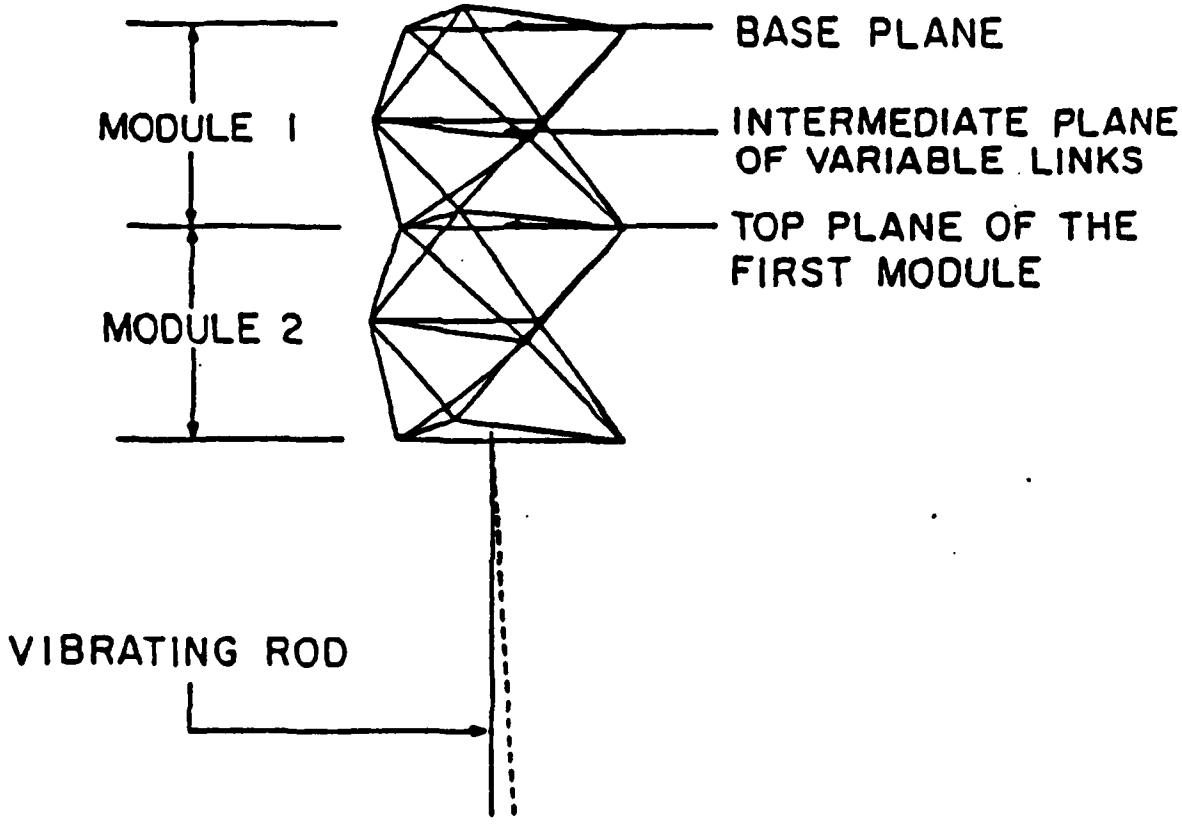

Figure 2. Spatial Variable Geometry Truss Actuator

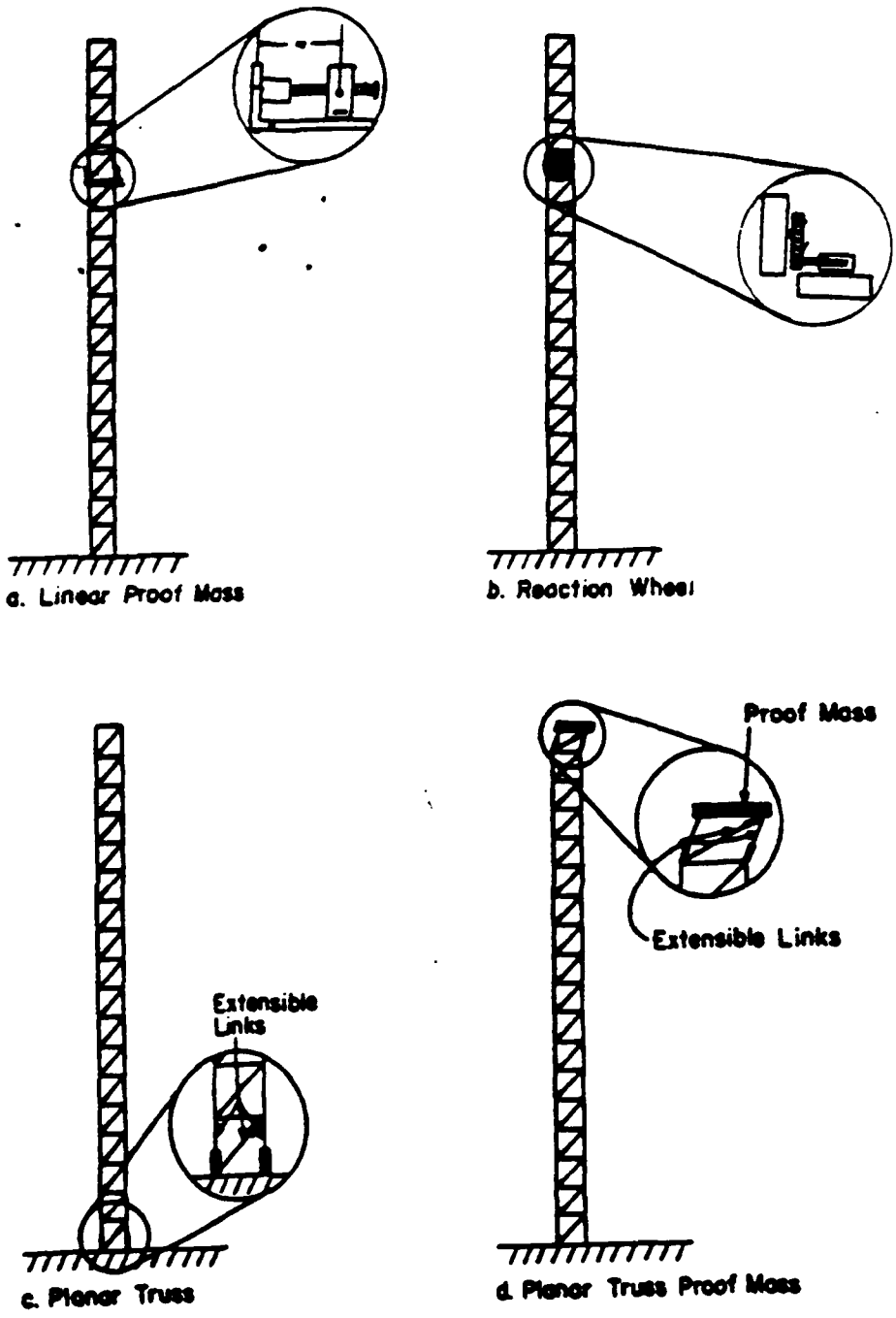

Figure 3. Illustration of Actuators Being Compared

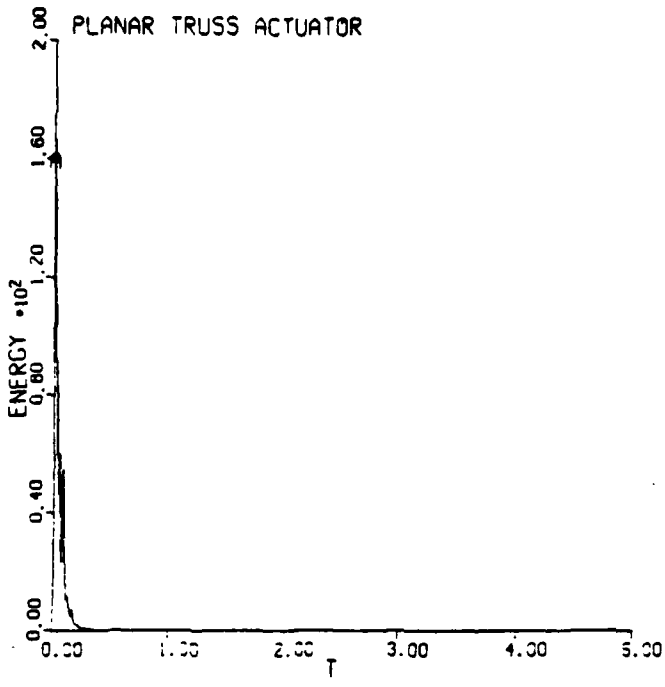

a. System Energy (Joules) vs. Time (sec)

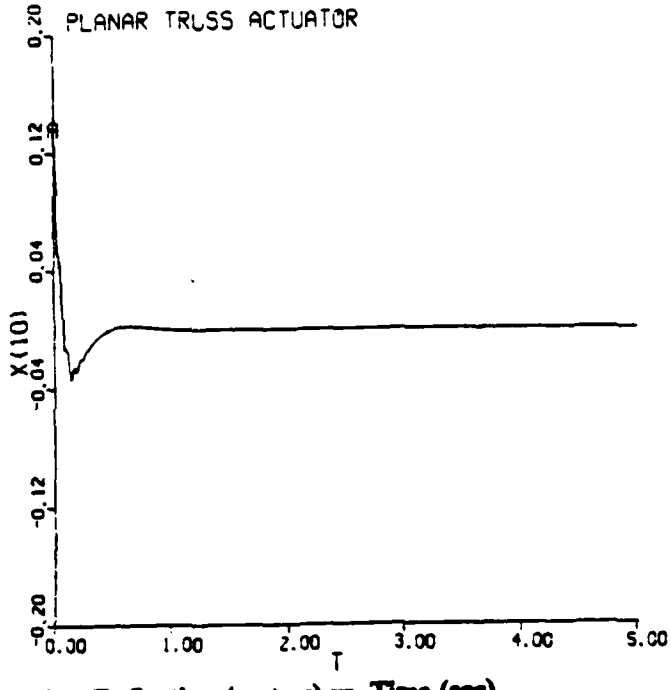

b. Beam Tip Deflection (meters) vs. Time (sec)

Figure 4. Response of Mini-Mast/VGT Actuator System to Initial Conditions

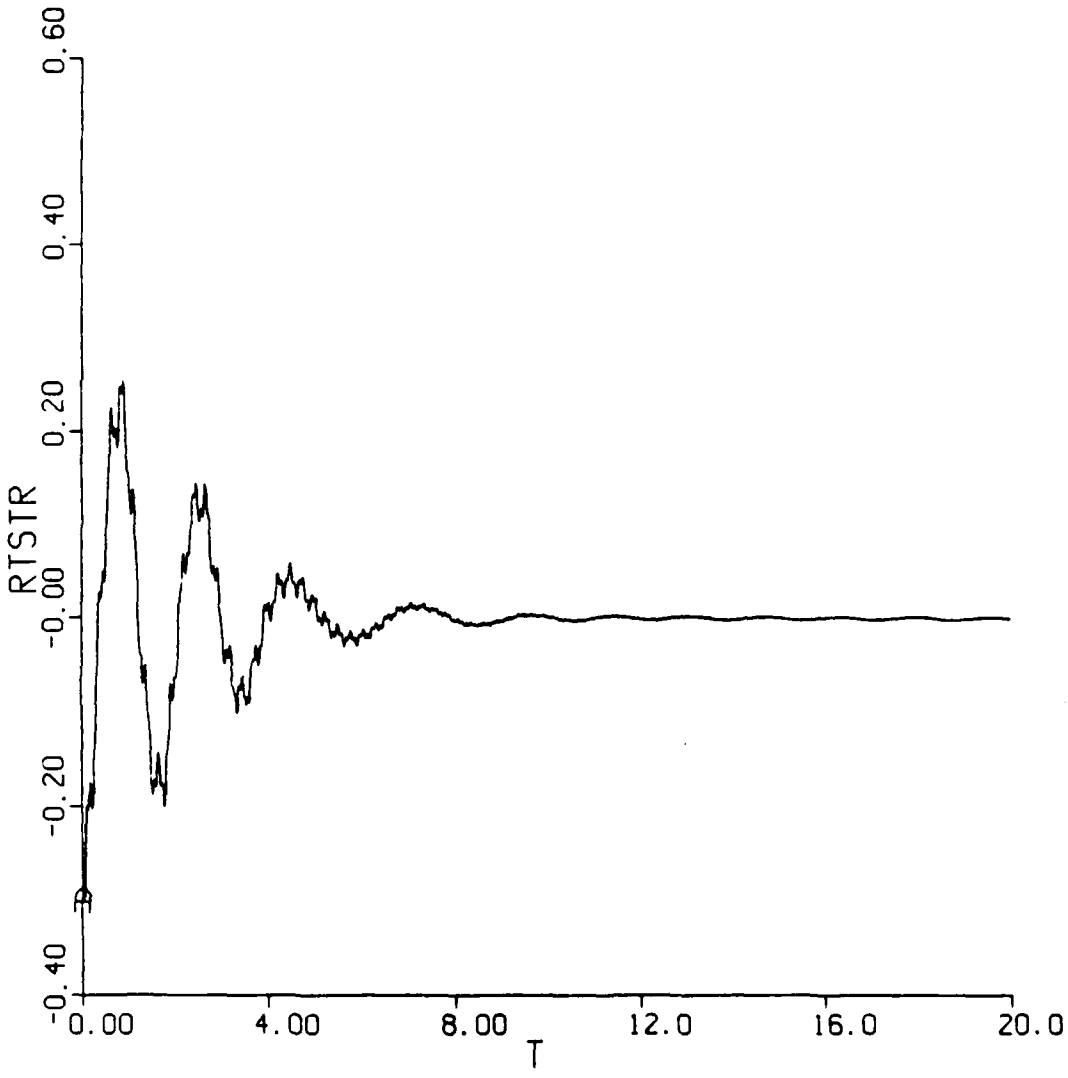

Figure 5. Root Strain of Beam Controlled by Planar VGT Actuator

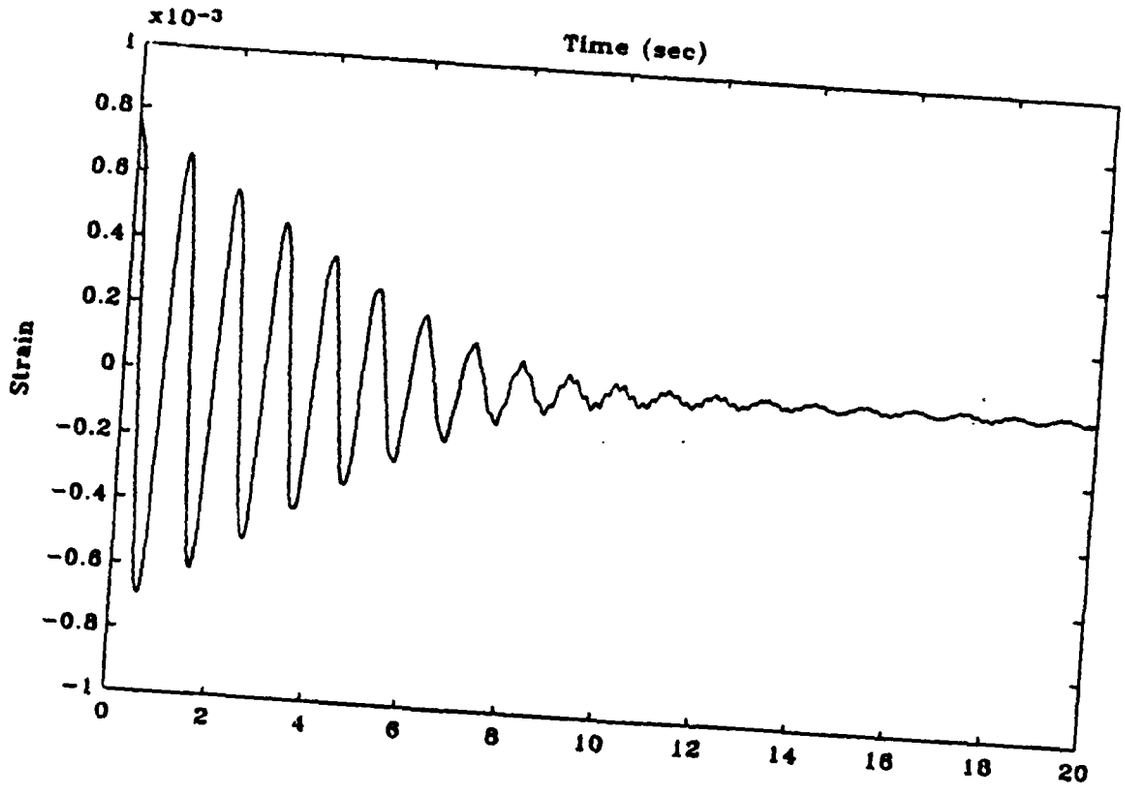

Figure 6. Root Strain of Rod Controlled by Spatial VGT Actuator-Experiment

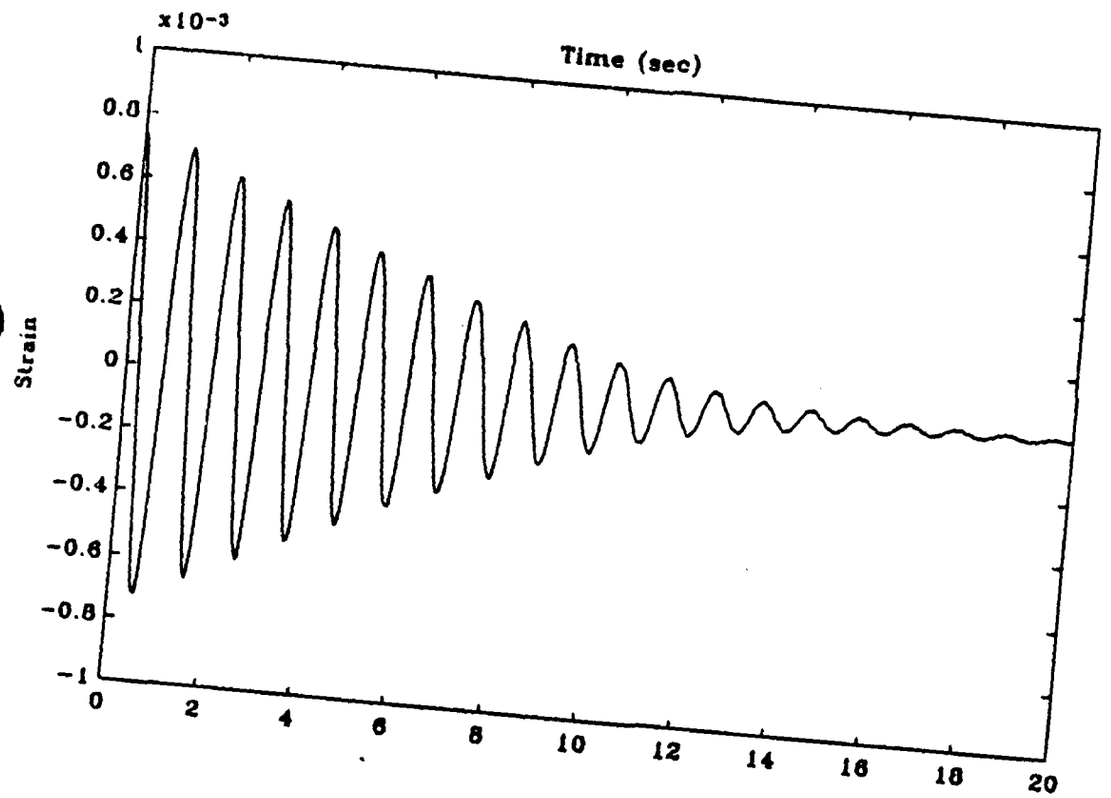

Figure 7. Root Strain of Rod Controlled by Spatial VGT Actuator-Simulation

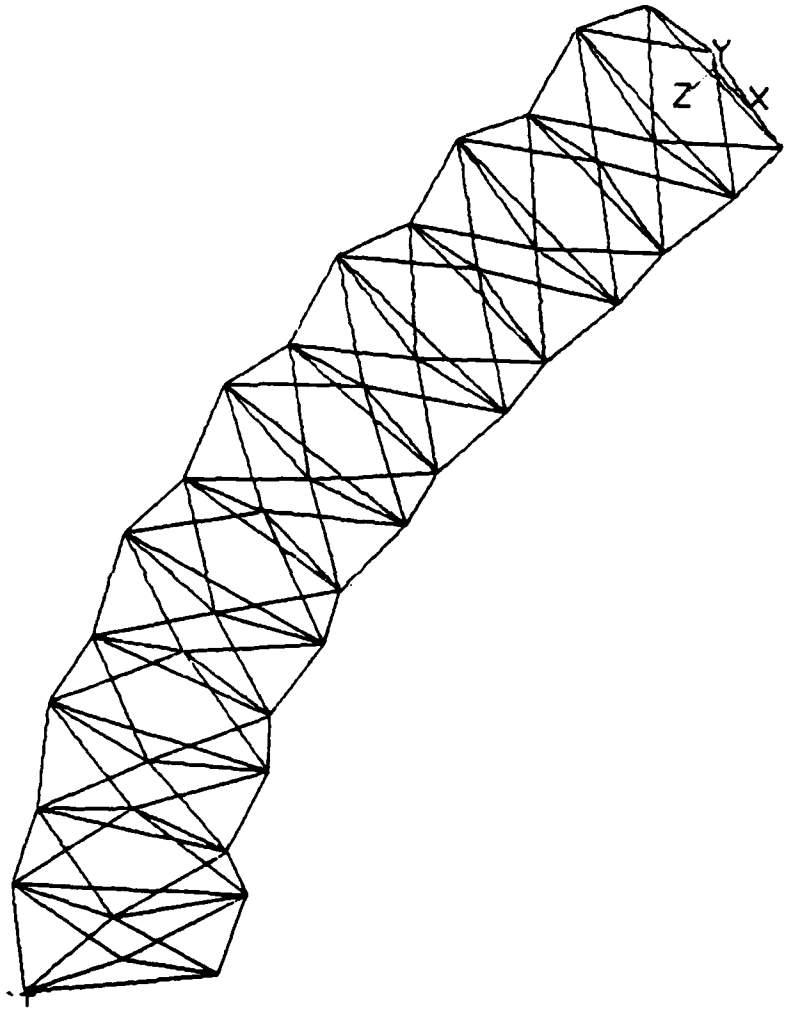

Figure 8. Twenty-One Degree of Freedom VGT

References

Anderson, W.W., and Groom, N.J., "The Annular Momentum Control Device (AMCD) and Potential Applications," NASA TN D-7866, March 1975.

Aubrun, J.N., "Analytical and Experimental Research in Large Space Structures Control," AIAA 23rd Aerospace Sciences Meeting, Reno, Nevada, January 14-17, 1985, pp. 1-15, AIAA Paper 85-0356.

Aubrun, J.N., "Theory of the Control of Structures by Low-Authority Controllers," *Journal of Guidance and Control*, Vol. 3, No. 5, September-October, 1980, pp. 444-451.

Bailey, T., and Hubbard J.E. Jr., "Distributed Piezoelectric-Polymer Active Vibration Control of a Cantilever Beam," *Journal of Guidance and Control*, Vol. 8, No. 5, September-October, 1985, pp. 605-611.

Clark, W. W., H. H. Robertshaw, and T. J. Warrington, "A Planar Comparison of Actuators for Vibration Control," submitted to the 30th Structures, Structural Dynamics, and Materials Conference, to be held April 3-5, 1989, Mobile, Alabama.

Doane, G.B., Waites, H., and Edgemon, G.D., "Development and Use of a Linear Momentum Exchange Device," Proceedings of the First NASA/DOD Control/structures Technology Conference, Norfolk, VA, Nov. 18-21, 1986, pp. 431-440.

Edberg, D.L., "Control of Flexible Structures by Applied Thermal Gradients," *AIAA Journal*, Vol. 25, No. 6, June 1987, pp. 877-883.

Fanson, J.L., and Chen, J-C., "Structural Control by the Use of Piezoelectric Active Members," Proceedings of the First NASA/DOD Control/Structures Interaction Technology Conference, Norfolk, VA, November 18-21, 1986, pp.809-829.

Ham, F.M., Hennings, B.L., and Greeley, S.W., Harris Corporation, AIAA Paper 87-2321.

Hanagud, S., Obal, M.W., and Calise, A.J., "Optimal Vibration Control By the Use of Piezoceramic Sensors and Actuators," Structures, Structural Dynamics, and Materials Conference, 28th, Monterey, CA, April 9-10, 1987, Technical Papers, Part 2B, pp.987-997, AIAA Paper 87-0959.

Joshi, N., "Mobility Analysis of Variable Geometry Trusses", MS Thesis, Department of Mechanical Engineering, VPI&SU, Blacksburg, VA, Feb. 1988.

Joshi, S.M., and Groom, N.J., "Modal Damping Enhancement in Large Space Structures Using AMCD's," *Journal of Guidance and Control*, Vol. 3, No. 5, September-October 1980, pp. 477-479.

Lovejoy, V.D., Robertshaw, H.H., Patten, W.N., and Horner, G.C., "Dynamics and Control of a Planar Truss Actuator," *Vibration Control and Active Vibration Suppression*, DE-Vol. 4, 1987, pp. 47-55.

Margulies, G., and Aubrun, J.N., "Geometric Theory of Single-Gimbal Control Moment Gyro Systems," *The Journal of the Astronautical Sciences*, Vol. XXVI, No. 2, April-June 1978, pp. 159-191.

Mills, R.A., "Active Vibration Control of a Cantilevered Beam: A Study of Control Actuators," Proceedings of the 34th International Astronautical Congress, Budapest, Hungary, October 10-15, 1983.

Natori, M., Iwasaki, K., and Kuwao, F., "Adaptive Planar Truss Structures and Their Vibration Characteristics," Structures, Structural Dynamics, and Materials Conference, 28th, Monterey, CA, April 6-8, 1987, Technical Papers, Part 2B, pp. 125-134, AIAA Paper 87-0743.

Patten, W. N., H. H. Robertshaw, D. Pierpont, and R. H. Wynn, "Active Vibration Mitigation of Distributed Parameter, Smart-Type Structures Using Psuedo Feedback Optimal Control," presented at Computational Aspects in the Control of Flexible Structures Workshop,NASA Langley Research Center, July 12-14, 1988.

Reinholtz, C. F., and D. Gokhale, "Design and Analysis of Variable Geometry Truss Robots", Proceedings of the 10th Applied Mechanisms Conference, Dec. 6-7, 1987, New Orleans, La.

Rhodes, M. D., and M. M. Mikulas, "Deployable Controllable Geometry Truss Beam", NASA Technical Memorandum 86366, June 1985.

Robertshaw, H. H., R. H. Wynn, Jr., H. F. Kung, S. L. Hendricks, and W. W. Clark, "Dynamics and Control of a Spatial Active Truss Actuator," Submitted to the 30th Structures, Structural Dynamics, and Materials Conference to be held April 3-5, 1989, Mobile, Alabama.

Salerno, R. J., C. F. Reinholtz, and H. H. Robertshaw, "Shape Control of High Degree-of-Freedom Variable Geometry Trusses", Using Psuedo Feedback Optimal Control," presented at Computational Aspects in the Control of Flexible Structures Workshop,NASA Langley Research Center, July 12-14, 1988.

Strunce, R.R., and Carman, R.W., "Active Control of Space Structures (ACOSS): A Status Report," Structures, Structural Dynamics, and Materials Conference, 25th, Palm Springs, CA, May 14-16, 1984, Technical Papers, Part 2, pp.348-356, AIAA Paper 84-1027.

Zimmerman, D.C., Inman, D.J., and Horner, G.C., "Dynamic Characterization and Microprocessor Control of the NASA/UVA Proof Mass Actuator," Structures, Structural Dynamics, and Materials Conference, 25th, Palm Springs, CA, May 14-16, 1984, Technical Papers, Part 2, pp. 573-577, AIAA Paper 84-1077.

PASSIVE SELF-ADAPTIVE STRUCTURES

Eugene I. Rivin
Department of Mechanical Engineering
Wayne State University
Detroit, Michigan 48202

Many critical applications of vibration isolators require adaptability to changing conditions (such as changing weight and weight distribution in the isolated object, rpm, ambient temperature, etc.), or easy adjustability (of selected natural frequencies of the isolation system, of effective damping, of stiffness ratios, etc.), or both. It is widely held that such properties can be achieved only through active control. Since the levels of cost, reliability and maintainability for active vibration control systems are presently not in the desirable range, the use of active systems is limited. However, it was shown (e.g., [2],[3],[4],[1]) that judiciously-designed passive nonlinear systems have an amazing potential for self-adaptation to changing conditions, as well as significant adjustability when subject to internal preload. For example, a single model of a constant natural frequency mount has been successfully used for installation of millions of very diverse industrial machines with weights-per-mount in the range of 400-10,000 lbs. [2]. Its performance characteristics are superior to conventional (linear) isolators, which are also more expensive and require lengthy computations and large inventories of mounts [4].

Our recent studies [5] have demonstrated that such desirable nonlinear characteristics can be obtained by very simple means, using elastomeric (rubber) elements simple streamlined shapes. It has also been shown that the use of streamlined elastomeric elements leads to reduced creep rates and to improved fatigue endurance, thus allowing the use of rubber blends with such desirable characteristics as high internal damping, which is usually associated with higher creep rates. The dimensions of the isolators can also be greatly reduced.

Benefits of streamlined elastomeric elements have also been demonstrated in torsionally flexible power transmission couplings [6],[7].

Nonlinear wire-mesh materials have a paradoxical double nonlinearity property - hardening nonlinearity at static and softening nonlinearity during vibratory loading [4]. the former property results in the constant natural frequency characteristic in a wide load range, ("smartness" for changing weight/weight distribution) while the latter property (which exhibits itself in strong amplitude dependences of effective stiffness and damping) provides a basis for "smart" behavior in complex vibratory environments. Stiffness at low amplitudes is very high, and damping is very low, while at high amplitudes stiffness is reduced while damping is very high (up to log decrements 2-3). Such characteristics are optimal, for example, for mounting

automotive engines: for large amplitude shake vibrations and for passage through resonance damping is very high, while at high frequencies which usually are associated with low amplitudes, low damping results in a good isolation.

If two nonlinear elements-1 and 2 in Fig. 1 (e.g., constant natural frequency isolators) are paired and subjected to internal preload (e.g. using preloading bolt 5 in Fig.1), then stiffness between object 3 and base 4 becomes dependent on the preload magnitude as illustrated by the plot in Fig. 1. This occurs due to shift of working points on load deflection characteristics with changing preload. This design could be made even "smarter" by using shape memory alloys or similar materials for preloader 5.

Use of "smart" passive nonlinear devices, some examples of which are briefly described above, in some cases supplemented with application of "smart" materials, can greatly improve performance of critical vibration control systems.

REFERENCE

1. Rivin, E.I., "Design and Application Criteria for Connecting Couplings," ASME J. of Mechan., Transmis., and Automation in Design, Vol. 108, 1986, pp. 96-105.
2. Rivin, E.I., "Principles and Criteria of Vibration Isolation of Machinery," ASME J. of Mechan. Design, Vol. 101, 1979.
3. Rivin, E.I., "Passive Engine Mounts-Some Directions for Future Development," SAE Technical paper 850481.
4. Rivin, E.I., "Application of Nonlinear Mechanical Systems for Advanced Machine Elements," Proceed. of 7th World Congress on Theory of Machines and Mechanisms, 1987, Vol. 3, pp. 1613-1618, Pergamon Press.
5. Rivin, E.I., Lee, B.S., "Frequency and Creep Characteristics of Streamlined Rubber Components in Compression," submitted to 1989 Pan American Congress on Mechanics.
6. Rivin, E.I., "Nonlinear Flexible Coupling Using Ideal Shape Elastomeric Members," Proceed. of 2nd World Congress on Gearing, Vol. 2, pp. 181-187, Paris, March 1986.
7. Rivin, E.I., "Nonlinear Torsionally Flexible Coupling", Patent disclosure, Wayne State University.

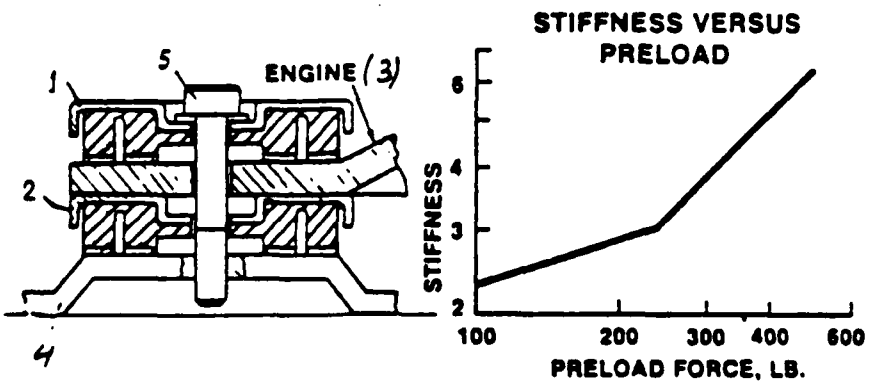
1
5
ENGINE (3)
2
4
STIFFNESS VERSUS
PRELOAD
STIFFNESS
6
4
3
2
100
200
300
400
600
PRELOAD FORCE, LB.

Figure 1

APPLICATIONS FOR SMART MATERIALS IN THE FIELD OF VIBRATION CONTROL

Theodore G. Duclos John P. Coulter Lane R. Miller

Lord Corporation
Thomas Lord Research Center
Cary, North Carolina 27512-8225, U.S.A.

ABSTRACT

Vibration isolation technology is a part of the general science of motion control. As such, the science of vibration isolation has grown and matured as motion control and, more specifically, transportation technology has become more sophisticated. The widespread availability of electronics and, more recently, digital "smart" electronics has broadened the performance capabilities of motion control systems and placed higher demands on vibration isolation technology. At the same time, new light materials and the placement of powerful powerplants on flexible and light structures has produced a need for new vibration isolation technologies for controlling the vibration problems caused by the new motion control and material technologies.

This paper discusses four general classes of vibration control problems, some commercial applications where they are important, and some of the newer vibration control technologies applicable to each area. The classes range from a single degree of freedom, spring, mass, damper system with a single disturbance input to flexible structures with distributed disturbance inputs.

INTRODUCTION

In the past ten years, controllable vibration isolation systems have become a commercial reality. The driving force behind the new isolation technology is the ability to achieve better isolation with controllable systems. Undoubtedly, the availability of microprocessors, controllable devices and smart materials is fueling the proliferation of controllable systems. As computing power increases and controllable hardware improves, the number of proposed applications for controllable isolation systems has and will continue to multiply.

The practicality of any controllable isolation system will depend on several factors. Cost, complexity, and reliability vs. the performance gains will determine the ultimate success of any proposed system. Reducing the complexity of a system will synergistically reduce the system cost, increase the reliability, and increase the practicality of the system. The ability to perform

multiple tasks such as vibration signature analysis for diagnostic purposes will increase the value of controlled isolation systems. Single component performance of multiple tasks will offset higher costs and system complexity normally associated with controllable systems.

To achieve low system complexity and still attain the benefits of control, the control strategy and the hardware must be complementary. The derivation of a control strategy realizable in hardware represents the first significant challenge to a system designer. Since a particular control strategy can be realized by many types of hardware, but not as efficiently in all cases, selecting hardware to most efficiently implement the control is the next major step. For example, a control requiring a force to be proportional to a velocity can be accomplished with a hydraulic actuator, but a linear damper is a much more efficient method of accomplishing the same thing. Successful integration of the hardware's passive characteristics into the control strategy is necessary to minimize system complexity.

In this paper, integration of control strategy and hardware is illustrated with four vibration isolation examples: 1) isolation of a mass with a single degree of freedom; 2) isolation of a mass with multiple degrees of freedom; 3) isolation of an engine on a structure; and 4) isolation of a structure from distributed inputs. The first example contains a detailed description of current control strategies and hardware illustrating the ability to integrate the hardware with the control strategy. The remaining three examples describe more complex vibration problems with less well developed control strategies and hardware solutions. In each of these examples, some solutions for the problems including the potential use of smart materials are considered and applications where the problems are prevalent are discussed. While not intended to be a comprehensive review of vibration isolation, the present discussion is aimed at providing a view of vibration isolation technology and add perspective to the current discussion of smart materials.

ISOLATION OF A MASS WITH A SINGLE DEGREE OF FREEDOM

Figure 1 shows the simplest, resonant, dynamic system imaginable -- a mass on a spring. In this example, the goal of the vibration isolation system is to hold up the mass, minimize the mass acceleration ($\ddot{x}_1$) and minimize the suspension travel (x_1-w). To illustrate the need to integrate the control strategy with the hardware, a desired control policy must first be derived. A quadratic performance criteria based on $\ddot{x}_1$ and (x_1-w) can be used with optimal control theory to derive a force control law based on the system states. The control law, which specifies the force applied to the mass has the form:

$$F = g_1 \dot{x}_1 + g_2 (x_1 - w) \tag{1}$$

Where g_1 and g_2 are gains specified by the designer. With the control law in hand, it is instructive to study five different isolation systems used to suspend masses. These five systems are: 1) a spring, 2) a spring and a damper; 3) a force generator; 4) a spring and a force generator; and 5) a spring and a controllable damper.

The first suspension system, a spring, is shown in figure 1. The force of the spring on the mass will be proportional to (x_1-w), therefore, this system can only produce a part of the desired control law given as equation (1). As a consequence, this system will not satisfy the performance criteria and the resulting tradeoff in this system is apparent from inspection of the transmissibility plot, presented as figure 2, between the mass velocity ($\dot{x}_1$) and the input velocity ($\dot{w}$). For this system, the resonant frequency, ω_n, is determined by the well known relation

$$\omega_n = \sqrt{\frac{K}{M}} \tag{2}$$

where K is the spring stiffness and M is the mass. The use of a soft spring will improve the isolation at lower frequencies by lowering the resonant frequency. Unfortunately, softer springs also have higher static displacements for given loads and provide large motions when a disturbance force is applied to the mass. Small changes in the mass can also produce large changes in the static displacement. In designs using this simple system the static displacement of the spring is traded off with the low frequency isolation.

If the input disturbances are broadband, impulsive, or have any way of exciting the resonance, then the system in figure 1 will not be acceptable because of the very high displacements near the resonance. Adding a damper as shown in figure 3 is an obvious solution for the resonance problem. Since the damper produces a force proportional to $(\dot{x}_1 - \dot{w})$, the force on the mass will be given by the equation:

$$F = K(x_1-w) + C(\dot{x}_1 - \dot{w}) \tag{3}$$

where K and C are the spring and damping constants respectively. Since the force on the mass is not the same as the optimal control force, this system also has a design tradeoff. As seen from the plot in figure 2, the addition of damping brings the transmissibility at the resonant frequency down, but at the price of less isolation in the higher frequency range.

In this system, the location of the resonant frequency will change if the mass changes (changing loads in a passenger car, for instance). Since the damping will be designed to tradeoff displacements at the resonant frequency against isolation at high frequencies, then the change in the resonant frequency means a different damping is needed to achieve the same tradeoff. The resonant frequency can theoretically be made invariant for a range of loads by using a non-linear spring [1]. If the non-linear spring gets stiffer as its deflection is increased, then the resonant frequency can be kept constant regardless of the load. However, this approach still cannot produce the optimal force nor compensate for the changes in material properties that can occur due to temperature fluctuations or aging. Another approach is needed.

The optimal control force can be produced by the passive system shown in figure 4. In contrast to the preceding system, the damper in figure 4 has been attached to an inertial ground. This change in the damper connection makes the damper force proportional to $\dot{x}_1$ and makes the force on the mass equal to

$$F = K(x_1-w) + C\dot{x}_1 \tag{4}$$

If the damping is adjusted to be critical, then the transmissibility between the mass velocity and the input velocity will be as shown in figure 2. This system controls the resonance and provides high frequency isolation. Unfortunately, since an inertial ground is not usually available, this hardware implementation of the optimal control law is generally not realizable. In fact, the control law cannot be satisfied using purely passive hardware.

The fully active suspension shown in figure 5 is a direct approach for achieving the proper control force and, in contrast to the passive solution, the fully active system is realizable in hardware. The

entire suspension consists of a force generator between the mass and the input. The desired optimal force is produced in this system by measuring $\dot{x}_1$ and (x_1-w), feeding the values to a microprocessor which multiplies them by selected gains and then outputs a control signal to the force generator. As seen from the transmissibility plot in figure 2, this system provides the correct force to the damper. Unfortunately, the system is not efficient because in real hardware, the system will use power to hold up the mass, even when the input disturbance is zero.

The efficiency of the fully active system can be markedly improved by borrowing pieces from the passive systems. For instance, the first suspension system, the spring, provided a part of the control force without using any power. If a spring is put in parallel with the force generator, as in figure 6, then the fully active system performance can be maintained and the efficiency is greatly improved. If $K=g_2$ in equation (1), then the actuator only needs to supply $g_1\dot{x}_1$ in equation (1) or $C\dot{x}_1$ in equation (4). Further modification of the system with a nonlinear spring would integrate another performance improvement from the passive suspensions.

The fully active system in figure 6 still has several drawbacks. First, malfunctions in the control system can cause the suspension to pump energy into the mass and create a safety problem or instability. Second, it will still use much more power than is actually necessary to achieve the desired performance. In figure 7, the force generator has been replaced by a controllable damper. This system is called a semi-active suspension system. If the damper in the semi-active system is controlled using the logic:

$$\text{If } \dot{x}_1(\dot{x}_1 - \dot{w}) < 0, \text{ then the damping is zero}$$
$$\text{If } \dot{x}_1(\dot{x}_1 - \dot{w}) > 0, \text{ then the damper force is } C\dot{x}_1,$$

then the suspension will produce the transmissibility plot shown in figure 2 [2]. As seen from the curve, the semi-active suspension produces nearly the same performance as the fully active system. Significantly, the performance is attained by using very little power. Also, unlike the fully active suspension, the semi-active suspension will never add energy to the system and in the case of breakdown, it will revert to a stable, damped, passive system.

In the future, smart materials could have a place in these suspension systems. Controllable springs made of memory metals could compensate for changing loads. They could also replace the hydraulic actuators presently used in fully active systems. Electrorheological fluids may simplify the design of controllable dampers and actuators and, at the same time, speed up the device responses. Piezoelectric materials are already used in sensors. Their incorporation into springs, dampers, or actuators could integrate the sensing functions into the suspension elements. This combination would fulfill some of the promise offered by smart materials.

SYSTEMS WITH MULTIPLE DEGREES OF FREEDOM

The single degree of freedom system provides an easily understood demonstration of the need to make the suspension hardware complement the control strategy. The insight gained from this system can be carried over to the study of more complex, multiple degree of freedom systems. Since most of the vibration isolation problems encountered in practice are multiple degree of freedom systems, relating the concepts discovered from the single degree of freedom system is crucial to their translation into engineering practice. The following examples demonstrate some ways to make the translation and offer guidance for future research.

ISOLATION OF A MASS WITH MULTIPLE DEGREES OF FREEDOM

A more complex isolation problem is shown in figure 8. In the figure, the mass is no longer constrained to move in one direction and forces are allowed to act on the mass. As it is drawn, the configuration is actually a schematic representation of an automobile, neglecting the so-called "unsprung mass" of the wheels and axles. The isolation system is represented by the four springs and the objective of the isolation system is to minimize the acceleration of the mass and the displacements of the suspension system.

The approaches to controlling the motions of the mass in figure 8 are similar to those used to control the single degree of freedom system. Using a performance criteria composed of the suspension displacements and the mass accelerations, an optimal force control law can be derived. Unlike the single degree of freedom control law, the multiple degree of freedom control law for controlling the mass in figure 8 will consist of four equations and all of the twelve state variables each multiplied by a gain will appear somewhere in the equations. In general, a control law developed for this type of system will have as many equations as there are suspension elements. In the case shown, there are four springs, therefore, there will be four equations.

The existence and form of an optimal force control law is dependent on the suspension geometry and the number of suspension elements. To preserve the generality of the discussion, an exact solution will not be given here. Rather, the tradeoffs between springs, dampers, force actuators and controllable dampers in the multiple degree of freedom system will be discussed with reference to the results found in the single degree of freedom system.

The six degree of freedom system shown in figure 8 has six distinct resonant frequencies. If, as shown in the figure, springs are used as the suspension system, then, as was the case in the single degree of freedom example, isolation will be good at high frequencies. Also, the displacements will be very high near the resonances and the static displacement will need to be traded off against high frequency isolation.

Putting dampers in parallel with the springs will help control the displacements near the resonant frequencies. However, unless the suspension geometry is carefully designed to uncouple them, the modes of the mass in figure 8 will be coupled. That is, the displacement of one spring or the application of a force to one point on the mass will excite more than one mode. If the modes are coupled (as they are in most systems), then critically damping one degree of freedom in figure 8 virtually guarantees that the other five degrees of freedom (or modes) will either be overdamped or underdamped.

In actual practice, this situation is not as bad as it seems, since the coupling between some modes is not strong and not all modes are excited. For example, in autos, the tradeoff made between the handling and the ride is really a tradeoff in the damping of one mode and the isolation of another. The tradeoff is similar to the tradeoff between the stiffness and damping in the single degree of freedom system, but it actually arises because the damping of one mode affects the isolation of the other.

This tradeoff can be seen by assuming that the configuration of figure 8 represents a car and that the suspension elements are rearranged such that they are parallel to the x direction. A measure of handling is the amount of roll produced about the y axis (assuming the y axis points along the traveling direction of the car) as the car enters a turn. The ride can be judged by the displacement of the mass in the x direction in response to inputs in the x-direction. Assuming the resonant frequency of the mass in the x-direction will be lower than the resonant frequency in the roll

direction, if the roll is critically damped with passive dampers, the ride will suffer because it will be overdamped. Conversely, if the ride is critically damped, then the roll will be underdamped and the handling will suffer. While this is an oversimplification of the problem, this essentially is the tradeoff seen in passenger cars. Smooth riding cars generally handle poorly while cars with excellent handling usually have harsh rides.

One answer to the handling versus ride tradeoff can be found on many newer cars. In these vehicles, the driver or a computer can change the dampers to soft or hard depending on the driving situation. While these adaptive solutions partially solve the problem, fully active or semi-active systems are better solutions. These systems are simply more complex versions of the controllable isolation systems discussed in reference to the single degree of freedom problem. In the fully active system, force generators are placed in parallel with springs. Similarly the semi-active system uses controllable dampers in parallel with springs.

The implementation of the control policies for these two systems are much more complex than the implementation of the single degree of freedom control law. For instance, to control each of the degrees of freedom, these systems require knowledge of the states of the system (twelve for the six degree of freedom system) and therefore, if observers or Kalman filters are not used in the control calculations, at least twelve independent sensors are required. Of course, in a real system all the modes are not important, therefore less than twelve sensors are usually used. Generally, the displacements of the springs are measured as well as the acceleration of the mass in at least the heave (motion along the x axis) and the roll about the y and z axes. The decisions of how to control the force generators or the dampers are based on a balance between spring deflection and accelerations in the measured directions. Since control of the various acceleration directions involve tradeoffs, weighting functions are used to balance the control. Although it is not possible to simultaneously control the mass acceleration optimally in each direction, with the proper weighting function it is possible to reduce the accelerations in each direction more with an active control or semi-active control than with a passive system [3].

As in the single degree of freedom example, the applications for smart materials in the control of the mass in figure 8 will be in controllable springs, dampers, sensors, and possibly actuators. Smart materials whose properties are independently controllable in several directions will be especially valuable. Since the control laws for the system in figure 8 will specify different forces in each direction, the simultaneous control of the forces in different directions by smart materials will reduce the amount of necessary hardware. For example, if the control law calls for damping in the x and y directions, then a smart material with controllable damping in two directions could perform the role of two passive dampers.

MASS ON A STRUCTURE

The isolation problem depicted in figure 9 represents a general engine mounting system. This system has multiple degrees of freedom and differs from the previous two problems in two respects. First, the structure is flexible and therefore cannot be modeled and handled as a rigid body, i.e., it will have an infinite number of modes. Secondly, the motions of both the mass and the structure need to be minimized. Cyclic disturbances come from the mass and must be isolated from the structure. Impulsive disturbances will be applied to the structure suspension and the responses of the structure and the mass to these disturbances must be minimized.

As in the previous example, the control law will be heavily dependent on the geometries of the suspension systems. In addition, the structure may not be easy to model. Therefore, the design of

the suspension systems, particularly the mass suspension system, will be discussed in general terms where the tradeoffs are related back to the single degree of freedom system.

The basic tradeoff encountered in systems of this type is the tradeoff between holding the mass up and keeping the disturbance vibrations from exciting the structure. Also, in response to sudden motions of the structure it is desirable to closely connect the mass to the structure to help reduce the structural motions. These desires are conflicting because the mounts must be stiff to hold up the mass and damped to closely connect the mass to the structure when the structure moves. In contrast, the mounts should be soft and lightly damped to isolate the vibrations from the structure.

One solution to the tradeoff is to use a property of multiple degree of freedom systems mentioned in the previous section. That is, if properly designed, the modes of the mass can be decoupled. The mounting system connecting the mass to the structure can be made very stiff to motions in the x direction yet very soft to roll motions about the y axis. This decoupling is the principle of focalized engine mounting systems. Although the concept can be easily demonstrated and has been used successfully in commercial products, there are some drawbacks. Most notably, a considerable amount of static torque windup can occur due to the soft roll stiffness.

The recently developed fluid filled mounts can also overcome some of the engine mounting system tradeoffs. Fluid filled mounts, such as the one shown in Figure 10, can be designed to have frequency dependent complex stiffnesses as shown in figure 11. If designed correctly, the mount can be tuned to accommodate the tradeoffs in the mounting system. With the proper internal structure, the mount can be made statically stiff, highly damped at a resonant frequency of the mass, and also either very stiff or very soft at higher frequencies depending on the engine speed and amplitude of the mount's displacement. Thus, this seemingly simple device can be made to sort out some of the complex vibration environment in figure 9.

Unfortunately, even the most complex passive internal structure of a fluid mount cannot produce a low dynamic stiffness over a wide frequency range -- a characteristic needed for many aircraft and automotive applications. This characteristic can only be achieved with an adaptive, semi-active, or fully active mounting system.

An adaptive system which has a low dynamic stiffness over a wide frequency range is described by Duclos [4]. This system uses electrorheological fluids and valves to tune a dynamic stiffness "notch". As the engine speed changes, the system adapts itself to tune the notch to the dominant vibration frequency. The system has been demonstrated on a car and the commercialization of tunable mounts is proceeding in several products.

Both fully active and semi-active systems have been applied to vibration problems of the type shown in figure 9, but they are only in the early prototype stages. Deciding on the control law is perhaps the most difficult aspect of the system designs. The total vibration environment of the system shown in figure 9 may be too complicated to ever yield analytic solutions to the control law problem.

Smart materials, distributed over the structure, may be a better method for controlling the structure vibrations. Both constrained and unconstrained layer passive damping materials are examples of currently available distributed control methods (figure 12) [5,6] and controllable materials have recently been proposed as possible future methods for controlling the structure vibrations [8]. Distributed control of the structure vibrations with smart materials may make the structure look like a rigid body to the suspension systems. This change would make the derivation of the suspension system control laws a more tractable problem. If distributed control of the structure by smart materials eliminated the need for the suspension systems, then this would be the best of all solutions.

DISTRIBUTED EXCITATION OF A FLEXIBLE STRUCTURE

The final vibration problem is shown in Figure 13. In this problem a flexible structure is excited by distributed forces. An example of this would be an airplane encountering turbulence in flight. Another example is airborne engine sound coupled to a car structure through the air.

Generally, the tradeoffs in these systems are complex, but as an example, in transportation applications an important tradeoff is made between the weight and stiffness of structural components. For efficiency, low mass is desirable but for fast response to control forces and few resonance problems, high stiffness is desirable. For a given material, lowering the mass of a structure generally means lowering its stiffness, therefore low mass and high stiffness are often conflicting requirements.

The constrained or unconstrained layer damping as shown in figure 12 is one method controls the structural resonances without significantly reducing the structural mass. This method will reduce the resonant peaks through the material damping without adding as much weight as an increase in stiffness would require. A drawback is that the increase in damping can generally only be optimized for specific narrow temperature and frequency ranges.

Most proposed methods for adaptive, semi-active, and fully active control of the vibration problem in figure 13 use smart materials. They consist of distributed actuators (memory metals, piezoelectric polymers, piezoelectric ceramics) or controllable modulus materials (phase transition controlled by temperature, electrorheological fluids). While many of these solutions have been proposed, only the control of piezoelectric layers has been developed to any great extent [7].

DISCUSSION

The vibration isolation problems presented have proceeded from the simple to the very complex. In parallel, the corresponding solutions proceed from the nearly perfect to the incomplete. A continuous thread through the problem and solution presentations is a need for control strategies and hardware in the solution. Together, the control strategy and the hardware form a complete solution to a vibration control problem. When passive hardware is used, the control strategy is defined by the hardware and vice versa. Controllable hardware places fewer restrictions on the control strategies. The price for this flexibility is system complexity and the need to develop appropriate control policies for controlling the hardware. As the complexity of the problems increase from single degree of freedom systems multiple degree of freedom rigid bodies and flexible structures, the number of sensors increases and the proper control strategy becomes more difficult to define. The success of controllable hardware will also depend as much on the successful derivation of practical control strategies as it will on the successful demonstration of the hardware.

Many fully active control strategies have been proposed in the literature for the use of discrete actuators to solve the structure and rigid body motion control problems. The control mathematics of distributed actuators has also received considerable attention. For semi-active systems, the control strategies are less developed, especially in the control of flexible structures. This situation is an opportunity for pioneering work covering a wide range of potential applications. The low power consumption and essentially fail-safe nature of semi-active control makes the approach ideal for vibration isolation applications.

The solutions, as presented here have been idealized. In real hardware, high frequency performance usually can only be attained at the cost of increased power consumption. In some cases, heat transfer limits will prevent proper high frequency performance altogether. As controllable hardware and smart materials are developed, they must overcome the limitations of high speed, power consumption and complexity present in the currently available hardware. Piezoelectrics and electrorheological fluids offer the promise of high speed performance. Memory metal composite structures present the possibility of solid state, high flexion actuators moving at reasonable speeds. Control of the heat transfer must be obtained before memory metal devices will become practical.

Smart materials can be used in the hardware for each of the four example motion control problems. Since these problems cover many of the motion control problems encountered in practice, the specific potential applications for smart materials are too numerous to be listed here. In addition, once these materials are used to solve motion control problems, their usefulness in performing other functions (such as diagnostic sensing) will become more apparent. Additional functionality, beyond vibration control, will enhance their value in vibration control systems and add to the list of potential applications. In some situations, dual role, smart materials could replace currently available vibration control technology and add capacities which are currently unattainable.

While many approaches are under research to tackle problems similar to the four presented here, the practicality of smart materials in real vibration control systems is still unclear. This uncertainty is especially true for the control of large structure motions and vibrations. It is easy to see how a simple cantilever beam or a plate may be controlled or damped with a controllable layer of material, but it is a giant leap from those simple situations to an airplane or a car.

REFERENCES

1. Riven, E. I., "Passive Engine Mounts - Some Directions for Further Development", *Society of Automotive Engineers technical paper 850481*, Warrendale, Pennsylvania, 1985.

2. Karnopp, D. C., Crosby, M. J., Harwood, R. A., "Vibration Control Using Semi-Active Force Generators," *ASME Paper No. 73-DET-122*, June 1974.

3. Miller, L. R., *An Approach to Semi-Active Control of Multiple Degree of Freedom Systems*, Ph.D Dissertation, North Carolina State University, Raleigh, North Carolina, 1988.

4. Duclos, T. G., "An Externally Tunable Hydraulic Mount which Uses Electro-Rheological Fluid," *Technical Paper #870963, Society of Automotive Engineers*,

5. Beranek, L. L., *Noise and Vibration Control*, McGraw-Hill, New York, 1971.

6. Nashif, A. D., Jones, D. I. G., and Henderson, J. P., *Vibration Damping*, John Wiley and Sons, New York, 1985.

7. Bailey, T., and Hubbard, J. E. Jr., "Distributed Piezoelectric-Polymer Active Vibration Control of a Cantilever Beam," *Journal of Guidance, Control, and Dynamics*, Vol. 8, No. 5, pp. 605-611, 1985.

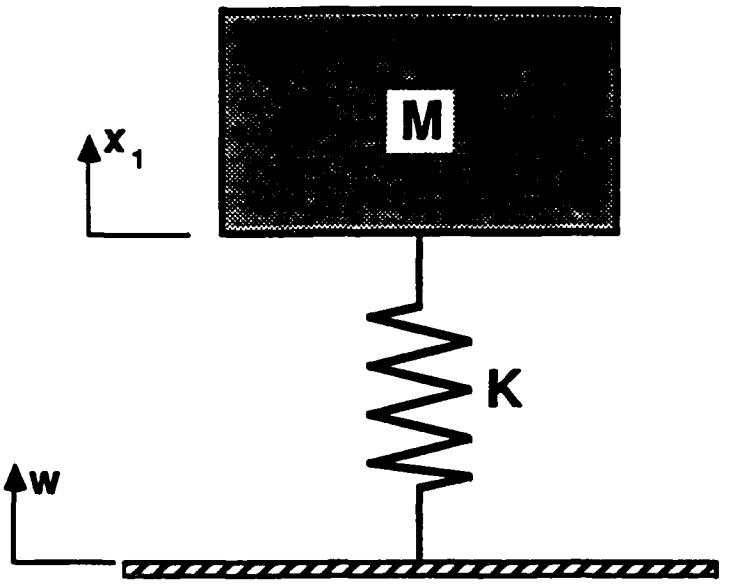

Figure 1: Single degree of freedom isolation of a mass.

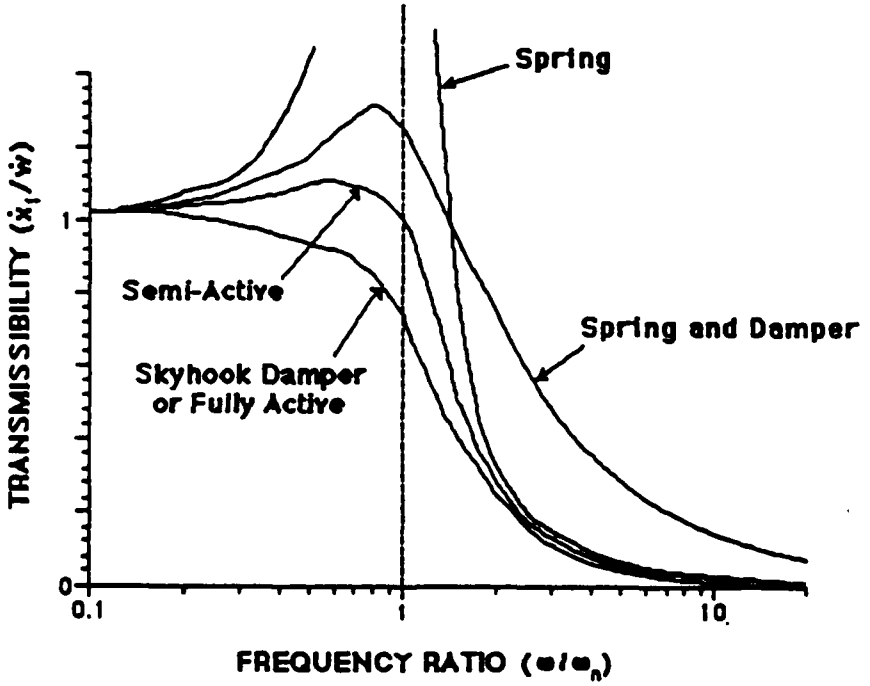

Figure 2: The variation of transmissibility ratio with frequency for undamped, passively damped, semi-active, and fully active single degree of freedom systems.

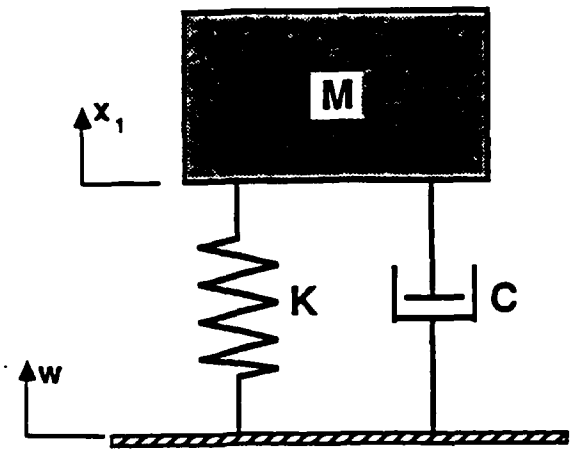

Figure 3: Single degree of freedom isolation of a mass including damping.

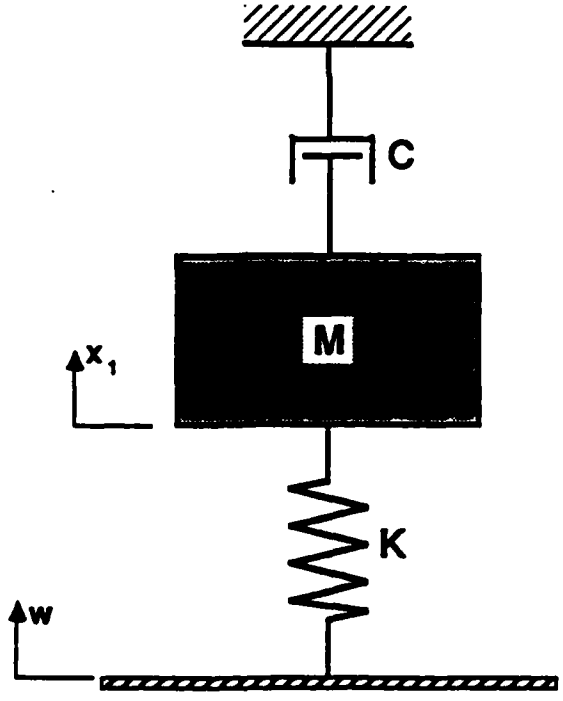

Figure 4: Single degree of freedom isolation encompassing a "skyhook" damper.

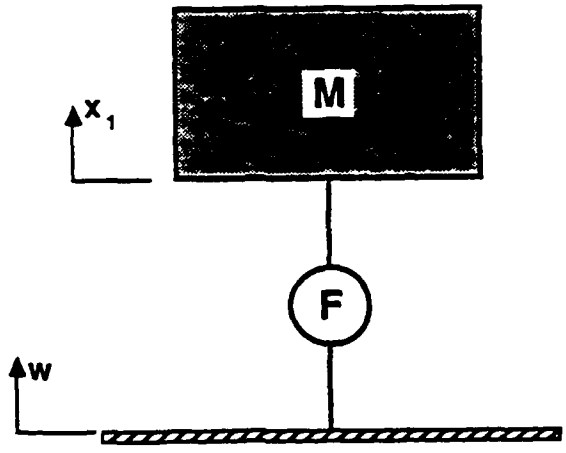

Figure 5: Single degree of freedom isolation utilizing fully active control.

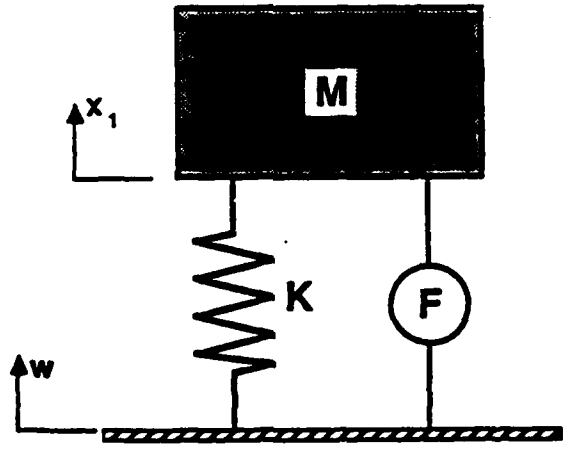

Figure 6: Single degree of freedom isolation with a spring and force actuator.

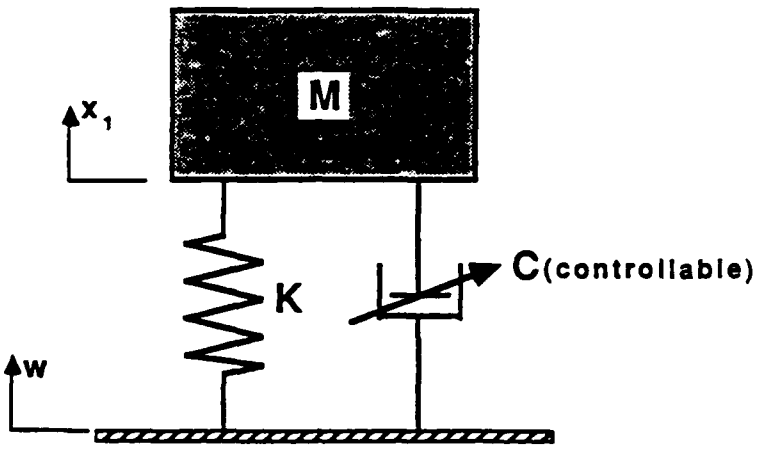

Figure 7: Single degree of freedom isolation with a spring and controllable damper.

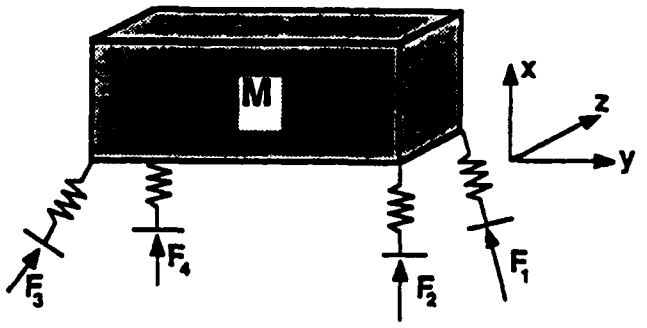

Figure 8: Multiple degree of freedom isolation of a mass.

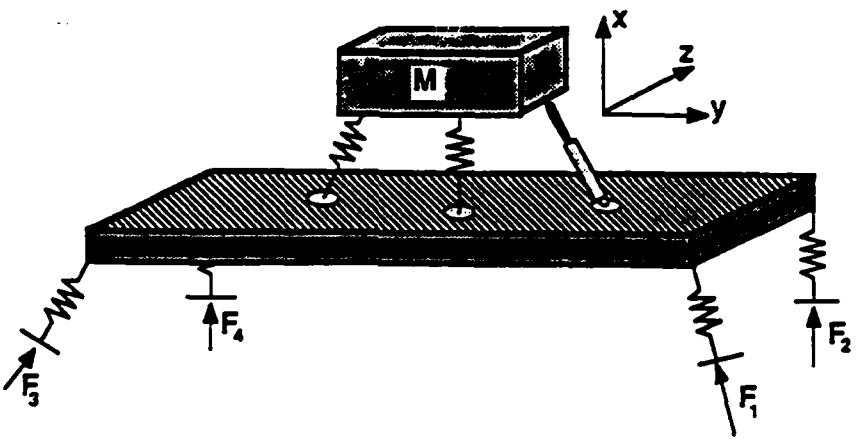

Figure 9: Schematic representation of a mass on a distributed flexible structure.

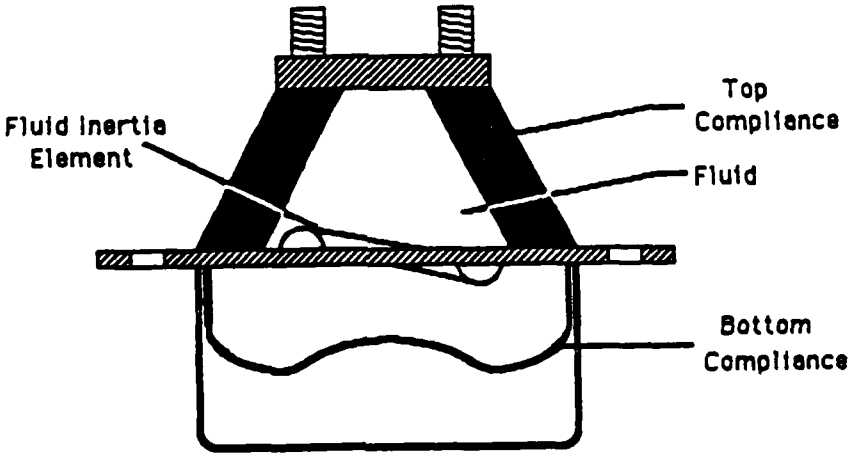

Figure 10: Typical configuration of a fluid filled structural mount.

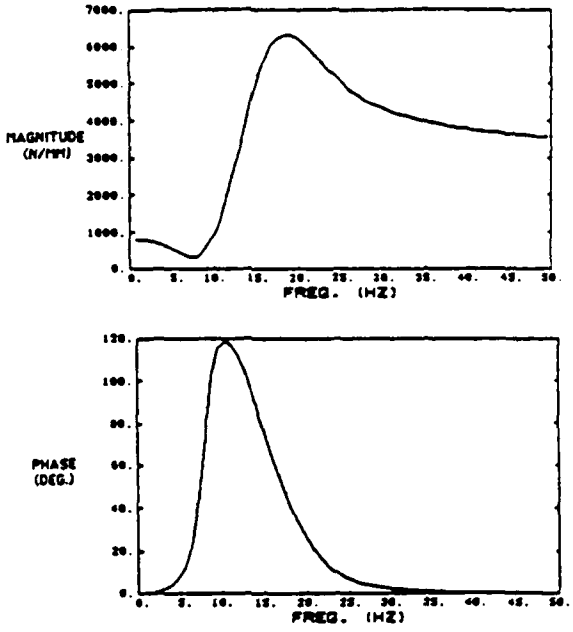

Figure 2: SIMULATED DYNAMIC STIFFNESS OF A SINGLE INERTIA ELEMENT HYDRAULIC MOUNT

Figure 11: Variation of complex stiffness of a fluid filled mount with *frequency*.

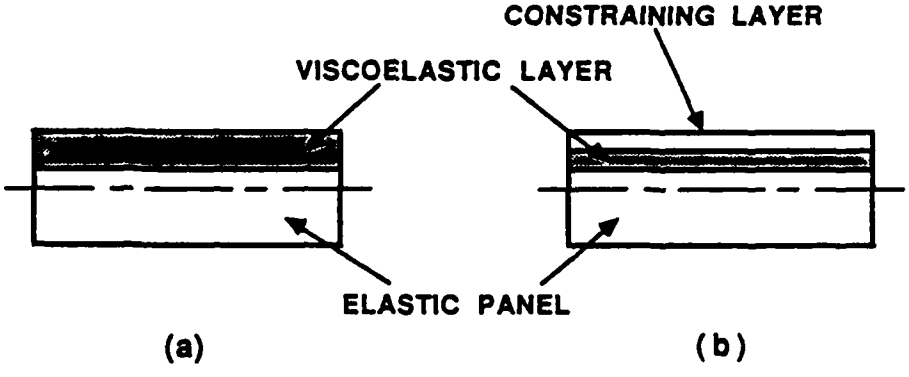

Figure 12: The control of structural response using constrained or unconstrained viscoelastic damping layer treatments; (a) unconstrained viscoelastic layer, (b) constrained viscoelastic layer.

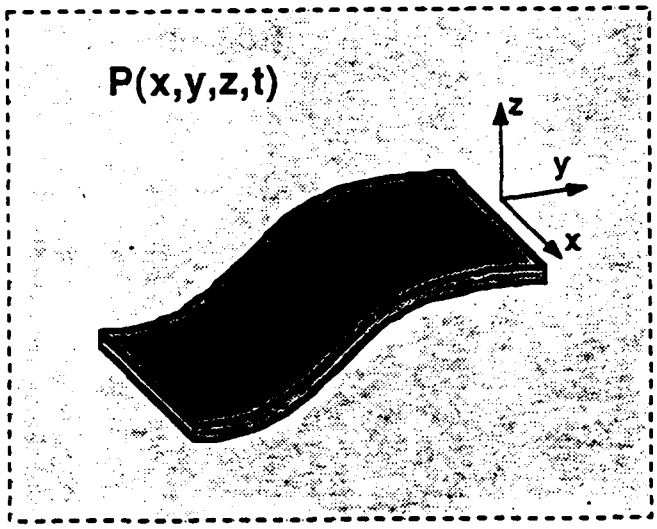

Figure 13: Distributed excitation of a flexible structure.

MATERIALS ISSUES FOR SMART STRUCTURES

Garth L. Wilkes
Chemical Engineering Department
Virginia Polytechnic Institute & State University
Blacksburg, Virginia 24061

ABSTRACT

The term "smart materials and structures" carries the implication that a given material or structure when provided a particular stimulus, will generate a specific response. What the specific stimuli are as well as the nature and magnitude of the response will depend upon the type of "smart structures" desired for a given application. This brief talk will focus on material parameter considerations with respect to generating smart structures and will illustrate a number of specific cases by example. While a somewhat higher emphasis will be given to those concerned with polymeric based materials, discussion will also consider those based on either metallic or ceramic systems as well. Finally, some new directions toward the development of new hybrid or complex material structures will be presented.

Session 2 - Smart Materials

G. L. Wilkes, "Materials Issues for Smart Structures", Abstract, Virginia Polytechnic Institute and State University.

R. E. Newnhan, "The Golden Age of Electroceramics", Pennsylvania State University.

B. B. Rath, "Self Assembly and 'Smart Materials'", Abstract, Naval Research Laboratory

R. D. James, "Basic Principles for the Improvement of Shape-Memory and Related Materials", University of Minnesota.

M. J. Furey, "Tribopolymerization: A New Concept of Boundary Lubrication", Abstract, Virginia Polytechnic Institute and State University.

Reprinted from Advanced Ceramic Materials, Vol. 3, No. 1, January 1988

The Golden Age of Electroceramics

ROBERT E. NEWNHAM*
Materials Research Lab, Pennsylvania State University, University Park, PA 16802

For 30 years I have collected gemstones and crystals; faceted stones of orange sphalerite, pink kunzite, pleochroic cordierite, purple apatite, and golden orthoclase continue to fascinate and delight me. Each gem is a beautiful piece of nature, cut and polished in a way to appeal to the human eye. Collectors classify gems according to the Seven Seas: composition, color, clarity, commoness, cutting, carats, and cost.

In many ways, thick film circuits, multilayer packages, and other electroceramics strike a similar chord. Each is a small bit of inorganic material carefully fashioned to carry out an electronic function. Much of the excitement (and hype!) of present-day electroceramics can also be summarized by the Seven Seas: conducting cuprates, ceramic circuitry, co-fired compatibility, curable chemicals, composite connectivity, core-clad couplers, and colloidal components.

ELECTROCERAMICS MARKET

The multibillion dollar electroceramics market (Fig. 1) includes Mn-Zn ferrites, PZT transducers, $BaTiO_3$ multilayer capacitors, ZnO varistors, Al_2O_3 packages, and SiO_2 optical fibers. Roughly speaking, the market is divided into six equal parts.[1] Rapidly developing technologies can be identified within each market segment: tellurium oxide coatings for video disks, barium hexaferrites for perpendicular recording, silver and copper electrode systems for multilayer capacitors, buried resistors and capacitors in ceramic packages, catalytic coatings for chemical sensors, and PZT piezoelectric motors. As in all rapidly evolving fields of science and engineering, there is a sense of excitement as a number of different technologies come together in a synergistic manner. The golden age of electroceramics involves the miniaturization and integration of ceramic components into a wide variety of optoelectronic systems.

STRUCTURE-PROPERTY RELATIONS

An overview of electroceramics is given in Fig. 2, which illustrates the various atomistic mechanisms utilized in ceramic circuit components. Multilayer capacitors, piezoelectric transducers, and PTC thermistors make use of the properties of ferroelectric perovskites with their high-dielectric permittivity, large piezoelectric coefficients, and anomalous electric conductivity. Similar domain phenomena are observed in ferrimagnetic oxide ceramics such as $NiFe_2O_4$. Hard and soft ferrites are analogous to hard and soft PZT and have found substantial markets in magnetic tape and electric motors.

Several kinds of mechanisms are operative in thermistors and other ceramics used as sensors. Most are based on changes in electrical resistivity, but the causes are different. The critical temperature thermistor involves a semiconductor-metal phase transition. NTC thermistors make use of the semiconducting properties of doped transition-metal oxides. Ionic conductivity is used in oxygen sensors and batteries. Stabilized zirconia is an excellent anion conductor, and β-alumina is one of the best cation conductors.

Humidity sensors make use of surface conduction. Adsorbed water molecules dissociate into hydroxyl and hydronium ions, which alter the electrical resistivity.

Grain-boundary phenomena are involved in boundary layer capacitors, varistors, and PTC thermistors. The formation of thin insulating layers between conducting grains is crucial to the operation of all three electroceramic components. Last, the importance of electroceramic insulators and substrates should not be overlooked. Here one strives to eliminate most of the interesting effects just described, but this is not always easy.

SUPERCONDUCTING CERAMICS

Until two years ago it was taken for granted that superconducting transition temperatures were limited to 25 K. But with the discovery of lanthanum strontium cuprate,[2] the temperature doubled, and doubled again with $YBa_2Cu_3O_7$, the so-called 1-2-3 compound.[3] The triple perovskite unit cell (Fig. 3) contains seven oxygen and two empty oxygen sites.

Ceramic and thin-film specimens both exhibit superconductivity above liquid air temperatures, opened up a large number of possible applications: frictionless generators, motors and high-speed trains; levitating toys and gimmicks; electronic Josephson junctions and resistanceless interconnects; large magnetic fields for NMR medical diagnosis, nuclear accelerators and hydrogen fusion; power transmission lines and closed-loop energy storage for load leveling; and radiation detectors for astronomy, oil exploration, and brain-wave research. The feasibility of many applications rests upon improvements in the critical current density. Ways must be found for stabilizing the superconducting phase under high magnetic fields and electric currents. Several interesting composite structures are under investigation.

But although ceramic superconductors have captured the imagination of thousands of scientists, the work is outside the mainstream of electroceramics. Until a major market is demonstrated, it will remain a curiosity. The main thrust in electroceramics research is not in the discovery of new materials but in the miniaturization and integration of components already known.

CERAMIC CIRCUITRY

Miniaturization and integration are technological goals in virtually all electronic materials. Several kinds of circuitry are under study by electroceramists, as shown in Fig. 4.

Electronic circuitry is the most advanced, especially in thick

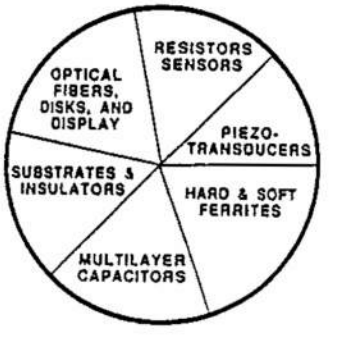

Fig. 1. Electroceramics market.

Member, the American Ceramic Society.

Presented at the 89th Annual Meeting, the American Ceramic Society, Pittsburgh, PA, April 27, 1987 (Orton Memorial Lecture, 1-O-87). Received August 12, 1987; approved September 28, 1987.

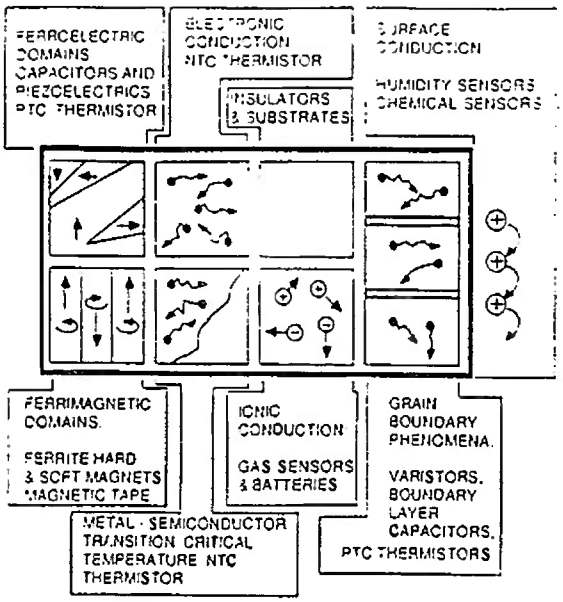

Fig. 2. Ionic and electronic mechanisms involved in electroceramic components.

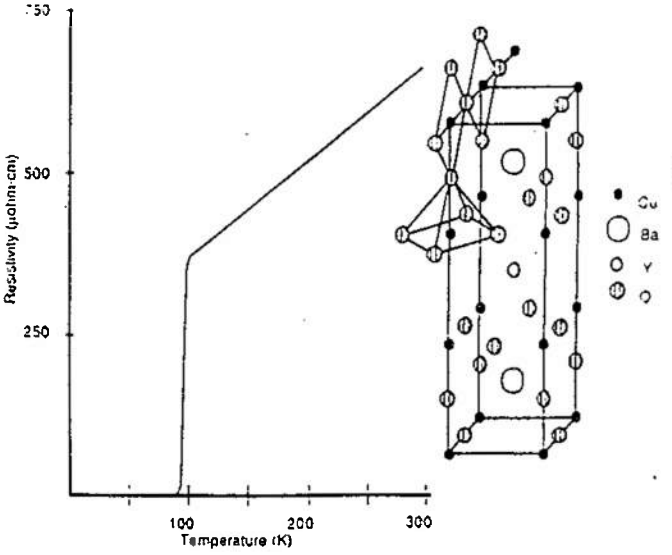

Fig. 3. Resistivity of the newly-discovered 1-2-3 cuprate ceramics; the structure contains many missing oxygen sites (Refs. 4 and 5).

film and multilayer packaging technology, where control of electrical conductivity (σ) and dielectric constant (K) are the key parameters. Integrated optic systems utilizing $LiNbO_3$ make use of small changes in refractive index (n) to guide and control light waves. Low absorption coefficients (α) are also important in optical circuitry. Thermal circuitry is important in packaging technology where heat must be removed as efficiently as possible. Thermal conductivity (k) and convective fluid flow velocities (v) are effective means of heat dissipation. Information storage utilizes magnetic circuitry made from high permeability (μ) and high conductivity (σ) materials to concentrate and manipulate regions of high magnetic flux. Electric flux concentration is used in ceramic actuators to produce large displacements with small voltages. Field concentration is accomplished with multilayer systems made up of internal electrodes (high conductivity σ) and high permittivity (K) dielectric layers. Multilayer capacitors operate on a similar flux concentration principle. Ionic movement in battery systems constitutes another type of circuitry in ceramics like β-alumina and stabilized zirconia. Ionic conductivities (σ) and diffusion coefficients (D) through intervening membranes are crucial property coefficients. Porous ceramics with high surface areas are used in fabricating chemical sensors. The movement of molecules and dissociation products constitutes a type of chemical circuitry controlled by diffusion coefficients (D) and surface electrical resistivity (ρ). Illustrations will be presented in succeeding sections.

PACKAGING MATERIALS

Important attributes of packaging materials for electronic circuitry include high thermal conductivity, high electrical resistivity, high mechanical strength, low dielectric constant, low dielectric loss, and good thermal expansion match with silicon.

Current research is focused on finding a replacement for alumina. High power transistor circuits generate an immense amount of heat; for this market, a substrate with high thermal conductivity is highly desirable. Aluminum nitride, beryllium oxide, cubic boron nitride, and diamond are candidate materials. The thermal conductivity of AlN and BeO is ten times higher than that of alumina ceramic, whereas that of BN and C is a hundred times better. Substrates of AlN made by hot-pressing are used as heat sinks for transistors and light-emitting diodes.[6] Recent experiments on the vapor deposition of diamond films give promise of even higher thermal conductivities. Thin diamond films have been grown on a silicon substrate using microwave plasma and methane and hydrogen gases.[7]

A second objective is the development of low dielectric constant materials for high-speed computer packages. Replacing alumina with a glass-bonded ceramic lowers the dielectric constant by 30% and greatly reduces the propagation delay. Further reductions have been achieved with porous silica nanocomposites prepared from colloidal silica gels.[8] To some extent the requirements for a large thermal conductivity and a small dielectric constant are mutually contradictory since introducing porosity decreases both K and k values.

INTEGRATED CERAMICS

The age of ceramic integration is upon us. Until recently multilayer ceramic packages consisted of dielectric strata with metallic circuitry printed on each layer and interconnected through metallized via holes between layers. Now additional circuit elements are being added. In the past two years buried capacitors and resistors have been added to the three-dimensional packages, and other components will follow shortly. Future devel-

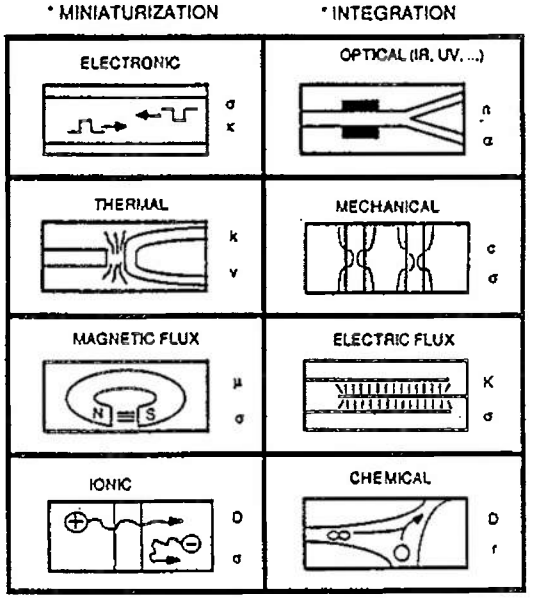

Fig. 4. Circuitry in ceramic materials for use in electronic packages, integrated optics, cooling systems, electromechanical transducers, magnetic recording, multilayer actuators, ionic batteries, and chemical sensors.

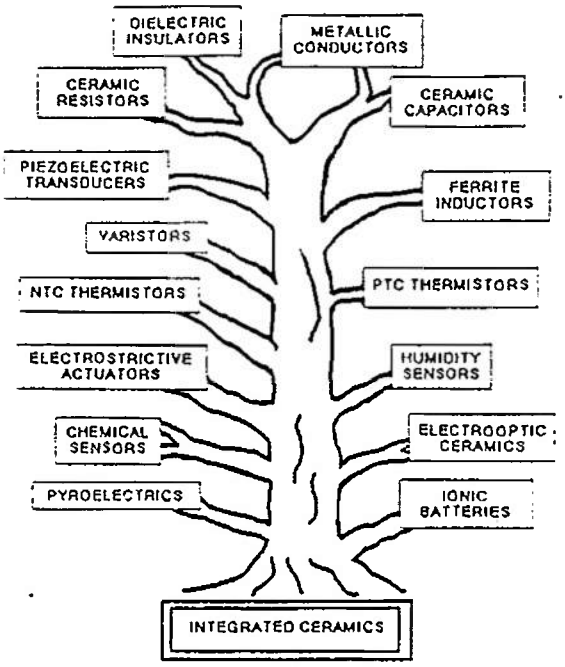

Fig. 5. Integrated ceramic packages of the future may incorporate many different components.

opments in the field of integrated ceramics are illustrated by the following tree in Fig. 5. Smart sensors, adaptive actuators, and ceramic packages with electroluminescent display panels, enclosed printing units, and voice modules are on the horizon. To conduct these functions it will be necessary to incorporate a wide variety of sensors, transducers, and actuators, together with thermistors and varistors to guard against current and voltage overloads.

The process of preparing co-fired multicomponent ceramic packages involves a marriage of tape casting and thick film technologies, augmented by photolithography, etching, sol-gel films, and fugitive phases (Fig. 6). In these multilayer packages, thick-film conductors, resistors, and dielectrics are screen-printed on green low-firing ceramic tapes to produce patterned circuitry in single layers. Vias are punched through the tapes and metallized to establish interconnects with adjacent layers. Low-permittivity tapes are used for signal transmission layers, and high-K tapes are used for the power plane.[9] After lamination into a single green body, the stack is sintered to produce a monolithic ceramic body with co-fired components buried within it. These substrate packages have the advantages of reduced size and fewer surface-mounted components, as well as low firing temperatures. Moreover, the buried capacitors, resistors, and metal interconnects are hermetically sealed within the ceramic package, thereby protecting the circuit elements against moisture, chemical attack, and mechanical damage.

In the NEC monolithic package,[9] the substrate material is a glass-ceramic composed of 55 wt% Al_2O_3 bonded with a lead borosilicate glass. The firing temperature was optimized at 900°C to allow co-firing with RuO_2 resistor compositions, Ag-Pd metal conductors, and tape-cast layers of lead iron tungstate-lead iron niobate capacitor formulations.

Similar systems have been developed by duPont, Sprague, and Narumi China. Sprague's multilythic packages are made by a wet laydown process in which a supporting substrate passes through a waterfall of substrate slip.[10] After the material is dried and screen-printed, it again passes through the waterfall curtain, producing additional layers in the multilayer package.

Liquid-cooled VLSI packages demonstrate the importance of thermal circuitry in integrated ceramic devices.[11] Multilayer alumina packages containing electronic circuitry and fine coolant channels have been fabricated. A series of mechanical punching and molding steps on the green tape is used to form

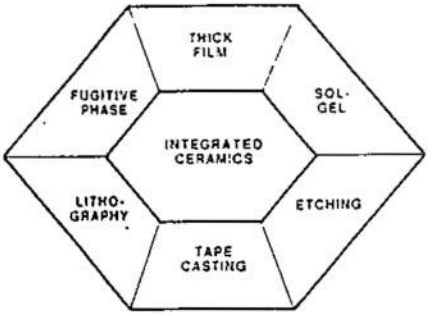

Fig. 6. Processing methods used in making multilayer, multicomponent ceramic packages.

the electrical vias and fluid distribution network.

Another approach to making fine-scale circuitry in ceramics is through the use of uv-curable pastes. The large-scale integration of high-speed computer systems requires high component density and fine line patterns. To meet these requirements, the photolithographic techniques used in semiconductor processing can be adapted to integrated electroceramic packaging.

A family of uv-curable pastes can be made by mixing the electroceramic powder within a photosensitive organic vehicle. Ceramists at Nippon Electric Company[12] have fabricated via holes by this method. A paste is made from a mixture of lead borosilicate glass and alumina powder. After the mixture is ball-milled, it is added to an organic medium consisting of methylmethacrylate copolymer together with a solvent, initiator, inhibitor, and some dyes.

To position via holes in the dielectric, the paste layer is laid down over a conductor pattern. The via regions are then covered with a mask and the surrounding areas exposed to uv radiation. After polymerizing the exposed photopolymer, the via regions are removed with a trichloroethane developer. The remaining dielectric tape is then fired to give a thin ceramic layer with via holes as small as 40 μm.

To process other electroceramics in the same way, it will be necessary to develop photoinitiators compatible with each type of ceramic component. Thioxanthone, benzathrone, and other commonly used photoinitiators are sensitive to wavelengths near 0.38 μm. Silica is transparent in this region but titania is not. New photofragmentation systems will be required for the ferroelectric titanates and niobates.

TRANSDUCERS AND FUGITIVE PHASE PROCESSING

There is a need for open space in many electroceramic devices for cooling systems, ink jets, resonant motion, and for backfilling with compliant polyers or conducting electrodes. The family of PZT-polymer transducers shown in Fig. 7 illustrates some of the geometries of interest.

Electromechanical transducers convert mechanical force to electric voltage. By concentrating the applied force on the piezoelectric portions of the transducer, greater sensitivity can be obtained. Force amplification is accomplished by utilizing the higher mechanical compliance of the polymer phase; the polymer transfers its stress to the stiffer piezoelectric ceramic in a type of mechanical circuitry (Fig. 4), thereby increasing the electrical response of the transducer. At the same time the capacitance of the transducer is reduced because of the smaller dielectric constant of the polymer. Reducing the capacitance increases the voltage coefficient of the piezoelectric composite. Several of the designs in Fig. 7 are effective as hydrophones for detecting weak pressure waves in fluids.

Polymer-ceramic composites can be made by a number of methods but the fugitive phase technique is especially versatile.[14] Transducers with 3-3 connectivity are fabricated by mixing polymer spheres in the ceramic slip. The spheres burn out during firing, leaving a porous ceramic skeleton that can be backfilled with epoxy.

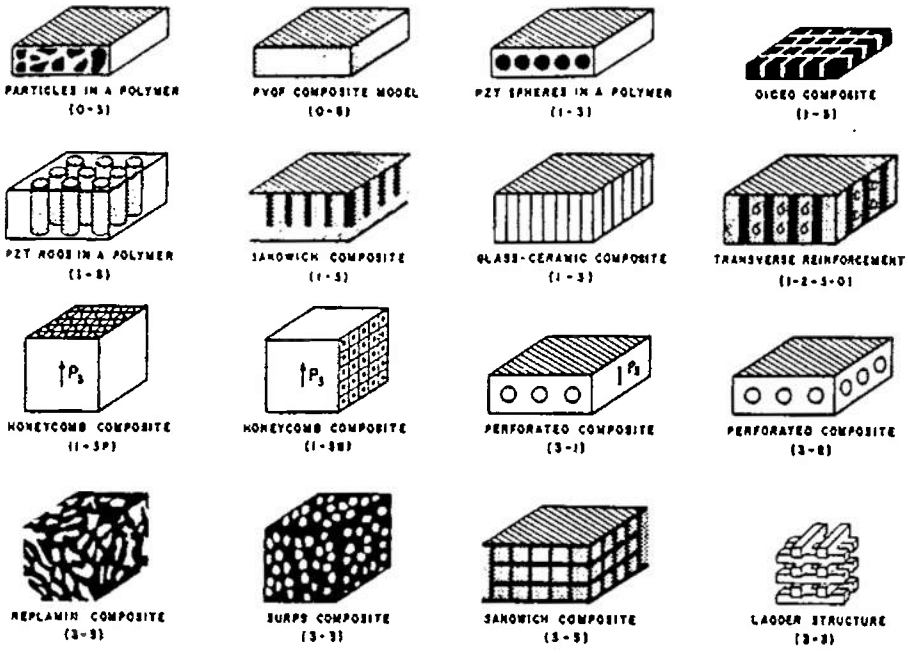

Fig. 7. Twelve PZT-polymer composites used as piezoelectric transducers; numbers refer to the connectivity pattern of the composite (Ref. 13).

Fig. 8. Spiral grooves etched into thickness mode resonators effectively damp lateral resonance modes (Ref. 14).

Transducers with checkerboard void patterns have been fabricated by Kahn *et al.*[15] A fugitive ink consisting of resin, carbon, PZT, and a solvent solution was screened onto PZT tape to produce the patterns.

The designed-space forming technology,[16] developed at N.E.C., combines tape-casting, photolithography, and a fugitive phase. A photosensitive polymer is deposited on a polyester carrier film and then exposed to uv light through a patterned mask. The photosensitive layer is then developed, leaving the irradiated portion of the pattern on the carrier film. This space-forming pattern is transferred to the tape-cast green ceramic and burns out during firing to leave a designed space within the multilayer package.

Drop-on-demand ink jets are made by this process.[17] Channel and reservoir spaces for the ink are incorporated within the piezoelectric printer made of PZT. Driving electrodes embedded within the poled ceramic provide the electric impulse required to propel ink droplets from the nozzle.

Humidity detectors and chemical sensors can be incorporated in the electroceramic packages in a similar way.[18] Fugitive electrodes have also been used to advantage in multilayer capacitors and multilayer boundary layer capacitors.

Photolithography and chemical etching have also been used in transducer design. A layer of uv-curable polymer is deposited on a thin wafer of piezoelectric ceramic. After the photopolymer is irradiated through a patterned mask, the unpolymerized regions are removed, exposing the PZT ceramic underneath. The exposed ceramic is then etched away in an acid bath. Tiny, double-cantilever transducers for measuring the viscosity and density of fluids are fashioned in this way. The transducer with an etched spiral shown in Fig. 8 has a very pure thickness mode vibration; coupled planar modes are dampened by the spiral groove.[19]

Unfortunately, the etching rates for most ceramics are rather slow, making it difficult to use on thick specimens. For many oxides the etching speed is only a few micrometers per minute, even in strong acids at elevated temepratures. Customized laser-assisted etching improves the rates markedly.[20]

ELECTRIC FIELD CONCENTRATION

The multilayer design used for ceramic capacitors is an effective configuration for concentrating electric fields. By interleaving metal electrodes and ceramic dielectrics in a 2-2 connectivity pattern, relatively modest voltages are capable of producing high electric fields.

Second harmonic generation and other nonlinear optical effects are well-known, but the corresponding low-frequency phenomena have not been thoroughly investigated. The recent upsurge of interest in actuators[21] is changing this situation. Electrostriction is a second-order electromechanical coupling between strain of electric field. For small fields, electrostrictive strains are small compared to piezoelectric strain, but this behavior is not true for the high fields generated in composite transducers.

Multilayer electrostrictive transducers made from relaxor ferroelectrics, such as lead magnesium niobate (PMN), are capable of generating strains larger than PZT. Since there are no macrodomains in PMN, there are no "walk-off" effects in electrostrictive micropositioners. Moreover, poling is not required, and there are no aging effects. The concentration of electric fields in composite transducers makes nonlinear effects increasingly important.

SCALING DOWN IN SIZE: NANOCOMPOSITES

An inexorable trend to smaller and smaller sizes is characteristic of the age of integration and miniaturization. It has been said, "There is plenty of room at the bottom," for electronic and optical systems. The dependence of ultrasonic and electromagnetic wavelengths on frequency is sketched in Fig. 9. A range of wavelengths is observed in ceramic materials because of differences in elastic constants and refractive indices.

Nonlinear optical devices are of special interest because of their importance in communication, computing, and nuclear fusion. A transparent nanocomposite for second harmonic generation is one such technical goal. To build such a window requires phase matching the fundamental and harmonic beams by balancing dispersion and birefringence. This procedure is possible in principle using aligned nanometer-size needles or platelets but has yet to be demonstrated. In addition, either the matrix phase or the dispersed particles must have sizable nonlinear optic coefficients, requiring the use of ferroic nanocrystals such as $PbTiO_3$.

INTRINSIC SIZE EFFECTS

In ferromagnetic materials, there are three kinds of magnetic structures for small particles.[22] Multidomain structures

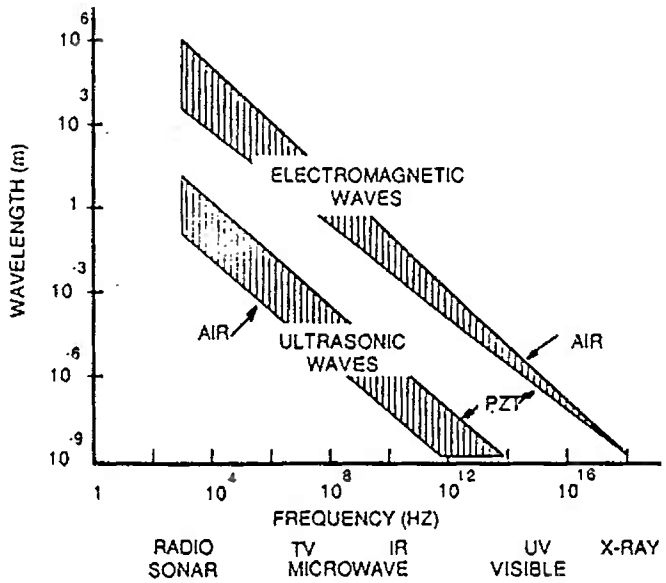

Fig. 9. High-frequency ultrasonic resonators and optical components require nanocomposite materials with very small particle sizes.

are common for particles larger than a critical size: magnetization in large particles takes place through domain wall motion. Below this critical size, single domain particles are observed, and switching takes place by rotation rather than wall movement, thereby increasing the coercive field. Very small particles exhibit a superparamagnetic effect in which the spins rotate in unison under thermal excitation. Only modest magnetic fields are required to align the spins of adjacent particles.

Analogous behavior in ferroelectric particles and ferroelastic particles has yet to be fully established, but a variety of interesting experimental results are accumulating.[23] In $BaTiO_3$ ceramics, single domain behavior is observed in grains less than 1 μm in size,[24] whereas dielectric phenomena resembling superparamagnetism are found in relaxor ferroelectrics. The fluctuating microdomains in this superparaelectric state are $\approx$20 nm across.[25]

Composite materials made up of single domain and superparaelectric particles have yet to be investigated in a systematic way with proper control of the connectivity and surrounding environment. The controlled synthesis of submicrometer ferroelectric grains will do much to stimulate research in this area.

SUMMARY

Rapid progress in the integration and miniaturization of ceramic components has led to the development of multipurpose electronic packages containing complex three-dimensional circuitry. At the same time, a wide variety of smart sensors, transducers, and actuators are being constructed utilizing composite materials to concentrate fields and forces. At present the processing methods make use of tape casting the thick film techniques, but several upset technologies loom on the horizon. During the years ahead we can expect electroceramic devices to follow in the footsteps of semiconductor technology as the component sizes drop below 1 μm, and nanocomposite devices become a reality.

A great deal has been written about the importance of scale in magnetic, optical, and semiconductor materials, and many of the same effects occur in electroceramics: critical domain sizes, resonance phenomena, electron tunneling, and nonlinear effects.

The Golden Age of electroceramics will not last forever. The age of integration, followed by the age of miniaturization, will inevitably lead to new ideas and new systems. Integrated ceramic systems will reach limits—grain size for one—as ceramists strive to make optoelectronic systems with extremely small feature size. A marriage of materials will result with several upset technologies emerging to replace integrated ceramic packages. Patterned thin film systems, involving oxides on silicon or silicon on oxide substrates, are already on the horizon, and others will follow. Sensor, actuator, and information processing systems as complex and compact as the human body one day will emerge.

REFERENCES

[1]Japan Electronics Almanac 1986, Dempa Publications, Inc., Tokyo; 412 pp.
[2]J. G. Bednorz and K. A. Muller, "Possible High T_c Superconductivity in the Ba-La-Cu-O System," *Z. Phys. B-Condensed Matter*, 64, 189–93 (1986).
[3]M. K. Wu, J. R. Ashburn, C. J. Torng, P. H. Hor, R. L. Meng, L. Gao, Z. J. Huang, Y. Q. Wang, and C. W. Chu, "Superconductivity at 93K in a New Mixed-Phase Y-Ba-Cu-O Compound System at Ambient Pressure," *Phys. Rev. Lett.*, 58 [9] 908–10 (1987).
[4]R. J. Cava, B. Batlogg, R. B. Van Doner, D. W. Murphy, S. Sunshine, T. Siegrist, J. P. Remeika, E. A. Rietman, S. Zahurak, and G. P. Espinosa, "Bulk Superconductivity at 91K in Single Phase Oxygen-Deficient Perovskite $Ba_2YCu_3O_{9-\delta}$," *ibid.* [16] 1676–79.
[5]F. Beech, S. Miraglia, A. Santoro, and R. S. Roth, "Neutron Study of the Crystal Structure and Vacancy Distribution of the Superconductor $Ba_2YCu_3O_{9-\delta}$," unpublished work.
[6]Y. Kurokawa, K. Utsumi, H. Takamizawa, T. Kamata, and S. Noguchi, "AlN Substrates with High Thermal Conductivity," *IEEE Trans. CHMT*, 8 [2] 247–52 (1985).
[7]A. Badzian, B. Simonton, T. Badzian, R. Messier, K. E. Spear, and R. Roy, "Vapor Deposition Synthesis of Diamond Films," *Proc. SPIE*, 683, 127–38 (1986).
[8]W. A. Yarbrough, T. R. Gururaja, and L. E. Cross, "Materials for IC Packaging with Very Low Permittivity via Colloidal Sol-Gel Processing"; unpublished work.
[9]K. Utsumi, Y. Shimada, T. Ikeda, and H. Takamizawa, "Monolithic Multicomponent Ceramic (MMC) Substrate," *Ferroelectrics*, 68, 157–79 (1986).
[10]G. R. Love, "Multilythics—A New Circuit Technology, IEEE Trans. CHMT, 9 [4] 341–46 (1986).
[11]T. Kishimoto and T. Ohsaki, "VLSI Packaging Technique Using Liquid-Cooled Channels," *ibid.*, 328–35.
[12]H. Takamizawa, K. Utsumi, and M. Suzuki, "Multilayer Ceramic Substrate with UV Curable Dielectric Paste for Multi-Chip Package," Proc. Int. Symp. on Microelectronics, 373–79 (1985).
[13]R. E. Newnham, D. P. Skinner, and L. E. Cross, "Connectivity and Piezoelectric-Pyrolectric Composites," *Mater. Res. Bull.*, 13 525–36 (1978).
[14]K. Rittenmyer, T. Shrout, W. A. Schulze, and R. E. Newnham, "Piezoelectric 3-3 Composite," *Ferroelectrics*, 4, 189–95 (1982).
[15]M. Kahn, A. Dalzell, and B. Kovel, "Ceramic-Air Composites for Hydrostatic Pressure Sensing," Proc. Sixth IEEE Int. Symp. on Appl. Ferroelectrics, June 8–11, 1986; pp. 273–76.
[16]K. Utsumi, M. Tsuzuki, M. Suga, and H. Takamizawa, "Designed-Space Forming Technology in Ceramics," *I.M.C. Proc.*, Kobe, May 28–30, 1986; pp. 36–42.
[17]M. Suga, K. Utsumi, M. Tsuzuki, and H. Takamizawa, "Drop-on-Demand Ceramic Ink-Jet Head Made from Piezoelectric Material," *S.I.D. Digest*, 193–96 (1986).
[18]T. Nitta, "Ceramic Humidity Sensor," *Ind. Eng. Chem. Prod. Res. Dev.*, 20, 669–74 (1981).
[19]S. Trolier, C. Geist, A. Safari, R. E. Newnham, and Q. C. Xu, "Etched Piezoelectric Structures," Proc. Sixth IEEE Int. Symp. on Appl. Ferroelectrics, June 8–11, 1986; pp. 707–10.
[20]T. Shiosaki, M. Tanizawa, H. Kamei, and A. Kawabata, "Laser Micromachining of Modified $PbTiO_3$ Ceramics in KOH Water Solution," *Jpn. J. Appl. Phys.*, 22, Suppl. 22-2, 109–12 (1983).
[21]K. Uchino, "Electrostrictive Actuators: Materials and Applications," *Am. Ceram. Soc. Bull.*, 65 [4] 647–52 (1986).
[22]I. S. Jacobs and C. P. Bean, "Fine Particles, Thin Films, and Exchange Anisotropy," pp. 271–350 in Magnetism, Vol. III. Edited by G. T. Rado and H. Suhl. Academic, New York, 1963.
[23]M. Multani; pp. 185–214 in The Finite Solid State Lattice, Preparation and Characterization of Materials. Edited by J. M. Honig and C.N.R. Rao. Academic, New York, 1981.
[24]Y. Ozaki, "Ultrafine Electroceramic Powder Preparation from Metal Alkoxides," *Ferroelectrics*, 49, 285–88 (1983).
[25]V. A. Bokov and I. E. Myl'nikova, "Electrical and Optical Properties of Single Crystals of Ferroelectrics with a Diffused Phase Transition," *Sov. Phys.-Solid State*, 3 613–19 (1961). □

Self Assembly and "Smart Materials"

B. B. Rath
Naval Research Laboratory
Washington, D. C. 20375

ABSTRACT

Phospholipids are an important example of a class of molecule that have the ability to self-organize into complex assemblies. These molecules comprise the major fraction of biological membranes. The specific arrangement of phospholipids in biological membranes. The specific arrangement of phospholipids in biological membranes and the matrix these lipids provide for membrane proteins, play an important functional membrane properties such as energy transduction and molecular recognition. All of which can be considered smart functions or properties. One of the goals of technological development in the area of lipid based self-assembly is to impart similar smart functionality into a designed microstructure. The study of the relationship of phospholopid molecular structure to assemblies of increaseing size and complexity may lead to applications in such diverse areas as electronic materials, drug delivery, improved composites, and advanced biosensors.

The research programs being pursued in NRL's Bio/molecular Engineering branch focus upon ways to utilize or emulate biological approaches for the fabrication of micron sized microstructures. Fundamental research in the design of molecular structure important to microstructure formation, the fabrication of these microstructures, and their subsequent characterization. Exploratory research programs that assess the utility of these structures, develops processing technology for the manipulation of sub micron structures, assess the requirements for and the potential of scale up, and determines the requirements and benefits for ultimate application also ongoing.

We have chosen lipid systems to be the initial trial for the design study of the fabrication of sub micron structures. This choice has proven to be quite fortuitous with respect to the development of smart materials. The resulting research and results are the basis for this talk.

BASIC PRINCIPLES FOR THE IMPROVEMENT OF SHAPE-MEMORY AND RELATED MATERIALS

R. D. James
Department of Aerospace Engineering
and Mechanics
University of Minnesota
Minneapolis, MN 55455

ABSTRACT

The goal of the research described here is to give reliable rules for making improved shape-memory and related materials.

INTRODUCTION

We give a brief survey of research on shape-memory and related piezoelectric and magnetostrictive materials. The goal of this research is to identify the important material parameters which are typically highly nonclassical and require the development of new tests for their measurement. Once the key material parameters are identified, the aim is the to relate the important material behavior to these parameters and to decide what choice of parameters gives optimum behavior. In the materials under consideration in which phase transformations play a crucial role, the mathematical problem of relating the material parameters to behavior is extremely difficult and has motivated the development of recent analytical techniques and has attracted the attention of leading analysts and constitutive theorists. The picture that is emerging for shape-memory materials is that only very special values of the material parameters lead to the interesting behavior. Finally, once this relationship has been found, it is then recognized that these material parameters are not really fixed but can be changed by changing the composition of the alloy. Often small changes of composition change the behavior dramatically, particularly the introduction of small percentages of rare-earths. The behavior is then optimized by pursuing compositions which give rise to the material parameters which in turn optimize the desired behavior.

At this stage we are developing and confirming experimentally a theory for shape-memory materials. This theory is sufficiently general to treat complex microstructures and general boundary conditions and therefore could serve as a vehicle for calculating the relation between material parameters and behavior. Below, we briefly describe this theory and indicate modifications necessary to discuss closely related piezoelectric and magnetostrictive materials.

THEORY OF STRUCTURAL PHASE TRANSFORMATIONS

We very briefly outline a theory for structural phase transformations in its simplest form. We begin with a lattice describing the high temperature phase, say described by lattice vectors

$$e_1, e_2, e_3. \tag{1}$$

The atoms of the high temperature phase are given by $n^i e_i$, where (n^1, n^2, n^3) are integers. Typically, these vectors change slightly with temperatures due to ordinary thermal expansion. Upon reaching the transformation temperature θ_c, these vectors change spontaneously into another set

$$f_1, f_2, f_3 . \qquad (2)$$

We consider a free energy function φ which depends on lattice vectors and temperature θ. We imagine that φ is minimized by e_i for $\theta > \theta_c$ and by f_i for $\theta < \theta_c$. Recognizing that two sets of lattice vectors may determine the same lattice and that we really want φ only to depend on the atomic positions, then φ inherits certain invariance properties. These properties are determined by a symmetry group G, which represents the symmetry of the lattice vectors e_i. It turns out that if the lattice vectors have been chosen properly, then the Born rule relating atomic to gross motion is reliable. This rule states that if u(x) represents the displacement field, then deformed lattice vectors $\hat{e}_i$ are related to reference lattice vectors, here for convenience chosen to be e_i, by the rule

$$\hat{e}_i = \big(\nabla u(x)\big)\, e_i, \quad i=1,2,3. \qquad (3)$$

A well-defined procedure, described in [1], can be used to define a free energy function $\varphi(\nabla u, \theta)$. The basic problem describing equilibrium configurations of a free crystal is

$$\min \int \varphi\,(\nabla u(x), \theta)\, dx . \qquad (4)$$

It turns out that the free energy functions that emerge from this argument have various **potential wells**. For $\theta > \theta_c$, φ is minimized at a matrix U_0 and all matrices of the form RU_0 where R is a rotation matrix and for $\theta < \theta_c$ φ is minimized at a set of matrices $U_1, \ldots, U_n$. The number n and the matrices $U_2, \ldots, U_n$ turn out to depend on the group G and on the **transformation strain** matrix U_1. In addition, φ is also minimized at $RU_1, \ldots, RU_1$ where R is any rotation matrix. Most of the free transformation behavior can be understood by calculating the minimizers of (4), which in turn relate to this potential-well structure of φ.

Piezoelectric and magnetostrictive materials have movement of atoms within the unit cell which cannot simply be described by three lattice vectors as in (1). Additional vectors called **shifts** are introduced to account for these movements and the free energy becomes a function of these as well.

SOME RESULTS

We give a brief qualitative description of predictions of this theory. One consequence is that minimizers can have planes of discontinuity of $\nabla u(x)$. The calculation of these planes then can be compared with experimentally observed twin planes for the alloy; this is an elementary check that the theory is set up correctly. A more sophisticated check is other minimizers, actually minimizing sequences [see 3], which model the austenite/martensite interface. The calculation of these microstructures agrees exactly with the Crystallographic Theory of Martensite. Such interfaces, which really distinguish martensitic materials from others, are only possible at special matrices U_1, and for special choices of the group G.

More generally, when we deform a shape-memory material, it deforms easily as long as it can simply rearrange variants, that is, rearrange displacement gradients among the potential wells. For large enough imposed deformations, this can no longer happen and the material suddenly "gets stiff." The point

at which this occurs has obvious importance. Current calculations involve the relation of this stiffening point to the pair U_1, G.

REFERENCES

1. R. D. James, Displacive phase transformations in solids, J. Mech. Phys. Solids **34** (1986), p. 359-394.

2. J. M. Ball and R. D. James, Fine phase mixtures as minimizers of energy, Arch. Ration. Mech. Anal. **100** (1987), p. 13-52.

3. R. D. James, The stability and metastability of quartz, in **Metastability and Incompletely Posed Problems** (*ed.* S. Antman, J. L. Ericksen, D. Kinderlehrer, I. Müller), Springer-Verlag (1987), p. 147-176.

T R I B O P O L Y M E R I Z A T I O N:

A NEW CONCEPT OF BOUNDARY LUBRICATION

by

Michael J. Furey
Department of Mechanical Engineering
Virginia Polytechnic Institute and State University
Blacksburg, Virginia 24061

ABSTRACT

This paper concerns tribology -- the study of friction, wear, and lubrication -- and in particular a new approach to the design of molecules which will act to form protective films in response to tribological conditions (e.g., high surface temperatures and pressures).

The concept of tribopolymerization as a new and potent mechanism of boundary lubrication is reviewed and discussed. By tribopolymerization, we mean the planned or intentional formation of protective polymeric films directly on tribological surfaces to reduce damage and wear by the use of minor (e.g., 0.1%, 1%) amounts of selected monomers capable of forming such polymer films "in situ." A diagrammatic and oversimplified representation of the tribopolymerization process is shown below.

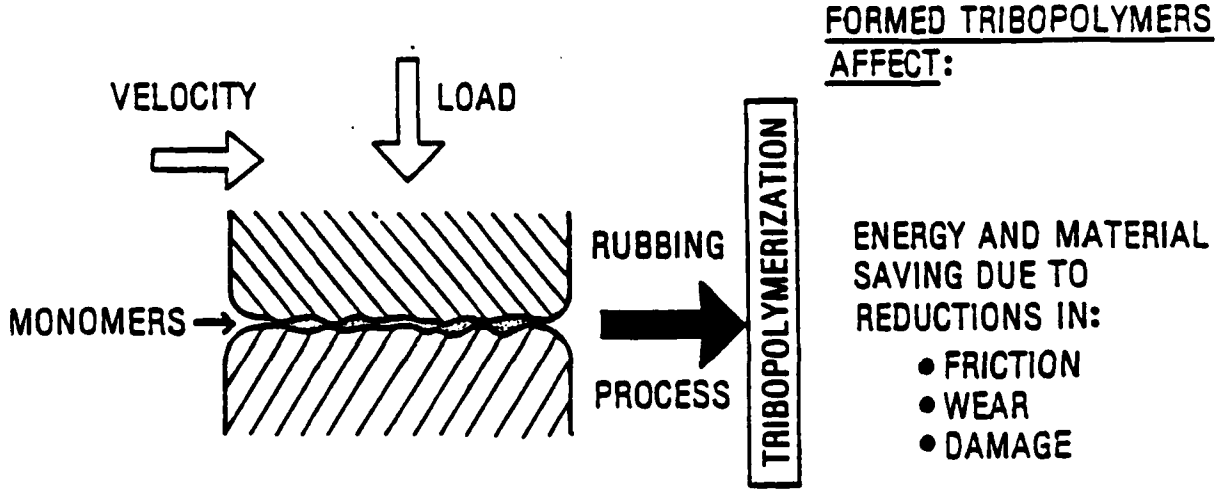

Tribopolymers are not to be confused with the collective term "friction polymer" which is often used in the literature and generally includes oxidative/degradative products formed from hydrocarbon and other lubricant components.

Furey's concept of tribopolymerization is described and key evidence in support of this concept is reviewed. Most of this work was carried out with compounds capable of forming polymers by a

polycondensation process (e.g., mixtures of long-chain diacids and glycols or single compounds containing both acid and glycol groups). An outstanding example is the class of monoesters made from C_{36} dimer acid and various glycols (e.g., ethylene glycol). These compounds are extremely effective in increasing the gear antiscuff ratings of hydrocarbon fuels and in reducing valve train wear in automotive engines. In the latter respect, they are equal in effectiveness in reducing wear (by over 90%) as the potent, commonly-used antiwear additive, zinc dialkyl dithiophosphate.

In addition, related research on tribopolymerization by Kajdas is discussed. This includes the role of the low-energy electron emission process (exoelectrons) on addition-type tribopolymerization (e.g., of vinyl type monomers).

Although there is considerable evidence in support of the use of the tribopolymerization process to reduce wear, several important fundamental questions remain. The authors present additional and more detailed hypotheses to help answer these questions. One hypothesis, offered to explain why monoesters of C_{36} dimer acid and glycols are extermely effective in reducing wear while tetraesters are relatively ineffective, involves the special orientation of these compounds on the surfaces prior to tribopolymerization. As can be seen in the diagram below, the surface density of adjacent -COOH and -OH pairs is greatest for the monoester; thus the probability of polymerization by condensation reactions on the surface is enhanced.

MONOESTER

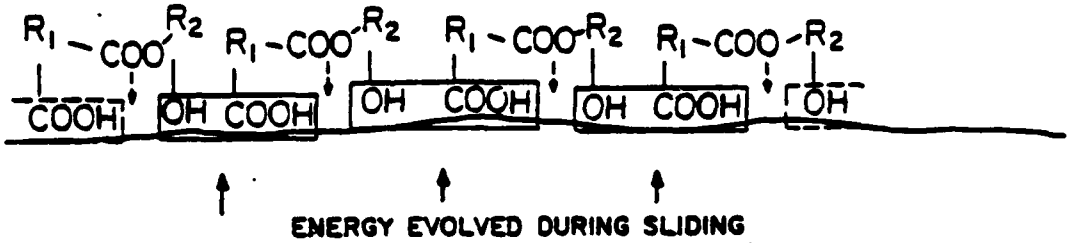

TETRAESTER

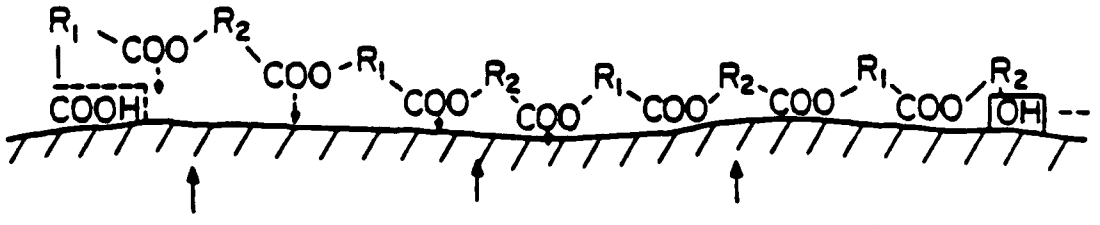

A plan of future research aimed at testing these hypotheses and at obtaining a better understanding of tripolymerization is described briefly. A key part of the planned research is the coupling of an infrared microscope system already used in tribology research at VPI&SU with advanced surface analytical techniques such as FTIRS and FTIRMA. Results of this collaborative research will be given in future papers.

REFERENCES

1. M. J. Furey, "Tribology" in M. B. Bever (Ed.), "Encyclopedia of Materials Science and Engineering," Pergamon Press, Oxford, New York, Toronto, Sydney, Frankfurt, 1986, pp. 5145-5147.

2. M. J. Furey, "The Formation of Polymeric Films Directly on Rubbing Surfaces to Reduce Wear," Wear, 26, 1973, pp. 369-392.

3. M. J. Furey, "The 'in situ' Formation of Polymeric Films on Rubbing Surfaces," Proceedings, International Colloquium on Polymers and Lubrication (Brest), published by Centre National de la Recherche Scientifique, No. 233, pp. 393-404, Paris, 1975.

4. M. J. Furey, "Infrared Measurements of Surface Temperatures Produced in Tribological Process," Proceedings, 3rd International Tribology Congress (EUROTRIB-81), Warsaw, 21-24 September, 1981, Vol. I, (Tribological Process in Solid Body Contact Areas), pp. 118-139.

5 M. J. Furey, and C. Kajdas, "The Planned Formation of Polymeric Films on Rubbing Surfaces to Reduce Wear," 61st Colloid Surface Science Symposium, American Chemical Society, The University of Michigan, Ann Arbor, 21-24 June 1987.

6. Furey, M. J., and C. Kajdas, "Tribopolymerization," Fourth International Tribology Conference, Budapest, Hungary, 22-24 September 1987.

7. Furey, M. J., and C. Kajdas, "Tribopolymerization as a Lubrication Mechanism for High-Energetic Contacts of Solids," 6th International Tribology Colloquim, Technische Akademie Esslingen, Esslingen, Federal Republic of Germany, 12-14 January 1988.

Session 3 - Mathematical Issues

R. V. Kohn, "Recent Progress in the Mathematical Modeling of Composite Materials", Courant Institute of Mathematical Sciences.

R. Rostamian, "Wave Propagation in Layered Elastic Media", Abstract, University of Maryland.

W. W. Hager, "Optimization and Homogenization for Elastic Materials", Abstract, University of Florida.

W. W. Hager, and R. Rostamian, "Wave Propagation in Anisotropic Elastic Media", University of Florida, University of Maryland Baltimore County.

C. Collins, and M. Luskin, "Computational Results for Phase Transitions in Shape Memory Materials", University of Minnesota.

M. Slemrod, "Admissibility Criteria for Phase Boundaries", University of Wisconsin-Madison

To appear in **Composite Material Response: Constitutive Relations and Damage Mechanisms**, G. Sih et. al. eds., Elsevier, 1988.

RECENT PROGRESS IN THE MATHEMATICAL MODELING OF COMPOSITE MATERIALS

Robert V. Kohn

Courant Institute of Mathematical Sciences

251 Mercer Street

New York, NY 10012

ABSTRACT

We review some of the recent mathematical progress on the effective moduli of composites. Specific attention is devoted to mathematically precise definitions of effective moduli, new methods for bounding effective moduli, new constructions of mixtures with explicitly computable properties, and applications to structural optimization.

1. INTRODUCTION

We are concerned with materials that are spatially heterogeneous on a suitably small length scale, and with linear models of material behavior, for example linear elasticity. The effective moduli of such a "composite" describe its overall, large-scale behavior. They have long been an object of study by physicists and materials scientists; selective reviews of the extensive literature include [14,22,68,69,72]. More recently, the study of effective moduli has attracted the attention of a growing community of mathematicians as well. The relatively new notions of homogenization and G-convergence provide a firm mathematical foundation [48,62,65,71]; moreover, the effective moduli of composites have been linked to fundamental issues arising in the optimal control of certain distributed parameter systems. and to deep questions involving the lower semicontinuity of variational functionals, see e.g. [1,12,28,30,32,38,39,49,50,58,67]. The specific questions about effective moduli raised by these new applications are sometimes different from those that were the focus of the older literature: for example, applications to structural optimization require the specification of all (anisotropic) composites attainable as mixtures of given components in specified

proportions. However, the mathematical tools developed to address such questions have also led to new results that are very much within the purview of the older theory. Examples include the simultaneous attainability of the Hashin-Shtrikman shear modulus and bulk modulus bounds [17,36,42,51]; the validity of a conjecture of Schulgasser about the effective conductivity of polycrystalline composites [5]; and the attainability of certain mean field theories [2,41].

The goal of this paper is to review selected aspects of this recent mathematical progress, which it is hoped will be of interest to a broad community of specialists in materials science. It should be emphasized that the ideas presented here are a synthesis of the work of many individuals, and that the selection of topics is somewhat arbitrary – in no way representing a comprehensive survey of the most important recent developments.

2. MATHEMATICALLY PRECISE DEFINITIONS OF EFFECTIVE MODULI.

We are concerned with mixtures of continua on a length scale small compared to that on which the loads and boundary conditions vary, but still large enough for continuum theory to apply. Such a "composite" is clearly an idealization: it represents the limiting behavior of a sequence of structures, as the ratio $\epsilon = \ell/L$ relating the "microscopic" length scale ℓ to the "macroscopic" one L tends to zero. There are in fact several distinct theories, differing as to the form assumed for the fine scale structure. A *periodic* composite is one whose microscopic structure is periodic with a specified unit cell; a *random* composite is one whose fine scale structure is a stochastic process with specified statistics. There is also a third approach which makes no such hypothesis on the fine scale structure, appealing instead to a compactness theorem for systems of partial differential equations. This last theory, known variously as G-*convergence* or *homogenization*, represents in a sense the most general approach.

To fix ideas, let us focus the discussion on mixtures of two isotropic, linearly elastic materials in $\mathbf{R}^d$ ($d = 2$ and $d = 3$ being, of course, the cases of physical interest). Each

of the component materials is characterized by a bulk modulus κ_i and a shear modulus μ_i $(i = 1, 2)$, determining a unique Hooke's law tensor A_i – a symmetric linear map on the space of symmetric tensors – such that

$$A_i e = \kappa_i (tr\ e) I + 2\mu_i (e - \frac{1}{d}(tre)I) \tag{2.1}$$

for any symmetric tensor e. The associated "elastic energy" quadratic form is the inner product of stress and strain:

$$(A_i e, e) = (\kappa_i - \frac{2\mu_i}{d})(tre)^2 + 2\mu_i |e|^2 \tag{2.2}$$

A structure which mixes the two materials will have a spatially varying Hooke's law, equal to either A_1 or A_2 at each material point x. Introducing a parameter ϵ, representing (at least in the periodic and random cases) the length scale of the microstructure, the spatially varying Hooke's law is

$$A^\epsilon(x) = \chi_1^\epsilon(x) A_1 + \chi_2^\epsilon(x) A_2, \tag{2.3}$$

where

$$\chi_i^\epsilon(x) = \begin{cases} 1 & \text{on the set occupied by material i} \\ 0 & \text{elsewhere} \end{cases} \tag{2.4}$$

so that $\chi_2^\epsilon = 1 - \chi_2^\epsilon$. By definition the structure is *periodic* (with cubic symmetry) if

$$\begin{aligned} &\chi_i^\epsilon(x) = \chi_i(\frac{x}{\epsilon}) \text{ for some function } \chi_i(y), \\ &\text{taking only the values 0 and 1, defined for all } y \in \mathbf{R}^d \\ &\text{and periodic in each component of } y \text{ with period 1.} \end{aligned} \tag{2.5}$$

An example would be a periodic array of spherical inclusions centered on a cubic lattice of mesh ϵ, each sphere having radius $\epsilon\rho$ $(\rho < \frac{1}{2})$. In the *random* case there is an additional

variable ω, belonging to a suitable probability space:

(2.6) $\chi_i^\epsilon(x,\omega) = \chi_i(\frac{x}{\epsilon},\omega)$ for some stochastic process $\omega \to \chi_i(y,\omega)$, defined for $y \in \mathbf{R}^d$ and ω in a probability space, and taking only the values 0 and 1. It is required that χ_i be translation invariant, in the sense that $\omega \mapsto \chi_i(y+c,\omega)$ gives the same stochastic process for each $c \in \mathbf{R}^d$. Furthermore, the translations are assumed to be ergodic, so that ensemble averaging is equivalent to spatial averaging.

An example would be a family of (possibly overlapping) spherical inclusions of radius $\epsilon\rho$ whose centers have a multidimensional Poisson distribution, the expected number of balls in a unit-sized region being of order ϵ^{-d}. The hypotheses (2.5) or (2.6) specify rather precisely the character of the fine scale structure. The G-*convergence* approach, by contrast, makes no such hypothesis:

(2.7) $\chi_1^\epsilon(x)$ is any family of functions taking only the values 0 and 1, parametrized by $\epsilon \to 0$, and $\chi_2^\epsilon = 1 - \chi_1^\epsilon$.

It is specifically *not* assumed in (2.7) that ϵ represents the length scale of the microstructure: even a sequence which has no clear separation of scales is permitted. Clearly (2.7) includes both the periodic case and the random one; indeed, in our opinion it includes any reasonable notion of a linearly elastic composite obtained by mixing two materials (with perfect bonding at all material interfaces).

The tensor of effective moduli A^* is simply the Hooke's law tensor of the composite. It represents the limiting behavior of the mixture as $\epsilon \to 0$. This means that for any (ϵ-independent) load f, the associated elastostatic displacement u^ϵ - which solves the equilibrium equations

(2.8)
$$\sigma^\epsilon = A^\epsilon e^\epsilon$$
$$e_{kl}^\epsilon = \frac{1}{2}(\frac{\partial u_k^\epsilon}{\partial x_l} + \frac{\partial u_l^\epsilon}{\partial x_k})$$
$$div\ \sigma^\epsilon = f$$

with an appropriate boundary condition – converges as $\epsilon \to 0$ to u^*, the solution of the corresponding system with A^ϵ replaced by A^*. The starting point of the mathematical theory is the *existence* of effective moduli. In the spatially periodic and stationary stochastic contexts (2.5), (2.6), translation invariance assures that the tensor A^* of effective moduli is constant. For periodic composites it can be given in terms of the solutions of certain canonical "cell problems," see e.g. [8,60], but we prefer this variational characterization, cf. [64]:

$$(A^*\xi,\xi) = \inf_{\phi} \int_Q (\tilde{A}(y)[\xi + e(\phi)], \xi + e(\phi))dy, \tag{2.9}$$

in which

$$\tilde{A}(y) = \chi_1(y)A_1 + \chi_2(y)A_2, \tag{2.10}$$

$Q = [0,1]^d$ is the unit cell of the periodic structure, ϕ varies over Q-periodic displacement fields, and $e(\phi) = \frac{1}{2}(\nabla\phi + \nabla\phi^T)$ is the linearized strain associated to ϕ. An entirely analogous formula is available in the random case, cf. [19,33,55,70]:

$$(A^*\xi,\xi) = \inf_{\mathbf{E}(e)=\xi} \mathbf{E}[(\tilde{A}e, e)], \tag{2.11}$$

in which $\mathbf{E}$ represents the ensemble average and e ranges over stationary, random strain fields with mean value ξ. In the more general G-convergence setting (2.7) there is no hypothesis of translation invariance, so the tensor of effective moduli $A^*(x)$ can vary with x. Moreover, there is obviously not enough structure to give a formula as explicit as (2.9) or (2.11). But it is nevertheless true that for any sequence χ_i^ϵ as in (2.7) there is a subsequence $\epsilon' \to 0$ for which there exists a limiting tensor of effective moduli $A^*(x)$, see for example [48,62,65,71].

We shall be interested in bounds for A^* in terms of the volume fractions of the component materials, so let us note here how to express these volume fractions in each of the different settings. For the periodic composite (2.5) the volume fraction of material i is the

proportion of the period cell occupied by it:

$$\theta_i = \int_Q \chi_i(y)\, dy. \tag{2.12}$$

Similarly, in the stationary, random case (2.6) it is the expected value of $\chi_i(y,\omega)$:

$$\theta_i = \mathrm{E}(\chi_i). \tag{2.13}$$

In the G-convergence context (2.7) it is instead given by the L^∞ – weak* limit

$$\theta_i(x) = \mathrm{wk}^* \lim_{\epsilon \to 0} \chi_i^\epsilon(x), \tag{2.14}$$

no longer necessarily constant, defined by the property that

$$\int \chi_i^\epsilon(x) g(x) dx \to \int \theta_i(x) g(x)\, dx \tag{2.15}$$

for continuous functions g.

These notions of effective moduli are easily seen to be equivalent to the operational definitions more commonly used in materials science, based on the average stress and strain or average elastic energy in a physical domain that is large compared with the microstructure but small compared with the length scale of the loads and boundary conditions, see e.g. [22,24]. They are important for the development of a proper mathematical theory, because they make it possible to give fully rigorous proofs of results about effective moduli. But why should they be of interest to a materials scientist? One answer lies in the following "density" result [16]: if an algebraic relation between the tensor of effective moduli the component volume fractions holds for all spatially periodic composites (or for all stationary, stochastic composites), then it holds in the more general context of G-convergence as well. Thus, *for bounds on effective moduli in terms of volume fractions alone, neither long-range disorder nor a definite separation of scales is relevant.* This resolves a point which has been the object of considerable controversy in the literature, see e.g. [22].

3. NEW METHODS FOR BOUNDING EFFECTIVE MODULI.

A typical goal of the new mathematical theory is the so-called G-*closure problem*: find the precise set of Hooke's laws A^* achievable by mixing two given isotropic, elastic materials in specified proportions. The motivation comes from applications to structural optimization, as we shall explain in section 5. The special case when A^* is isotropic was considered by Hashin and Shtrikman [23], under the further hypothesis that the component materials are well-ordered, *i.e.* that

$$\mu_1 \leq \mu_2, \quad \kappa_1 \leq \kappa_2. \tag{3.1}$$

They gave upper and lower bounds for the effective bulk and shear moduli, κ^* and μ^*, which are now known to be simultaneously achievable [17,51]. An improvement of the Hashin-Shtrikman bounds can be found in [10,47], but the precise set of attainable isotropic composites is still not known. In any event, results of this kind – concerning A^* with specified symmetry – are not adequate for applications to structural optimization, since the best composites for use in an optimal structure can (and generally will) be fully anisotropic. While the complete solution of the G-closure problem seems beyond the reach of current methods, the analogues of the Hashin-Shtrikman bounds on κ^* and μ^* are now understood for fully anisotropic composites [3,4,45]. In particular, we now know those parts of the boundary of the G-closure which represent the "strongest" and the "weakest" anisotropic composites.

In the course of exploring these and other bounds for effective moduli, a number of powerful new tools have been introduced. The well-known Hashin-Shtrikman variational principles have been applied in new ways [3,4,26,34,45], and new variational principles have been introduced, obtained from more classical ones by the addition of a quadratic null-Lagrangian [5,27]. In addition, entirely new approaches have been introduced: one is based on an equivalence between bounds for effective moduli and the lower semicontinuity of certain variational functionals [30,32,63]; another uses the fact that the effective moduli

depend analytically on the component properties [9,19,25,44]; a third uses "compensated compactness" to construct certain lower semicontinuous functionals [17,18,35,37.66], and a fourth makes use of Hilbert space decompositions and continued fractions [43]. (These references represent a mere sampling of the relevant literature in each area.) The interested reader will find several of thse new methods applied to a single problem in a self-contained manner in [27]. The power and limitations of these various methods are just beginning to be understood, as are the relationships among them [46].

To convey some of the flavor of these new developments, we present in detail one of the recently established bounds, an upper bound on the elastic energy quadratic form. There is of course a well-known bound due to Paul [56]:

$$(A^*\xi,\xi) \le \theta_1(A_1\xi,\xi) + \theta_2(A_2\xi,\xi), \tag{3.2}$$

where θ_i is the volume fraction of the i^{th} material, $i = 1, 2$. This bound is sharp, in the sense that for certain choices of the "average strain" ξ there is a microstructure whose associated A^* achieves equality in (3.2). However, for *most* choices of ξ (3.2) is not saturated by any composite; therefore a better bound

$$(A^*\xi,\xi) \le F(\theta_1,\theta_2,\mu_1,\mu_2,\kappa_1,\kappa_2,\xi) \tag{3.3}$$

is possible. We shall in fact prove the *optimal* bound of this type, in other words one which is saturated, for each ξ, by an appropriately chosen mixture of the two given materials. The method, which is based on the Hashin-Shtrikman variational principle, requires that the component materials be well-ordered. Our presentation follows that of [26]; equivalent results can be found presented somewhat differently in [3,4] and [45]. The function F on the right of (3.3) is given by (3.16) below, as the extremal value of a finite-dimensional mathematical programming problem.

As discussed in Section 2, it is sufficient to prove the bound for spatially periodic composites. We may therefore fix $Q = [0,1]^d$ as the period cell; the microstructure is

determined by the indicator functions $\chi_1(y)$ and $\chi_2(y) = 1 - \chi_1(y)$, $y \in Q$, constrained by the given volume fractions (2.12); and the effective Hooke's law is determined by (2.9).

The first step is to derive the Hashin-Shtrikman variational principle:

$$
\begin{aligned}
(A^*\xi, \xi) \leq & -2\int_Q (\sigma, \xi + e(\phi))\chi_1 dy \\
& + \int_Q ((A_2 - A_1)^{-1}\sigma, \sigma)\chi_1 dy \\
& + \int_Q (A_2(\xi + e(\phi)), \xi + e(\phi))dy
\end{aligned} \tag{3.4}
$$

for any Q-periodic displacement field ϕ, and any Q-periodic field of symmetric tensors σ. The proof is elementary: expanding the pointwise inequality

$$
|(A_2 - A_1)^{1/2}(\xi + e(\phi)) - (A_2 - A_1)^{-1/2}\sigma|^2 \geq 0 \tag{3.5}
$$

and multiplying by χ_1 gives

$$
-\chi_1((A_2 - A_1)(\xi + e(\phi)), \xi + e(\phi)) \leq -2(\sigma, \xi + e(\phi))\chi_1 + \chi_1((A_2 - A_1)^{-1}\sigma, \sigma). \tag{3.6}
$$

The left side equals

$$
((\tilde{A} - A_2)(\xi + e(\phi)), \xi + e(\phi)); \tag{3.7}
$$

therefore integrating over Q and applying (2.9) we conclude (3.4).

The next step is to specialize to *constant* σ, and to evaluate the integrals in (3.4) wherever possible. This gives

$$
\begin{aligned}
((A^* - A_2)\xi, \xi) + 2\theta_1(\sigma, \xi) - \theta_1((A_2 - A_1)^{-1}\sigma, \sigma) \\
\leq -2\int_Q (\sigma\chi_1, e(\phi))dy + \int_Q (A_2 e(\phi), e(\phi))dy,
\end{aligned} \tag{3.8}
$$

for any Q-periodic displacement field ϕ.

The third step is to minimize the expression on the right over ϕ. This amounts to solving the elastostatic equilibrium equation

$$
DIV(A_2 e(\phi)) - DIV(\sigma\chi_1) = 0 \tag{3.9}
$$

with a periodic boundary condition. It is convenient to use Fourier analysis: since A_2 and σ are constant, (3.9) determines the Fourier transform of ϕ at each frequency $k \in \mathbf{Z}^d$ directly in terms of the transform of χ_1 at the same frequency. After some algbra, one finds that the extremal value of the right side of (3.8) is

$$-\sum_{k\neq 0} |\hat{\chi}_1(k)|^2 (f(\frac{k}{|k|})\sigma, \sigma) \tag{3.10}$$

where

$$\chi_1(y) = \sum_{k\in\mathbf{Z}^d} e^{2\pi i k\cdot y}\hat{\chi}_1(k), \tag{3.11}$$

and for any unit vector $v \in \mathbf{R}^d$, $f(v)$ is the "degenerate Hooke's law" defined by

$$\begin{aligned} f(v)\sigma = &\frac{d}{d\kappa_2 + 2(d-1)\mu_2}(\sigma v, v)v\odot v \\ &+ \frac{1}{\mu_2}[(\sigma v)\odot v - (\sigma v, v)v\odot v]. \end{aligned} \tag{3.12}$$

Here σ is any symmetric tensor, and we use the notation $v\odot w = \frac{1}{2}(v\otimes w + w\otimes v)$ for the symmetric tensor product of two vectors in $\mathbf{R}^d$.

It remains to eliminate the explicit dependence of the bound on χ_1, which is after all arbitrary except for the volume fraction constraint. We use this constraint to see that

$$\int_Q (\chi_1 - \theta_1)^2 dy = \theta_1\theta_2, \tag{3.13}$$

whence by Plancherel's theorem

$$\sum_{k\neq 0} |\hat{\chi}(k)|^2 = \theta_1\theta_2. \tag{3.14}$$

This gives a bound on the "nonlocal" term:

$$(3.10) \leq -\theta_1\theta_2 \min_{|v|=1}(f(v)\sigma, \sigma). \tag{3.15}$$

Substitution into (3.8) gives a bound on A^* which still depends on the choice of a symmetric tensor σ, and minimization over σ gives a result of the desired form $(A^*\xi,\xi) \leq F$, with

$$F = (A_2\xi,\xi) + \theta_1 \cdot \min_{\sigma}\{-2(\sigma,\xi) + ((A_2 - A_1)^{-1}\sigma,\sigma) - \theta_2 \min_{|v|=1}(f(v)\sigma,\sigma)\}. \tag{3.16}$$

Our interest in this bound lies in the fact that it is the *best possible* bound for $(A^*\xi, \xi)$ in terms of the given parameters $\xi, \theta_1, \theta_2 = 1 - \theta_1$, and the bulk and shear moduli of the component materials $\kappa_1 \leq \kappa_2$, $\mu_1 \leq \mu_2$. This will be proved in the next section, as an application of the formula for the effective behavior of a sequentially laminated composite.

4. CONSTRUCTION OF MIXTURES WITH EXPLICITLY COMPUTABLE EFFECTIVE MODULI.

For most microstructures there is no explicit, algebraic formula for the tensor of effective moduli A^*; one must make do instead with a variational principle such as (2.9) or (2.11), or perhaps with the partial differential equation characterizing its extremal. If this were the only available tool it would be virtually impossible to establish the optimality of any bound! Fortunately there are certain, rather special microstructures for which the effective moduli *are* computable; and, remarkably, this class of composites is rich enough to demonstrate the optimality of a variety of bounds, including (3.3).

There are some simple and more or less classical examples of composites with explicitly computable properties. One example is that of a layered microstructure [6.11,40]; another is the "concentric sphere construction," which was used by Hashin in [73] to prove the optimality of their bulk modulus bounds. It is natural enough to iterate such constructions, for example layering together two composites each of which has its own fine-scale structure, obtained perhaps by layering or by a version of the concentric sphere construction. This idea, which can be found in Bruggeman's work [11], has been rediscovered by various individuals and applied to prove the attainability of many different bounds, e.g. [3-5,17,18.26,34,35,37,38,42,61,66].

An important new development concerns the attainability of certain mean field theories. The formulas they predict for the tensor of effective moduli A^* were originally intended as approximations, not as exact results. Nevertheless, it has recently been shown that certain effective medium theories are *exactly* attainable by composites with approximately chosen microstructures [2,36,41]. Obviously, this result greatly expands the class of

composites with explicitly computable effective moduli – particularly since these effective medium theories (the "coherent potential approximation" and the "differential effective medium theory ") have been widely studied in the mechanics literature, see e.g. [74,75].

The microstructures that arise from these constructions are, it should be understood, somewhat idealized materials. They are highly ordered, neither periodic nor stochastic in character, and they frequently involve multiple length scales. It may seem like cheating that we allow the use of such microstructures to establish the attainability of a bound, whereas the proof of the bound may make use of special structure such as periodicity. This is in fact perfectly legitimate; indeed, it is here that we use the power of the mathematical theory. The point is that these constructions fit perfectly into the mathematical context of G-convergence (see especially [2]); therefore, by the "density" result mentioned at the end of Section 2, their effective moduli can be approximated arbitrarily well by those of spatially periodic composites. Actually, it is quite natural to use the most restrictive possible setting for proving bounds, and the most general one for showing that they are achieved.

The remainder of this section is devoted to a discussion of *sequentially laminated* composites, and to a proof of the attainability of the new upper bound (3.3). Closely related ideas and results can be found in [3,4,26,45]. The construction of a sequentially laminated composite is an iterative procedure, producing a microstructure that has several different length scales. A ***laminar composite of rank*** 1 is obtained by layering two initially given materials, specifying the proportion of each and the layer direction, and using a small parameter ϵ_1 as the layer thickness. As $\epsilon_1 \to 0$, the elastic behavior is described by an effective Hooke's law C_1. A ***laminar composite of rank*** 2 is obtained by layering two laminar composites of rank 1, again specifying the proportion of each and the layer direction, and using another small parameter ϵ_2 for the layer thickness. As $\epsilon_1, \epsilon_2 \to 0$ with $\epsilon_1 << \epsilon_2$, the elastic behavior is described by an effective Hooke's law C_2. This process can clearly be continued indefinitely: the general sequentially laminated composite of rank

r is obtained by layering together two sequentially laminated composites of rank $r-1$. We shall consider here only a special case, in which *one of these two materials is the isotropic one with shear modulus μ_2 and bulk modulus κ_2 at each successive stage.* An elegant, iterative formula for representing the effective moduli of such a composite was derived in [17], following a method developed for scalar equations in [66]. We now give a derivation of this result.

The basic building block is a formula for the effective tensor C corresponding to a layered mixture of the isotropic material with Hooke's law A_2 and a general elastic material with Hooke's law B, using layers orthogonal to the unit vector $v \in \mathbf{R}^n$, and using proportions ρ_2 and $\rho_B = 1 - \rho_2$ of A_2 and B, respectively:

$$\rho_B (A_2 - C)^{-1}\sigma = (A_2 - B)^{-1}\sigma - \rho_2 f(v)\sigma \tag{4.1}$$

for any symmetric tensor σ. Here $f(v)$ is the *same* degenerate Hooke's law that arose in our proof of the bound, defined by (3.12). In writing (4.1) we have implicitly assumed that $A_2 - C$ and $A_2 - B$ are invertible, when viewed as symmetric linear maps on the space of symmetric tensors. This is the case whenever $B < A_2$, since then $C < A_2$ as well, by Paul's bound (3.2); this ordering hypothesis will be sufficient for our purposes, since we are concerned with mixtures of two well-ordered isotropic materials, *i.e.* (3.1) holds. (There is a version of (4.1) without invertibility hypotheses, see for example [17].) To prove (4.1), one must of course begin with a characterization of C. In a layered composite of the type under consideration, the local values of the stress and strain are essentially constant within each component. Therefore, arguing for example as in [40], the calculation of $C\xi$ given ξ is easily reduced to this algebraic problem: find a pair of symmetric matrices ξ_2 and ξ_B (representing the strain in the layers occupied by materials A_2 and B respectively) such that

$$\begin{aligned} &\rho_2\xi_2 + \rho_B\xi_B = \xi \\ &\xi_B - \xi_2 = v \odot w \text{ for some } w \in \mathbf{R}^n, \\ &(A_2\xi_2 - B\xi_B)v = 0. \end{aligned} \tag{4.2a-c}$$

The first relation says that ξ is the average strain; the second is the consistency condition for the existence of a deformation with the specified piecewise constant strain (recall that $v \odot w = (v \otimes w + w \otimes v)/2$); and the third represents the continuity of the normal stress at the layer interface. In terms of these quantities, $C\xi$ is determined by

$$C\xi = \rho_2 A_2 \xi_2 + \rho_B B \xi_B , \tag{4.2d}$$

which identifies it as the average stress. The solution of (4.2a-d) is easiest to represent in terms of $\sigma = (A_2 - C)\xi$. One calculates that ξ_2 and ξ_B are given in terms of σ by

$$\xi_B = \rho_B^{-1}(A_2 - B)^{-1}\sigma, \quad \xi_2 = \xi_B - v \odot w, \tag{4.3}$$

where $w \in \mathbf{R}^n$ is chosen so that

$$\rho_B A_2(v \odot w) = 2(\sigma v) \odot v - (\sigma v, v)v \odot v, \tag{4.4}$$

whence

$$\rho_B [A_2(v \odot w)]v = \sigma v. \tag{4.5}$$

The unique w satisfying (4.4) is

$$w = \rho_B^{-1}[\frac{d}{d\kappa_2 + 2(d-1)\mu_2}(\sigma v, v)v + \frac{1}{\mu_2}(\sigma v - (\sigma v, v)v)], \tag{4.6}$$

and it has the property that

$$\rho_B v \odot w = f(v)\sigma \tag{4.7}$$

with $f(v)$ defined by (3.12). Therefore

$$\begin{aligned} (A_2 - C)^{-1}\sigma = \xi &= \rho_B \xi_B + \rho_2 \xi_2 \\ &= \xi_B - \rho_2 v \odot w \\ &= \rho_B^{-1}(A_2 - B)^{-1}\sigma - \rho_B^{-1}\rho_2 f(v)\sigma, \end{aligned} \tag{4.8}$$

which is precisely the desired formula (4.1).

Now consider a sequence $C_0, C_1, C_2, \ldots$ of effective tensors such that

(4.9a) $C_0 = A_1$ represents an isotropic material with bulk modulus κ_1 and shear modulus μ_1,

and, for $r \geq 1$,

(4.9b) C_r is obtained by layering A_2 with C_{r-1} in volume fractions α_r and $(1-\alpha_r)$ respectively, using the unit vector v_r as the layer normal.

Evidently, C_r represents the effective behavior of a certain sequentially laminated composite of rank r. The volume fraction of A_2 in C_r is

$$\beta_r = 1 - \prod_{i=1}^{r} (1-\alpha_i), \quad r \geq 1; \quad \beta_0 = 0. \tag{4.10}$$

A formula for C_r is easily obtained by iterating (4.1):

$$(1-\beta_r)(A_2 - C_r)^{-1} = (A_2 - A_1)^{-1} - \sum_{i=1}^{r} (\beta_i - \beta_{i-1}) f(v_i). \tag{4.11}$$

Let us terminate this process at $r = N$, and write

$$\begin{aligned} \theta_2 = \beta_N &= \text{ overall volume fraction of } A_2 \\ \theta_1 = 1 - \beta_N &= \text{ overall volume fraction of } A_1 \\ A^* = C_N &= \text{ effective Hooke's law of the associated rank } N \text{ composite.} \end{aligned} \tag{4.12}$$

It is easy to see that the sequence

$$m_i = (\beta_i - \beta_{i-1})/\beta_N, \quad 1 \leq i \leq N, \tag{4.13}$$

can be any nonnegative sequence which sums to 1, by making an appropriate choice of the parameters $\{\alpha_i\}$. Thus we have shown that *for any integer $N \geq 1$, any unit vectors $\{v_i\}_{i=1}^N$ in $\mathbf{R}^d$, any real numbers $\{m_i\}_{i=1}$ with $0 \leq m_i \leq 1$ and $\sum m_i = 1$ and any real number θ_2, $0 < \theta_2 < 1$, there is a sequentially laminated composite made by mixing A_1*

and A_2 as in (4.9), *using overall volume fractions $\theta_1 = 1 - \theta_2$ and θ_2 respectively, whose effective Hooke's law A^* is characterized by*

$$\theta_1(A_2 - A^*)^{-1} = (A_2 - A_1)^{-1} - \theta_2 \sum_{i=1}^{N} m_i f(v_i). \tag{4.14}$$

We now apply this construction to establish the optimality of the new upper bound (3.16). Our task is to show that for each symmetric tensor ξ there is a choice of the parameters $\{v_i, m_i\}$ such that A^*, defined by (4.14), satisfies $(A^*\xi, \xi) = F$ with F as in (3.16). Now, (3.16) gives F in terms of a mathematical programming problem

$$\min_{\sigma}\{-2(\sigma, \xi) + ((A_2 - A_1)^{-1}\sigma, \sigma) - \theta_2 \min_{|v|=1}(f(v)\sigma, \sigma)\} \tag{4.15}$$

over symmetric tensors σ, so it is reasonable to expect the proper choices of $\{v_i, m_i\}$ to emerge from the optimality conditions for (4.15). Since the last term is not a smooth function of σ, it is natural to use the methods of "nonsmooth analysis," see for example [15]. To this end we rewrite (4.15) as

$$\min_{\sigma}\{-2(\sigma, \xi) + g(\sigma)\} \tag{4.16}$$

with

$$g(\sigma) = \max_{|v|=1}((A_2 - A_1)^{-1} - \theta_2 f(v)]\sigma, \sigma). \tag{4.17}$$

For each fixed v the expression on the right is a positive, quadratic function of σ (one way to establish positivity is to make use of (4.1)). Therefore g is convex, and the optimality condition for (4.17) is that for any extremal σ^*

$$2\xi \in \partial g(\sigma^*), \tag{4.18}$$

where $\partial g(\sigma^*)$ is the subdifferential of g at σ^* (see e.g. [15, 2.3.1-2.3.3 and Corollary 1, §2.3]). Moreover, $\partial g(\sigma^*)$ is the closed convex hull of the differentials of the various quadratic forms in (4.17) as v ranges over all extremals (see e.g. [15, §2.8, Corollary 1]). Since the space

of symmetric tensors is finite dimensional, each element of the closed convex hull is in fact a convex combination of finitely many extreme points. Therefore the optimality condition (4.18) becomes

$$\xi = (A_2 - A_1)^{-1}\sigma^* - \theta_2 \sum_{i=1}^{N} m_i f(v_i)\sigma^*, \tag{4.19}$$

with $m_i \geq 0$, $\Sigma m_i = 1$, $|v_i| = 1$, $N < \infty$, and

$$g(\sigma^*) = ((A_2 - A_1)^{-1}\sigma^*, \sigma^*) - \theta_2(f(v_i)\sigma^*, \sigma^*), \quad 1 \leq i \leq N. \tag{4.20}$$

Comparing (4.19) with (4.14), we see that

$$\xi = \theta_1(A_2 - A^*)^{-1}\sigma^*, \tag{4.21}$$

where A^* is the sequentially laminated composite of rank N constructed using $\{m_i, v_i\}_{i=1}^{N}$. We claim that this A^* satisfies $(A^*\xi, \xi) = F$. Indeed, the value of F is

$$F = (A_2\xi, \xi) + \theta_1\{-2(\sigma^*, \xi) + g(\sigma^*)\}, \tag{4.22}$$

using (3.16) and the fact that σ^* is extremal for (4.15). We have

$$(\sigma^*, \xi) = g(\sigma^*) \tag{4.23}$$

by (4.19) and (4.20), so (4.22) becomes

$$F = (A_2\xi, \xi) - \theta_1(\sigma^*, \xi). \tag{4.24}$$

But $\theta_1\sigma^* = (A_2 - A^*)\xi$ by (4.21), and substitution gives the desired result $F = (A^*\xi, \xi)$.

5. APPLICATIONS TO STRUCTURAL OPTIMIZATION.

The recent interest in optimal bounds on the effective moduli of composites has been stimulated in large part by applications to structural optimization, see e.g. [1,28,38,39,49,50,67]. That discipline is concerned with choosing the geometry or composition of a load-bearing structure so as to use the available materials as efficiently as possible. The subject has a rich history and an extensive literature; books and articles reviewing various aspects include [7,21,53,57]. Initially attention was focused primarily on analytical methods – optimality conditions, conformal mapping, isoperimetric inequalities, and so forth. More recently, with the growing feasibility of large scale computing, attention has naturally been turned to methods for the direct, numerical calculation of optimal structures.

To fix ideas, let us consider a particular problem involving shape optimization and plane stress. We begin with a homogeneous, isotropic elastic body occupying a region $\Omega \subset \mathbf{R}^2$, loaded along its boundary $\partial\Omega$ by a specified traction f. We desire to lighten this body by removing material from a subset $H \subset \Omega$, consisting of one or more holes of arbitrary size and shape. The goal is to achieve the *minimum possible weight*, i.e. to maximize the area of the "holes" H, subject to a *performance constraint* on the stress σ_H or displacement u_H of the resulting elastic structure. Typical constraints are

(5.1a) that the work done by the load ("compliance") be not too large : $\int_{\partial\Omega} u_H \cdot f \leq C$; or

(5.1b) that the average displacement on a subdomain Ω_1 be not too large : $\int_{\Omega_1} |u_H| \leq C$; or

(5.1c) that the pointwise maximum stress be not too large : $\sup_{x \in \Omega} \|\sigma_H(x)\| \leq C$.

Highly efficient and sophisticated algorithms have been developed for the numerical solution of such problems; [21] gives an excellent review. Typically, one begins by deciding

how many holes to consider. Each hole boundary is determined by finitely many points, for example using splines. The resulting domain is triangulated, and the equations of elastostatics are modeled as a finite system of linear equations using the finnite element method. The design problem is thus transformed to a (highly nonlinear!) mathematical programming problem, and one can seek an "optimal" design – or at least an improvement of a given design – using streepest descent, or perhaps some more sophisticated method.

Though its utility is beyond disupte, this "conventional" approach has one troublesome aspect: the gross features of the design – especially, the number of holes – must be chosen at the outset; they are not a part of the optimization. Thus the output is likely to be a local optimum, or at best an optimum among all designs with a specified number of holes. In fact, numerical attempts at *global* optimization for related model problems have led in some cases to "optimal" designs that vary on the scale of the mesh size itself, with no convergence evident as the mesh size tends to zerro [1,13]! This phenomenon is now well-understood. In the context of shape optimization, the situation is as follows: consider first the best design with one hole, then that with two, and so forth. As the number of holes gets larger, the performance may get better (depending, of course, on the specific problem under consideration). In the limit of infinitely many holes one thus finds a global optimum which is not a "conventional" design at all, but instead a structure made from ***composite materials obtained by perforation.***

With hindsight it seems almost obvious: if one is prepared to consider designs with many small holes, then one ought also to consider their limits. We thus arrive at a new approach to structural optimization: if the goal is to find a global optimum then it is best to work from the start in the class of all ***structures made up of composite materials obtainable by perforation from the one initially given.*** It should be emphasized that the underlying problem is *not* being changed, since we allow *only* composites achievable by perforation, and we are careful to model them properly. However, the resulting optimization problem looks quite different: whereas initially we were considering structures made up of a single

material (or the absence thereof), now we propose to allow a continuum of materials – each representing a perforated composite with a different microscopic geometry. (As a technical matter, the mathematical theory discussed in the preceding sections does not quite apply to perforated composites, since it requires $\mu_i > 0$ and $\kappa_i > 0$. This can be circumvented, at least for compliance optimization problems, by the methods of [30,32]. Alternatively, we can simply treat the "holes" as though they were filled with a very weak elastic material.)

The introduction of composites as generalized designs – sometimes called the *relaxation* of the design problem – has been studied extensively by several groups over the past ten years, see e.g. [20,30,38,50,52,54,58,59,67]. From a theoretical standpoint, the principal advantage of relaxation is that it assures the *existence* of an optimal design; roughly, this means that a numerical solution of the relaxed problem will converge as the mesh size tends to zero. There is also a practical advantage, based on the fact that the initial material and the absence of material are included (as extreme cases) among the candidate composites: evidently, for a given finite element subdivision the introduction of composites serves to enlarge the design space and hence to *improve the performance* of a numerically obtained optimal design. Moreover, precisely because it has the effect (within a finite element context) of enlarging the design space, the process of relaxation can *destroy local minima* – making it easier to locate a globally optimal design. Finally, since the relaxed problem is known to have a solution, it is meaningful to use the associated *optimality conditions*; this has led in some contexts to closed-form examples of optimal designs making use of composites, e.g. [29,30,31]. The method of relaxation has its limitations: the optimal designs obtained this way may be difficult or even impossible to manufacture, because of the presence of composites. Even so, these solutions can be used as *benchmarks* against which to compare the output of a more conventional algorithm.

The process of relaxation is conceptually simple: we must simply reformulate the design problem in a form that permits perforated composites as admissible materials. The actual execution, however, is not so simple: it requires specific knowledge about the prop-

erties of the relevant composites. For a local performance criterion such as the maximum stress (5.1c) we would have to know optimal bounds relating the effective Hooke's law, the density of holes, the average stress, and the local maximum stress in a general perforated composite. This represents a challenge for the future: no such result is presently known. For a performance criterion involving some integral of the displacement, such as (5.16), it would suffice to know the solution of the G-closure problem – in other words, to know the class of all effective Hooke's laws obtainable using perforations that remove a given fraction of the material. The analogous problem has been solved for scalar equations [37,66], and it has been applied to solve various optimization problems involving conductivity, see e.g. [12,20,30,38,50,67]; but unfortunately the G-closure problem for elasticity remains open at this time except in certain rather special cases [34,35]. However, problems involving compliance constraints such as (5.1a) do not require the full solution of the G-closure problem; rather, bounds of the type presented in Sections 3 and 4 are sufficient. To explain why, we note that it is not really necessary to consider *all* composites; one might as well consider just those that can actually occur in an optimal design. Now, by Green's formula the compliance is equal to the internal elastic energy:

$$\int_{\partial\Omega} u \cdot f = \int_{\Omega} (A(x)e(u), e(u))\, dx, \tag{5.2}$$

where $A(x)$ is the spatially varying tensor of elastic moduli and u the associated displacement. A structure which minimizes weight for fixed compliance will also minimize compliance for given weight; it is not hard to see from this that $A(x)$ should *maximize* $(Ae(u), e(u))$ at each point x in an optimal design. Thus the values that $A(x)$ can take in an optimal design are restricted to those that maximize $(A\xi, \xi)$ for some tensor ξ.

The preceding discussion shows that we have enough information to solve optimal design problems with compliance constraints, but it falls short of specifying an algorithm to do so. How, operationally, should one proceed? Following [30], we advocate an algorithm based on the principle of minimum complementary energy, a variational principle for the

stress whose extremal value is equal to the compliance:

$$\int_{\partial\Omega} u \cdot f = \min_{div\ \sigma=0, \sigma\cdot n=f} \int_{\Omega} (A^{-1}(x)\sigma, \sigma)\ dx. \tag{5.3}$$

Introducing a Lagrange multiplier for the performance constraint (5.1a) our design problem is

$$MIN_{designs}\{WEIGHT + \lambda \cdot COMPLIANCE\}. \tag{5.4}$$

The outer minimization over designs is quantified by introducing functions $\theta(x)$ and $A(x)$, the density and effective Hooke's law, constrained by the pointwise conditions

$$\begin{aligned} &0 \le \theta \le 1, \text{ and } A \text{ is the effective Hooke's law of a} \\ &\text{perforated composite obtained by removing volume} \\ &\text{fraction } 1-\theta \text{ of the initially given material.]}cr \end{aligned} \tag{5.5}$$

The compliance is itself a minimum, according to (5.3), so (5.4) becomes

$$\min_{\theta, A}\{\int_{\Omega} \theta(x)\ dx + \lambda \cdot \min_{div\ \sigma=0, \sigma\cdot n=f} \int_{\Omega} (A^{-1}(x)\sigma, \sigma)\ dx\}. \tag{5.6}$$

The order of minimization is unimportant, and switching it gives

$$\min_{div\ \sigma=0, \sigma\cdot n=f} \int_{\Omega} \Phi_{\lambda}(\sigma)\ dx \tag{5.7}$$

with

$$\Phi_{\lambda}(\sigma) = \min_{\theta, A}[\theta + \lambda(A^{-1}\sigma, \sigma)]. \tag{5.8}$$

The minimization in (5.8) is over real numbers θ and tensors A, constrained by (5.5). This is slightly different than the problem we treated in Sections 3 and 4, but *it can be solved by exactly the same method* – as can considerably more general problems, for example the analogue of (5.8) when there are compliance constraints under two or more loads.

The next step, of course, is to evaluate (5.8) analytically or numerically, and to carry out the optimization by solving (5.7) for realistic design problems. Work in these directions

is currently in progress. The minimization of (5.8) was executed in [30] for the special case of an elastic material in plane stress with Poisson's ratio zero – i.e. when $\mu = \kappa = \frac{1}{2}E$. where E is Young's modulus – using a different method, based on quasiconvexification. The answer is surprisingly simple: scaling $\lambda = E = 1$ for simplicity,

$$\Phi_1(\sigma) = \begin{cases} 1 + \sigma_1^2 + \sigma_2^2, & |\sigma_1| + |\sigma_2| \geq 1 \\ 2(|\sigma_1| + |\sigma_2|) - 2|\sigma_1\sigma_2|, & |\sigma_1| + |\sigma_2| \leq 1 \end{cases}$$

where σ_1 and σ_2 are the principal stresses (the eigenvalues of σ).

ACKNOWLEDGEMENTS: This work was supported in part by NSF grant DMS-8312229, ONR grant N00014-83-K-0536, DARPA contract F49620-87-C-0065, and the Sloan Foundation.

REFERENCES

[1] Armand, J.-L., Lurie, K.A. and Cherkaev, A.V., "Optimal control theory and structural design," in *New Directions in Optimum Structural Design*, E. Atrek et al., eds., John Wiley and Sons, p.211, 1984.

[2] Avellaneda, M., "Iterated homogenization, differential effective medium theory, and applications," *Comm. Pure Appl. Math. 40*, p. 527, 1987.

[3] ————, "Optimal bounds and microgeometries for elastic composites," *SIAM J. Appl. Math. 47*, p. 1216, 1987.

[4] ————, "Bounds on the effective elastic constants of two-phase composite materials," to appear in *Proc. Sem. Collège de France.*

[5] ————, Cherkaev, A. V., Lurie, K. A. and Milton, G. W., "On the effective conductivity of polycrystals and a three-dimensional phase interchange inequality," *J. Appl.Phys.* to appear, 1988.

[6] Backus, G. E., "Long-wave elastic anisotropy produced by horizontal layering," *J. Geophys. Res. 67*, p. 4427, 1962.

[7] Banichuk, N. V., *Problems and Methods of Optimal Structural Design*, Plenum. 1983.

[8] Bensoussan, A., Lions, J.-L., and Papanicolaou, G., *Asymptotic Analysis for Periodic Structures*. North-Holland, 1978.

[9] Bergman, D. J., "The dielectric constant of a composite material - a problem in classical physics," *Phys. Rep. C43*, p. 377, 1978.

[10] Berryman, J. G. and Milton, G. W., "Microgeometries of random composites and porous media," *J. Phys. D*, to appear, 1988.

[11] Bruggeman, D. A. G., "Berechnung verschiedener physikalischer konstanten, von heterogenen substanzen," *Ann. Phys. 5*, p.636, 1935; also "Elastizität konstanten von kristallaggragaten", Ph.D. Thesis, Utrecht, 1930.

[12] Cabib, E. and Dal Maso, G., "On a class of optimum problems in structural design," *J. Opt. Th. Appl.56*, to appear, 1988.

[13] Cheng, K.-T. and Olhoff, N., "An investigation concerning optimal design of solid elastic plates," *Int. J. Solids Struct. 17*, p. 305, 1981.

[14] Christensen, R. M., *Mechanics of Composite Materials*, Wiley Interscience, 1979.

[15] Clarke, F. H., *Optimization and Nonsmooth Analysis*, John Wiley and Sons, 1983.

[16] Dal Maso, G. and Kohn, R., "The local character of G-closure," in preparation.

[17] Francfort, G. A. and Murat, F., "Homogenization and optimal bounds in linear elasticity," *Arch. Rat. Mech. Anal. 94*, p. 307, 1986.

[18] Gibianski, L. V. and Cherkaev, A. V., "Design of composite plates of extremal rigidity," Ioffe Physicotechnical Institute preprint, 1984.

[19] Golden, K. and Papanicolaou, G., "Bounds for effective parameters of heterogeneous media by analytic continuation," *Comm. Math. Phys. 90*, p. 473, 1983.

[20] Goodman, J., Kohn, R. V., and Reyna, L., "Numerical study of a relaxed variational problem from optimal design," *Comp. Meth. Appl. Mech. Eng. 57*, p. 107, 1986.

[21] Haftka, R. T. and Grandhi, R. V., "Structural shape optimization - a survey," *Comp. Meth. Appl. Mech. Eng. 57*, p. 91, 1986.

[22] Hashin, Z., "Analysis of composite materials: a survey," *J. Appl. Mech. 50*, p. 481.

1983.

[23] Hashin, Z. and Shtrikman, S., "A variational approach to the theory of the elastic behavior of multiphase materials," *J. Mech. Phys. Solids 11*, p. 127, 1963.

[24] Hill.R., "Elastic properties of reinforced solids: some theoretical principles," *J. Mech. Phys. Solics 11*, p. 357, 1963.

[25] Kantor, Y. and Bergman, D. J., "Improved rigorous bounds on the effective elastic moduli of a composite material," *J. Mech. Phys. Solids, 32*, p. 41, 1984.

[26] Kohn, R. V. and Lipton, R., "Optimal bounds for the effective energy of a mixture of two incompressible elastic materials," *Arch. Rat. Mech. Anal.*, to appear, 1988.

[27] Kohn, R. V. and Milton, G. W., "On bounding the effective conductivity of anisotropic composites," in *Homogenization and Effective Moduli of Materials and Media*, J. Ericksen et al., eds., Springer-Verlag, p. 97, 1986.

[28] Kohn, R. V. and Strang, G., "Structural design optimization, homogenization, and relaxation of variational problems," in R. Burridge et al., *Macroscopic Properties of Disordered Media*, Springer-Verlag, p. 131, 1982.

[29] Kohn, R. and Strang, G., "Optimal design for torsional rigidity," in *Hybrid and Mixed Finite Element Methods*, S. N. Atluri et al., eds., John Wiley and Sons, p. 281, 1983.

[30] Kohn, R. and Strang, G., "Optimal design and relaxation of variational problems I-III," *Comm. Pure Appl. Math. 39*, pp. 113, 139, and 353, 1986.

[31] Kohn, R. V. and Strang, G., "The constrained least gradient problem," in *Non-Classical Continuum Mechanics*, R. J. Knops and A. A. Lacey, eds., Cambridge Univ. Press, p. 226, 1987.

[32] Kohn, R. V. and Vogelius, M., "Relaxation of a variational method for impedance computed tomography," *Comm. Pure Appl. Math. 40*, p. 745, 1987.

[33] Kozlov, S. M., "The averaging of random operators," *Math. USSR - Sbornik 37*, p. 167, 1980.

[34] Lipton, R., "On the effective elasticity of a two dimensional homogenized incompress-

ible elastic composite," *Proc. Roy. Soc. Edinburgh*, Ser. A, to appear, 1988.

[35] Lurie, K. A. and Cherkaev, A. V., "G-closure of some particular sets of admissible material characteristics for the problem of bending of thin elastic plates," *J. Opt. Th. Appl. 42*, p. 305, 1984.

[36] Lurie, K. A. and Cherkaev, A. V., "Optimization of properties of multicomponent isotropic composites," *J. Opt. Th. Appl. 46*, p. 571, 1985; also "The problem of formation of an optimal isotropic multicomponent composite," Ioffe Physicotechnical Institute preprint no. 895.

[37] Lurie, K. A. and Cherkaev, A. V., "Exact estimates of the conductivity of a binary mixture of isotropic components," *Proc. Roy. Soc. Edinburgh*, Ser. A., 104, p. 21, 1986.

[38] Lurie, K. A. and Cherkaev, A. V., "The effective properties of composites and problems of optimal design of constructions," (in Russian), *Uspekhi Mekhaniki*, No. 2, 1987.

[39] Lurie, K. A., Cherkaev, A. V., and Fedorov, A. V., "Regularization of optimal design problems for bars and plates I, II," *J. Opt. Th. Appl. 37*, pp. 499 and 523, 1982.

[40] McConnell, W. H., "On the approximation of elliptic operators with discontinuous coefficients," *Ann. Sc. Norm. Sup. Pisa*, 3, p. 121, 1976.

[41] Milton, G. W., "The coherent potential approximation is a realizable effective medium theory," *Comm. Math. Phys. 99*, p. 465, 1985.

[42] Milton, G. W., "Modeling the properties of composites by laminates," in *Homogenization and Effective Moduli of Materials and Media*, J. Ericksen et al., eds., Springer-Verlag, p. 150, 1986.

[43] Milton, G. W., "Multicomponent composites, electrical networks, and new types of continued fractions I, II," *Comm. Math. Phys.*, to appear, 1988.

[44] Milton, G. W. and Golden, K., "Thermal conduction in composites," in *Thermal Conductivity 18*, T. Ashworth and D. R. Smith, eds., Plenum, p. 571, 1985.

[45] Milton, G. W. and Kohn, R. V., "Variational bounds on the effective moduli of anisotropic composites," in preparation.

[46] Milton, G. W. and McPhedran, R. C., "A comparison of two methods for deriving bounds on the effective conductivity of composites," in *Macroscopic Properties of Disordered Media*, R. Burridge et al., eds., Springer-Verlag, p. 183, 1982.

[47] Milton, G. W. and Phan-Thien, N., "New bounds on the effective elastic moduli of two-dimensional materials," *Proc. Roy. Soc. London A380*, p. 305, 1982.

[48] Murat, F., "H-convergence," mimeographed lecture notes, Univ. d'Alger, 1978.

[49] Murat, F., "Control in coefficients," in *Systems and Control Theory Encyclopedia: Theory, Technology, Applications*, Pergamon Press, 1986.

[50] Mura F. and Tartar, L., "Calcul des variations et homogénéization," in *Les Méthodes de l'Homogenéization: Theorie et Applications en Physique*, Coll. de la Dir. des Etudes et Recherches d'Electricité de France, Eyrolles, p. 319, 1985.

[51] Norris, A. N., "A differential scheme for the effective moduli of composites," *Mech. of Materials 4*, p. 1, 1985.

[52] Olhoff, N., Lurie, K. A., Cherkaev, A. V., and Fedorov, A. V., "Sliding regimes and anisotropy in optimal design of vibrating axisymmetric plates," *Int. J. Solids Struct. 17*, p. 931, 1981.

[53] Olhoff, N. and Taylor, J., "On structural optimization," *J. Appl. Mech. 50*, p.1139, 1983.

[54] Ong, T.-G.,Rozvany, G. I. N., and Szeto, W. T., "Least weight design of perforated elastic plates for given compliance: non-zero Poisson's ratio," to appear.

[55] Papanicolaou, G. and Varadhan, S. R. S., "Boundary value problems with rapidly oscillating random coefficients," in *Colloquia Mathematica Societatis Janos Bolyai 27*: Random Fields, North Holland, p. 835, 1982.

[56] Paul, B., "Prediction of elastic constants of multiphase materials," *Trans. A.S.M.E. 218*, p. 36, 1960.

[57] Pironneau, O., *Optimal Shape Design for Elliptic Systems*, Springer-Verlag, 1984.

[58] Raitum, U. E., "On optimal control problems for linear elliptic equations," *Soviet*

Math. Dokl. 20, p. 129, 1979.

[59] Rozvany, G. I. N.; Ong, T. G.; Szeto, W. T.; Sandler, R.; Olhoff, N.; and Bendsoe, M. P., "Least-weight design of perforated elastic plates I,II," *Int. J. Solids Struct. 23*, pp. 521 and 537, 1987.

[60] Sanchez-Palencia, E., *Non-homogeneous Media and Vibration Theory*, Lecture Notes in Physics 127, Springer-Verlag, 1980.

[61] Schulgasser, K., "Relationship between single-crystal and polycrystal electrical conductivity," *J. Appl. Phys. 47*, p. 1880, 1976.

[62] Spagnolo, S., "Convergence in energy for elliptic operators," in *Numerical Solution of Partial Differential Equations III Synspade* 1975, B. Hubbard. ed., Academic Press, 1976.

[63] Strang, G. and Kohn, R. V., "Optimal design of a two-way conductor," in *Non-Smooth Mechanics*, P. D. Panagiotopoulos, et al., eds., Birkhauser, 1988.

[64] Suquet, P., "Une méthode duale en homogénéisation: application aux milieux élastiques." *J. Mech. Theor. Appl.*, special issue, p. 79, 1982.

[65] Tartar, L., Cours Peccot, Collège de France, 1977.

[66] Tartar, L., Estimations fines des coefficients homogénéisés," in *Ennio de Giorgi's Colloquium*, P. Krée, ed., Pitman, p. 168, 1985.

[67] Tartar, L., "The appearance of oscillations in optimization problems," in *Non-Classical Continuum Mechancis*, R. J. Knops and A. A. Lacey, eds., Cambridge Univ. Press, p. 129, 1987.

[68] Willis, J. R., "Variational and related methods for the overall properties of composite materials," in C. S. Yih, ed., *Advances in Applied Mechanics*, 21, p. 2, 1981.

[69] Willis, J. R., "Elasticity theory of composites," in *Mechanics of Solids*, H. G. Hopkins and M. J. Sewell, eds., Pergamon, p. 653, 1982.

[70] Yurinskii, V. V., "Average of an elliptic boundary value problem with random coefficients." *Siberian Math. J. 21*, p. 470, 1980.

[71] Zhikov, V. V., Kozlov, S. M., Oleinik, O.A., and Ngoan, K. T., "Averaging and G-convergence of differential operators," *Russian Math. Surveys 34*, p. 69, 1979.

[72] Watt, P. J., "The elastic properties of composite materials," Rev.Geophys. and Space Phys. 14, p. 541, 1976.

[73] Hashin, Z., "The elastic moduli of heterogeneous materials," ASME J. Appl. Mech. 29, p. 143, 1962.

[74] Berryman, J. G., "Long wavelength propagation in composite elastic mmedia I. II." J. Acoust. Soc. Amer. 68, p. 1809, 1980.

[75] Elliott, R. J., Krumhansl, J. A., and Leath, P. L., "The theory and properties of randomly disordered crystals and related physical systems," Rev. Mod. Phys. 46, p. 465, 1974.

Wave Propagation in Layered Elastic Media

Rouben Rostamian
Department of Mathematics
University of Naryland Baltimore County
Baltimore, MD 21228

In a joint work with William Hager we have studied propagation of plane waves in layered, linearly elastic media. An elastic material is *layered* if its properties depend only on one coordinate of a Cartesian coordinate system. Consider an elastic body consisting of a homogeneous half-space attached to a layered half-space, and a plane wave traveling in the homogenrous half-space and obliquely impinging onto the layered interface. We compute the strengths of the resulting reflected and refracted waves. As a special case, we consider the situation where a layered elastic slab is sandwiched between two homogeneous half-spaces. An important problem in submarine technology is to determine the mechanical properties of the sandwiched layer to minimize the strength of the reflected waves. We will describe our results in the isotropic case and outline our ongoing research for the anisotropic case. This leads to some interesting problems in homogenization and optimization which will be discussed here and in W. Hager's talk.

Wave Propagation in Anisotropic Elastic Media *

William W. Hager
Department of Mathematics
University of Florida, Gainesville
Gainesville, FL 3261

Rouben Rostamian
Department of Mathematics
University of Maryland Baltimore County
Baltimore, MD 21228

1. Introduction

In this paper we describe a generalization to anisotropic materials of our theory [3] of analysis of reflection and refraction of obliquely incident, plane, time-harmonic waves in stratified elastic media. Specifically, we address the following questions: What is the fraction of energy that is reflected from a stratified slab sandwiched between two homogeneous half-spaces? What is the fraction of energy transmitted through the slab? By a stratified medium, we mean a generally anisotropic, linearly elastic material whose mechanical properties vary in only one direction in an arbitrarily prescribed way. The ability to handle general stratifications is an important feature of our approach. Furthermore, in the optimal design of coatings, cf. [3], this generality is essential.

To determine the reflection and transmission tensors for a stratified slab, we introduce the concept of *impedance tensor* which contains information about the local mechanical properties of the medium and wave propagation directions. An overall impedance tensor is then obtained for a stratified slab by integrating a Riccati equation across the thickness of the slab; the local impedance tensor enters into the coefficients of the Riccati equation. The reflection and transmission tensors of a stratified slab then can be expressed in terms of its global impedance tensor.

The specific application that motivated our formulation for the reflectivity and the transmissivity concerns the design of an optimal coating that minimizes reflected

*Research supported by grants from NSF, ONR and ARO

energy from a surface for waves in some frequency band. The optimization is subject to design constraints such as upper and lower bounds for the Lamé moduli in the isotropic case, for the dissipation coefficient, and for the density within the coating; however, the dependence of mechanical properties on the depth in the coating is not specified a priori. In order to implement gradient-based optimization algorithms, we need a formula for the gradient of the reflectivity with respect to parameters describing the coating. It turns out (see [2]) that i) these gradients can be expressed compactly in terms of the impedances, ii) the optimal mechanical properties have a bang-bang structure over part of the coating while they vary continuously over the remaining part of the coating, and (iii) if we focus on waves of a specific frequency (rather than a frequency band), then the optimal coating is completely bang-bang. (By a bang-bang structure, we mean that the coating is composed of homogeneous layers, and in each layer the mechanical properties are either at the upper bound or at the lower bound.) The bang-bang structure for the optimal coating can be deduced from the minimum principle of control theory and the way the mechanical properties enter in the Riccati equation.

2. Notation

$\mathcal{E}$ denotes the three-dimensional euclidean space (set of points) and $\mathcal{V}$ is the associated vector space. We topologize $\mathcal{V}$ by the usual dot product. A second order tensor is a linear mapping of $\mathcal{V}$ into $\mathcal{V}$; $\mathcal{L}$ denotes the linear space of the second order tensors. We topologize $\mathcal{L}$ by using the inner product $\mathbf{E} \cdot \mathbf{F} \stackrel{\text{def}}{=} \text{tr}(\mathbf{E}^T\mathbf{F})$, where 'tr' denotes the trace and the superscript T denotes the transpose (same as adjoint.) We use $\| \ \|$ do denote norms both on $\mathcal{V}$ and $\mathcal{L}$. The tensor product $\mathbf{a} \otimes \mathbf{b}$ of two elements $\mathbf{a}$ and $\mathbf{b}$ of $\mathcal{V}$ is the second order tensor that assigns to each vector $\mathbf{u} \in \mathcal{V}$ the vector $(\mathbf{b} \cdot \mathbf{u})\mathbf{a}$:

$$(\mathbf{a} \otimes \mathbf{b})(\mathbf{u}) = (\mathbf{b} \cdot \mathbf{u})\mathbf{a} \qquad \forall \mathbf{u} \in \mathcal{V}.$$

The inner product induces a natural orthogonal decomposition $\mathcal{S} \oplus \mathcal{K}$ of the $\mathcal{L}$ where $\mathcal{S}$ and $\mathcal{K}$ are, respectively, the linear spaces of symmetric and skew-symmetric second order tensors.

The (fourth order) elasticity tensor at each point $\mathbf{x}$ of an elastic body $\mathcal{B} \subset \mathcal{E}$ is a linear operator $\mathsf{C} : \mathcal{V} \to \mathcal{V}$ satisfying the following hypotheses:

1. C is self-adjoint
2. $\ker \mathsf{C} = \mathcal{K}$
3. C is strongly elliptic, i.e., there exists a positive constant α such that

$$\mathbf{U} \cdot \mathsf{C}_{\mathbf{x}}[\mathbf{U}] \geq \alpha \|\mathbf{U}\|^2$$

for all $\mathbf{x} \in \mathcal{E}$ and all rank-one second order tensors $\mathbf{U}$ in $\mathcal{S}$.

Note that $\mathbf{U} \in \mathcal{S}$ is of rank-one if and only if $\mathbf{U} = \mathbf{u}_1 \otimes \mathbf{u}_2$ for some $\mathbf{u}_1$ and $\mathbf{u}_2$ in $\mathcal{V}$.

When necessary, we explicitly indicate the dependence of C on $\mathbf{x}$ by writing $\mathsf{C}_\mathbf{x}$ or as $\mathsf{C}(\mathbf{x})$. We assume throughout that C is bounded and measurable as a function of $\mathbf{x}$. The equation of motion of a linearly elastic material $\mathcal{B}$ is

$$\rho\ddot{\mathbf{v}} = \operatorname{div} \mathsf{C}[\nabla \mathbf{v}] \tag{2.1}$$

where $\mathbf{v} = \mathbf{v}(\mathbf{x}, t)$ is is the (infinitesimal) displacement at time t and at point $\mathbf{x}$, ρ is the mass density, and superimposed dots denote time derivatives. In general, ρ and C are functions of $\mathbf{x}$. Subsets of $\mathcal{B}$ where C and ρ are independent of $\mathbf{x}$ are said to be *homogeneous*.

Consider a homogeneous elastic material that occupies the entire space $\mathcal{E}$. A *plane wave* is a motion of the form

$$\mathbf{v}(\mathbf{x}, t) = \mathbf{a} f(t - \mathbf{x} \cdot \mathbf{p}/c) \tag{2.2}$$

that satisfies the equation of motion (2.1). Here $\mathbf{a}$ is the *amplitude vector*, $\mathbf{p}$ is the *propagation direction vector*, and if $\mathbf{p}$ is of unit length, then c is the speed of propagation. The function f is the *wave profile*. Substitution of equation (2.2) in the equation of motion (2.1) implies that

$$\rho\mathbf{a} = \frac{1}{c^2}\mathsf{C}[\mathbf{a} \otimes \mathbf{p}]\mathbf{p}. \tag{2.3}$$

The *acoustic tensor* is a function $\mathbf{A} : \mathcal{E} \to \mathcal{L}$ defined by

$$\mathbf{A}(\mathbf{p})\mathbf{a} = \frac{1}{\rho}\mathsf{C}[\mathbf{a} \otimes \mathbf{p}]\mathbf{p}, \qquad \mathbf{a} \in \mathcal{E}. \tag{2.4}$$

Thus we may write (2.3)as an eigenvalue problem:

$$\mathbf{A}(\mathbf{p})\mathbf{a} = c^2\mathbf{a}. \tag{2.5}$$

Proposition 1 (Cf. Gurtin[1]) *Assume that the hypotheses on the elasticity tensor* C *stated above hold. Then for any nonzero vector* $\mathbf{p} \in \mathcal{E}$, *the second order tensor* $\mathbf{A}(\mathbf{p})$ *is symmetric and positive-definite.*

The formula (2.2) describes a plane wave if and only if the parameters $\mathbf{a}$, $\mathbf{p}$, and c satisfy the eigenvalue problem (2.5). In any direction given by a unit vector $\mathbf{p}$, the symmetric and positive-definite matrix $\mathbf{A}(\mathbf{p})$ has three real, positive eigenvalues c_1^2, c_2^2, c_3^2 and a corresponding orthonormal set of eigenvectors $\{\mathbf{a}_1, \mathbf{a}_2, \mathbf{a}_3\}$. Order the eigenvalues such that $c_1 \leq c_2 \leq c_3$, and set $\mathbf{p}_i(\mathbf{p}) := \mathbf{p}/c_i$ for $i = 1, 2, 3$. Equation (2.5) then implies that

$$\mathbf{A}(\mathbf{p}_i)\mathbf{a}_i = \mathbf{a}_i, \qquad i = 1, 2, 3. \tag{2.6}$$

Definition 1 The three surfaces

$$S_i = \{\mathbf{x} \in \mathcal{E} : \mathbf{x} = 0 + \mathbf{p}_i(\mathbf{p}), \quad |\mathbf{p}| = 1\} \qquad i = 1, 2, 3$$

are called the *descriptor surfaces* for the elastic material with the elasticity tensor $\mathbf{C}$.

Here, and in what follows we denote the arbitrarily fixed origin in $\mathcal{E}$ by 0. Note that since $\mathbf{A}$ is quadratic in $\mathbf{p}$ then each S_i is symmetric with respect to 0.

Observation 1 A vector $\mathbf{r} \in \mathcal{V}$ such that $0 + \mathbf{r}$ is in one of descriptor surfaces determines a plane wave that propagates in the direction of $\mathbf{r}$ at speed $1/|\mathbf{r}|$, and an amplitude vector $\mathbf{a}$ such that, by (2.6), $\mathbf{A}(\mathbf{r})\mathbf{a} = \mathbf{a}$.

Example 1: The elasticity tensor for isotropic material has the following simple representation in cartesian coordinates:

$$C_{ijkl} = \mu(\delta_{ik}\delta_{jl} + \delta_{il}\delta_{jk}) + \lambda\delta_{ij}\delta_{kl}.$$

where μ and λ are the Lamé moduli. It may be shown that $\mathbf{C}$ is strongly elliptic if and only if $\mu > 0$ and $2\mu + \lambda > 0$. It follows that

$$\mathbf{A}(\mathbf{p}) = \frac{\mu}{\rho}|\mathbf{p}|^2\mathbf{I} + \frac{\mu + \lambda}{\rho}\mathbf{p} \otimes \mathbf{p}$$

where $\mathbf{I}$ is the identity in $\mathcal{L}$. We thus have

$$\det\left(\mathbf{A}(\mathbf{p}) - c^2\mathbf{I}\right) = (\frac{\mu}{\rho}|\mathbf{p}|^2 - c^2)^2\Big[(\frac{2\mu + \lambda}{\rho}|\mathbf{p}|^2 - c^2\Big],$$

whence, with $|\mathbf{p}| = 1$ we get

$$c_1 = c_2 = \sqrt{\frac{\mu}{\rho}} \qquad c_3 = \sqrt{\frac{2\mu + \lambda}{\rho}}.$$

Moreover, $\mathbf{a}_3 = \mathbf{p}$, and the eigenvectors $\mathbf{a}_1$ and $\mathbf{a}_2$ may be taken as any orthonormal pair of vectors in the orthogonal complement of span of $\mathbf{p}$. The lengths of the vectors $\mathbf{p}_i = \mathbf{p}/c_i$ of Definition 1 in this case are fixed and are independent of the vector $\mathbf{p}$. The descriptor surfaces S_i therefore are spheres:

$$S_1 = S_2 = \{\mathbf{x} \in \mathcal{E} : \mathbf{x} = 0 + \mathbf{r}, |\mathbf{r}| = \frac{\rho}{\mu}\},$$

$$S_3 = \{\mathbf{x} \in \mathcal{E} : \mathbf{x} = 0 + \mathbf{r}, |\mathbf{r}| = \frac{\rho}{2\mu + \lambda}\}.$$

Example 2: The elasticity tensor of an originally isotropic material with added reinforcing fibers running along the direction of a unit vector $\mathbf{h}$ is

$$C_{ijkl} = \mu(\delta_{ik}\delta_{jl} + \delta_{il}\delta_{jk}) + \lambda\delta_{ij}\delta_{kl} + \kappa h_i h_j h_k h_l$$

where the constant κ measures the tensile strength of the reinforcement. It follows that

$$\mathbf{A}(\mathbf{p}) = \frac{\mu}{\rho}|\mathbf{p}|^2\mathbf{I} + \frac{\mu+\lambda}{\rho}\mathbf{p}\otimes\mathbf{p} + \frac{\kappa}{\rho}(\mathbf{p}\cdot\mathbf{h})^2\mathbf{h}\otimes\mathbf{h}.$$

A representative set of descriptor surfaces for this material is shown in the figure at the end of this paper.

3. Wave propagation in a homogeneous half-space

Consider a homogeneous elastic half-space $\mathcal{B}$ with boundary $\partial\mathcal{B}$, elasticity tensor $\mathbf{C}$ satisfying the hypotheses of Section 2. Let n denote the unit external normal at $\partial\mathcal{B}$. Consider a plane wave in the form

$$\mathbf{v}(\mathbf{x},t) = \alpha\mathbf{a}f(t - \mathbf{x}\cdot\hat{\mathbf{p}})$$

for some propagation vector $\hat{\mathbf{p}}$ in one of the descriptor surfaces S_i for the material. We assume that $\mathbf{p}\cdot\mathbf{n} > 0$; this may be interpreted as asserting that the wave is 'coming from infinity.' The unit vector $\mathbf{a}$ is determined from (2.6) (see also Observation 1), and α is a scalar coefficient. The line $L : 0 + \hat{\mathbf{p}} + k\,\mathbf{n}$, $k \in (-\infty,\infty)$, intersects the descriptor surfaces S_1, S_2, S_3 in a total of six points in general, one of which is $0 + \hat{\mathbf{p}}$ corresponding to $k = 0$. Denote these points, in the order of increasing k, by $\mathbf{r}_3, \mathbf{r}_2, \mathbf{r}_1, \mathbf{p}_1, \mathbf{p}_2, \mathbf{p}_3$. The assumption $\mathbf{p}\cdot\mathbf{n} > 0$ implies that $\hat{\mathbf{p}} \in \{\mathbf{p}_1, \mathbf{p}_2, \mathbf{p}_3\}$. The letter $\mathbf{r}$ is chosen as a mnemonic for reflection as we will show that the reflected waves generated by the incident wave $\hat{\mathbf{p}}$ propagate in the directions of the vectors $\mathbf{r}_1, \mathbf{r}_2, \mathbf{r}_3$. In fact, any one of the three incident wave of the type

$$\mathbf{v}(\mathbf{x},t) = \alpha_i\mathbf{a}_i f(t - \mathbf{x}\cdot\mathbf{p}_i)$$

gives rise to a combination of reflected waves in all three directions $\mathbf{r}_1, \mathbf{r}_2, \mathbf{r}_3$. Extending an idea in our previous work[3] we thus look at a slightly more general problem, where instead of one incident wave in the direction $\mathbf{p}_i$ we have three simultaneous incident waves in directions $\mathbf{p}_1$, $\mathbf{p}_2$, $\mathbf{p}_3$.

Definition 2 A *wave ensemble* is a superposition of three plane waves of the form

$$\mathbf{v}(\mathbf{x},t) = \sum_{i=1}^{3}\alpha_i\mathbf{a}_i f(t - \mathbf{x}\cdot\mathbf{p}_i), \tag{3.1}$$

where for $i = 1, 2, 3$

1. the vectors $\mathbf{p}_i$ are in the descriptor surfaces S_i
2. $\mathbf{p}_i \cdot \mathbf{n} > 0$ for all i or $\mathbf{p}_i \cdot \mathbf{n} < 0$ for all i
3. $\mathbf{a}_i$ are unit vectors and (2.6) holds
4. For $j \neq i$, $\mathbf{p}_j - \mathbf{p}_i$ is parallel to $\mathbf{n}$

The incident wave ensemble (3.1) upon interaction with the boundary $\partial\mathcal{B}$ gives rise to the reflected wave ensemble

$$\mathbf{v}(\mathbf{x}, t) = \sum_{i=1}^{3} \beta_i \mathbf{b}_i f(t - \mathbf{x} \cdot \mathbf{r}_i). \tag{3.2}$$

When $\mathbf{x} \in \partial\mathcal{B}$ the arguments of f in (3.1) and (3.2) by their construction are identical. The motion generated at the boundary by (3.1) is proportional to $\mathbf{a} \stackrel{\text{def}}{=} \sum_{i=1}^{3} \alpha_i \mathbf{a}_i$ and the motion generated by (3.2) is proportional to $\mathbf{b} \stackrel{\text{def}}{=} \sum_{i=1}^{3} \beta_i \mathbf{b}_i$. We now proceed to define the concept of the *impedance tensor* which plays a central role in the remainder this paper.

The traction at the boundary of the half-space due to the wave (3.1) is $\mathbf{Sn}$, where the stress $\mathbf{S}$ is given by $\mathsf{C}[\nabla \mathbf{v}]$:

$$\text{traction} = \mathbf{Sn} = \mathsf{C}[\nabla \mathbf{v}]\mathbf{n} = -\sum_{i=1}^{3} \alpha_i \mathsf{C}[\mathbf{a}_i \otimes \mathbf{p}_i]\mathbf{n} f'. \tag{3.3}$$

Fix an arbitrary set of cartesian coordinates and temporarily (with an abuse of notation) let us use $\mathbf{a}_i$ to denote the representation of $\mathbf{a}_i$ as a 3×1 matrix. Define the 3×3 matrix

$$\mathsf{A} = \begin{bmatrix} \mathbf{a}_1 & \vdots & \mathbf{a}_2 & \vdots & \mathbf{a}_3 \end{bmatrix} \tag{3.4}$$

and the 3×1 matrix

$$\mathsf{B} = \begin{bmatrix} \mathsf{C}[\mathbf{a}_1 \otimes \mathbf{p}_1]\mathbf{n} & \vdots & \mathsf{C}[\mathbf{a}_2 \otimes \mathbf{p}_2]\mathbf{n} & \vdots & \mathsf{C}[\mathbf{a}_3 \otimes \mathbf{p}_3]\mathbf{n} \end{bmatrix} \tag{3.5}$$

and let

$$\mathbf{H} = \mathsf{B}\mathsf{A}^{-1}. \tag{3.6}$$

It may be verified that $\mathbf{H}$ is represents a second order tensor which is independent of the choice of coordinates. We now state a definition in a somewhat more general context.

Definition 3 *Let the triple of vectors $\mathbf{p}_i$, $i = 1, 2, 3$, be such that $\mathbf{0} + \mathbf{p}_i \in S_i$ for each i, where S_i are the descriptor surfaces of an elastic material. Let the unit vectors $\mathbf{a}_i$ be the solutions of the equation (2.6). With an arbitrary unit vector $\mathbf{n}$ construct the matrices A and B as in (3.4) and (3.5), and the tensor $\mathbf{H}$ as in (3.6). We call $\mathbf{H}$ the* ***impedance tensor*** *of the elastic material with respect to the the incident wave system $\{(\mathbf{p}_i, \mathbf{a}_i)\}_{i=1}^{3}$ and the normal vector $\mathbf{n}$.*

Recalling the notation $\mathbf{a} = \sum_{i=1}^{3} \alpha_i \mathbf{a}_i$ we may write

$$\mathbf{a} = \mathsf{A} \begin{pmatrix} \alpha_1 \\ \alpha_2 \\ \alpha_3 \end{pmatrix} \qquad \text{or, equivalently} \qquad \begin{pmatrix} \alpha_1 \\ \alpha_2 \\ \alpha_3 \end{pmatrix} = \mathsf{A}^{-1}\mathbf{a}. \tag{3.7}$$

Therefore we rewrite (3.3) as

$$\text{traction} = \mathbf{Sn} = -\mathsf{B} \begin{pmatrix} \alpha_1 \\ \alpha_2 \\ \alpha_3 \end{pmatrix} f' = -\mathsf{B}\mathsf{A}^{-1}\mathbf{a}f' = -\mathbf{H}\mathbf{a}f'. \tag{3.8}$$

4. Reflection at the interface of two homogeneous half-spaces

Consider two homogeneous elastic half-spaces, $\mathcal{B}_1$ and $\mathcal{B}_2$, with a common boundary $\mathcal{I}$, and unit external normal vectors $\mathbf{n}_1$ and $\mathbf{n}_2$ at their respective boundaries. Assume that no slippage occurs at the boundary, and that the elasticity tensors C_1 and C_2 each satisfy the hypotheses of Section 2.

Consider an ensemble (cf. Definition 2) of the form

$$\mathbf{v}^{(inc)}(\mathbf{x}, t) = \sum_{i=1}^{3} \alpha_i \mathbf{a}_i f(t - \mathbf{x} \cdot \mathbf{p}_i), \tag{4.1}$$

representing a triple of plane waves traveling in $\mathcal{B}_1$. Assume that $\mathbf{p}_i \cdot \mathbf{n}_1 > 0$, that is the waves are originated at infinity. Let the ensemble

$$\mathbf{v}^{(refl)}(\mathbf{x}, t) = \sum_{i=1}^{3} \beta_i \mathbf{b}_i f(t - \mathbf{x} \cdot \mathbf{r}_i) \tag{4.2}$$

represent the resulting reflected wave system as constructed in Section 2. We wish to compute the amplitude coefficients β_i in terms of α_i. The success of the computation will implicitly validate the form (4.2) that we have adopted for representing the reflected waves. The intensity of the reflected waves in $\mathcal{B}_1$ of course depend on the properties of the adjoining half-space $\mathcal{B}_2$. We now proceed to describe the wave pattern in $\mathcal{B}_2$.

The starting point of construction of the ensembles involved in (4.1) and (4.2) is the construction of the line $L_1 : 0 + \mathbf{p}_i + k\,\mathbf{n}_1$, as described in the beginning of Section 3. The choice of index i is immaterial, since by part 4 of Definition 2 all such lines will coincide. The next stage of the construction of the ensemble involves the descriptor surfaces which depend on material properties. Thus the properties of the half-space $\mathcal{B}_1$ are implicitly involved in the representation (4.1) and (4.2).

Consider now the line $L_2 : 0 + \mathbf{p}_i + k\,\mathbf{n}_2$ which coincides (for any i) with the line L_1 except that the parameter k orients it in the opposite direction. This line intersects the descriptor surfaces of the elastic material $\mathcal{B}_2$ in six points which we label, in the increasing direction of k, with $\mathbf{t}_3, \mathbf{t}_2, \mathbf{t}_1, \mathbf{s}_1, \mathbf{s}_2, \mathbf{s}_3$. The vectors $\mathbf{t}_i$, $i = 1, 2, 3$ are the directions of the transmitted (i.e. refracted) waves. The transmitted wave in the half-space $\mathcal{B}_2$ then has the following representation:

$$\mathbf{v}^{(trans)}(\mathbf{x}, t) = \sum_{i=1}^{3} \gamma_i \mathbf{c}_i f(t - \mathbf{x} \cdot \mathbf{t}_i) \tag{4.3}$$

The unknown amplitude factors β_i and γ_i are determined by equating the displacements and by balancing the tractions at the interface. The equality of displacements $\mathbf{v}^{(inc)} + \mathbf{v}^{(refl)} = \mathbf{v}^{(trans)}$ at the interface immediately gives

$$\sum_{i=1}^{n} \alpha_i \mathbf{a}_i + \sum_{i=1}^{n} \beta_i \mathbf{b}_i = \sum_{i=1}^{n} \gamma_i \mathbf{c}_i$$

which, with the notation

$$\mathbf{a} = \sum_{i=1}^{n} \alpha_i \mathbf{a}_i \qquad \mathbf{b} = \sum_{i=1}^{n} \beta_i \mathbf{b}_i \qquad \mathbf{c} = \sum_{i=1}^{n} \gamma_i \mathbf{c}_i \tag{4.4}$$

reduces to

$$\mathbf{a} + \mathbf{b} = \mathbf{c}. \tag{4.5}$$

To match the tractions, we use the expression in terms of impedances (3.8) in Section 3. We need to distinguish, however, three impedances, based on three different sets of parameters, as follows.

The impedance $\mathbf{H}_1$, based on the elasticity tensor C_1, the incident wave descriptors $\{(\mathbf{p}_i, \mathbf{a}_i)\}_{i=1}^{3}$, and the normal vector $\mathbf{n}_1$.

The impedance $\dot{\mathbf{H}}_1$, based on the elasticity tensor C_1, the reflected wave descriptors $\{(\mathbf{r}_i, \mathbf{b}_i)\}_{i=1}^{3}$, and the normal vector $\mathbf{n}_1$.

The impedance $\dot{\mathbf{H}}_2$, based on the elasticity tensor C_2, the transmitted wave descriptors $\{(\mathbf{t}_i, \mathbf{c}_i)\}_{i=1}^{3}$, and the normal vector $\mathbf{n}_2$.

Then, according (3.8) the tractions measured in terms of external vectors at the interface of the two half-spaces are given by

$$-\mathbf{H}_1 \mathbf{a} f' - \dot{\mathbf{H}}_1 \mathbf{b} f' \quad \text{on } \mathcal{B}_1 \qquad \text{and} \qquad -\dot{\mathbf{H}}_2 \mathbf{c} f' \quad \text{on } \mathcal{B}_1,$$

whence

$$\mathbf{H}_1 \mathbf{a} + \dot{\mathbf{H}}_1 \mathbf{b} + \dot{\mathbf{H}}_2 \mathbf{c} = 0. \tag{4.6}$$

Solving equations (4.5) and (4.6) for $\mathbf{b}$ and $\mathbf{c}$ we get

$$\mathbf{b} = \mathbf{R}\mathbf{a}, \qquad \mathbf{c} = \mathbf{T}\mathbf{a},$$

where

$$\mathbf{R} = -(\hat{\mathbf{H}}_1 + \hat{\mathbf{H}}_2)^{-1}(\mathbf{H}_1 + \hat{\mathbf{H}}_2), \qquad \mathbf{T} = -(\hat{\mathbf{H}}_1 + \hat{\mathbf{H}}_2)^{-1}(\mathbf{H}_1 - \hat{\mathbf{H}}_1). \tag{4.7}$$

We refer to $\mathbf{R}$ and $\mathbf{T}$ as the *reflection and transmission tensors at the interface*.

Using these values for $\mathbf{b}$ and $\mathbf{c}$, the coefficients β_i and γ_i of the reflected and refracted waves (4.2), (4.3) then may be computed from (4.4) as in (3.7).

5. Layered media

In Section 3 we introduced the concept of impedance for a homogeneous elastic half-space and used it in Section 4 to compute the reflectivity of the interface of two homogeneous half-spaces. In this section we extend the definition of impedance to layered media and then use it to compute the reflectivity of the interface of two half-spaces, one of which is homogeneous and the other is layered. For technical reasons we restrict our attention to steady-state sinusoidal waves. As in [3], we approach the problem via invariant imbedding. This is done in two steps:

Step 1: Solve the auxiliary problem of computing reflectivities in the case of a homogeneous slab sandwiched between a homogeneous half-space and a layered half-space.
Step 2: Compute limits as the thickness of the slab in Step 1 approaches zero.

This leads to the concept of localized impedance and a differential equation satisfied by it.

5.1. The auxiliary problem

Consider a homogeneous slab $\mathcal{B}_2$ of thickness τ interposed between a a homogeneous half-space $\mathcal{B}_1$ and a stratified half-space $\mathcal{B}_3$. We denote the variables associated with the homogeneous half-space, the homogeneous slab, and the stratified half-space by indices 1, 2. and 3, respectively. We denote the interface of $\mathcal{B}_1$ and $\mathcal{B}_2$ by $\mathcal{I}_{12}$, the interface of $\mathcal{B}_2$ and $\mathcal{B}_3$ by $\mathcal{I}_{23}$, the unit external normals to the boundaries of $\mathcal{B}_1$ and $\mathcal{B}_3$ by $\mathbf{n}_1$ and $\mathbf{n}_3$, and the unit external normals at the boundaries $\mathcal{I}_{ij}$ of $\mathcal{B}_2$ by $\mathbf{n}_{ij}$. We assume that the origin $\mathbf{0}$ of $\mathcal{E}$ is contained in $\mathcal{I}_{23}$. The reflectivity of the interface $\mathcal{I}_{12}$ with respect to waves impinging from the $\mathcal{B}_1$-side depends on the thickness τ of the slab and is denoted by $\mathbf{R}(\tau)$. The reflectivity of the interface $\mathcal{I}_{23}$ with respect to waves impinging from the $\mathcal{B}_2$-side will be denoted by $\mathbf{R}_0$. Note that $\mathbf{R}_0$ does not equal $\mathbf{R}(0)$ in general since these represent reflectivities of the boundary of $\mathcal{B}_3$ with respect to waves traveling in two deferent media $\mathcal{B}_1$ and $\mathcal{B}_2$. Our objective in this subsection is to compute $\mathbf{R}(\tau)$ in terms of $\mathbf{R}_0$.

As in Section 4 consider the ensemble

$$\mathbf{v}^{(inc)}(\mathbf{x},t) = \sum_{k=1}^{3} \alpha_k \mathbf{a}_k \exp[i\omega(t - (\mathbf{x} - \tau\mathbf{n}_3)\cdot\mathbf{p}_k)] \tag{5.1}$$

which travels in $\mathcal{B}_1$ such that $\mathbf{p}_k \cdot \mathbf{n}_1 > 0$ for $k = 1,2,3$. This represents a triple of plane, steady-state, sinusoidal incident waves. Let the ensemble

$$\mathbf{v}^{(refl)}(\mathbf{x},t) = \sum_{k=1}^{3} \beta_k \mathbf{b}_k \exp[i\omega(t - (\mathbf{x} - \tau\mathbf{n}_3)\cdot\mathbf{r}_k)] \tag{5.2}$$

represent the resulting reflected ensemble in $\mathcal{B}_1$.

In $\mathcal{B}_2$ we construct the propagation vectors $\mathbf{t}_3, \mathbf{t}_2, \mathbf{t}_1, \mathbf{s}_1, \mathbf{s}_2, \mathbf{s}_3$ as in Section 4 and the ensembles corresponding to them:

$$\mathbf{v}^{(aux_1)}(\mathbf{x},t) = \sum_{k=1}^{3} \gamma_k \mathbf{c}_k \exp[i\omega(t - (\mathbf{x} - \tau\mathbf{n}_3)\cdot\mathbf{t}_k)] \tag{5.3}$$

$$\mathbf{v}^{(aux_2)}(\mathbf{x},t) = \sum_{k=1}^{3} \delta_k \mathbf{d}_k \exp[i\omega(t - (\mathbf{x} - \tau\mathbf{n}_3)\cdot\mathbf{s}_k)]. \tag{5.4}$$

Figuratively, (5.3) and (5.3) represent the resultant of the reverberation set up in $\mathcal{B}_2$ by the incident wave system.

In what follows we will use the following notation:

$$\mathbf{a} = \sum_{k=1}^{3} \alpha_k \mathbf{a}_k \qquad \mathbf{b} = \sum_{k=1}^{3} \beta_k \mathbf{b}_k \qquad \mathbf{c} = \sum_{k=1}^{3} \gamma_k \mathbf{c}_k \qquad \mathbf{d} = \sum_{k=1}^{3} \delta_k \mathbf{d}_k$$

$$\mathbf{c}_0 = \sum_{k=1}^{3} \gamma_k \mathbf{c}_k \exp[i\omega\tau\mathbf{n}_3\cdot\mathbf{t}_k)] \qquad \mathbf{d}_0 = \sum_{k=1}^{3} \delta_k \mathbf{d}_k \exp[i\omega\tau\mathbf{n}_3\cdot\mathbf{s}_k)].$$

Furthermore, temporarily fix a cartesian coordinate system and construct the matrices

$$\mathsf{C} = [\ \mathbf{c}_1 \ \vdots\ \mathbf{c}_2 \ \vdots\ \mathbf{c}_3\ ] \qquad \mathsf{D} = [\ \mathbf{d}_1 \ \vdots\ \mathbf{d}_2 \ \vdots\ \mathbf{d}_3\ ]$$

and set

$$\mathbf{C}(\tau) = \mathsf{C}\ \mathrm{diag}[\exp(-i\omega\tau\mathbf{n}_3\cdot\mathbf{t}_1),\ \exp(-i\omega\tau\mathbf{n}_3\cdot\mathbf{t}_2),\ \exp(-i\omega\tau\mathbf{n}_3\cdot\mathbf{t}_3)]\ \mathsf{C}^{-1} \tag{5.5}$$

$$\mathbf{D}(\tau) = \mathsf{D}\ \mathrm{diag}[\exp(-i\omega\tau\mathbf{n}_3\cdot\mathbf{s}_1),\ \exp(-i\omega\tau\mathbf{n}_3\cdot\mathbf{s}_2),\ \exp(-i\omega\tau\mathbf{n}_3\cdot\mathbf{s}_3)]\ \mathsf{D}^{-1} \tag{5.6}$$

where diag$\{\ \}$ denotes the diagonal matrix of the given elements. It is readily seen that $\mathbf{C}(\tau)$ and $\mathbf{D}(\tau)$ are tensors hence independent of the specific choice of coordinates. The vectors $\mathbf{c}, \mathbf{c}_0, \mathbf{d}, \mathbf{d}_0$ are related by

$$\mathbf{c}_0 = \mathbf{C}(\tau)\mathbf{c} \qquad \mathbf{d}_0 = \mathbf{D}(\tau)\mathbf{d}. \tag{5.7}$$

The reflectivities $\mathbf{R}_0$ and $\mathbf{R}(\tau)$ then satisfy the relations

$$\mathbf{d}_0 = \mathbf{R}_0\mathbf{c}_0 \tag{5.8}$$

and

$$\mathbf{b} = \mathbf{R}(\tau)\mathbf{a}. \tag{5.9}$$

The continuity of the displacement at the interface $\mathbf{I}_{12}$ is expressed:

$$\mathbf{a} + \mathbf{b} = \mathbf{c} + \mathbf{d}. \tag{5.10}$$

To express the balance of traction at $\mathcal{I}_{12}$ we introduce the following four impedances:

- The impedance $\mathbf{H}_1$, based on the elasticity tensor C_1, the incident wave descriptors $\{(\mathbf{p}_k, \mathbf{a}_k)\}_{k=1}^3$, and the normal vector $\mathbf{n}_1$.
- The impedance $\dot{\mathbf{H}}_1$, based on the elasticity tensor C_1, the reflected wave descriptors $\{(\mathbf{r}_k, \mathbf{b}_k)\}_{k=1}^3$, and the normal vector $\mathbf{n}_1$.
- The impedance $\dot{\mathbf{H}}_2$, based on the elasticity tensor C_2, the transmitted wave descriptors $\{(\mathbf{t}_k, \mathbf{c}_k)\}_{k=1}^3$, and the normal vector $\mathbf{n}_{12}$.
- The impedance $\mathbf{H}_2$, based on the elasticity tensor C_2, the transmitted wave descriptors $\{(\mathbf{s}_k, \mathbf{d}_k)\}_{k=1}^3$, and the normal vector $\mathbf{n}_{12}$.

Then, using (3.8), we compute and equate the traction vectors at the interface $\mathcal{I}_{23}$ and obtain:

$$\mathbf{H}_1\mathbf{a} + \dot{\mathbf{H}}_1\mathbf{b} + \dot{\mathbf{H}}_2\mathbf{c} + \mathbf{H}_2\mathbf{d} = \mathbf{0}. \tag{5.11}$$

We may solve (5.7), (5.8), (5.10), (5.11) as a system of five equations in five unknowns $\mathbf{b}, \mathbf{c}, \mathbf{d}, \mathbf{c}_0, \mathbf{d}_0$. In particular we obtain

$$[\dot{\mathbf{H}}_1 + \mathbf{G}(\tau)]\mathbf{b} = -[\mathbf{H}_1 + \mathbf{G}(\tau)]\mathbf{a}, \tag{5.12}$$

where we have let

$$\mathbf{G}(\tau) = \left(\dot{\mathbf{H}}_2 + \mathbf{H}_2\mathbf{D}(\tau)^{-1}\mathbf{R}_0\mathbf{C}(\tau)\right)\left(\mathbf{I} + \mathbf{D}(\tau)^{-1}\mathbf{R}_0\mathbf{C}(\tau)\right)^{-1}. \tag{5.13}$$

Comparing with (5.9) we see that

$$\mathbf{R}(\tau) = -(\hat{\mathbf{H}}_1 + \mathbf{G}(\tau))(\mathbf{H}_1 + \mathbf{G}(\tau)). \tag{5.14}$$

Thus we have obtained a relationship between the reflectivities $\mathbf{R}(\tau)$ and $\mathbf{R}_0$. Note the similarity between the expressions (5.14) and (4.7). In particular, $\mathbf{G}(\tau)$ in (5.14) plays the role of the impedance tensor $\hat{\mathbf{H}}_2$ in (4.7). For this reason, we consider $\mathbf{G}(\tau)$ as the impedance of the boundary $\mathcal{I}_{12}$ of the stratified half-space $\mathcal{B}_3 \cup \mathcal{B}_2$. This will be further clarified in the following subsection.

5.2. Derivative of $\mathbf{G}(\tau)$ at $\tau = 0$

Let us now compute the rate of change of $\mathbf{G}(\tau)$ with respect to the thickness τ of the slab. In particular, we are interested in computing the derivative $\mathbf{G}'(0)$ which expresses the rate of change of the impedance of the stratified half-space $\mathcal{B}_3$ due to the addition of an 'infinitesimal' veneer with mechanical properties equal to that of $\mathcal{B}_2$. For this, let

$$\mathbf{L}(\tau) = \mathbf{D}(\tau)^{-1}\mathbf{R}_0\mathbf{C}(\tau) \tag{5.15}$$

and rewrite (5.13) as

$$\mathbf{G}(\tau) = (\hat{\mathbf{H}}_2 + \mathbf{H}_2\mathbf{L}(\tau))(\mathbf{I} + \mathbf{L}(\tau))^{-1}. \tag{5.16}$$

Then we have

$$\begin{aligned} \mathbf{G}'(\tau) &= \mathbf{H}_2\mathbf{L}'(\mathbf{I}+\mathbf{L})^{-1} - (\hat{\mathbf{H}}_2 + \mathbf{H}_2\mathbf{L})(\mathbf{I}+\mathbf{L})^{-1}\mathbf{L}'(\mathbf{I}+\mathbf{L})^{-1} \\ &= (\mathbf{H}_2 - \hat{\mathbf{H}}_2)(\mathbf{I}+\mathbf{L})^{-1}\mathbf{L}'(\mathbf{I}+\mathbf{L})^{-1}. \end{aligned} \tag{5.17}$$

To simplify this, compute $\mathbf{L}$ in (5.16):

$$\mathbf{L} = (\mathbf{G} - \mathbf{H}_2)^{-1}(\hat{\mathbf{H}}_2 - \mathbf{G}),$$

whence

$$\mathbf{I} + \mathbf{L} = (\mathbf{G} - \mathbf{H}_2)(\hat{\mathbf{H}}_2 - \mathbf{H}_2).$$

Substitute in (5.17) to get

$$\mathbf{G}'(\tau) = -(\mathbf{G} - \mathbf{H}_2)\mathbf{L}'(\hat{\mathbf{H}}_2 - \mathbf{H}_2)^{-1}(\mathbf{G} - \mathbf{H}_2). \tag{5.18}$$

Now we proceed to compute $\mathbf{L}'(\tau)$, and $\mathbf{L}'(0)$ in particular. Recall the definition of $\mathbf{L}(\tau)$ in (5.15) those of $\mathbf{C}(\tau)$ and $\mathbf{D}(\tau)$ in (5.5) and (5.6). Observe that $\mathbf{C}(0) = \mathbf{D}(0) = \mathbf{I}$, and let

$$\mathbf{C}^0 \stackrel{\text{def}}{=} \mathbf{C}'(0) = -i\omega\mathbf{C}\ \mathrm{diag}[\mathbf{n}_3 \cdot \mathbf{t}_1,\ \mathbf{n}_3 \cdot \mathbf{t}_2,\ \mathbf{n}_3 \cdot \mathbf{t}_3]\ \mathbf{C}^{-1} \tag{5.19}$$

$$\mathbf{D}^0 \stackrel{\text{def}}{=} \mathbf{D}'(0) = -i\omega \mathsf{D}\ \mathrm{diag}[\mathbf{n}_3 \cdot \mathbf{s}_1,\ \mathbf{n}_3 \cdot \mathbf{s}_2,\ \mathbf{n}_3 \cdot \mathbf{s}_3]\ \mathsf{D}^{-1} \tag{5.20}$$

Then

$$\begin{aligned} \mathbf{L}'(0) &= -\mathbf{D}^0\mathbf{R}_0 + \mathbf{R}_0\mathbf{C}^0 \\ &= -\mathbf{D}^0\mathbf{L}(0) + \mathbf{L}(0)\mathbf{C}^0 \\ &= -\mathbf{D}^0\Big[(\mathbf{G}(0) - \mathbf{H}_2)^{-1}(\dot{\mathbf{H}}_2 - \mathbf{G}(0))\Big] \\ &\quad + \Big[(\mathbf{G}(0) - \mathbf{H}_2)^{-1}(\dot{\mathbf{H}}_2 - \mathbf{G}(0))\Big]\mathbf{C}^0. \end{aligned} \tag{5.21}$$

Let $\tau = 0$ in (5.18), substitute for $\mathbf{L}'(0)$ from (5.21), use the matrix identity

$$\begin{aligned} &(\mathbf{G} - \mathbf{H}_2)^{-1}(\dot{\mathbf{H}}_2 - \mathbf{G})(\dot{\mathbf{H}}_2 - \mathbf{H}_2)^{-1}(\mathbf{G} - \mathbf{H}_2) \\ &= (\mathbf{G} - \mathbf{H}_2)^{-1}\Big[(\dot{\mathbf{H}}_2 - \mathbf{H}_2) + (\mathbf{H}_2 - \mathbf{G})\Big](\dot{\mathbf{H}}_2 - \mathbf{H}_2)^{-1}(\mathbf{G} - \mathbf{H}_2) \\ &= (\dot{\mathbf{H}}_2 - \mathbf{H}_2)^{-1}(\dot{\mathbf{H}}_2 - \mathbf{G}) \end{aligned}$$

and simplify the result to arrive at

$$\begin{aligned} \mathbf{G}'(0) &= (\mathbf{G}(0) - \mathbf{H}_2)\mathbf{D}^0(\dot{\mathbf{H}}_2 - \mathbf{H}_2)^{-1}(\dot{\mathbf{H}}_2 - \mathbf{G}(0) \\ &\quad - (\dot{\mathbf{H}}_2 - \mathbf{G}(0))\mathbf{C}^0(\dot{\mathbf{H}}_2 - \mathbf{H}_2)^{-1}(\mathbf{G}(0) - \mathbf{H}_2). \end{aligned} \tag{5.22}$$

5.3. The Riccati equation

Equation (5.22) shows the effect on the impedance at the boundary of the stratified half-space $\mathcal{B}_3$ due to an augmentation by an infinitesimal layer at its boundary. We may build up a stratified slab of finite thickness and a prescribed distribution of mechanical properties by 'integrating' (5.22) over the width of the slab. Specifically, as before, let $\mathcal{B}_3$ be a stratified half-space and $\mathcal{B}_1$ be a homogeneous half-space. However, in contrast to what we have done thus far, let $\mathcal{B}_2$ also be a stratified, rather than a homogenous, slab of some finite thickness a. Suppose that we know the reflectivity $\mathbf{R}_0$ of the interface eqna created by bringing the half-spaces $\mathcal{B}_3$ and $\mathcal{B}_1$ in contact.[1]. We wish to interpose $\mathcal{B}_2$ between $\mathcal{B}_1$ and $\mathcal{B}_3$ and to compute the reflectivity of the boundary of the composite half-space $\mathcal{B}_3 \cup \mathcal{B}_2$. The crux of the invariant imbedding idea is to replace this problem with the one-parameter family of problems where instead of augmenting $\mathcal{B}_3$ by the slab $\mathcal{B}_2$ of thickness a, one gradually 'builds up' to the desired thickness a by gradual addition of infinitesimal layers, accounting for the change of reflectivity at each step, and integrating the changes over the whole process.

Thus let the parameter τ denote the thickness of the partially formed slab $\mathcal{B}(\tau)$ of thickness τ and let $\mathbf{G}(\tau)$ denote the impedance of the boundary of the composite half-space $\mathcal{B}_3 \cup \mathcal{B}(\tau)$. When this half-space is further augmented by adding an infinitesimal

[1] For instance, if $\mathcal{B}_3$ is homogeneous then $\mathbf{R}_0$ may be computed from (4.7)

veneer of material with the desired mechanical properties, the rate of change of $\mathbf{G}$ can be computed using equation (5.22) as

$$\begin{aligned}\mathbf{G}'(\tau) &= (\mathbf{G}(\tau)-\mathbf{H}(\tau))\mathbf{D}^0(\tau)(\hat{\mathbf{H}}(\tau)-\mathbf{H}(\tau))^{-1}(\hat{\mathbf{H}}(\tau)-\mathbf{G}(\tau) \\ &\quad -(\hat{\mathbf{H}}(\tau)-\mathbf{G}(\tau))\mathbf{C}^0(\tau)(\hat{\mathbf{H}}(\tau)-\mathbf{H}(\tau))^{-1}(\mathbf{G}(\tau)-\mathbf{H}(\tau)). \quad (5.23)\end{aligned}$$

Here $\mathbf{H}(\tau)$ is the impedance tensor based on the local properties of the material found at distance τ from the surface of $\mathcal{B}_3$. Note that the propagation vectors $\mathbf{t}_3, \mathbf{t}_2, \mathbf{t}_1$ and $\mathbf{s}_1, \mathbf{s}_2, \mathbf{s}_3$ that enter in the computation of $\mathbf{H}(\tau)$ are now functions of τ. The tensors $\mathbf{C}^0$ and $\mathbf{D}^0$, which were defined in (5.19) and (5.20) for the special case $\tau = 0$ are now also functions of τ since they depend on the propagation vectors $\mathbf{s}_k$ and $\mathbf{t}_k$.

The Riccati differential equation (5.23) may be integrated on the interval $(0, a)$ to compute $\mathbf{G}(a)$. The reflectivity of the boundary of the composite half-space $\mathcal{B}_3 \cup \mathcal{B}_2$ then may be computed from (5.14). See [3] for further analysis of special cases in the context of isotropic materials.

References

[1] M. E. Gurtin, *The Linear Theory of Elasticity*, Handbuch der Physik, vol. VIa/2, Springer-Verlag, Berlin, 1972.

[2] W. Hager and R. Rostamian, Optimal Coatings, Bang-bang Controls, and Gradient Techniques, *Optimal Control: Applications and Methods* **8**, 1–20, 1987.

[3] W. Hager and R. Rostamian, Reflection and refraction of elastic waves for stratified materials, *Wave Motion*, to appear.

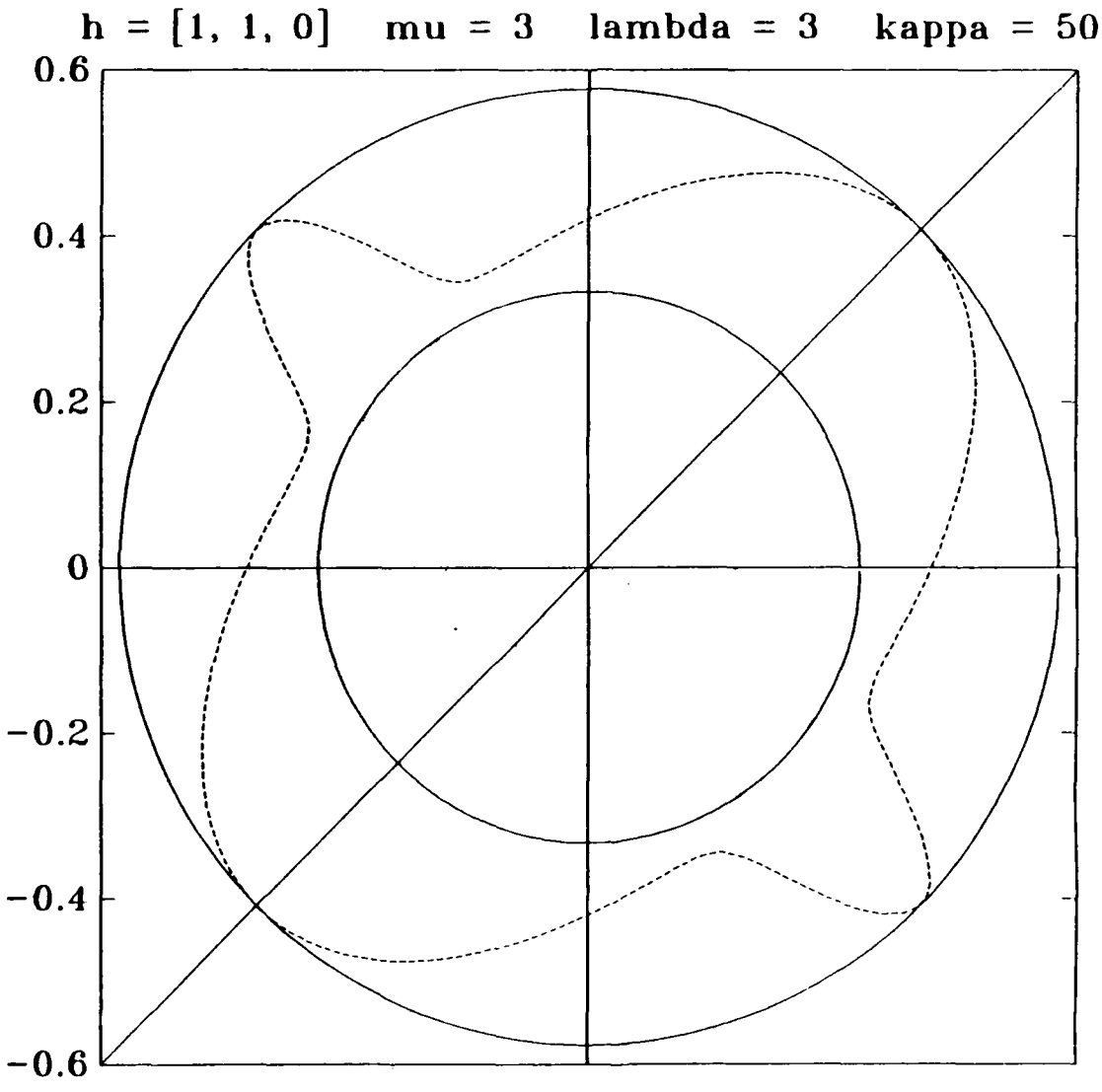
h = [1, 1, 0] mu = 3 lambda = 3 kappa = 50
0.6
0.4
0.2
0
−0.2
−0.4
−0.6

COMPUTATIONAL RESULTS FOR PHASE TRANSITIONS IN SHAPE MEMORY MATERIALS†

CHARLES COLLINS‡ AND MITCHELL LUSKIN‡
School of Mathematics and Minnesota Supercomputer Institute
University of Minnesota
Minneapolis, Minnesota 55455.

Abstract. We give computational results for the martensitic-austenitic phase transition in the indium-thalium alloy. We use the free energy density developed by Ericksen for cubic-tetragonal phase transitions. We have developed numerical algorithms and a finite element code to compute approximate minima for the bulk energy functional. Our numerical results give twinning on the scale of the grid . We are also able to compute an austenitic - finely twinned martensitic interface.

1. Introduction. Much of the interesting behavior of shape memory materials is associated with the fact that loads and temperature changes influence martensitic phase transitions. The austenitic-martensitic phase transition is a solid-solid phase transition usually characterized by a decrease in crystal symmetry at a transition temperature. The indium-thallium alloy with composition near 20 atomic % thallium exhibits such a phase transition from a high temperature solid phase with cubic symmetry (austenite) to a low temperature solid phase with tetragonal symmetry (martensite) [5]. It is observed that the martensitic phase is often "finely twinned" along planes related to the crystal lattice and that an austenitic-finely twinned martensitic interface can be observed at the transition temperature along special planes related to the crystal lattice [5]. In this paper, we give results which demonstrate that the experimentally observed phenomena of fine scale martensitic twinning and the austenitic-finely twinned martensitic interface can be obtained by numerical computations based on the Ericksen theory for cubic-tetragonal phase transitions [9,10].

The Ericksen theory gives a free energy density for first-order cubic-tetragonal phase transitions. The moduli have been determined by R. D. James to match the transformation strain and the linear elastic moduli for the martensitic phase at the transition temperature. Ball and James [2] and Chipot and Kinderlehrer [6,15] have explained how the Ericksen theory gives the interesting phenomena of fine scale twinning and of an austenitic-finely twinned martensitic interface.

We have developed numerical algorithms and a three-dimensional finite element code to compute approximate minima for the bulk energy functional [8]. Our numerical results

†Proceedings of the ARO Smart Materials, Structures, and Mathematical Issues Workshop, Virginia Polytechnic Institute and State University, September 15-16, 1988.

‡This research was supported by the National Science Foundation, Grants DMS 835-1080 and DMS 871-8881, the Cray Research Foundation, ARO Grant DAAL03-88-K0170, and the Minnesota Supercomputer Institute.

give twinning on the scale of the grid and an austenitic-finely twinned martensitic interface on the planes predicted by the Ball-James theory [2].

Alt, Hoffman, Niezgódka, and Sprekels have given a numerical study of a one-dimensional mathematical model for the dynamics of the austenitic-martensitic phase transition [1]. Silling has used a non-physical bulk energy in two space dimensions to numerically simulate martensitic transformation and twinning [16].

2. Continuum Theory. Let the reference configuration for the crystal, $\Omega \subseteq \mathbf{R}^3$, be undistorted austenite at the critical temperature, θ_c. Let $y(x) : \Omega \to \mathbf{R}^3$ be the deformation. As usual, we assume that $y(x)$ is continuous, injective, and orientation preserving [7]. The deformation gradient is given by $F(x) = \nabla y(x)$ and the right Cauchy-Green strain tensor is given by $C = F^T F$ [13]. We denote the temperature by θ and the free energy per unit volume by $\phi(F, \theta)$. The bulk energy for the deformation $y(x)$ at the temperature θ is then given by

$$\mathcal{J}(y) = \int_\Omega \phi(\nabla y(x), \theta) dx.$$

We want our constitutive equation to be invariant under observer changes [13], so we want ϕ to satisfy

$$\phi(F, \theta) = \phi((F^T F)^{1/2}, \theta) \tag{2.1}$$

and we define

$$W(C, \theta) = \phi(C^{1/2}, \theta) = \phi(F, \theta).$$

Since the reference configuration has cubic symmetry, we want W to satisfy

$$W(R_i C R_i^T, \theta) = W(C, \theta) \tag{2.2}$$

for $R_i \in \mathcal{G}$ where $\mathcal{G} = \{R_1, \ldots, R_{24}\}$ is the cubic symmetry group of proper rotations.

In an unstressed state, the Cauchy-Green strain for the martensitic phase is given by one of the variants

$$\begin{aligned} C_1 &= C_1(\theta) = \operatorname{diag}(1 + 2\epsilon, 1 - \epsilon, 1 - \epsilon), \\ C_2 &= C_2(\theta) = \operatorname{diag}(1 - \epsilon, 1 + 2\epsilon, 1 - \epsilon), \\ C_3 &= C_3(\theta) = \operatorname{diag}(1 - \epsilon, 1 - \epsilon, 1 + 2\epsilon), \end{aligned}$$

where $\epsilon = \epsilon(\theta)$. Note that

$$\{R_i C_1 R_i^T | i = 1, \ldots, 24\} = \{C_1, C_2, C_3\}.$$

We also define the right stretch tensors

$$U_i = C_i^{1/2}.$$

Our energy density must predict that in an unstressed state the austenitic phase is stable for $\theta > \theta_c$. the austenitic phase and the martensitic phase can coexist for θ near θ_c, and the martensitic phase is stable for $\theta < \theta_c$. More precisely, we must have that

$$W(C,\theta) > W(I,\theta) \qquad (2.3)$$
$$\text{for } C \neq I,\ \theta > \theta_c,$$
$$W(C,\theta) > W(C_1,\theta) = W(C_2,\theta) = W(C_3,\theta) \qquad (2.4)$$
$$\text{for } C \neq C_1, C_2, C_3,\ \theta < \theta_c,$$

and

$$W(C,\theta_c) > W(I,\theta_c) = W(C_1,\theta_c) = W(C_2,\theta_c) = W(C_3,\theta_c) \qquad (2.5)$$
$$\text{for } C \neq C_1, C_2, C_3, I.$$

Ericksen has proposed the following energy density for a constrained elastic crystal [10]

$$W(C,\theta) = b(\theta)J + c(\theta)K + d(\theta)J^2,$$
$$J = \frac{1}{6}\{(\lambda_1 - 1)^2 + (\lambda_2 - 1)^2 + (\lambda_3 - 1)^2\}$$
$$K = \frac{1}{2}(\lambda_1 - 1)(\lambda_2 - 1)(\lambda_3 - 1),$$
$$\lambda_1 = C_{11}, \quad \lambda_2 = C_{22}, \quad \lambda_3 = C_{33}$$

subject to the constraints

$$C_{12} = C_{23} = C_{13} = 0, \quad \text{tr } C = 3.$$

Ericksen has shown that the coefficients b, c, and d can be chosen so that W satisfies (2.1)-(2.5). Ericksen also proposed to the authors that the constraints could be replaced by adding penalty terms to the energy density to obtain

$$W(C,\theta) = bJ + cK + dJ^2 +$$
$$\frac{e}{2}(C_{12}^2 + C_{13}^2 + C_{23}^2 + C_{21}^2 + C_{31}^2 + C_{32}^2) + f(\text{tr } C - 3)^2,$$

$$J = \frac{1}{6}\{(\lambda_1 - 1)^2 + (\lambda_2 - 1)^2 + (\lambda_3 - 1)^2\},$$
$$K = \frac{1}{2}(\lambda_1 - 1)(\lambda_2 - 1)(\lambda_3 - 1), \qquad (2.6)$$

where the λ_i are modified so that

$$\lambda_i = \frac{3C_{ii}}{\text{tr } C} \qquad \text{for } i = 1,2,3.$$

R. D. James has determined coefficients for W so that (2.1)-(2.5) are satisfied, so that W matches available experimental linear elastic moduli at $\theta = \theta_c$ for the martensitic phase ($F = U_1$), and so that C_1, the Cauchy-Green strain for the unstressed martensitic phase, matches experimental data at $\theta = \theta_c$ for the indium-thallium alloy with 20.5 atomic % thallium. James' coefficients also match experimental data [5] for the effect of uniaxial stress on transition temperature. James' moduli are (θ in $^\circ C$ and moduli in gigapascals)

$$\begin{aligned} b &= 0.38 + (1.22 \times 10^{-3})(\theta - 70) \\ c &= -29.23 \\ d &= 562.13 \\ e &= 3.26 \\ f &= 5.25 \end{aligned}$$

The critical temperature, the temperature at which (2.5) holds, is $\theta_c = 70$ for these coefficients.

3. Internally Twinned Martensite. For an unstressed solid at $\theta < \theta_c$ the above theory allows the existence of minimum energy deformations which have deformation gradients which are discontinuous across twin planes [2,6,8,9,10,15]. Ball and James [2] have shown that there exists a proper rotation, R, such that

$$RU_1 = U_3 + a \otimes n$$

where

$$\begin{aligned} n &= \frac{1}{\sqrt{2}}(e_1 + e_3), \\ a &= \frac{3\sqrt{2}\epsilon}{2+\epsilon}((1-\epsilon)^{1/2}e_1 - (1+2\epsilon)^{1/2}e_3). \end{aligned} \tag{3.1}$$

Planes orthogonal to n are twin planes. It then follows that

$$y(x) = U_3 x + a \int_0^{x \cdot n} \beta(t)dt,$$

where $\beta(t)$ takes only the values 0 and 1, is a deformation which has minimum energy and which has a discontinuous deformation gradient if $\beta(t)$ is not constant. We note that

$$\begin{aligned} \nabla y(x) &= U_3 \qquad \text{where} \quad \beta(x \cdot n) = 0 \\ \nabla y(x) &= RU_1 \qquad \text{where} \quad \beta(x \cdot n) = 1. \end{aligned}$$

The mathematical properties of the Ericksen energy density is very different from the properties of the energy density of linear elastic materials. The Ericksen energy density is clearly not convex since

$$\frac{\phi(U_1) + \phi(U_3)}{2} > \phi(\frac{U_1 + U_3}{2}).$$

The energy densities of linear elastic materials are quadratic and convex. We saw above that there are minimun energy deformations with discontinuous deformation gradients if the energy density attains its minimun value at distinct deformation gradients which differ by a rank-1 matrix. A nontrivial energy density with distinct minima clearly cannot be convex.

As a consequence of the lack of convexity of the Ericksen energy density, for some boundary conditions there do not exist deformations which achieve the miminum energy. Instead, deformations attempt to attain the minimun energy by having arbitrarily fine scale twinning. In the language of mathematical analysis, our bulk energy is not **lower semi-continuous**[2,6,15]. To see this, let $\beta(t)$ be periodic of period 1 and define

$$y_k(x) \equiv k^{-1} y(kx).$$

Then

$$y_k(x) \rightharpoonup y^*(x) \equiv (U_3 + \lambda a \otimes n)x \qquad \text{uniformly}$$

and

$$\int_{\mathcal{D}} \nabla y_k(x)\, dx \rightharpoonup \int_{\mathcal{D}} \nabla y^*(x)\, dx$$

as $k \rightharpoonup \infty$ for all domains $\mathcal{D} \subseteq \Omega$. However, $y^*(x)$ is not a deformation with minimum energy even though all of the $y_k(x)$ are deformations with minimum energy. We note that convex bulk energy functionals are lower semi-continuous and thus do not allow fine scale twinning[2,6,15].

Now for $\theta < \theta_c$ and $0 < \lambda < 1$ the bulk energy function, $\mathcal{J}(y)$, cannot attain its minimum value on the set of admissible deformations [3]

$$\mathcal{A} = \{y(x) \mid y(x) = (U_3 + \lambda\, a \otimes n)x \text{ for } x \in \partial\Omega\}.$$

This is because the deformation gradients of minimizing sequences attempt to take values which minimize the energy density. This results in fine twinning to give compatibility with the boundary conditions. The information to be obtained from the minimizing sequences for this problem can be summarized using the concept of the Young measure [6,15]. In fact, any minimizing sequence for this problem gives a unique, nontrivial Young measure which converges to a single laminate [3].

We are interested in the possibility of numerically computing minima of the bulk energy on finite-dimensional approximations of the set of admissible deformations as a

means toward understanding the material microstructure given by minimizing sequences. For our numerical experiments we let our reference configuration be

$$\Omega = \{x = (x_1, x_2, x_3) | 0 < x_i < 1 \text{ for } i = 1, 2, 3\}.$$

To construct our finite element approximation to $\mathcal{A}$ we let N be a positive integer, $h = 1/N$, and

$$\Omega_{ijk} = \{x = (x_1, x_2, x_3) | ih < x_1 < (i+1)h,\ jh < x_2 < (j+1)h,\ kh < x_3 < (k+1)h\}$$

for $i, j, k = 0, \ldots, N-1$. We then define the space of trilinear polynomial functions

$$Q_1 = \{\xi(x) | \xi(x) = \sum_{i,j,k=0}^{1} \alpha_{ijk} x_1^i x_2^j x_3^k \text{ for } \alpha_{ijk} \in \mathbf{R}^3\}$$

and the space of continuous, piecewise trilinear deformations by

$$\mathcal{M}_h = \{y(x) | y(x) \text{ is continuous for } x \in \Omega \text{ and } y|_{\Omega_{ijk}} \in Q_1 \text{ for } i, j, k = 0, \ldots, N-1\}.$$

We approximate the set of admissible deformations by the finite-dimensional space

$$\mathcal{A}_h = \{y \in \mathcal{M}_h \mid y(x) = (U_3 + \lambda\, a \otimes n)x \text{ for } x \in \partial\Omega\}. \tag{3.2}$$

We then wish to compute $\tilde{y} \in \mathcal{A}_h$ such that

$$\mathcal{J}(\tilde{y}) \leq \mathcal{J}(y), \qquad \forall y \in \mathcal{A}_h. \tag{3.3}$$

Note that we have not required deformations in $\mathcal{A}$ and $\mathcal{A}_h$ to be orientation preserving ($\det \nabla y > 0$). This is acceptable since our computed solutions to (3.3) have all been orientation preserving. We have approximated the integrals in (3.3) by mid-point quadrature, and we have used the gradient method and the Fletcher-Reeves version of the conjugate gradient method [11,12] to compute minima of (3.3). Of course, both the gradient method and the conjugate gradient method can converge to local minima.

We were unable to obtain a fine scale twinned minima for (3.2). The reason seems to be that the twin planes (planes across which the deformation gradient is discontinuous) should be orthogonal to $n = \frac{1}{\sqrt{2}}(e_1 + e_3)$, but the deformations in $\mathcal{A}_h$ are not allowed to have discontinuities in their deformation gradients across planes orthogonal to n. However, we have obtained martensitic twinning on the scale of the mesh if the reference configuration is rotated so that the expected twin planes lie along planes for which the deformations in $\mathcal{A}_h$ can have discontinuous deformation gradients. This is easily done by rotating the reference configuration by $\frac{\pi}{4}$ about the x_2-axis. We shall continue to denote the coordinates in the

new reference configuration by $x = (x_1, x_2, x_3)$ and the displacement by $y(x)$. We assume that the body in the new coordinates is described by

$$\Omega = \{x = (x_1, x_2, x_3) | 0 < x_i < 1 \text{ for } i = 1, 2, 3\}.$$

The energy density is now given by

$$\hat{\phi}(F, \theta) = \phi(FS, \theta)$$

where S is the rotation of $\frac{\pi}{4}$ about the x_2-axis, and the bulk energy is given by

$$\hat{\partial}(y) = \int_\Omega \hat{\phi}(\nabla y, \theta) dx.$$

The martensitic strains are now given by

$$\hat{C}_i = SC_iS^T$$

and

$$\hat{U}_i = SU_iS^T,$$

and we set

$$\hat{a} = Sa \text{ and } \hat{n} = Sn = e_1.$$

The set of admissible deformations for the continuous problem is now

$$\mathcal{A} = \{y(x) \mid y(x) = (\hat{U}_3 + \lambda \hat{a} \otimes \hat{n})x \quad \text{for } x \in \partial\Omega\}$$

and the finite element subspace is

$$\mathcal{A}_h = \{y \in \mathcal{M}_h | y(x) = (\hat{U}_3 + \lambda \hat{a} \otimes \hat{n})x \quad \text{for } x \in \partial\Omega\}.$$

The problem is then to compute $\tilde{y} \in \mathcal{A}_h$ such that

$$\tilde{\partial}(\tilde{y}) \leq \tilde{\partial}(y), \qquad \forall y \in \mathcal{A}_h.$$

In order to see the effect of twinning more easily in our graphical output of the deformed state, we have replaced b by $16b$ and c by $4c$. This has the effect of replacing $\epsilon(\theta_c)$ by $4\epsilon(\theta_c)$. Thus, $\epsilon(\theta_c)$ for the new coefficients equals .104.

The most dramatic technique for showing the finely twinned structure we obtained from our numerical computation for this problem is to mark each cell in our reference

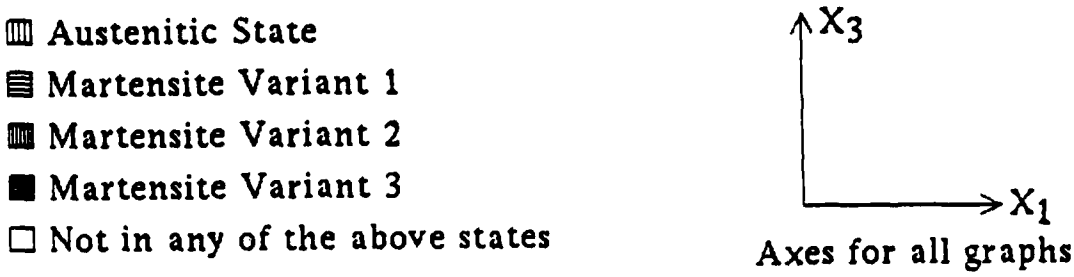

Figure 1. Key to later figures.

configuration to denote whether the right Cauchy-Green strain at the mid-point is close to the austenitic state, $C = I$, or any of the martensitic variants, $C_i(\theta)$. In Figure 2 and Figure 3 we show our results for the case $\lambda = 1/2$ and $\theta = 69$ (recall that $\theta_c = 70$) after 700 iterations of the gradient method with $h = 1/16$. The initial state is $y(x) = (\hat{U}_3 + \lambda \hat{a} \otimes \hat{n})x$. We consider a cell to be in the austenitic state if at the midpoint,

$$\|C - I\| \leq \text{minimum}\{\|C - C_1\|, \|C - C_2\|, \|C - C_3\|, (.02)^{1/2}\}$$

where the matrix norm is defined by

$$\|B\| = (\text{tr } B^T B)^{1/2} = \left(\sum_{i,j=1}^{3} B_{ij}^2 \right)^{1/2}.$$

We consider a cell to be in variant i of the martensitic state if at the midpoint

$$\|C - C_i\| \leq \text{ minimum}\{\|C - C_j\| \text{ for } j \neq i, \|C - I\|, (.02)^{1/2}\},$$

and we consider a cell to be not in a austenitic or a martensitic state if

$$\text{minimum}\{\|C - I\|, \|C - C_1\|, \|C - C_2\|, \|C - C_3\|\} \geq .02^{1/2}.$$

Figure 1 gives a key for all of the later figures.

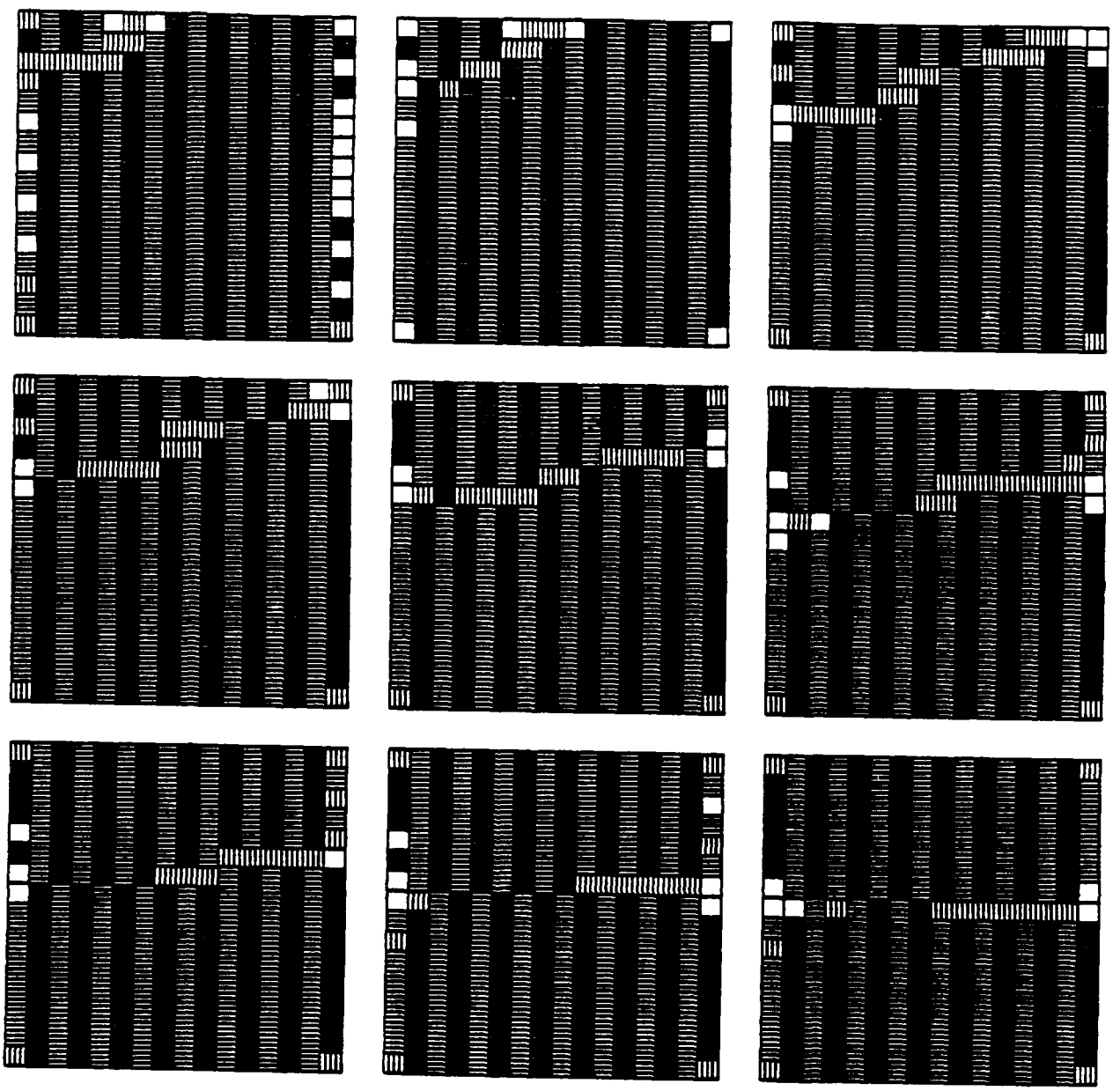

Figure 2. Planar cross-sections for $x_2 = (i + \frac{1}{2})h$ for $i = 0, \ldots, 8$ with $\lambda = 1/2$.

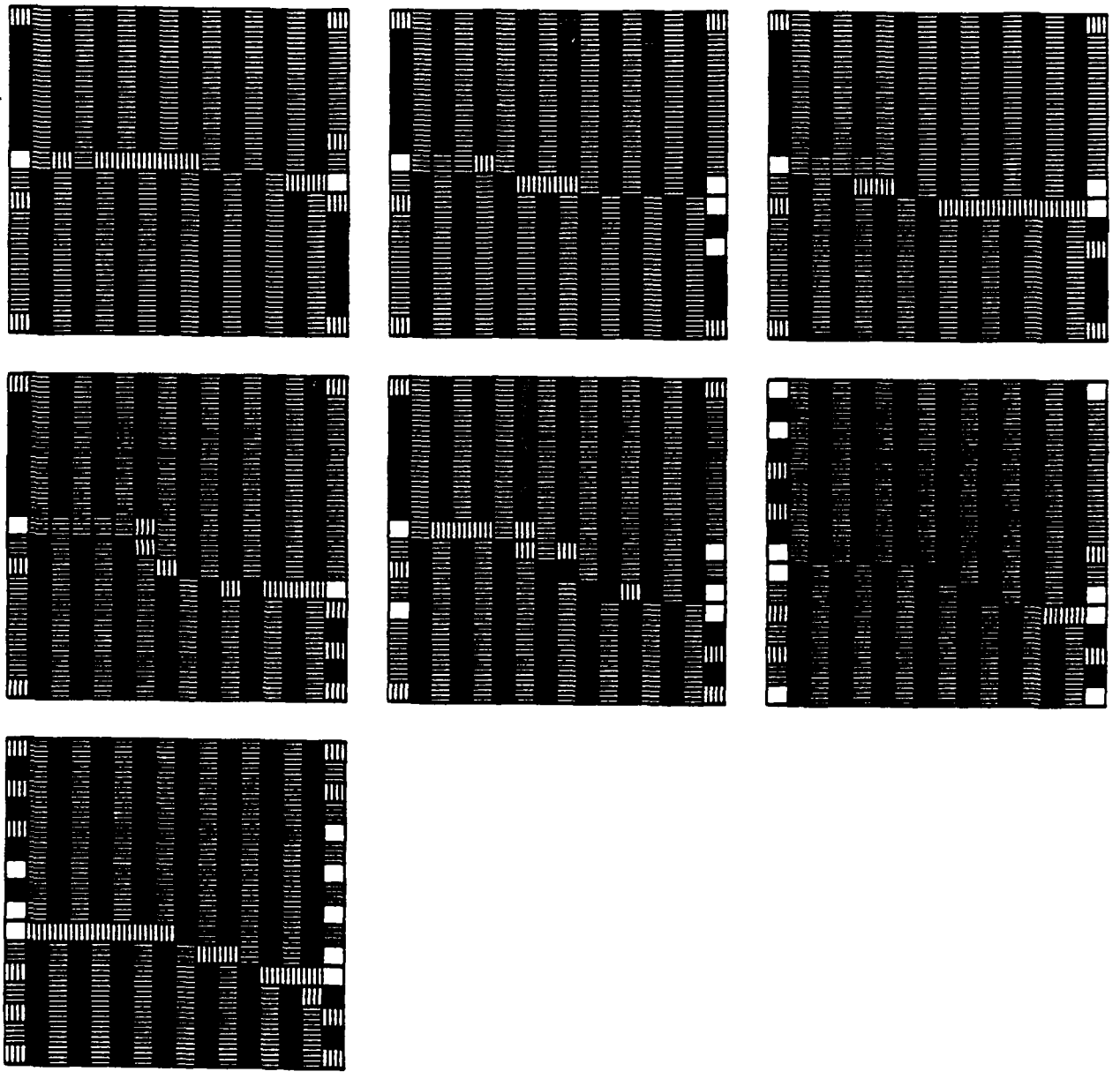

Figure 3. Planar cross-sections for $x_2 = (i + \frac{1}{2})h$ for $i = 9, \ldots, 15$ with $\lambda = 1/2$.

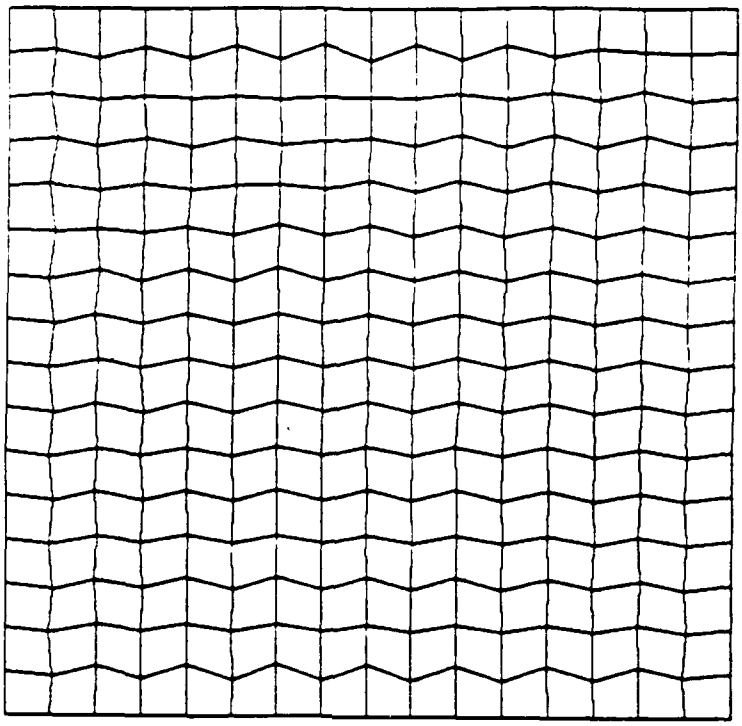

Figure 4. Planar cross-section of the deformation for $x_2 = \frac{3}{16}$ with $\lambda = 1/2$.

It is also informative to study the deformation of the crystal. In Figure 4 and Figure 5 we show the x_1-x_3 deformation of the crystal for the planar cross-sections $x_2 = \frac{3}{16}$ and $x_2 = \frac{1}{2}$. It is easy to see the shearing in the planar layers. It is also evident from Figures 2-5 that there is a planar defect in the crystal which is characterized by a change in the martensitic variant in the layers. This defect indicates that we are stuck in a local minimum. The final distribution of states is given by

austenitic state	221
martensite variant 1	1894
martensite variant 2	0
martensite variant 3	1889
not in any of the above states	92

We note that

$$\lambda_{\text{calc}} \equiv \frac{\#\text{ of states in martensite variant 1}}{\#\text{ of states in martensite}} = .50066$$

which is in excellent agreement with $\lambda = 1/2$.

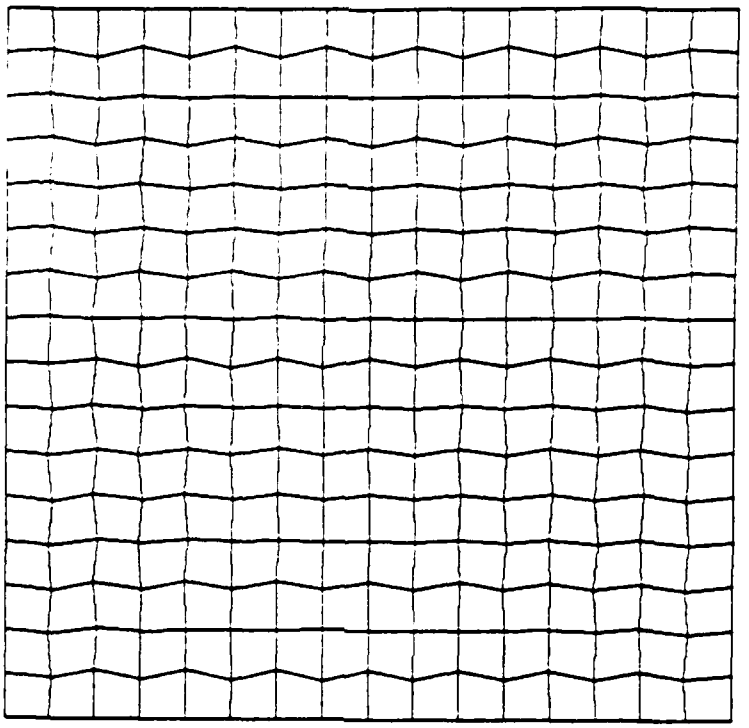

Figure 5. Planar cross-section of the deformation for $x_2 = 1/2$ with $\lambda = 1/2$.

§4. **The Austenitic-Finely Twinned Martensitic Interface.** Ball and James have shown how the existence of an austenitic-finely twinned martensitic interface can be explained by the theory of finite elasticity and minimizing sequences [2]. To construct the interface, they show that there exists λ^* such that $0 < \lambda^* < 1$ and that there exists a proper rotation, Q, such that

$$\hat{U}_3 + \lambda^* \hat{a} \otimes \hat{n} = Q(I + \hat{b} \otimes \hat{m}) \tag{4.1}$$

where

$$\begin{aligned}
\hat{m} &= Sm, \\
m &= \left(-\frac{1}{2}(1-\tau),\ 1,\ \frac{1}{2}(1+\tau)\right), \\
\hat{b} &= Sb, \\
b &= \left(-\frac{1}{2}\zeta(1-\tau),\ \beta,\ \frac{1}{2}\zeta(1+\tau)\right), \\
\tau &= (1-4\epsilon)^{1/2}, \\
\zeta &= \epsilon(1+(1+2\epsilon)^{1/2})^{-1}, \\
\beta &= -\epsilon(1+2\epsilon)^{1/2}(1+(1+2\epsilon)^{1/2})^{-1}, \\
\lambda^* &= \frac{1}{2}\left[1-\left(1-\frac{4}{9}(2+\epsilon)\right)^{1/2}\right].
\end{aligned}$$

As before, we then compute $\hat{y} \in \mathcal{A}_h$ such that

$$\hat{\partial}(\hat{y}) \leq \hat{\partial}(y), \qquad \forall y \in \mathcal{A}. \tag{4.2}$$

We have solved (4.1) by the gradient method with the initialization $y(x) = y^*(x)$ at interpolation points (grid points) in Ω.

In Figure 6 and Figure 7 we give our results for the right Cauchy-Green strain for $\alpha = 1/\sqrt{2}$, $h = 1/16$ and $\theta = \theta_c = 70$ after 350 iterations. The interface is clearly given as the boundary between an austenitic region and a finely twinned region. We note the presence of some twin planes oriented orthogonal to the twin planes which are orthogonal to $\hat{n}$. The final gradient distribution is given by

austenitic state	1492
martensite variant 1	992
martensite variant 2	0
martensite variant 3	1566
not in any of the above states	46

We note that

$$\lambda_{\text{calc}} \equiv \frac{\#\text{ of states in martensite variant 1}}{\#\text{ of states in martensite}} = .388$$

whereas $\lambda^* = .372$. In Figure 8 and 9 we give the deformation of the plane $x_2 = \frac{5}{16}$ and $x_2 = \frac{1}{2}$ for the above problem.

As a consequence of (4.1) they show that at $\theta = \theta_c$, for any $\alpha \in \mathbf{R}$, there exists a minimizing sequence y_k of deformations such that

$$\hat{\mathcal{J}}(y_k) \to 0,$$
$$y_k \to y^* \qquad \text{uniformly}$$

and

$$\int_{\mathcal{D}} \nabla y_k \, dx \to \int_{\mathcal{D}} \nabla y^* \, dx$$

as $k \to \infty$ for all domains $\mathcal{D} \subseteq \Omega$ and where

$$y^*(x) = \begin{cases} Qx & \text{for } x \cdot \frac{\dot{m}}{|\dot{m}|} < \alpha \\ \alpha Q \frac{\dot{m}}{|\dot{m}|} + (\hat{U}_3 + \lambda^* \hat{a} \otimes \hat{n})(x - \alpha \frac{\dot{m}}{|\dot{m}|}) & \text{for } x \cdot \frac{\dot{m}}{|\dot{m}|} > \alpha. \end{cases}$$

Further, outside of a boundary layer about $x \cdot \frac{\dot{m}}{|\dot{m}|} = \alpha$ whose width, $w(k)$, converges to zero as $k \to \infty$,

$$\nabla y_k = \begin{cases} Q & \text{for } x \cdot \frac{\dot{m}}{|\dot{m}|} < \alpha \\ \hat{U}_3 + \beta(k\, x \cdot \hat{n}) \hat{a} & \text{for } x \cdot \frac{\dot{m}}{|\dot{m}|} > \alpha + w(k) \end{cases}$$

where β is a function which takes only the values 0 and 1, which is periodic with period 1 and which satisfies

$$\lambda^* = \int_0^1 \beta(t) dt.$$

Note that

$$\hat{\mathcal{J}}(y^*) \neq 0.$$

Thus, the crystal is in the austenite state for $x \cdot \frac{\dot{m}}{|\dot{m}|} < \alpha$ and is in a finely twinned martensite state for $x \cdot \frac{\dot{m}}{|\dot{m}|} > \alpha$. The plane of the interface satisfies $x \cdot \frac{\dot{m}}{|\dot{m}|} = \alpha$.

We now consider the minimization of $\hat{\mathcal{J}}(y)$ on the set of admissible deformations

$$\mathcal{A} = \{y(x) \mid y(x) = y^*(x) \text{ for } x \in \partial\Omega\}.$$

We think that the minimum of $\hat{\mathcal{J}}$ is not attained in the set $\mathcal{A}$ [4], although this has not yet been rigorously proven. However, minimizing sequences give an austenitic-finely twinned martensitic interface as described above.

We have been able to numerically compute such an austenitic-finely twinned martensitic interface. We approximate $\mathcal{A}$ by the finite dimensional space.

$$\mathcal{A}_h = \{y \in \mathcal{M}_h | y(x) = y^*(x) \text{ for } x \text{ at interpolation points in } \partial\Omega\}.$$

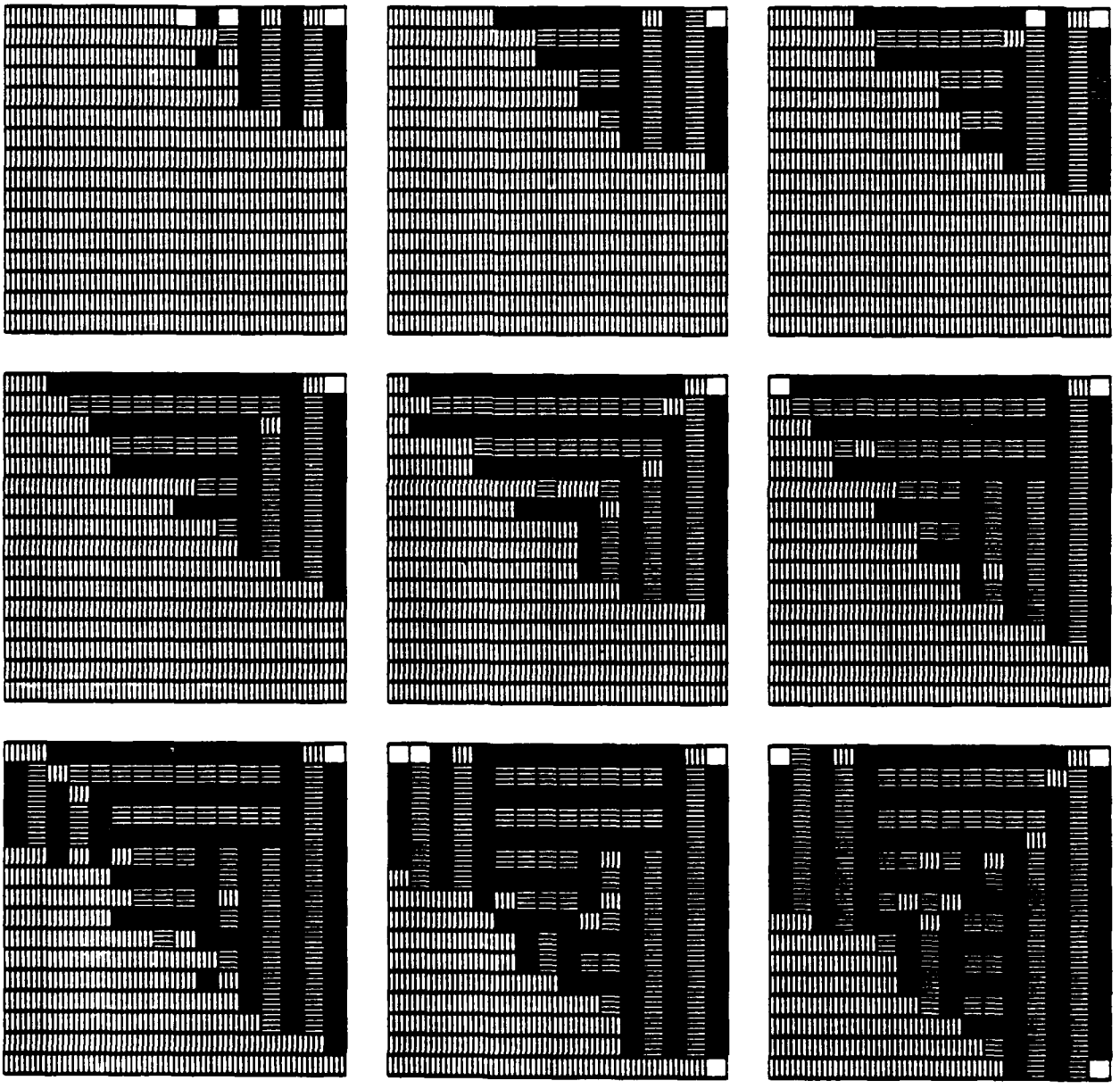

Figure 6. Planar cross-sections for $x_2 = (i + \frac{1}{2})h$ for $i = 0, \ldots, 8$ for the austenite/finely twinned martensite interface.

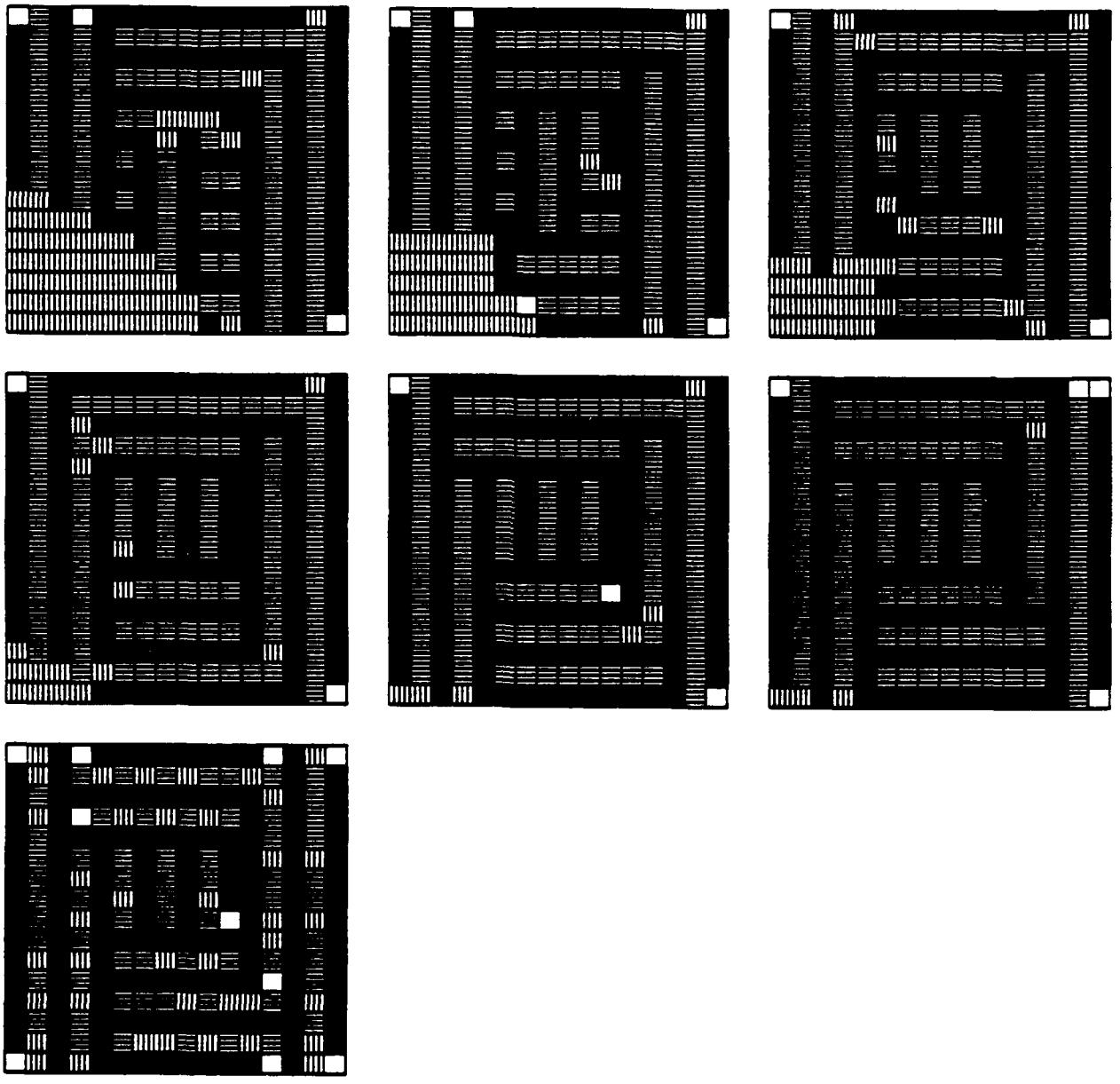

Figure 7. Planar cross-sections for $x_2 = (i + \frac{1}{2})h$ for $i = 9, \ldots, 15$ for the austenite/finely twinned martensite interface.

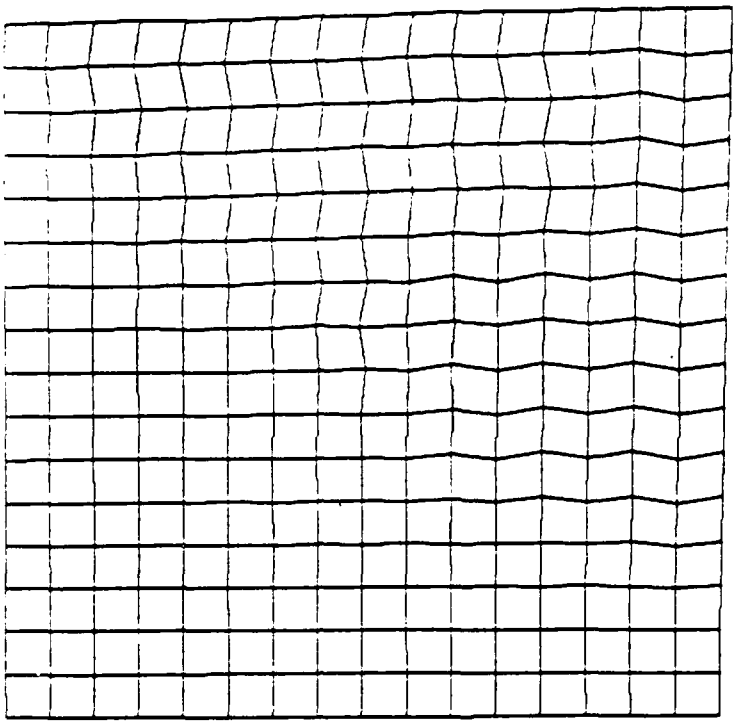

Figure 8. Planar cross-sections of the deformation for $x_2 = 5/16$ for the austenite/finely twinned martensite interface.

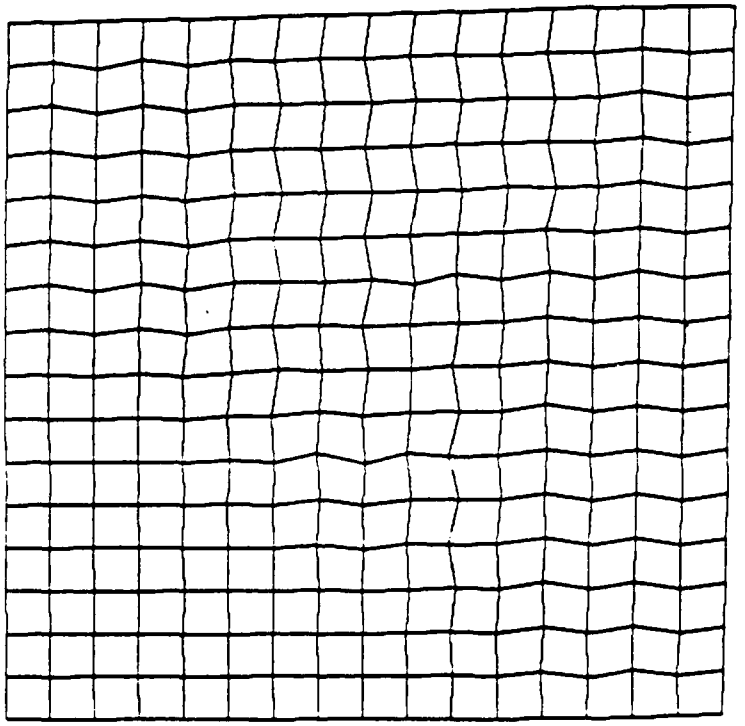

Figure 9. Planar cross-sections of the deformation for $x_2 = 1/2$ for the austenite/finely twinned martensite interface.

§5. Numerical Methods. In this section, we shall describe the gradient method and the conjugate gradient methods that we have used to find minima of the functional, $\hat{\mathcal{J}}$.

The gradient method starts with an initial guess, $y^\circ \in \mathcal{A}_h$, and determines an iteration sequence, $y^n \in \mathcal{A}_h$, such that (under appropriate conditions) $y^n \to \hat{y}$. After $y^n \in \mathcal{A}_h$ has been computed, we compute $y^{n+1} \in \mathcal{A}_h$ as follows. First, we compute the gradient, $g^n \in \mathcal{A}_h$, by

$$\int_\Omega g^n \cdot z \, dx = \int_\Omega \frac{\partial \hat{\phi}}{\partial F}(\nabla y^n, \theta) \cdot \nabla z \, dx, \qquad \forall z \in \mathcal{A}_h. \tag{5.1}$$

Then we compute $\rho_n \in \mathbf{R}$, $\rho_n > 0$ such that

$$\hat{\mathcal{J}}(y^n - \rho_n g^n) \leq \hat{\mathcal{J}}(y^n - \rho g^n) \qquad \forall \rho > 0. \tag{5.2}$$

Finally, we set

$$y^{n+1} = y^n - \rho_n g^n.$$

We note that (5.2) is a univariate optimization problem for $\rho > 0$. In practice, we compute the first local minima for $\rho > 0$ in (5.2).

It is well-known that even for quadratic, convex functionals the gradient method can converge slowly [11]. For such problems the conjugate gradient method often converges in an order of magnitude fewer iterations.

The Fletcher-Reeves variant of the conjugate gradient method is initialized by an initial guess $y^\circ \in \mathcal{A}_h$ and an initial search direction $d^\circ \equiv g^\circ \in \mathcal{A}_h$ is computed. After $y^n \in \mathcal{A}_h$ and the search direction $d^n \in \mathcal{A}_h$ have been computed, we compute

$$y^{n+1} = y^n - \rho_n d^n$$

where $\rho_n \in \mathbf{R}$, $\rho_n > 0$ is the solution to the one-dimensional minimization problem

$$\hat{\mathcal{J}}(y^n - \rho_n d^n) \leq \hat{\mathcal{J}}(y^n - \rho d^n), \qquad \forall \rho > 0.$$

We then compute the new gradient, $g^{n+1} \in \mathcal{A}_h$, by

$$\int_\Omega g^{n+1} \cdot z \, dx = \int_\Omega \frac{\partial \hat{\phi}}{\partial F}(\nabla y^{n+1}, \theta) \cdot \nabla z \, dx, \qquad \forall z \in \mathcal{A}_h.$$

The new search direction, $d^{n+1} \in \mathcal{A}_h$, is then computed by

$$d^{n+1} = g^{n+1} + \lambda_n d^n$$

where

$$\lambda_n = \left[\int_\Omega g^{n+1} \cdot g^{n+1} dx\right] / \left[\int_\Omega g^n \cdot g^n \, dx\right]$$

Our computational experiments have show that the energy of the iterates for the conjugate gradient method initially decays faster than the energy of the iterates for the gradient method. However, the gradient method reaches our criterion for convergence as fast as the conjugate gradient method. In Figure 10, we give a comparison of the decay of the energy for iterates of the gradient method and the conjugate gradient method for the internally twinned martensite problem with $\lambda = 1/2$ as described in section 3.

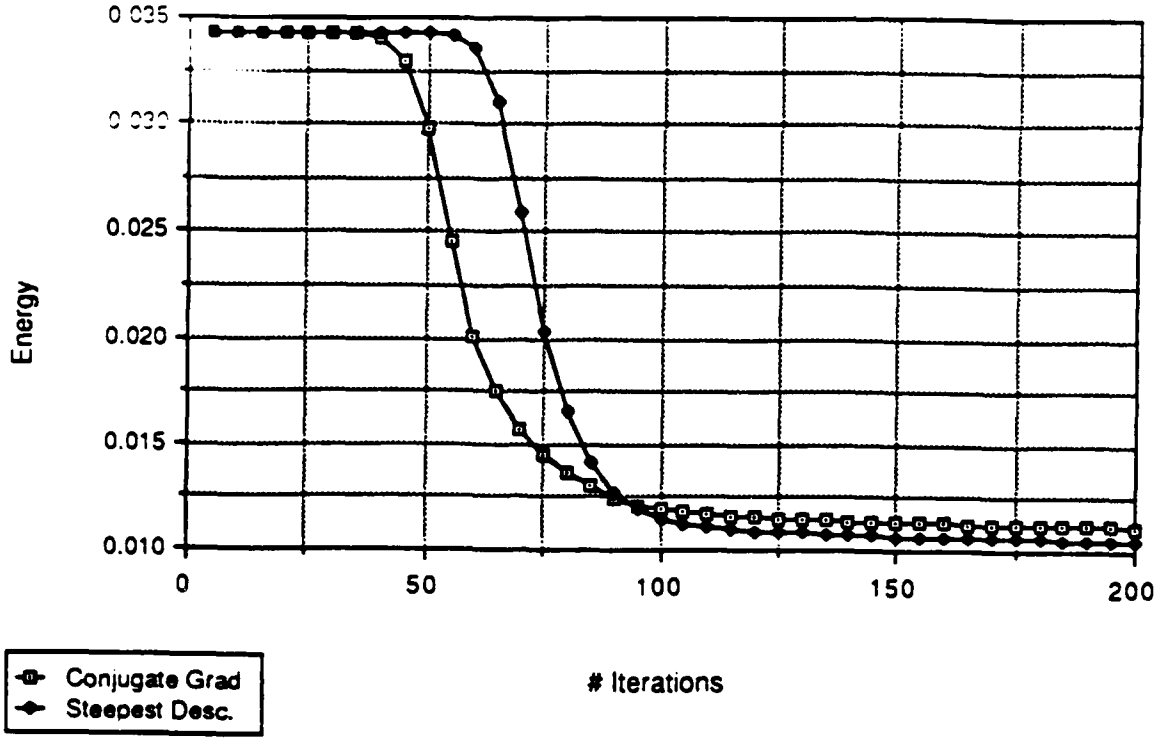

Figure 10. Comparison of the decay of the energy for iterates computed with the gradient method and the conjugate gradient method for the internally twinned martensite problem with $\lambda = 1/2$.

REFERENCES

[1] F. W. Alt, K.-H. Hoffmann, M. Niezgódka, J. Sprekels, *A numerical study of structural phase transitions in shape memory alloys*, Preprint #90, Institut für Mathematik, Universitat Augsburg, 1985.

[2] J. M. Ball and R. D. James, *Fine phase mixtures as minimizers of energy*, Arch. Rational Mech. Anal., 100 (1987), pp. 13-52.

[3] J. M. Ball and R. D. James, *Experimental tests of a theory of fine microstruture*, preprint, August, 1988.

[4] J. M. Ball, R. D. James, and D. Kinderlehrer, in these proceedings.

[5] M. W. Burkart and T. A. Read, *Diffusionless phase change in the indium-thallium system*, Trans. AIME J. Metals, 197 (1953), pp. 1516-1524.

[6] M. Chipot and D. Kinderlehrer, *Equilibrium configurations of crystals*, to appear, Arch. Rational Mech. Anal.

[7] P. G. Ciarlet, *Mathematical Elasticity, Volume 1: Three-Dimensional Elasticity*, North-Holland, Amsterdam, 1988.

[8] C. Collins and M. Luskin, *The computation of the austenitic-martensitic phase transition*, University of Minnesota Supercomputer Institute preprint #88/75, July, 1988, to appear in Partial Differential Equations and Continuum Models of Phase Transitions (ed. M. Rascle, D.Serre, and M. Slemrod), Springer-Verlag.

[9] J. L. Ericksen, *Some constrained elastic crystals*, (ed. J. M. Ball), Oxford University Press, 1987. pp. 119-137.

[10] J. L. ERICKSEN, *Constitutive theory for some constrained elastic crystals*, Int. J. Solids and Structures, 22 (1986), pp. 951-964.
[11] P. GILL, W. MURRAY, AND M. WRIGHT, *Practical Optimization*, Academic Press, London, 1981.
[12] R. GLOWINSKI, *Numerical Methods for Nonlinear Variational Problems*, Springer-Verlag, New York, 1984.
[13] M. E. GURTIN, *Topics in Finite Elasticity*, SIAM, Philadelphia, 1981.
[14] R. D. JAMES, *Microstructure and weak convergence*, in Material Instabilities in Continuum Mechanics and Related Problems, (ed. J. M. Ball), Oxford University Press, 1987, pp. 175-196.
[15] D. KINDERLEHRER, *Remarks about equilibrium configurations of crystals*, in Material Instabilities in Continuum Mechanics and Related Problems (ed. J. M. Ball), Oxford University Press, 1987, pp. 217-242.
[16] S. A. SILLING, *Phase changes induced by deformation in isothermal elastic crystals*, preprint.

Marshall Slemrod
Center for the Mathematical Sciences
University of Wisconsin-Madison
Madison, WI 53705

ABSTRACT

Dynamics of Phase Transitions

Smart materials such as materials with shape memory often exhibit the ability to change phase. In this report I will discuss two approaches to understanding the dynamics of phase transitions. There are (i) phenomological continuum modeling based on the van der Waals equation of state for a compressible fluid and (ii) reductionist modecular kinematic modeling based on the Becker-Döring cluster equations. Both approaches yield conditions for dynamic change of phase though the mathematical issues in each case are quite distinct.

ADMISSIBILITY CRITERIA FOR PHASE BOUNDARIES

M. Slemrod#
Department of Mathematical Sciences
Rensselaer Polytechnic Institute
Troy, N. Y. 12180

The purpose of this note is to review some ideas on admissibility criteria for phase boundaries in materials. Specifically we are concerned with one dimensional motions of elastic fluids or elastic solids which possess a constitutive relation of the form shown in Figure 1.

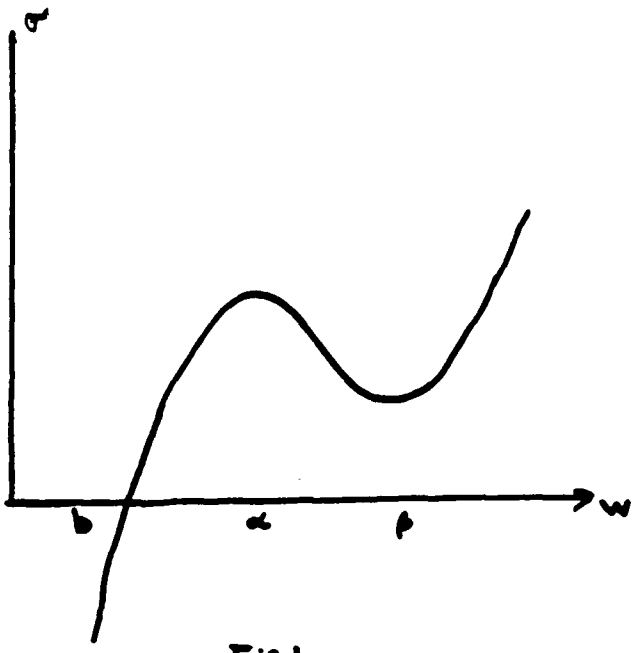

Fig.1

#Research supported by the Air Force Office of Scientific Research, Air Force Systems Command, USAF, under Contract/Grant No. AFOSR-85-0239. The United States Government is authorized to reproduce and distribute reprints for Government purposes not withstanding any copyright herein.

Here σ is Piola-Kirchoff stress and w is the specific volume (= (density)$^{-1}$ for an elastic fluid (the deformation gradient for an elastic solid.)

We let u(x,t) denote the velocity of the fluid (solid) at Lagrangian coordinate x and time t. The balance of mass and momentum can be expressed by the 2×2 system of conservation laws

$$\begin{aligned} u_t &= \sigma(w)_x \ . \\ w_t &= u_x \ , \quad t > 0 \ , \ -\infty < x < \infty \ . \end{aligned} \tag{1}$$

Of course (1) should be coupled with initial conditions for the motion

$$u(x,0) = u_0(x) \ , \ w(x,0) = w_0(x) \ . \tag{2}$$

Due to the fact that $\sigma' < 0$ in (α,β) and $\sigma' > 0$ elsewhere, (1) is a mixed hyperbolic-elliptic system.

An ambitious program would be to investigate solvability of (1) . (A less ambitious task is to study solvability for a simpler test problem namely the Riemann problem where

$$\begin{aligned} u_0(x) &= u_r \ , \ w_0(x) = w_r \ , \ x > 0 \ , \\ u_0(x) &= u_\ell \ , \ w_0(x) = w_\ell \ , \ x < 0 \ , \end{aligned} \tag{3}$$

u_r, u_ℓ, w_r, w_ℓ constants. We may then try to piece together a solution of the Riemann problem in terms of elementary waves. As usual the waves of interest are shock waves whose speed of propagation s satisfies the Rankine-Hugoniot jump condition

$$\begin{aligned} -s[u] &= [\sigma] \ , \\ -s[w] &= [u] \ , \end{aligned} \tag{4}$$

rarefaction waves, and a contact discontinuity for which $[\sigma] = 0$. Here $[u] = u_+ - u_-$, etc. where + , - denotes the limits of u from the right and left of the shock. When w_+ , w_- lies (b,α) or (β,∞) or vice-verse the shock is said to be a phase boundary.

This concept of phase boundary just reflects the usual elementary notions of a model like that in Figure 1. That is $w\in(b,\alpha)$ and $w\in(\beta,\infty)$ are supposed to denote different phases of the same material, e.g. (b,α) = liquid phase, (β,∞) = vapor phase in a van der Waals fluid.

Of course as is well known even for strictly hyperbolic problems we cannot expect a unique weak solution for the Cauchy initial value

problem. We need some admissibility criteria for choosing preferred solutions.

In this note we consider four admissibility criteria: the viscosity criterion, the entropy criterion, the viscosity-capillarity criterion, and the entropy rate criterion. To keep matters simple we shall consider the simplest Riemann problem exhibiting a phase transition i.e. the case where $w_\ell \in (b,\alpha)$, $w_r \in (\beta,\infty)$ and u_ℓ, u_r, w_ℓ, w_r are constants consistent with the Rankine-Hugoniot jump condition for some s. In this case the shock wave solution

$$\begin{aligned} &w = w_\ell \ , \ x < st \ ; \ w = w_r \ , \ x > st \ , \\ &u = u_\ell \qquad\qquad\quad u = u_r \end{aligned} \tag{5}$$

is a <u>phase boundary</u>.

(I) <u>The viscosity criterion</u>.

Our phase boundary (5) is admissible according to the viscosity criterion if the wave is a limit as $\mu \to 0+$ of traveling wave solutions

$$u = \hat{u}\left(\frac{x-st}{\mu}\right) \ , \ w = \hat{w}\left(\frac{x-st}{\mu}\right) \tag{6}$$

to the viscous problem

$$\begin{aligned} u_t &= \sigma(w)_x + \mu u_{xx} , \\ w_t &= u_x \ . \end{aligned} \tag{7}$$

Traveling wave solutions $\hat{u}$, $\hat{w}$ satisfy

$$\begin{aligned} -s\hat{u}' &= \sigma' + \hat{u}'' \ , \\ -s\hat{w}' &= \hat{u}' \ , \end{aligned}$$

where $' = \frac{d}{d\xi}$, $\xi = \frac{x-st}{\mu}$.

Since we wish $\hat{u} \to u_\ell$, $\hat{w} \to w_\ell$, $x < st$;

$\hat{u} \to u_r$, $\hat{w} \to w_r$, $x > st$; as $\mu \to 0_+$

it is natural to impose the boundary conditions

$$\hat{u}(-\infty) = u_\ell , \ \hat{u}(+\infty) = u_r , \ \hat{w}(-\infty) = w_\ell , \ \hat{w}(+\infty) = w_r . \tag{9}$$

Integration of (8) coupled with (9) yields

$$\begin{aligned} -s(\hat{u}-u_\ell) &= \sigma(\hat{w}) - \sigma(w_\ell) + \hat{u}' \ , \\ -s(\hat{w}-w_\ell) &= \hat{u}-u_\ell \ , \end{aligned}$$

or simply

$$s\hat{w}' + s^2(\hat{w}-w_\ell) - \sigma(\hat{w}) + \sigma(w_\ell) = 0 \ . \qquad (10)$$

The equilibrium points of (10) are w_ℓ, w_r, and possibly an intermediate value w where the chord connecting $(w_\ell, \sigma(w_\ell))$ and $(w_r, \sigma(w_r))$ cuts the graph of σ. For (10) to have a <u>continuous</u> solution satisfying (9) it is impossible to have such a middle equilibrium point. For example a solution $s = 0$, $u_\ell = u_r = 0$, $\sigma(w_\ell) = \sigma(w_r)$ as shown in Fig. 2 would not be admissible from this point of view.

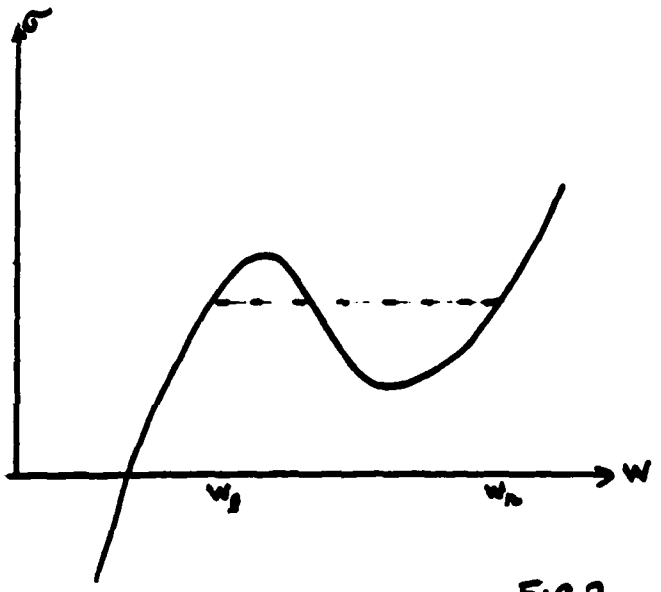

Fig.2

On the other if one allows <u>discontinuous</u> traveling waves then $\hat{w} = w_\ell \quad \xi < 0$; $\hat{w} = w_r$, $\xi > 0$; is a solution of (10).

If one allows such discontinuous traveling waves Shearer [1] has proven existence of solutions to the general Riemann problem (1), (3) whose solutions are admissible according to the viscosity criterion.

(II) <u>Entropy criterion</u>.

The entropy criterion postulates that there is a non-trivial function $H(u,w)$ which satisfies an additional conservation law

$$H_t + Q_x = 0 \qquad (11)$$

for smooth solutions (u,w) of (1) but for which $H_t + Q_x$ has a preferred sign for non-smooth solutions. For example in our problem

the natural "entropy" is the total mechanical energy

$$H(u,w) = \frac{1}{2}u^2 + \int^w \sigma(\xi)d\xi \ .$$

It is easy to check that (11) is satisfied for smooth solutions of (1) with $Q(u,w) = -u\sigma(w)$. For non-smooth solutions the entropy criterion asserts

$$H_t + Q_x \leq 0 \ . \tag{12}$$

Mechanistically (12) reflects that the fact that an isothermal non-conductor of heat with no heat sources will dissipate mechanical energy. More simply, shock formation does mechanical work.

For our simple solution (12) implies

$$-s\left\{\left(\frac{\sigma(w_r)+\sigma(w_\ell)}{2}\right)(w_\ell - w_r) + \int_{w_\ell}^{w_r}\sigma(\xi)\theta\xi\right\} \geq 0 \ . \tag{13}$$

This inequality also has a geometric interpretation: The phase boundary joining the state (u_ℓ, w_ℓ) to (u_r, w_r) must have area > area B for $s > 0$. area A < area B for $s < 0$. For $s = 0$ all equilibria satisfying $\sigma(w_\ell) = \sigma(w_r)$ are admissible as was the case in the viscosity criterion (I).

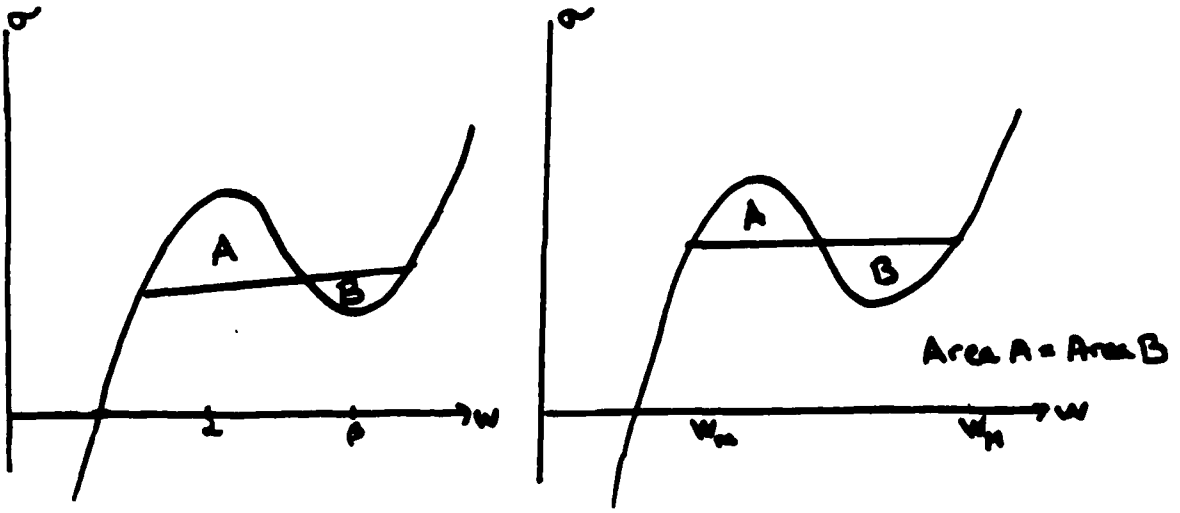

(III) Viscosity-capillarity criterion.

A third approach to the phase boundary problem admissibility criterion was proposed in [2]. In that paper it was suggested that perhaps viscosity and capillarity should play a role in studying shock structure. The idea of including capillarity in studying

interfaces in phase transitions can be traced to the work of van der Waals [3] and has been reconsidered by many others since then, e.g. Cahn and Hilliard [4], Aifantis and Serrin [5].

Simply put in the framework of our problem we amend the balance law (1) by including the effects on viscosity and capillarity:

$$\begin{aligned} u_t &= \sigma(w)_x + \mu u_{xx} - \mu^2 A w_{xxx} \, . \\ w_t &= u_x \, . \end{aligned} \tag{14}$$

As in (I) we wish to approximate the discontinuous phase boundary solution by traveling wave solution $u = \hat{u}\left(\frac{x-st}{\mu}\right)$.

$w = \hat{w}\left(\frac{x-st}{\mu}\right)$ as $\mu \to 0_+$. Here A is a positive constant.

A simple argument shows

$$\begin{aligned} &A\hat{w}'' + s\hat{w}' + s^2(\hat{w}-w_\ell) - \sigma(\hat{w}) + \sigma(w_\ell) = 0 \\ &\hat{w}(-\infty) = w_\ell \, , \quad \hat{w}(+\infty) = w_r \, , \\ &\hat{w}'(-\infty) = 0 \, , \quad \hat{w}'(+\infty) = 0 \, . \end{aligned} \tag{15}$$

For fixed (u_ℓ, w_ℓ) in (b, α) there is always some state to which it can be connected by a phase boundary. This result and several others may be found in the papers of Slemrod [2], Hagan and Slemrod [6], Shearer [7,8]. It is easy to see, however, that where $s = 0$ w must satisfy

$$A\hat{w}'' - \sigma(\hat{w}) + \sigma(w_\ell) = 0. \tag{16}$$

Multiply (16) by w' and integrate from $\xi = -\infty$ to $\xi = +\infty$. This shows

$$\int_{-\infty}^{\infty} (\sigma(w(\xi)) - \sigma(w_\ell))\, \hat{w}'(\xi) d\xi = 0$$

or

$$\int_{w_\ell}^{w_r} (\sigma(w) - \sigma(w_-)) dw = 0 \tag{17}$$

i.e. the only equilibrium states consistent with a stagnant phase boundary must have area A = area B. (The Maxwell equal area rule.)

Notice the difference between this highly restricted stagnant phase boundary condition and the continuum of possibilities in (I) and (II). We also note that phase boundaries satisfying the viscosity-capilarity criterion satisfy the entropy criterion (see [2]).

In a remarkable paper [8] Shearer has shown existence of a solution to the general Riemann problem for w_ℓ, w_r close to w_m, w_M all of whose shocks satisfy the viscosity-capillarity criterion.

(IV) Entropy rate criterion.

The entropy rate criterion was proposed by Dafermos [9] for the study of admissible solutions to hyperbolic conservation laws. It has been extended by Hattori [10],[11], to the case of van der Waals like materials.

The idea behind the entropy rate criterion is as follows. The total mechanical energy on any interval [a,b] satisfies at time τ

$$\frac{D^+}{D\tau} \int_a^b H(u,w)dx = \sum_{\substack{\text{jump} \\ \text{discontinuities}}} \sigma(\tau)\, A(w_-,w_+) \qquad (18)$$

for any piecewise smooth solutions u,w of (1) which possesses a finite number of shock waves. Here $\sigma(\tau)$ is the speed of the jump discontinuity and

$$A(w_-,w_+) = \frac{1}{2}\,(\sigma(w_-)+\sigma(w_+)(w_+-w_-)) - \int_{w_-}^{w_+} \sigma(\xi)d\xi.$$

Thus (18) computes the rate of energy dissipation. The entropy rate criterion says that among all solutions which agree up to time τ the preferable one is the one that maximizes the rate of energy dissipation at time τ, i.e. we choose the process which renders

$$\sum_{\substack{\text{jump} \\ \text{discontinuities}}} \sigma(\tau)A(w_-,w_+)$$

a minimum. Philosophically the criteria asks that nature should choose a solution which renders the already decaying mechanical energy decay as rapidly as allowed by the balance laws and constitutive equations.

The difficulty in applying the entropy rate criterion is the need to check a candidate for an admissible solution against all other solution competitors at each time τ. To check the admissibility of shocks Dafermos [9] has suggested a modified version of the entropy rate criterion. In the modified version the shock is admissible when compared against solutions of the Riemann problem (defined by the shock) made up of the usual fan of shocks, rarefaction waves, contact discontinuities. Hattori [10] has applied this

modification to check admissiblity of phase boundaries for (1).

As an illustrative example consider once again the equilibrium Riemann problem $u_\ell = u_r = 0$. $\sigma(w_\ell) = \sigma(w_r)$. Hattori has shown that if $\sigma(w_\ell)$. $\sigma(w_r)$ are not on the Maxwell line (given by the equal area rule) there is another solution of the Riemann problem which dissipates energy more rapidly at $\tau = 0_+$. Hence such a solution will <u>not</u> be admissible according to the entropy rate criterion. Moreover if $\sigma(w_\ell)$. $\sigma(w_r)$ are on the Maxwell line i.e. $w_\ell = w_m, w_r = w_M$. Hattori has shown that when compared against competitive solutions made up of shocks, rarefraction waves, and phase boundaries (in a manner motivated by Dafermos's entropy rate shock criterion) this Maxwell solution dissipates energy most rapidly. These results are similar to those given by the viscosity-capillarity criterion (III).

In conclusion we see the viscosity criterion and entropy criterion play no role in distinguishing stagnant phase boundaries. On the other hand the viscosity-capillarity criterion and entropy rate criterion do. In fluids the classical theory of phase transitions (both theoretically and experimentally) gives a preferred equilibrium with co-existing phases. Hence for fluid problems one might think either the viscosity-capillarity criterion or entropy rate criterion will be appropriate. For solids where viscous forces may dominate Pego [12] has argued for the viscosity criterion. Pending further results (theoretical, numerical, and experimental) I would be hesitant to say there is any "correct," universal admissibility criteria for all materials modeled by (1).

References

1. M. Shearer, The Riemann problem for a class of conservation laws of mixed type, J. Differential Equations 46(1982), 426-443.

2. M. Slemrod, Admissibility criteria for propagating phase boundaries in a van der Waals fluid, Arch. Rational Mechanics and Analysis 81(1983), 301-315.

3. J. D. van der Waals, Translation of J. D. van der Waals, "The Thermodynamic theory of capillarity under the hypothesis of the continuous variation of density" by S. Rowlinson, J. Statistical Physics 20(1979), 197-244.

4. J. W. Cahn and J. E. Hilliard, Free energy of a nonuniform system, J. Chemical Physics 28(1958), 258-267.

5. E. C. Aifantis and J. B. Serrin, The mechanical theory of fluid interfaces and Maxwell's rule, J. Colloid and Interface Science 96(1983), 517-529.

6. R. Hagan and M. Slemrod, The viscosity-capillarity criterion for shocks and phase transitions, Archive for Rational Mechanics and Analysis 83(1984), 333-361.

7. M. Shearer, Admissibility criteria for shock wave solutions of a system of conservation laws of mixed type, Proc. Royal Soc. Edinburgh 93A(1983), 233-244.

8. M. Shearer, Nonuniqueness of admissible solutions of Riemann initial value problems for a system of conservation laws of mixed type, to appear J. Differential Equations.

9. C. Dafermos, Hyperbolic systems of conservation laws, in Systems of Nonlinear Partial Differential Equations, ed. J. M. Ball, Reidel (1984).

10. H. Hattori, The Riemann problem for a van der Waals fluid with entropy rate admissibility criterion, isothermal case, to appear Archive for Rational Mechanics and Analysis.

11. H. Hattori, The Riemann problem for a van der Waals fluid with entropy rate admissibility criterion, nonisothermal case, to appear J. Differential Equations.

12. R. Pego, Phase transitions: stability and admissibility in one dimensional nonlinear viscoelasticity, Institute for Mathematics and its Applications, Univ. of Minnesota, Preprint No. 180 (1985).

List of Attendees

Iqbal Ahmad
Materials Science Division
U.S. Army Research Office
P.O. Box 12211
Research Triangle Park, NC 27709-2211
(919) 549-0641 ex. 284

Dr. Gary Anderson
Structures & Dynamics
Engineering Sciences Division
P.O. Box 12211
Research Triangle Park, NC 27709-2211
(919) 549-0641

Dr. Felton Bartlett
Aerostructures Directorate
M.S. 266
NASA Langley Research Center
Hampton, VA 23665
(804) 865-2866

Mr. Joseph Burns
Wright Patterson AFB
Wright Patterson, OH 45433

Dr. J. Chandra
Director of Mathematical Sciences
U.S. Army Research Office
P.O. Box 12211
Research Triangle Park, NC 27709-2211
(919) 549-0641

Dr. S.C. Chou
SLCMT-MRD Bldg. 313 North
405 Arsenal Street
Army Materials Technology Laboratory
Watertown, MA 02172
(617) 923-5115

Professor R.O. Claus
Fiber & Electro-Optics Research Center
Dept. of Electrical Engineering
VPI&SU
Blacksburg, VA 24061
(703) 961-7203

Dr. Ted Duclos
Thomas Lord Research Center
P.O. Box 8225
Cary, NC 27512-8225
(919)469-3443 ex. 304

Mr. Gary Farley
U.S. Army Aerostructures
NASA Langley Research Center
Hampton, VA 23665

Professor Mukesh Gandhi
Dept. of Mechanical Engineering
Michigan State University
East Lansing, MI 48824-1226
(517) 355-1744

Mr. Tony Gerardi
Wright Patterson AFB
AFWAL/FIBE
Wright Patterson, OH 45433
(513) 255-2544

Bob Gordon
Wright Patterson AFB
Wright Patterson, OH 45433

Professor Barry Grossman
Department of Electrical and
Computer Engineering
Florida Institute of Technology
Melbourne, Florida 32901-6988
(305) 768-8000 ex. 7429

Professor William Hager
Dept. of Mathematics
University of Florida
Gainesville, FL 32611
(904) 392-0286

Professor Sathya Hanagud
School of Aerospace Engineering
Georgia Institute of Technology
Atlanta, GA 30332
(404) 894-3040

Professor Richard James
Dept. of Aerospace
Engineering & Mechanics
University of Minnesota
110 Union St., SE
Minneapolis, MN 55455
(612) 625-8000

Professor Robert Kohn
Courant Institute of
Mathematical Science
New York University
251 Mercer Street
New York, NY 10012
(212) 998-3217

Professor Mitchell Luskin
School of Mathematics
University of Minnesota
Minneapolis, MN 55455
(612) 625-6565

Mr. Wayne R. Mantay
Mail Stop 340
NASA Langley Research Center
Hampton, VA 23665
(804) 865-2867

Dr. Arje Nachman
Air Force Office of
Scientific Research
Bolling Air Force Base
Washington, DC 20332-6448
(202) 767-5028

Professor R.E. Newnham
Pennsylvania State University
Materials Research Laboratory
University Park, PA 16802
(814)865-1612

Mr. Mark Nixon
U.S. Army Aerostructures
NASA Langley Research Center
Hampton, VA 23665

Dr. Bhakta Rath
Naval Research Labs
Code 6000
4555 Overlook Ave., S.W.
Washington, DC 20375-5000
(202) 767-3566

Professor Eugene Riven
Dept. of Mechanical Engineering
Wayne State University
Detroit, MI 48282
(313) 977-3898

Professor H.H. Robertshaw
Smart Materials & Structures
Dept. of Mechanical Engineering
VPI&SU
Blacksburg, VA 24061
(703) 961-7196

Professor Craig Rogers
Smart Materials & Structures
Dept. of Mechanical Engineering
VPI&SU
Blacksburg, VA 24061
(703) 961-7194

Professor Rouben Rostamian
Department of Mathematics
University of Maryland
Baltimore, MD 21228
(301) 455-2412 ex. 2458

Dr. John Shipley
Aerospace Structures Group
Harris Corporation
Melbourne, FL 32902

Professor Marshall Slemrod
Mathematics Research
University of Wisconsin
Madison, WI 53706
(608) 262-2881

Professor Michael Thursby
Dept. of Electrical &
Computer Engineering
Florida Institute of Technology
Melbourne, Florida 32901-6988
(305) 768-8000 ex. 7183

Professor Garth Wilkes
Chemical Engineering Department
VPI&SU
Blacksburg, VA 24061
(703) 961-5498

Dr. Julian Wu
U.S. Army Research Office
P.O. Box 12211
Research Triangle Park, NC 27709-2211

Professor M.J. Furey
Mechanical Engineering Department
VPI&SU
Blacksburg, VA 24061
(703) 961-7193

Professor C.F. Reinholtz
Mechanical Engineering Department
VPI&SU
Blacksburg, VA 24061
(703) 961-7820

Professor J.B. Kosmatka
Mechanical Engineering Department
VPI&SU
Blacksburg, VA 24061
(703) 961-7355